Studies of the Physical Aspects of Intumescence Using Advanced Diagnostic Methods

By:

Mr Hussain Saeed

This thesis is submitted to the University of Sheffield for the degree of Doctor of Philosophy

Combustion and Flow Diagnostic Research Group

Department of Mechanical Engineering

Submission Date

01st March 2017

Declaration

The work presented in this thesis is that of the author and has not been submitted for any other awards or degree at the University of Sheffield or any other university/institution. Where other sources of information or help from other parties has been used this has been acknowledged.

Dedication

To my Family, my lovely niece and most importantly my wife, Ayesha Mubarik Hussain.

Acknowledgements

Publications

H. Saeed and Y. Zhang, 'Studies of the physical aspects of intumescence using advance diagnostic methods.' 8th International Symposium on Measurement Techniques for Multi-Phase Flows 2013; http://dx.doi.org/10.1063/1.4872104

Abstract

Commercial testing of Intumescent paints can be extremely expensive. There is a need to develop lab scale systems that can cost effectively both study and test intumescent paints under conditions that are closer to commercial and real time fire tests. This research aims to present a strong case for using an impinging flame based rig to test intumescent coatings. The main feature of using flame impingement is the heterogeneous absorption of heat along the wall surface. This property is a great advantage because intumescent paints under complex fire conditions can be simulated more realistically. The heating technique is coupled with advance diagnostics methods to highlight behaviour that has not been observed before. Physical aspects of commercial coatings, under the new setup, are compared to the cone calorimeter – traditional testing setup

The process of intumescence was observed through the use of diagnostic techniques such as Schlieren, thermal and digital imaging. Cross sectional area and surface textures were captured using digital images of fully intumesced char samples that revealed distinct internal structures and surface textures. Temperature of the substrate, T_b, was recorded using a thermocouple attached to the back surface of the panel under different heating conditions.

Schlieren technique, based on the refraction of light phenomenon, has never been use to examine the physical aspects of intumescence. It helped highlight the interaction between the flame and paint surface. The impingement of non-reactive fuel, at low separations was clearly visible and was responsible for influencing mode shape of the resulting char. The expulsions phenomenon observed using this technique has not been visually observed before. It occurred during the pustule appearance phase offering conclusive evidence that invisible gases escape from the surface of the paint. The measurement of char expansion and its rate of growth whilst engulfed in luminous diffusion flames is a methodology developed using this technique. The results revealed that formulations tested had unique expansion behaviours and growth pattern. Furthermore, an expansion activation temperature (EAT) range with respect to substrate temperature was identified for each formulation, which was found to be consistent under a variety of experimental conditions.

The distinctive yellow colour of a diffusion flames engulfs a coating during a test. Due to this, the process of intumescence has not been observed visually. Thermal imaging was used in this study because it allowed the user to bypass the flame and observe intumescence as it occurred.

Using thermal imaging, the physical aspects of intumescence were studied in extensive detail and salient characteristics were identified. The appearance of surface pustules followed by majority of the expansion were characterised as the two distinct phases in the intumescence process. Analysis of the surface temperature revealed that the thermal profile of the surface was non-uniform and highly localized in nature. This was attributed to the higher temperature of the pustules relative to the paint surface. Results from thermal imaging combined well with the Schlieren technique to develop a coherent understanding of the expansion process.

Diagnostic equipment, particularly thermal and digital imaging, were also used on tests conducted in a cone calorimeter. The results between cone heater and impinging flame-based tests were compared. The degree of intumescence, surface temperature profile and various characteristics were found to be different between both methods.

Finally, the use of the techniques was extended to study the process of intumescence and complex char growth patterns on T-shaped panels coated with intumescent formulations. Char growth was observed to be complex and non-linear as compared to flat panel systems. A novel Image processing algorithm using the thermal imaging data from the cone calorimeter was developed marking a further advancement to the use of this technique and gain insight into the growth mechanism when examining a complicated three dimensional system such T-panels.

Table of Contents

List of figures and tables

Nomenclature

Uppercase Roman Letters

A	Area	[mm^2]
C	Carbon	
C	Centigrade	
CV	Calorific Value	
D	Diameter	[mm]
EAT	Expansion Activation Temperature	[^{0}C / K]
H/h	Height	[mm/m]
H	Hydrogen	
J	Joule	
K	Kelvin	
Kg	Kilogram	
N	Nitrogen	
O	Oxygen	
T	Temperature	[^{0}C]
P	Pressure	[Pa]
Pa	Pascal	
$\dot{Q}$	Heat Flux	[KW/m^2]
R	Radius	[mm]
R	Ideal Gas constant	[J/kg.K]
Re	Reynolds Number	
S	Speed	
TTF	Time to Failure	[s]
TTF$_m$	Time to Failure – modified	[s]

U/u	Exit Velocity	[m/s]
V	Velocity	[m/s]
W	Radiance	[KW/sr·m^2]
W	Watts	

Lowercase Roman Letters

c	Speed of light	[m/s]
f	Frequency	[Hz]
k	Thermal Conductivity	[KW/m.K]
l	Litres	
m	Meter	
mm	Millimetre	
min	Minute	
n	Refractive Index	
r	Radius	[mm]
s	Second	
t	Film Thickness	[mm]
v	Fuel Flow rate	[m^3/s]
x	Axial position	
x,y	Spatial Coordinates	
z	Depth	

Lowercase Greek Letters

$\alpha_{A,B}$	Seebeck coefficient	
β	Number of hydrogen	
ε (e)	Emissivity	
λ	Wave Length	[μm]

μ	Dynamic Viscosity	[Pa.s]
ϕ	Equivalence Ratio	
ρ	Density	[kg/m^3]
θ	Angle	[^{0}]

Subscripts

∞	Ambient/Far field
a	Air
α, β, γ	Molar quantities Carbon, Hydrogen and Oxygen respectively
b	Back Face/Substrate
c	conduction
cv	Convection
f	Fluid Temperature
f	Fuel
h	Convective heat transfer coefficient
L	Laminar
m	modified conditions
p	Pore
r	Radiation
s	Surface
surr	Surrounding
st	Stoichiometric

Acronyms/Abbreviations

1D	One-dimensional
2D	Two-dimensional
APP	Ammonium Polyphosphate
ASTM	American Society for Testing and Materials

CC	Cone Calorimeter
CO_2	Carbon Dioxide
CFD	Computational Fluid Mechanics
CPF	Cellulosic Paint Formulation
DAQ	Data Acquisition system
Deg	Degrees
DTA	Differential Thermogravimetric Analysis
Di-PER	Di- Pentaerythritol
EG	Expandable Graphite
ER	Expansion Ratio
FFT	Fourier Frequency Transformation
FPS	Frames Per Second
FTIR	Fourier Transform Infra Red
H_2O	Water
HPF	Hydrocarbon Paint Formulation
HRR	Heat Release Rate
ISO	International Organisation for Standardisation
LL01	Line tool (Thermal)
LOI	Limiting Oxygen Index
LW	Long Wave
MW	Medium Wave
MEL	Melamine
MELP	Melamine Phosphate
NH_3	Ammonia
NTP	Nozzle to Plate
PA-6	Poly Amide 6

PER	Pentaerythritol
PU	Polyurethane
QWIP	Quantum Well Infrared Photo Detector
SP01	Spot Tool (Thermal)
SW	Short Wave
TGA	Thermo Gravimetric Analysis
Tri-PER	Tri- Pentaerythritol
UL	Underwriters Laboratories
VOC	Volatile Organic Compounds
VI	Virtual Instrument

Chapter1.   Introduction

The cost of fire damages has been estimated to be approximately \$400 billion (USD) and close to 1% of the world's GNP (2004)[1]. In addition to loss of assets, risk of human casualties is a primary concern. The need for fire protection methods has been realised and made its way in almost all safety practices. One such method of passive fire protection is the use of intumescent paints.

Intumescence literally means 'to swell'. A small layer of paint can swell up to 100 times its original size. They work on a very simple principle. When the temperature increases, chemical reactions under the paint surface result in the release of gases to form a foam-like cellular structure and a crisp outer carbon rich char. The endothermic nature of the reaction absorbs the heat released by the fire. The expanding paint uses the available oxygen in the atmosphere and protects the substrate. Finally, the expanding foam layer has a porous structure comprised of numerous gas pockets resulting in a low thermal conductivity that helps provide good insulation to the substrate.

There are various physical advantages of intumescent paints over traditional fire proofing systems. They offer thin film coatings that allow maximum utilisation of space. They are lightweight and aesthetically pleasing. Other desirable characteristics include good weatherability, corrosion endurance over time, water solubility and aesthetic qualities [2].

A typical intumescence is shown in Fig.1.1.
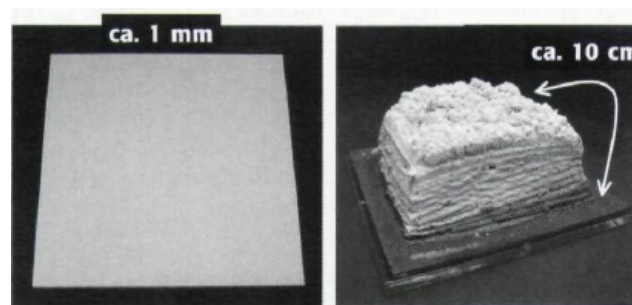
Figure 1.1 Intumescence resulting in a 100mm layer of foamed char from a 1mm layer of paint[1].

The main focus of industrial research has been on the use of coatings in the construction industry. Specifically, on critical weight bearing steel columns [1, 3]. In case of a fire, the temperature of steel can rise to 500 ^{0}C in less than five minutes and loose up to half its

structural strength resulting in the collapse of the structure. Intumescent coatings are applied over the steel substrate and are expected to reduce the transfer of heat for many hours under conditions where temperatures can be in excess of $1100^{o}C$[3]. The coatings are capable of curbing the rate of temperature increase. Under a suitable thickness, it can take up to 90 minutes before the failure temperature of $500\ ^{0}C$ is achieved. This can provide valuable evacuation times especially in high-rise buildings.

1.1   Research Motivation

The interaction between intumescent paints and fires is not understood in great detail. This is because a typical fire has a very complicated structure with uneven thermal gradients, heat flux and propagation patterns based on factors such as environment, scale and nature of fire. To overcome this unpredictability, industrial standards have evolved so that rigorous full-scale fire tests are required before a paint coating is made available in the market.

The problems with these tests are that they are extremely expensive to conduct. It is very difficult to use any diagnostic equipment to study what is happening during such tests. Thermocouples are the only instrumentation attached to the substrate to study the heating rate under the action of a jet fire. Typically, a sample fails as the intumescing char is either deteriorated or it pulls away to expose the substrate surface. This is indicated when a steep change in the temperature measured by the thermocouple is registered. Thus, there is a risk that a coating may fail and have to be retested.

Large scale furnace and jet fire tests under ISO 22899-1[4] are pre-dominantly used to test market ready formulations. Samples are heated up to $1100\ ^{0}C$ and data is gathered by positioning thermocouples to monitor the temperature and inspect the resulting char at the end of the testing phase. Consequently, very limited information is gained on the performance of coatings in these tests.

Overall, industrial methods, especially large furnace tests, are very expensive and can be considered very coarse when the aim is to study what happens while the sample undergoes intumescence. Hence, there is an urgent need for cost effective methods where the performance of the pre-market formulation can be visually inspected during intumescence [5].

One such cost effective method is the cone calorimeter heater. The sample can be visually inspected from beginning to the end of intumescence. They are tested under an electric cone heater that provides a uniform radiative heat flux[6-8]. However, a uniform heat flux is not a true representative of a real fire scenario. Hence, the need for test that can simulate real fire conditions at lab scale is still unmet.

This research aims to take advantage of the impinging flame configuration to create lab scale models of various fire modes in order to test intumescent formulations under conditions similar to those of a full-scale fire test. Impinging flames have been widely used at lab scale because they exhibit simple flow dynamics and allow ease of instrumentation access. Furthermore, they are capable of exhibiting all major modes of heat transfer.

Flame impingement includes the contact of flame with the surface that is being processed utilising all modes of heat transfer, but predominantly forced convection. It is used widely in industries to mould metal and glass. The cost of running such a system is higher compared to the conventional radiation or electric heating furnaces. However, a higher heat transfer rate, enhanced productivity, flexibility in heating regimes, reduced heating time, fuel consumption and emissions are many of the advantages that enhance the efficiency of the procedure[9]. The main feature of using flame impingement is the heterogeneous absorption of heat near the stagnation point on the surface. To the research in this project, this property is a great advantage because the intumescent paint under complex fire conditions can be simulated using an impinging flame.

This research also aims to identify and use novel diagnostic equipment such as thermal imaging to enhance the benefits of visual observation. Advance visualisation techniques have rarely been utilised to study any scale of testing. Therefore, there is no precursor to what techniques are best suited for studying the behaviour of intumescence. The intention at the start of this research was to conduct exploratory experimental research through the use of various temperatures and flow visualisation based diagnostic techniques. Based on their potential, certain techniques were utilised in greater detail to justify their merit towards lab scale tests, as an economic way for future research in the field of fire protection.

1.2   Objectives

The expected outcomes of this research are summarised below.

- Devise a new experimental methodology in order to investigate the process of intumescence using impinging flames.

- Validate currently established features of intumescence, through observations of the process, by using an impinging flame configuration as the primary source of heat.

- Highlight new physical characteristics through the use of various temperature and flow visualisation based diagnostic techniques.

- Characterise the physical aspects of intumescence using a simple structural element such as a square flat panel.

- Extended analysis from flat panels tests to determine behaviour in complex structural elements such as the T-panel.

- Compare and evaluate the performance of various formulations under different heating conditions using an impinging flame.

- Establish that an impinging flame is a powerful lab scale configuration to characterise performance expected in large-scale tests.

- Compare the use of impinging flame configuration with cone calorimeter.

1.3   Thesis Outline

The chapters in this thesis are as follows:

Chapter 1 provides and overview of the research topic. A list of expected outcomes and the outline of the thesis are also presented.

Chapter 2 presents current academic research and industrial practices in regards to intumescent paints and impinging flames. A review of current application of the diagnostic techniques used, as part of the research is also presented.

Chapter 3 presents an overview of the experimental methodology in support of this research work

Chapter 4 presents the experimental results of flat panels tested under different experimental conditions using an impinging flame setup. Various physical aspects are highlighted and discussed.

Chapter 5, the results from flame-based setups are compared with cone heater setup. The experiments performed using T-panel were compared to a) flat panels tested under similar conditions b) T-panels tested using cone calorimeter and the results form the char tracking technique, developed exclusively in this work.

Chapter 6 presents a conclusion and makes recommendation for future work and improvements in the current setup to continue research using flame-based setups.

Chapter2.   Literature review

2.1   Intumescent Paints

Uncontrolled fires are caused by accidents or negligence. There are many examples in history where accidental fires have resulted in huge losses. Especially in high-rise building, e.g. Gold plaza tower, Taiwan and Windsor Tower, Madrid in 2005 where loading bearing steel columns collapsed after prolonged exposure to heat.

Global urbanisation is resulting in the construction of high-rise buildings where evacuation times, in case of a fire, increase. The protocols for fire protection are struggling to keep up and ensure safety of lives. Hence, there is a constant need to develop safer and efficient fire protection techniques. Commonly used building materials are concrete, wood and steel. These materials lose strength when exposed to fire. Concrete spalls and wood burns. Steel does not burn but it can lose significant strength at temperatures above 500 ^{0}C [3]. Since, it is the most commonly used material in buildings, the focus of application of intumescent paints has been on preventing key steel structural components from exceeding a failure temperature of 400^{0}C.

A virgin coating and the char after exposure to heat are shown in figure 2.1. A schematic illustrating the reaction sequence is shown in figure 2.2. Upon exposure to heat, intumescence results in a series of complex chemical reactions. The matrix expands as the gases try to escape. The end product is a swollen carbon rich char with a high porosity and low thermal conductivity that acts as a thermal barrier between the heat source and the substrate surface [10].
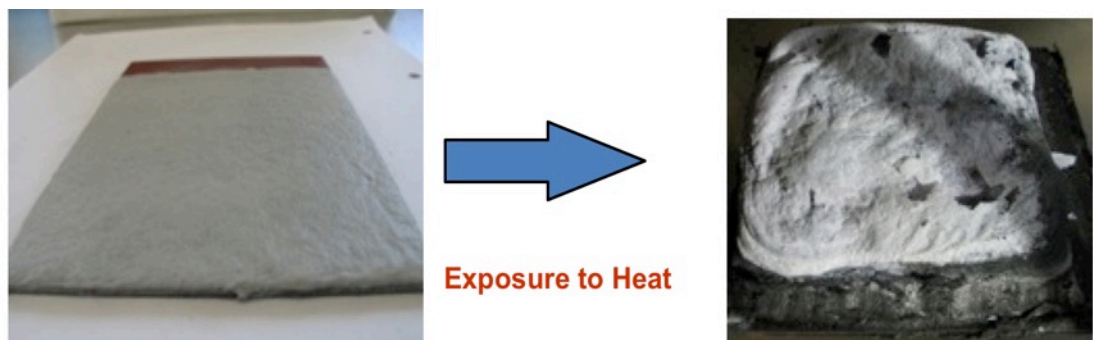
Exposure to Heat

Figure 2.1. Virgin coating changes to voluminous char upon exposure to heat.
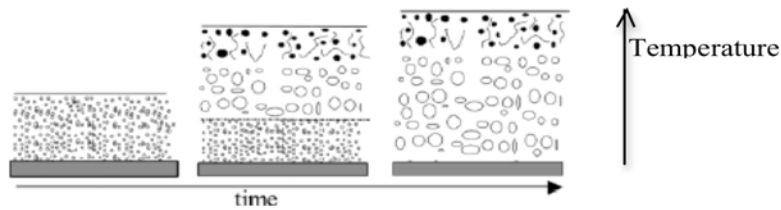
Figure2.2. Foaming process exhibiting growth and cellular internal structure in intumescence as temperature increases, Adapted from [8].

2.1.1 Intumescence- how it works?

The basic Intumescent system contains four ingredients [11, 12]:

1.   Inorganic acid e.g. Ammonium Polyphosphate (APP) that also acts as a catalyst

2.   Char forming 'Carbonific' Carbon-rich Polymer based compound e.g. Pentaerythritol (PER) [13].

3.   Gas evolving blowing agent 'spumific' organic amine or amide-Nitro based compounds e.g. melamine (MEL)

4.   Organic Binders – Epoxy or Acrylic resin.

Acid component initiates the reaction sequence. *Carbonific* is the main source of the carbonaceous char. *Spumific* or *blowing agent*, is responsible for the production of non-flammable gaseous bi-products like CO_2, NH_3 and H_2O [2]. The gases rise from under the surface of the char resulting in intumescence. A *mineral/inorganic acid* is added to control the process and act as a catalyst. *Binder* component ensures contact with the substrate surface. Commonly used binders also engage and help the process of intumescence [14].

The most commonly referenced components of intumescent paints are APP, melamine (MEL) and pentaerythritol (PER). Boubigot [13, 15, 16], Levchick *et al*. [12, 17-20] and other leading researchers have published studies on the mechanism of intumescence using the APP/PER/MEL combination. These systems have been extensively studied. Time to failure (TTF), defined as the time to reach a critical temperature of 400 ^{o}C, was found to be highest when a combination of these components were used [2, 3, 13, 18, 19, 21-28].

Vandersall [11], in his famous research paper, provided a piecewise mechanism of intumescence. He proposed that as the temperature was increased:

I. The dehydrating agent decomposed forming of a mineral acid around 215^0C.

II. The acid reacted with the hydroxyl (OH) part of the carbonising substance that resulted in the formation of an ester.

III. The ester then decomposed and the ample supply of Carbon surfaced as a dehydrated char.

IV. The secondary product of the ester decomposition released gaseous products like CO_2, NH_3 and H_2O (blowing agent).

V. The binder simultaneously softened and helped char adhere to the steel as it solidified at temperatures of around $360\ ^0$C.

The mechanism is still considered to be accurate. The complete review is still a very good starting point for any research.

The techniques in this research aim to highlight the steps discussed in the mechanism above. It envisages using a small lab scale setup and flat steel panels with various coatings under an impinging flame. As the coating will intumesce:

- Thermocouples attached to the substrate surface would monitor its temperature until a failure criterion is achieved, $400\ ^o$C.
- Thermal imaging will be used to monitor the stepwise intumescing mechanism.
  - These steps will be linked to the surface and substrate temperature
  - Physical characteristics of the surface would also be studied in detail.
- Schlieren flow visualisation technique would
  - Visualise the flame paint interaction
  - Identify changes in the interaction as the char expands
  - Measure rate of char growth
  - Observe the release of gaseous products

2.1.2 Experimental Methods and Techniques

2.1.2.1   Cone calorimeter

Cone calorimeter (CC) became the benchmark for studying organic compounds and their Heat Release Rate (HRR) properties. In 1990, this led to the publication of the first standardised test using this technique as ASTM E-1354-90 followed by ISO 5660-1 standardisation in 1993 [29]. A schematic of a typical CC setup is illustrated in figure 2.3. The three main components in the assembly are the cone heater, exhaust system and the load cell.
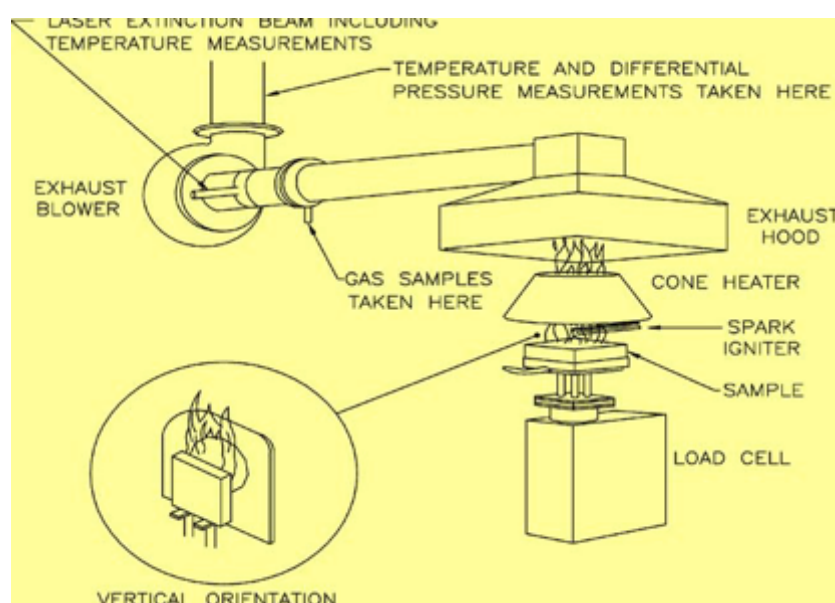
Figure2.3. Typical Cone calorimeter setup highlighting key components- Adapted from [30].

There are many advantages of using the CC setup to study intumescent coatings. Varying the heat flux from 0 to 100 kW/m^2 can simulate fire conditions under a uniform heat flux. It is relatively inexpensive lab scale equipment that offers the ability to observe the sample as it intumesces. The ease of instrumentation access allows additional equipment to be used in conjunction and offer a detailed quantitative analysis.

Various studies showed that CC equipment is best utilised to study synergistic effect of additives and binders[31-33] and the performance of new formulation compared to traditional APP/PER formulations [34, 35].

To summarise, cone calorimeter testing marked a significant milestone in bench scale testing methods for intumescent coatings. However, some academics propose that

simulated conditions require significant improvement before they can be relied upon to predict performance in real fire scenarios. Schartel [36] and Bisby [37] highlighted there are severe challenges with scaling of small scale tests to represent real fire performance. The range of fire scenarios is vast and equipment like CC only allows study of certain aspects of a typical fire. Furthermore, correlation of results with real fires has been difficult and unpredictable.

One of the main outcomes from this research is to compare sample test data using a cone calorimeter (standard fire tests) to impinging flame (non standard fire regime) and analyse various differences with respect to the process of intumescence.

2.1.2.2   Limiting Oxygen Index (LOI) and UL-94

Limiting Oxygen Index (LOI) is an ASTM test that is used to determine the flammability of a specimen. Similarly, UL-94 flammability rating is used in conjunction with LOI to a polymer's flammability. These test are certainly not conclusive but many researchers have used them [38]. Especially, when the mixing ratio of components is unknown. They can provide a reasonably quick analysis on which mixing proportions would be suitable for further investigation.

2.1.2.3   Furnace tests

Large-scale furnace have standardised testing procedures that can be used to predict performance under real fire conditions- particularly closed configuration fires. There are various heat transfer modes involved during the tests but convective heat transfer is the dominant mode of heat transfer. Furthermore, various standardised testing procedures have been drafted and implemented which include Underwriters Laboratories UL-1709 [39], ISO 834 , ASTM E-119 or BS-EN13381-8 [40].

Test standards comprise of square steel panels primed and coated with the specimen formulation. Jiminez [5] reported on details of the testing standard- it comprised of 300x300 mm or 150 x 150 mm square panels and a thickness of 3.5mm with 5 thermocouples attached at the back to measure average substrate temperature. In the furnace, they were secured using well-insulated frames in a vertical orientation. Typically up to four samples were examined in a test. The heating rate was set to 200^0C/min up until a temperature of 1200 ^{0}C was achieved in the furnace.

Most companies use fire resistive furnace tests before a commercial coating is brought into the market. The tests are very expensive to conduct and mandatory in order to achieve commercial certification. The tests only indicate whether a sample can withstand simulated fire condition that is representative of real fire conditions. If a formulation fails during the test, it is very difficult to establish the under lying cause of failure. This is a key limitation of furnace tests.

Quantitative information obtained from the test includes the thermocouple temperature-time curve. The time taken to achieve the failure temperature indicates the performance of the sample. The sample can only be viewed through a very small quartz optical window during the test. If a sample fails, the cause of failure can only analysed at the end of a test. Samples would usually fail due to cracking or peeling of char during intumescence. It is not possible for all formulations to be tested through furnace tests unless you commit huge financial resource because the biggest disadvantage is that these tests are extremely expensive to run.

Some new techniques are already being developed. The Fire research group in University of Edinburgh has developed a Heat-transfer rate inducing system (H-TRIS) [37]. It can simulate standardised furnace heating rates and allows instrumentation access which is advantageous. However, it uses electric heaters to generate heat transfer via radiation as the main mode of heat transfer. This can be expensive and still not fully represents a real fire.

Unlike furnace tests, impinging flame systems are easily scalable. Ramp rates similar to furnace tests can be replicated at lab scale. The greatest advantage will be the ability to monitor the process of intumescence. In doing so, one can gain more insight failure.

2.1.2.4   Other techniques

Thermogravimetric Analysis (TGA) has been widely used to study intumescent formulation and components. This technique monitors the mass loss/gain of a sample with respect to temperature. TGA is a powerful quantitative tool. If reaction sequence is known, TGA allows the key stages of chemical activity and their associated temperature to be studied.

FTIR spectroscopy is a broad-spectrum quantitative tool that allows the investigator to identify unknown materials in a sample. It is a powerful diagnostic technique in order to understand intumescence. The technique has its merit and has helped significantly to understand the process of intumescence. It is still used to develop new formulations and study the effects of new components.

Other techniques such as Nuclear Magnetic Resonance (NMR) [41], X-ray Diffraction [22], Differential Scanning Calorimetric (DSC) [42] and Scanning Electron Microscopy (SEM) [35] are also used to study intumescent formulations. Aspects such as improving formulations in terms of mechanical strength, heat release rate, thermal degradation, nature and quality of char products have well studied. All these experimental technique assume a constant heating rate to degrade samples where applicable. The use of more realistic fire conditions is still an area that needs further investigation.

2.2   Combustion, Fire and Impinging Flames

The ability to generate and control fire or harness its energy is one of the most significant steps towards civilisation. Combustion and its associated application has become the centre of study in various field including safety and fire protection. This section would introduce fires and various types of flames classifications, heat transfer mechanism and the properties of jet or impinging flame setups. Their use in relevant literature is also discussed.

2.2.1 Fires

Fire is as an uncontrolled combustion reaction distinguished into various categories based on its physical state. They are typically diffusion flame based in which the rate of burning is regulated by the diffusion of chemical species. The mechanism of movement is shown in the figure 2.4. Buoyancy and air entrainment are key factors that contribute towards rate of heat release and propagation of fire.

The movement of air into the flammable mix is defined as air entrainment. Air entrainment is dependent on buoyancy forces. Hot gases around the flame rise up due to buoyancy forces and are replaced by denser cold air currents that are entrained to sustain combustion [43]. The entrainment phenomenon is also responsible for the flame geometry. The balance of momentum exchange between the mixing fuel and oxidiser

species limits the boundaries of flame region. The stability of a diffusion flame system is highly dependent on the air entrainment [43]. Laminar flames, at Reynolds number of less than 2000, can suffer from flickering instability due to the presence of dominant shear forces [44]. Furthermore, fire chemistry and fire dynamics can vary significantly based on the conditions such as closed or open room configuration, ceiling height, ventilation and availability/design/type of combustible solid fuel. This makes the task of modelling any fire scenario extremely difficult.
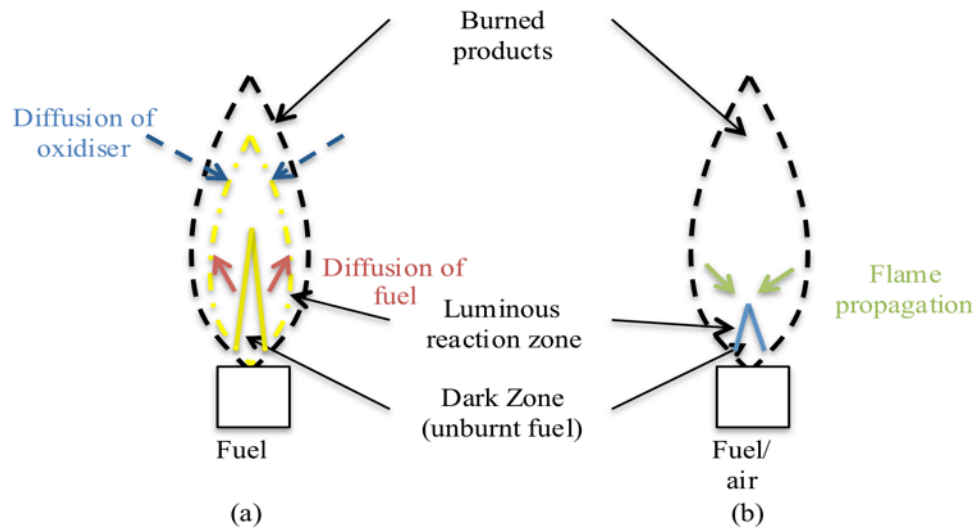
Figure2.4. (a) Reaction zone, movement of fuel and oxidiser species as they behave in a diffusion flame system and (b) premixed flame system, its reaction zone and contour of burnt products making up the flame boundary (right) - adapted from [45].

Two main types of fires are discussed, *Buoyancy* driven fire plumes and momentum driven *jet* fires. In Buoyancy driven fires the gaseous hot products above the visible laminar diffusion flame would rise above the buoyant plume. The convective plume would increase air entrainment until the mixture of combustion products and air would rise and start to impinge on the ceiling. The rate of air entrainment, flame height and the rising buoyant plume would be important factors towards fire growth [46].

In momentum driven jet fires, a high-pressure fuel pipe will combust and, in the presence of surrounding air as the oxidiser, generate highly turbulent flows. The enhanced air entrainment and turbulent mixing accompanying the increased jet velocity; promote in turn, increased combustion efficiency and reactant consumption [46].

Drysdale has cited research as far back as the early 1930's on attempts to model the behaviour of fire [44]. Although both types are well studied, a realistic fire scenario

13

would lie somewhere in between these two extremes driven by a list of factors. These include:

- Rate of burning
- Rate of spread of fire
- Air entrainment and effect of ventilation/wind
- Flame bed diameter

These are a few key factors that have been used to build fire models. Ultimately the task of determining a unanimous fire model is difficult because there are too many variables involved in a fire scenario. One can remove all external factors and focus on constructing a basic model highlighting two salient features [44].

1. An infinitesimally small point ignition source

2. A rising axisymmetric plume to a height where buoyancy forces become too weak to overcome viscous drag of surrounding air and hence limit entrainment.

Such a model is represented in figure 2.5, originally proposed by Heskestad [47]. A variation to the model utilises a real circular fuel bed with a diameter D extrapolated to a virtual origin. The flow is also modelled to impinge on a ceiling to add the effect from compartmental boundaries [44].
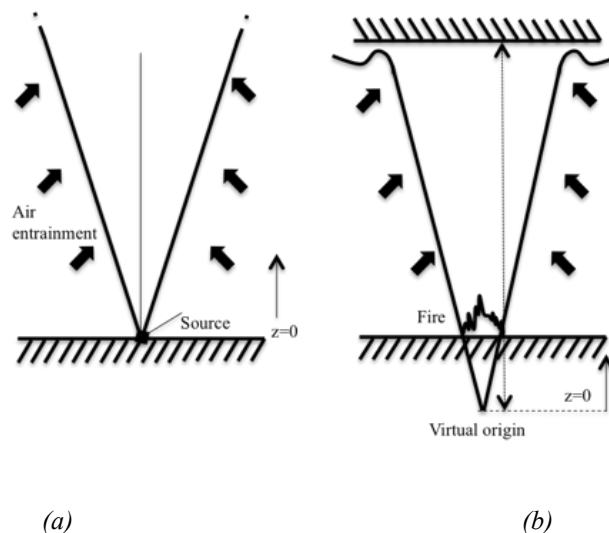
Figure 2.5. (a) Heskestad proposed model of an axi-symmetric conical fire (b) improved model based on real fire source and impinging ceiling (right)- adapted from [47].

McCaffery identified that a fire plume can be made of three distinct regimes tabulated below and illustrated in figure 2.6 [48]:

I. The region near the burner surface consists of a continuous flame and an accelerating flow of burning products.

II. Region in which there is intermittent flaming and a near-constant flow velocity

III. A flickering buoyant plume with decreasing velocity and temperature
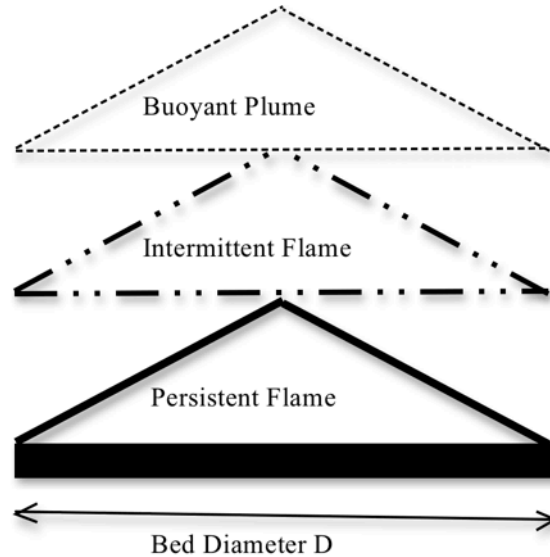
Figure 2.6. Mccaffery's illustration of the regions in a typical fire plume-adapted from [48].

The advantage of the model in figure 2.5 is that it uses common characteristics from both buoyant and jet fires such as buoyancy driven mixing in zone III and diffusion of species in zone II and I. It is a diffusion based flame system and air entrainment is a key-driving factor. The flow impinges on a ceiling that is a) representative of a room fire-the most common occurring fire hazard and b) addresses the main aim of this research that is **to study interaction between fire and intumescent paint coatings on flat and 3-D surfaces.**

There is relatively little literature on experimental studies using impinging flame setup to study buoyant diffusion flames at low Re number. Weng And Hasemi [49] used a low Re number, impinging flame experimental setup to study the radial heat flux distribution, flame height, convective and radiative heat transfer effects on a non confined ceiling, at a variable height, H, using various burner diameters, D. A schematic of their setup is illustrated in the figure 2.7. They used burners of diameter 0.3m, 0.5m and 1.0m with maximum ceiling height of 1.8m. A relevant model based on a virtual ignition source and an axisymmetric distribution was also created for comparison. The experimental results were compared to modelling results and were found to be in good agreement.
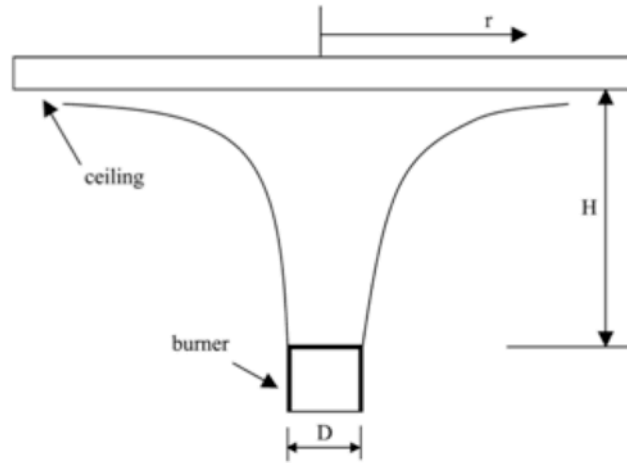
Figure 2.7. Weng and Hasemi's experimental setup schematic with burner of diameter, D at a distance H from the ceiling- adapted from [49].

Heat transfer mechanisms play a vital role in understanding the behaviour of fire. A variety of experimental and modelling works have been conducted to understand the role of heat transfer mechanisms in a range of fire scenarios. Diffusion buoyant flames are sooty, therefore the impact of radiation can be significant. A generic understanding is that, in propane based flames, the effect of radiative heat transfer can be up to 50 % of the total heat transfer [44].

Heat transfer form radiation and convection had a very high impact on ceiling temperature during the initial stages of a fire because of the temperature difference between ambient conditions and the flame [49]. A reduction was observed in their impact as the separation distance was increased. The impact also decreased as temperature differences reduce with time until a stable value was achieved. In buoyant plumes, generated using burners with variable diameters, the effect of convective heat transfer was higher at small nozzle diameters [49, 50].

Various other studies have investigated similar phenomenon [47, 51-53]. Gross [52] focused on variation in burner nozzle to ceiling distance and the power output at the burner. He found good agreement between the experimental results and available empirical and modelling data.

Drysdale [44] identified up to 9 various dimensionless parameters including Reynolds number to study fire behaviour. He suggested that creating a model where all parameters could be scaled is impossible and hence focus should be on choosing some relevant parameters. Ma [54] encountered similar problems in his modelling study and concluded

16

that scaling laws are still a subject of investigation. Some agreement has been achieved however the results can vary significantly based on the fire regime.

Therefore, fire modelling and experimentation is very sensitive to the scale of the setup. The dynamics, mechanics and various other characteristics like flame height and air entrainment factor can differ. However dimensionless parameters such as nozzle to plate distance and thermal loading/power at the burner nozzle exit can be modelled at a smaller scale. Experimental studies surrounding impinging flames have found great success in investigating turbulent jet fire scenarios. There is evidence of using the same technique to study buoyant diffusion fire plumes as well. For the purpose of this study, where the impinging flame setup is being used as a heating source, variation in nozzle to plate distance allows the study of heating rates in all zones that can be found in a fire. Fuel flow rate variation can help create various power/thermal loadings and laminar to turbulent flame regimes that can represent fire scenarios from buoyant leading to momentum jets.

Consequently, to target the research aims of generating a fire model and impinge it on paint coated surface. We have used impinging flames which have similar characteristics to the model described earlier in figure 2.5. **At a lab scale, the flow rate of the fuel will be varied to generate conditions of laminar and turbulent flame patterns exhibiting both buoyancy and jet flame properties. The height of the sample would be adjusted to study the effect of all three zones and their associated heating rates. Finally, the flow near the paint surface (ceiling) and its associated heat flux characteristics can also be analysed.**

2.2.1.1 Jet Fire tests of intumescent coatings and the need for non-standard fire condition based testing

ASTM and ISO certification standards are constantly scrutinised to regulate coating performance and demand higher protection times. Protection times deemed satisfactory for commercial application have risen from 60 minutes up to 240 minutes. Also, It doesn't help when various stakeholder come into play with difference in opinion on performance characteristics. Formulators might focus on aspects such as performance, nature of additives and type of protection etc. whereas; architects will consider aesthetic appeal and thickness. Environmental aspects such as release of volatile organic

compounds (VOC) can be an issue. Insurance companies and safety compliance bodies can also have their own agenda. The cost of construction can have major effects as well since coatings require special application which adds into construction time [55]. All these factors have made the development of formulation a difficult prospect.

ISO testing standard is the ISO 22899-1, determination of the resistance to jet fires of passive fire protection materials [4] is an important testing standard. The test is designed to simulate fire conditions when hydrocarbon fuels can leak at high pressures to produce jet flames that can reach up to 150 m/s [56]. Such conditions are significantly probable in locations like offshore oilrigs or refineries. OTI-95634 standard jet fire test illustrated in the figure 2.8 is an example of a typical jet fire test and very similar to the ISO 22899-1 specification. The temperature time curve is very steep reaching up to 1000^0 C in approximately 4 minutes.
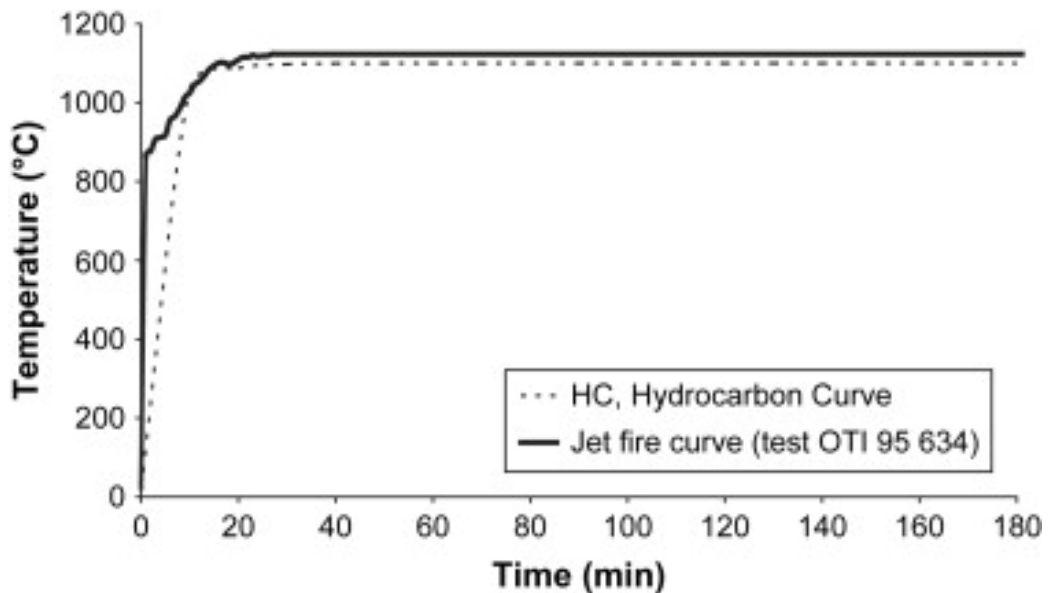
Figure2.8. Hydrocarbon and jet fire test heating curves as used in certification tests [56].

A brief overview of the test specifications is summarised here. The test setup comprises of four items. A schematic of the setup in figure 2.9 highlights the salient features and a table of dimensions is illustrated in table 2.1:

1. Jet nozzle position   2.Flame recirculation chamber   3.Protective chamber
4.Panel
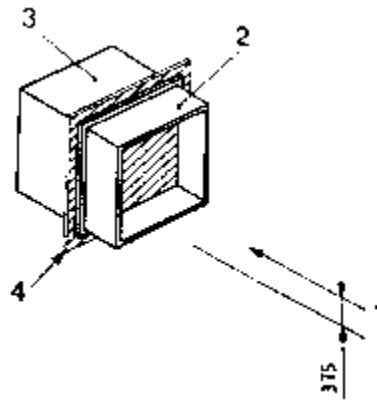
Figure2.9. Internal configuration schematic of a typical test element in ISO 22899-1, adapted from [4].

Table2.1. Dimensions of salient components in ISO-22899 test setup

Component	Length [mm]	Outer diameter [mm]	Inner diameter [mm]
1. Nozzle	200	52	17.8
		Width [mm]	Height [mm]
2. Recirculation chamber	1500	1500	500
3. Protective chamber	1500	1500	1000
4. Painted panel	1620	1620	10

A few variations can also be tested in addition to the standard flat panel configuration. An important variation relevant to this work is the structural steel work test specimen. This configuration allows simulation of complex char movement as expected in real structural components e.g. an I-beam. A typical I-beam and the corresponding test schematic are shown in figure 2.10. A central web 20mm thick and 250mm deep is slotted and welded protruding normal to the surface of the painted surface in the recirculation chamber. The cross-section of the setup would look like a T-panel. They have been used in this research to study complex multi dimensional char movement, as expected in jet fire tests.
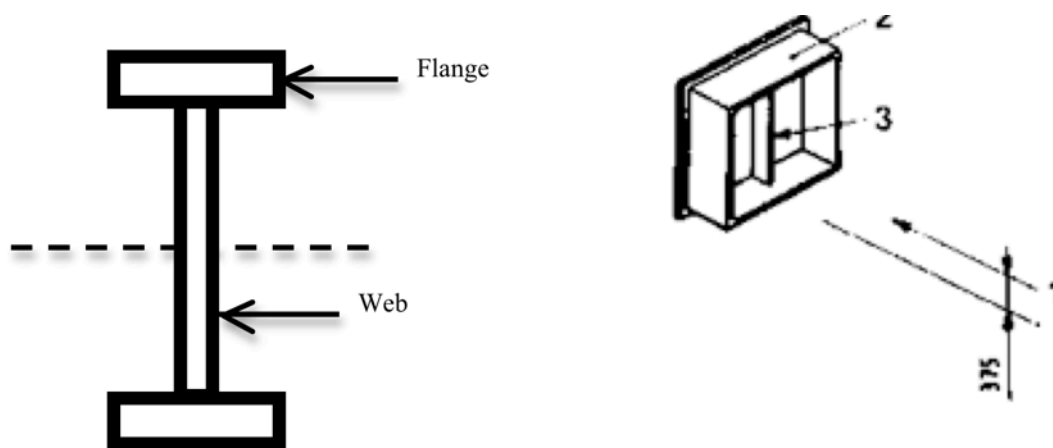
Figure2.10. (Left) Typical I-beam cross-section, component used in construction industry; (Right) ISO test schematic with web (part 3 highlighted) simulating performance of I-beam system[4]

The nozzle is positioned at a distance of 1000mm and normal to the face of the protected surface. The centre of the nozzle is 375mm above the inner surface face of the base panel, illustrated in figure 2.10. The fuel used would be propane vapour with a mass flow rate of 0.3kg/s continually monitored every 30s. Temperature measurements would be recorded through thermocouples drilled and positioned form the back face of the panel. The number and positioning of thermocouples would be different depending on the test case.

At the end of the test result, the sample is expected to withstand the endurance time specified by the formulator. The resulting char is inspected at the end of the test. The heat flux from the jet fire is non-uniform. Therefore, the thermocouples will have significant variation however; the maximum temperature achieved at each location during the test is recorded. It is used as a performance indicator for maximum protection time. A sudden or sharp increase in the rate of temperature change at any location is also recorded which implies possible failure in the coating at or near that location has occurred. The most significant failure criterion is the exposure of substrate under the test conditions. If that happens then the test samples fails however various other criterion are recorded and subjected to analysis before a conclusive rating is given.

An interesting paragraph in the document is quoted. The document states that ' ... *the method specified has been designed to simulate some of the condition that occur in a jet fire, it cannot reproduce them all exactly. The results of this test do not guarantee safety but may be used as elements of a fire risk assessment for structures or plants.*'

'... the criterion of performance, provided by the test, is the minimum time required to reach the critical temperature associated with the fire scenario to be protected against...' [4].

It can be interpreted that the test is still a simulation of real fire conditions. The results do not guarantee safety of usage in real fire conditions and only criterion considered is time to failure (TTF). It is well documented that scaling up fires is a difficulty faced in many fields of research. These tests are extremely expensive to run even for formulations that have been tested rigorously. If jet fire tests are inherently simulating fire conditions at a relatively large scale, it just makes logical sense to conceive lab scale test methods to test formulations in conditions similar to the jet fire test at a smaller scale.

This is the primary reason why impinging flame configurations have been considered and used as part of this research.

- They exhibit many properties similar to those of jet fire tests.

- The cost of running such a setup is insignificant compared to just one jet fire test with additional benefit of instrumentation access.

- The luminosity from a propane flame used in jet fire test makes it impossible for any diagnostic equipment to be used to monitor the performance of the sample. This is extremely beneficial for lab scale setups where various diagnostic tools can provide insight into the process of intumescent under jet fire conditions.

2.2.2 Impinging Flames

Impinging flame offers a highly effective heat transfer rate as the flame is forced to change its direction when it comes in contact with a surface. Research has focused to study the temperature and heat flux behaviour of the flow in the stagnation and wall jet region. Figure 2.11 illustrates different regions that are found in a typical impinging flame arrangement.
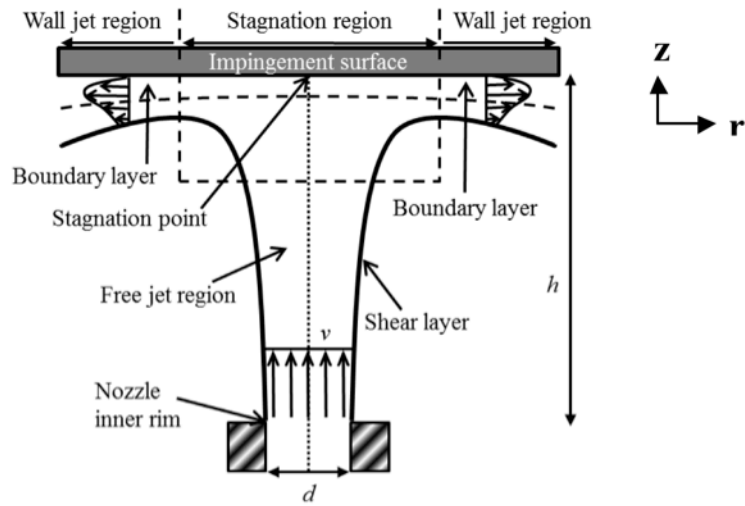
Figure2.11. Illustration of the free jet region, stagnation region and wall jet region in a typical impinging jet-Adapted from [57].

Prior to impingement is the *free jet region.* The axis through the centre of the nozzle meets the target at its centre- this is the location of the *stagnation point* where the velocity of the flow is equal to zero. The jet experiences a change in direction radially parallel to the direction of target plate from the *stagnation region* into the wall *jet region* [57].

Similar to the three distinct zones defined in an arbitrary fire (figure 2.6), figure 2.12 illustrates the developing stages of a free non-reacting jet. Three distinct zones are *potential core* zone, *developing* zone and fully developed *zone.*
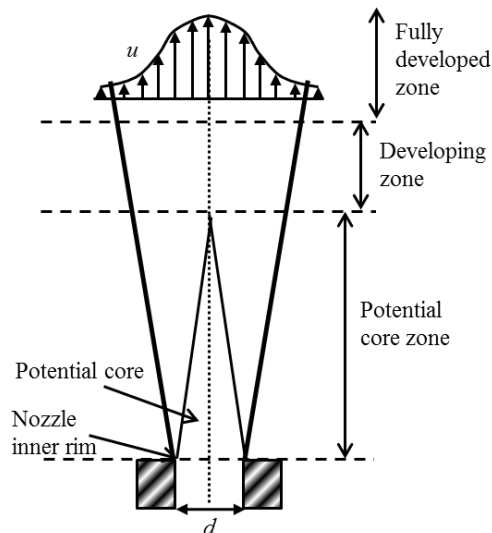
Figure2.12. Illustration of the potential core zone, developing zone and fully developed zone in the flow regimes of a free non-reacting jet- Adapted from [57].

Viskanta[57] summarised the structure of the impinging jet. In the potential core zone the flow velocity is equal to nozzle exit velocity of the fuel/oxidiser mixture. Downstream in

the developing zone, the velocity profile decays as a result of air entrainment caused by large shear stresses due to turbulence at the jet boundary. The combustion efficiency increases in this zone and the temperature of the jet is higher than the potential core [58]. Further downstream the developing zone becomes a fully developed zone, where a broadening of jet and decay in axial velocity was observed to be linear. The temperature, pressure and velocity distribution is different in all three zones.

Temperature profiles on the target plate have been the focus of study and it has been reported that the maximum thermal efficiency is achieved between the developing and fully developed zone [59]. The velocity profile is reported to be fully developed after the flame has travelled a certain distance 'H' away from the nozzle depending on the fuel exit velocity, U, Reynolds number, Re, and nozzle diameter, D.

Many researchers have studied impinging flame jets in an experimental and modelling context. Baukal, Gebhart [60-64], Chander and Ray[65] provided a review of a significant number of research papers available. This has helped combine relevant experimental and numerical work between 1949-2005 conducted by other researchers using different methodologies but reporting on similar parameters. The idea behind the consensus was to provide insight into what had been done so far and what areas should be explored for future research.

Table 2.2 summarises all the parameters that were varied:

Table2.2. Different tests conducted in flame impingement research [65].

Configurations- with respect to nozzle axis	Normal to a cylinder
	Normal to a flat pate
	Parallel to a plane surface
	Parallel to a hemi-spherical nosed cylinder
Fuels	Fuel/Air mixtures (Methane, Propane and Butane)
	Fuel/Oxidiser mixture
	Fuel/Oxygen mixtures
Equivalence ratio	Diffusion flame system
	Premixed system with $\Phi < 1$
	Premixed system with $\Phi = 1$

	Premixed system with $\Phi > 1$
Firing Rates	Variable [majority ranging between 5-25 kW]
Reynolds number	0-2300 Laminar
	2300-above Turbulent [mostly turbulent studies]
Burner geometries	Single, isothermal, coflow and multiple jets
Nozzle diameter	0-100mm
Nozzle to Plate distance	Variable 3<H/D<75
Target	Material- metals and ceramics
	Size-300mm nominal diameter
	Surface preparation- Rough, smooth, Polished
	Surface temperatures
Entrainment effect of outside cold air	Effects of air entrainment

Chander and Ray [9, 58], van der Meer [66] and Fairweather *et al.[67]* reported heat transfer measurements for stagnation point using methane/air flames for low Reynolds number laminar and turbulent jet flames. They provided valuable insight into the temperature variation along the central axis measured axially (x) at different radial positions (z) using thermocouples for temperature and probe sensors for heat flux measurement.

They also analysed the occurrence of high heat flux near the tip of the inner premixed zone as shown in Fig. 2.13 [9, 58] between 2007 and 2011 respectively and suggested that heat transfer characteristics were significantly dependent on whether the inner reaction zone was impinging on the target. Hou and Ko [59] shared similar findings stating that the thermal efficiency of the flame changed with flame height. The highest efficiency was reported to occur near the tip of the inner reaction zone
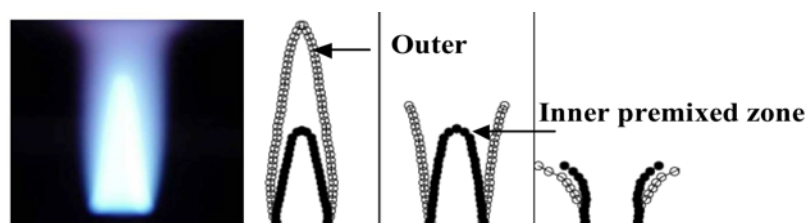
Figure2.13 Characterising different flame zones as found in a typical premix flame system – adapted from [59]

Chander and Ray [9, 58] summarised the effect of various other experimental conditions. Some relevant conditions are summarised here. It was observed that maximum heat

transfer rate decreased and the maximum heat flux position moved further away axially from the stagnation point in fuel rich mixtures, figure 2.14. This was due to excess fuel in the air/fuel mixture and lack of oxidiser (air) to support complete combustion resulting in cold fuel impinging on the target surface. The cold fuel reduced the temperature at the stagnation point. Furthermore, as the flow moved radially along the target plate, the reduced momentum allowed air entrainment and combustion of the unburnt fuel resulting in a higher temperature away from the centre of the target.
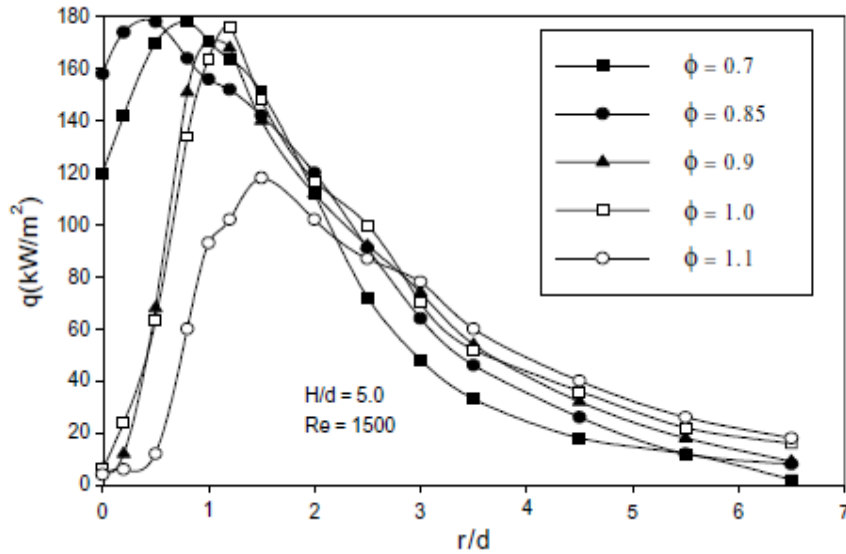
Figure2.14 Heat flux distribution at different E.R, Φ for an premixed flame setup impinging on a flat plate target – adapted from [65].

It was observed that the maximum heat transfer rate increased with Re number, figure 2.15. The heat flux position moved further away axially and a cool central core appeared as unreacted fuel impinged on the target surface, similar to equivalence ratio studies. It became larger in size as Re was increased.
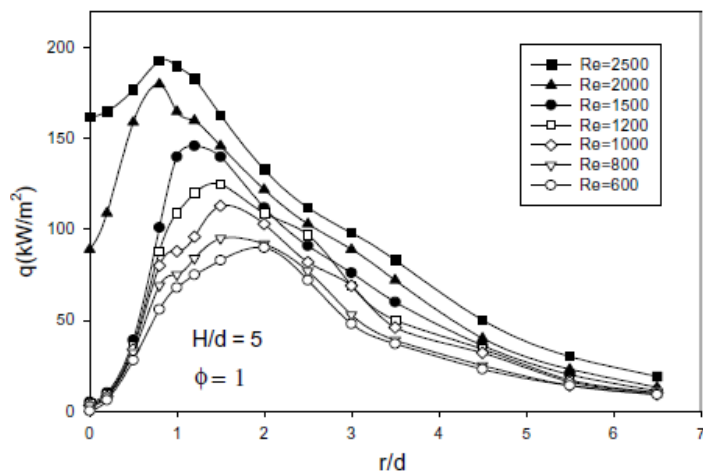
Figure 2.15. Heat flux distribution at different Re measured axially for a premixed flame impinging on a flat steel target.[65]

Chander and Ray[65] also reviewed the effect of NTP distance on heat transfer and stagnation point heat flux values. They reported that at larger seperations, air entrainment into the flame increased. This resulted in reduced flame temperature and heat transfer rates. The stability of diffusion flames decreased due to buoyancy effects. The bell shape also became flatter and uniform as H/D was increased as shown in figure 2.16 below. Dong [68] investigated the same phenomenon using premixed impinging jets. He summarised that at the stagnation point:

1. The cool central core appeared on unreacted fuel at very small separation distances and was the smallest value of heat flux over the complete radial profile.

2. This value becomes the maximum heat flux value over the complete radial profile as separation was increased and unreacted reactions species concentration was reduced to almost negligible. At such separations, the tip of the inner premixed zone was in contact with the plate, which was the hottest part of the flame.

3. As the separation was increased future, the maximum heat flux remained at the stagnation point however, the profile along the distribution was flatter with smaller variations in the radial direction.
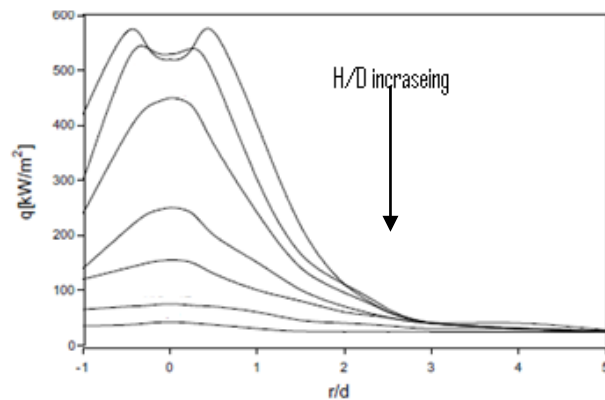
Figure2.16. Effect of H/D on heat flux measured axially on a flat steel plate target using an impinging flame geometry-adapted from [65]

This literature survey has been intended to offer a convincing assessment that an impinging flame setup is an effective lab scale system that can be used to conduct fire research. Relevant excerpts from a vast array of detailed research highlighting the use of this system and its associated characteristics have been presented in an effort to enlighten the reader. Furthermore, in this research, the intention is to use this review as a foundation to establish a sound methodology for experimental work.

Nozzle to Plate distance variation has been chosen as a key part of this study because it offers a significant number of experimental conditions. It is a versatile and easy to implement method to study the variation in overall heating rate and heat flux profiles on the surface as illustrated in figure 2.16. Similar to variation of ceiling height mentioned in section 2.2.1, NTP changes will allow us to study the impact on intumescence as the distance between the ignition source and protected surface is varied. The interaction of a protected surface as it interacts with the three distinct zones in a fire structure can also be examined through variation in NTP distance.

A variation in Reynolds number to generate laminar and turbulent flame structures can suffer from problem of stability. A range of buoyant fire plumes to momentum jet fires can be regenerated by increasing Reynolds number through fuel flow rate conditions. There is also the added advantage of analysing the effect of increased thermal loading on the protected surface. This work would explore variations in fuel flow rate at a constant distance between target surface and burner nozzle to study the effect on intumescence.

Endurance time or Time to Failure (TTF) of a formulation is a key performance indicator. Therefore, variation of coating thickness would also be discussed and presented in more detail in the latter half of this thesis. The next part of this review would present the experimental diagnostic tools that have been used as part of this work.

2.2.3 Thermal Conductivity and its role in heat transfer calculations

Heat transfer mechanisms play an important role in heat transfer calculations and therefore the thermal performance of fire protective coatings [69] The heat transfer mechanisms are divided into two categories namely macroscopic and microscopic. Considering the coated panel and the flame as a single control volume, the heat transfer mechanisms is a result of the interaction between the flame and the intumescent coating which are defined as macroscopic mechanisms (figure 2.17).

Anderson Jr. and Buckmaster [70-72] have developed and reported various numerical models to describing various physical process involved during intumesce. They applied conservation of mass, energy and momentum equations, relevant boundary conditions and the contribution of conduction, convection and radiation to generate models which offered good agreement with experimental results. The relevant equation of conduction,

convection and radiation were applied using temperatures of the flame, char surface and the substrate. They considered a zonal model dividing the process into three distinct phases. These were called pre-heating phase, expansion phase and char phase.
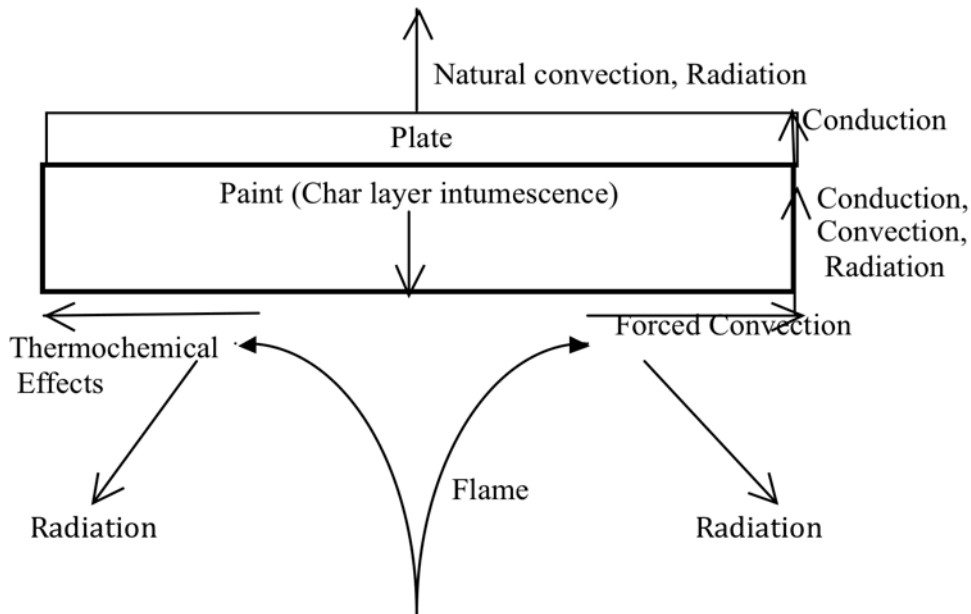
Figure 2.17.Illustartion of all the macroscopic heat transfer mechanisms involved in an intumescent system exposed to a heating source.

As the heat from the source moves through the intumescing char towards the substrate, complex microscopic heat transfer mechanism interact under the surface of the char. This is due to its porous and carbonaceous nature. Staggs [10] and Kantorovich [69]summarised that the thermal conductivity of porous chars was dependent upon the internal structure of char. This included the porosity of the char, char height and pore/particle distribution. It was also dependent on particle content and the temperature. Porosity was defined as the ratio of the cumulative volume of voids to the total volume of the char.

Of the three major modes of heat transfer, the effect of convection on the thermal conductivity calculation was considered negligible for pores with diameter less than 1cm. Therefore, conduction and radiation dominate. This is because a majority of porosity is microscopic in nature. Staggs [10] reported that char structures had a physical porosity, defined as pores visible by naked eyes, typically in the range of 30 to 40%. However, analysis under scanning electronic microscopy (SEM) and other microscopic techniques, he found chars, with expansion ratios up to 20, had an overall porosity of 80-95%. Based on this observation, it is relatively safe to assume that most pores are considerably smaller than 1cm.

28

The mechanisms of conduction and radiation were found to be co-dependent. Conduction is one of the key parameter in calculating the thermal performance of an intumescing system. A combined effect known as radiation enhanced conduction mechanism has also been reported, this is defined as the additional heat flux due to radiated heat across pores into the solid char walls [10] and expressed using the equation 2.1:

$$Q_r = 4\sigma\varepsilon_p\, n^2 T^3 R \qquad\qquad (2.1)$$

Where σ is the Stefan-Boltzmann constant, ε_p is the emissivity of the pore usually assumed equal to 1, n is the refractive index of the gas, assumed to be air (temperature dependent), T is the temperature and R is the pore radius. Therefore, the effect of radiation-enhanced conduction cannot be neglected especially at high temperatures. The detailed mechanism of heat transfer is still a subject of further research and study. Staggs made the following observations in his experiments [10]. He reported that the thermal conductivity decreased as the porosity in the char increased. Based on equation 2.1 and the effect of radiation-enhanced conduction, thermal conductivity increased as the pore size increased. Even though in his experiments showed the importance of porosity based thermal conductivity calculations, the sample with the highest char height exhibited the lowest overall thermal conductivity.

The unpredictable and complex nature of fires already presents a problem. Complex heat transfer mechanism occurs under the char surfaces are still not fully understood. Hence, adding further difficulty towards understanding the behaviour of fire protective coatings in real fire conditions.

2.3 Experimental Diagnostic Techniques

2.3.1 Introduction

Experimental diagnostic techniques used in this research have been discussed. Schlieren imaging, a technique commonly used in studies of combustion, was used for the first time to study intumescence. Thermocouples are frequently used in intumescent studies. They were combined with thermal imaging to understand the process of intumescence as it happened.

2.3.2   Thermocouples

Thermocouples have been used since early 19th century and their principal application is to measure temperature. Hence they have found significant application in the field of thermodynamics and temperature measurement [73]. The principle behind the temperature measuring capability of a thermocouple is that, if there is a temperature difference, an electric current is generated at the junction of two conducting materials. The most commonly used thermocouple is Type-K thermocouple.

2.3.2.1   Use and limitations

Thermocouples have found their use in many temperature related study. Their advantages include price, ease of use, compatibility, reliability and large temperature measuring range [74]. A thermocouple junction is attached to the surface for which temperature measurement is required. It is also attached to a data logging that can log and display live temperature variations. In this research thermocouples were used extensively. The thermocouple was used in order to measure the temperature characteristics of the substrate until the failure temperature of 400 ^{0}C was achieved.

They are easy to use and convenient to measure surface temperatures. However, they have their limitations.

- They are an intrusive and have to be in direct contact with the surface of measurement.
- They can affect certain characteristics e.g. the dynamics of an impinging flame on a surface or influence the intumescing of a paint sample during tests.
- They degrade upon repeatable usage that can lead to uncertainties in the measurements.
- The voltage registered by thermocouples is small meaning specialist measuring equipment is required.

Other techniques such as Thermographic phosphors and [75]reference-beam interferometry [76] offer non-contact measurement overcoming limitations encountered by thermocouples. However, thermocouples are much cheaper and easier to implement and still remain the best-applied technique to experimental purposes.

2.3.3 Digital Imaging

Digital imaging has many advantages. It gives the ability to edit and observe tiny details in high-resolution images. The advances in the field of electronics that has resulted in smaller and more powerful components like the coupled device chips (CCD) (and more recently CMOS chops) combined with modern manufacturing techniques to produce high-grade lenses has led to the production of digital cameras with high responsiveness, acute light sensitivity, shutter and aperture speed control among various other features. This has resulted in digital cameras and their use in a vast variety of fields.

2.3.4 Schlieren/Shadowgraph technique

The Schlieren (Germen word meaning streaks) is a flow visualisation technique that has found its application in many modern day fields such as combustion [77-79] and high-speed aerodynamics[80, 81]. Schlieren relies on the bending of light due to natural phenomena of refraction.

Robert Hooke originally laid down the principles and foundation of visualising flows in the 17th century. In his experiments, as illustrated in figure 2.18, the light source illuminated a relatively large area. A disturbance, the likes of a lit candle, was present in the test area that will cause a straight beam of light to refract at an angle θ from its original path A to an alternative path ending at point B at a distance δz, away from point A. This would result in a dark point at point A and a brighter point at point B. If there was no disturbance, there would be a uniform distribution on the screen.
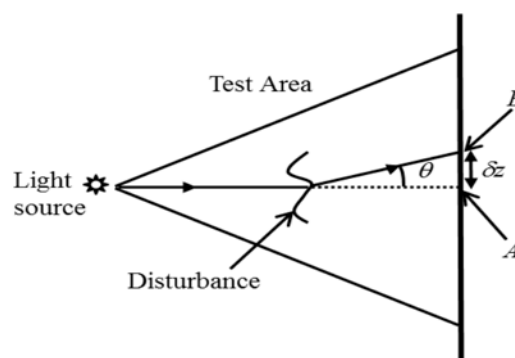
Figure2.18. Illustration of the shadowgraph method highlighting the bending of light away from its original path-adapted from [82].

He continued his work and developed the first lens-based setup illustrating the principles of the Schlieren technique as illustrated in the figure 2.19.
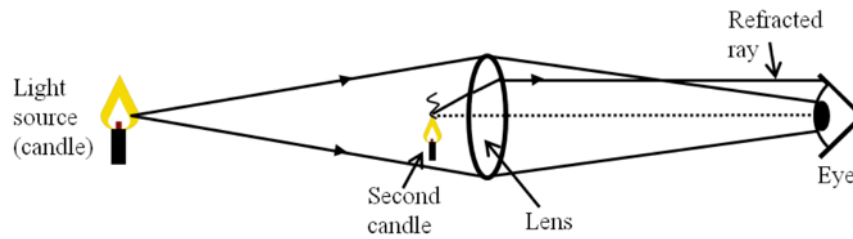
Figure2.19. Robert Hookes' original Schlieren setup-adapted observing hot gas plume over a candle from [82].

The setup comprised of a first candle placed at a relatively large distance away from the lens to act as a light source and illuminated the entire lens diameter to the observer at the opposite side of the lens. A second candle flame was then positioned close to the lens. The light beams from the first candle were refracted at angles large enough that they fell outside the pupil. Consequently, these refracted light beams could not be observed by the user thus, revealing the invisible convective plume to the observer[82].

2.3.4.1 The z-type mirror system

The z-type uses parabolic mirrors. They have an advantage of using less space, offer large field of view and ease of maintenance over other configurations. A typical schematic of such a setup is illustrated in figure 2.20. In a z-type Schlieren setup, the first parabolic mirror is aligned so that the light beams from the light source are converted into straight parallel beams. Any density fluctuations within the test section bend the direction of the light. The knife-edge is positioned on the focal point of the second parabolic mirror. It acts as an aperture controlling the light that is focused through the lens onto the screen or camera. Typically, half of the light is blocked using the aperture in a Schlieren setup making it much more sensitive to density variations in the test section [83].
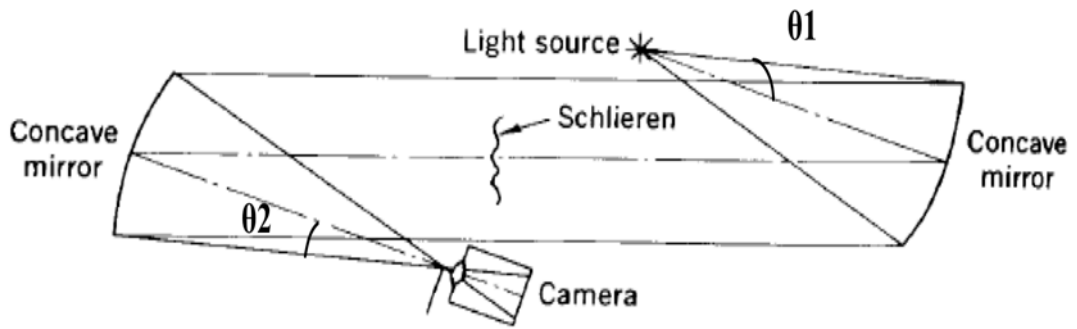
Figure2.20. the mostly commonly employed Z-type Schlieren setup- adapted from [82]

The problem of astigmatism cannot be eliminated from a z-type system but can be controlled significantly by ensuring mirrors are aligned properly.[82] Coma occurs due to the tilting of the parabolic mirror off its optical axis. This results in a point light source being smeared and focused as set of point appearing in the form of a line and is highly dependent on the angle between the light source and the optical centre of the mirror. The problem can easily be rectified if both mirrors in the z-type setup are aligned at equal and opposite angles $\theta1 = \theta2$.

2.3.4.2   Uses and Limitations

The effectiveness of the Schlieren technique is enhanced when it is coupled with high-speed imaging. High-speed cameras can capture information at extremely high frame rates. Therefore, allowing high temporal resolution and observation of physical phenomenon in slow motion to observe instantaneous events. This feature offers great benefits in studies of impinging flame where tiny detail of instantaneous events, which may not be visible to the naked eye, near or far field can be recorded and observed.

Staggs [84] conducted detailed experiments on intumescent paint formulations under various heating regimes and found that, for the same initial thickness, the amount of intumescence can vary. Therefore, the heating regime has a significant impact on the process of intumescence. In this research, the impact of heating regime is analysed using the Schlieren method. It is adopted to analyse the complex interaction between the flame front and the intumescing paint boundary. The changes in the overall flame structure will also be observed with respect to growing char boundary.

Characteristics, which are usually blocked by the luminous nature of diffusion flames, will be clearly visible and offer new insight into the dynamics of intumescence. Furthermore, the growing char would block certain part of the light allowing us to measure char growth with respect to time and temperature. Finally, the application of this technique is a novel method and has not been attempted before with respect to intumescent paint formulation. The methodology and the results are discussed in the respective sections, which make up the latter part of this thesis.

2.3.5 Thermal Imaging

Any object at a temperature above the absolute zero (-273 ^{o}C) will emit electromagnetic radiation. Thermal imaging utilises this phenomenon to its advantage by measuring the amount of radiation and relating it to the temperature of the object.

Thermal imaging cameras are designed to operate in the infrared region of the electromagnetic spectrum. The equipment is designed to operate in three distinct ranges defined as long wave (LW) λ= 7-12 μm, medium wave (MW) λ = 3-5 μm and short wave (SW) λ = 0.9-1.8 μm. Most IR cameras work in long and medium wave range and specialised products can be designed to tackle short wave range of the spectrum.
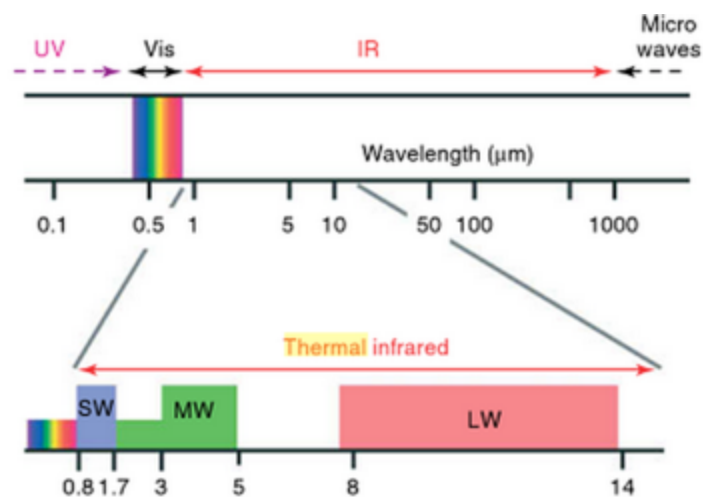
Figure2.21. Categories of IR wave lengths, short wave (SW), medium wave (MW) and long wave (LW)- adapted from [85].

The equipment, which performs in the LW range, is ideal when small changes against the ambient temperature are under consideration. However, MW is used for most industrial application where higher temperatures are considered.

Thermal imaging provides an ideal platform for mapping 2-D images of temperature distribution. Early research into the measurement of thermal radiance through optical equipment was restricted to military purposes. However, research has grown vastly within the civil sector over the last 40 years [85, 86].

The SC3000 thermal imaging camera, figure 2.22, is used in this research to study the intumescent behaviour of different paint samples under flame impingement. The camera is built using Quantum Well Infrared Photo detector (QWIP) that are made by using a combination of different detection materials. This allows it to operate over a very wide range of wavelengths λ= 3-20 μm. The temperature range covered by SC3000 is between -10 and 2000°C and primarily focuses in visualising 2-D images of objects which emit radiation at λ= 8-9 μm. It allows the user to see through diffusion flames by adjusting the temperature scales. This allows the user to examine the changes in the surface of the paint. The thermal sensitivity is reported to be 20mK at 30^{0}C and accuracy of ±1% and ±2% at temperatures below and above 150$^{=}$C respectively. The in-house software supplied with the camera captures high-resolution images nominally at 60Hz NTSC with further capabilities of recording videos at a resolution of 320 x 240 pixels. The temperature range is split into three tiers, -10 to 150 ^{o}C, 100 to 500 ^{o}C and 300 to 2000 ^{o}C. This makes the camera a powerful visualisation tool for temperature based research studies both of quantitative and qualitative nature [87].

Figure 2.22. FLIR SC-3000 thermal camera and associated software illustration[88]

2.3.5.1   Application and limitation

Academia and industry have both required non-invasive temperature measurement methods. Thermal imaging has successfully found its place in research where non-

intrusive and non-obstructive techniques are needed to study temperature and heat-transfer based studies. McDaid [89], Lytle and Webb [90] have used thermal imaging to study heat transfer characteristics through thermal imaging [91-93]. Most studies investigated the non-impinged side of an object because thermal imaging systems failed to measure flame temperature accurately. This is primarily because of the high spectral range of species produced from flames. Furthermore, the temperature distribution in a typical propane flame can be fairly large resulting in a wide range of emissivity thus limiting its use.

In the intumescent paint industry, thermocouples attached to the back of the substrate's surface have been the dominant method of measurement. This helps highlight areas where rapid temperature changes can occur. The occurrence of these changes is primarily due to inadequate protection provided by the intumescing sample. Furthermore, quality compliance regulations and ISO certification [4] have required such measurements to be made before a product is deemed acceptable for commercial purposes. During testing, the temperature measured through various thermocouples allows identification of sections where protection through intumescence is not sufficient. Cracking and peeling can occur at joints and flanges in steel columns. They fail to identify what reasons have caused such failures and the char structure can only be examined once failure has occurred. Thus one of the main research aims of this thesis was conceived- Use of thermal imaging systems to study the process of intumescence.

Literature pertaining to the use of thermal imaging to study the process of intumesce is almost non-existent. The dynamics of the paint before, during, after failure and instantaneous temperature measurements have not been explored or reported. Thermal imaging systems have their limitation however, one advantage of thermal imaging is the ability to see past a diffusion flame and observe the object. Although accurate temperature measurement cannot be made, the ability to observe a sample as it intumesces offers a huge advantage. A methodology designed to overcome the presence and influence of a flame to study surface temperature will be discussed in the methodology section. Consequently, the core part of this research would utilise thermal imaging to enhance understanding of the physical aspects that occur during intumescence.

2.4 Literature Review conclusion

Advances in technology, computational power and theoretical understanding have provided increased our understanding of the nature of fire and control it into advantageous industrial processes. However, there is always a risk of accidental fires. This has increased our awareness of fire safety and the need for development of sophisticated techniques for fire protection. One solution is the use of intumescent paint systems as a passive fire protection technique. The physical aspects of intumescence need greater understanding. Therefore, efforts must be directed to understand in greater detail for better fire protection systems in the future.

Screening techniques such as LOI, UL94 and TGA have been highlighted followed by the issue of expensive large-scale furnace and jet fire tests. These tests are expensive but mandatory before paint systems can be made commercial. They replicate some conditions in a real fire but there is still discrepancy among the expected and actual performance. This is primarily because fire is a complex phenomenon. Its nature is greatly dependent on the permutations of possible initial conditions.

Leading researchers have recognised the need for lab scale setups where conditions in large-scale fire setups can be modelled at a more economic scale. They also have the added benefit of instrumentation access to achieve a better understanding of the physical aspects of intumescence- an aspect which has not received its due research attention.

Efforts have been directed towards understanding fire and its effect on its surrounding environment through small-scale setups where a flame impinges on a ceiling. However, the use of impinging flames to study intumescent paint systems is limited to large-scale jet fire tests. Therefore, there is definite research gap to explore the possibility of testing paint systems at a relatively smaller scale laboratory environment.

This work aims to address this research gap, add greater value by exploring various temperature measurements techniques such as thermocouple, thermal imaging and flow visualisation techniques like Schlieren and high-speed imaging.

The formulations; two each designed for high temperature hydrocarbon jet fires (HTHF) and low temperature cellulosic fires (LTCF) would be tested using flat square panels. This is followed by application on a complex shape, referred to as the T-panel, to

understand complex movement of the char. The Nozzle to Plate (NTP) distance would be altered to vary the distance between the ignition source and the impinging plate covered with various coating thicknesses under a variety of thermal loading conditions. These experimental variations have been carefully selected to analyse intumescence behaviour under a variety of fire conditions, varying from diffusion buoyant plumes to high momentum turbulent jet fires at close or distant proximities.

Various techniques and their application, used as part of this research, are summarised in the table 2.3 below

Table2.3. Summery of diagnostic techniques and the measured intumescent properties

Technique	Measured property	Description
Thermocouple	Temperature	• Monitor the temperature-time *heating curve* as the sample intumesces • Compare Time to Failure for different formulation under varying fire conditions
Thermal imaging	Temperature Physical process	• Study the surface temperature in conjunction with the thermocouple measurements • Observe the physical characteristics of intumescence beyond the luminous flame • Analyse the characteristics of failure conditions
Schlieren Flow visualisation Technique	Flame paint interaction	• Changes in flame structure, hot gas layer both up and downstream during intumescence • Visualise mixing regions, turbulent and convective structures. • Flame wall and paint surface interactions • Rate of Char growth in different paint formulations • The phenomenon of expulsions – bursting pockets of gases through the char surface
Digital imaging	Physical properties	• Char structures • Surface and internal structural features

One of the greatest benefits to this work is the ability of IR system to see beyond the visible yellow luminesce of a diffusion flame completely. The sample can be viewed as it intumesces to study its physical characteristics. However, the radiation from the flame would dominate and limit the use of the camera to viewing the sample only. To by-pass this limitation, burnouts would be introduced at discrete times. The flame would be switched off allowing the camera to record the temperatures on the paint surface. Such methods and efforts to understand the behaviour of different coatings in a variety of fire scenarios have not been widely studied.

Overall, the theory and application of the various subject matters involved in this work have been discussed. This has been followed by a review of the different diagnostic techniques that would be used to study intumescent paint system. The section to follow will lead the discussion on the design of the test rig and burner setup. Furthermore, the experimental methodology adapted would be discussed followed by the instrumentation setup.

Chapter 3.   Experimental Setup

3.1   Introduction

The experimental methodology, the main components used in the experimental setup and their applications are presented in this chapter. The uses of various diagnostic techniques that have been reviewed in Chapter 2 are also presented.

3.2   Cone Calorimeter and Burner

The test setup consisted of two different test rigs. - The cone calorimeter and flame burner. The cone calorimeter setup comprised of a cone heater mounted above a loading cell. It was made up a multitude of coils that produced a uniform heating flux over the specimen using an adjustable controller. The controller was adjusted until a target heat flux was achieved. A thick circular steel section mounted in front of the cone heater acted as a shutter. The shutter was closed when the cone was heating up and only opened when making heat flux measurements or to conduct an experiment. A schematic of the setup is illustrated in the figure 3.1 and 3.2.
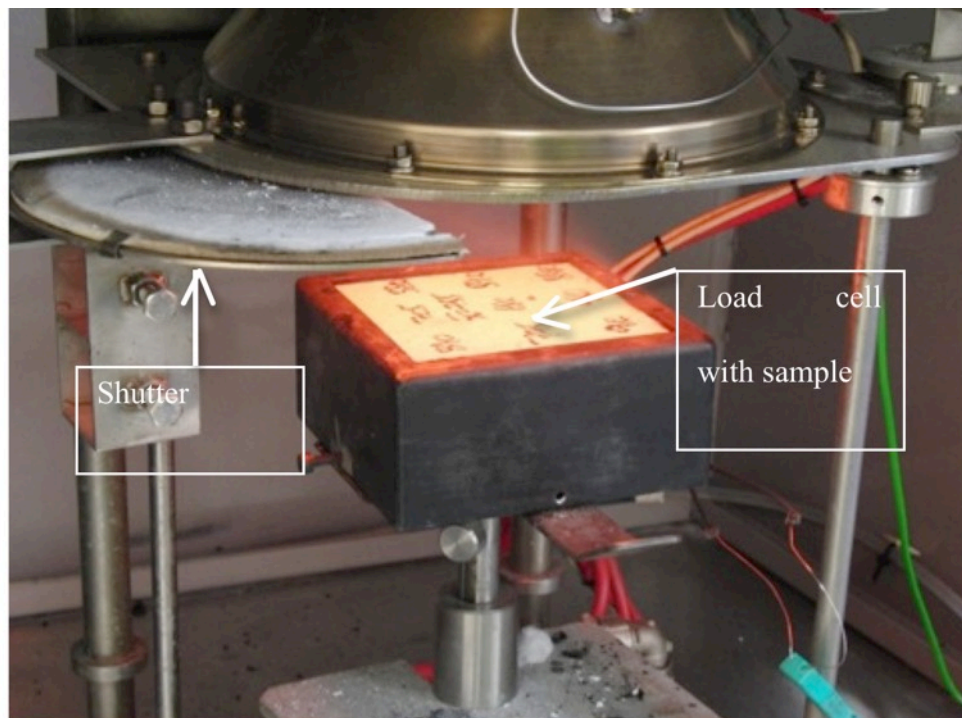
Figure 3.1. Loading cell, cradle and test sample assembly highlighted under an open cone heater.
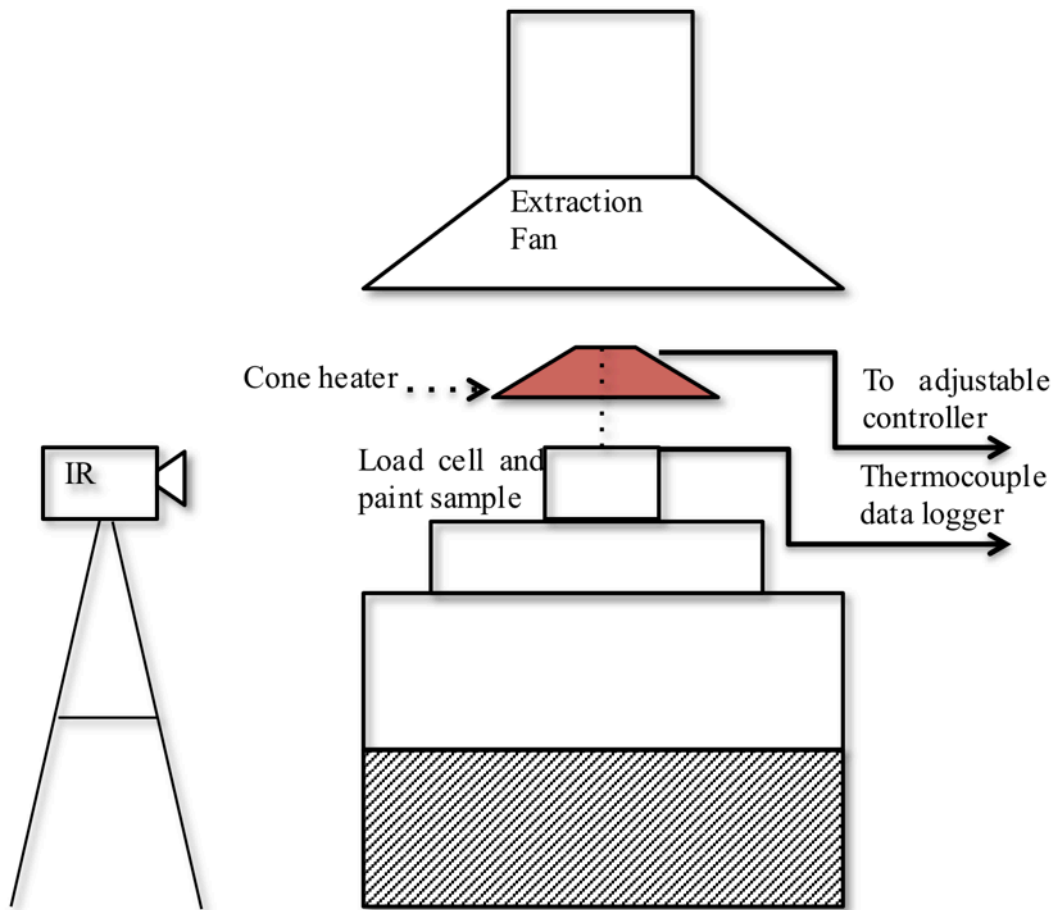
Figure 3.2. Schematic of the Cone calorimeters experimental rig used as part of this research.

The heat flux was measured using a heat flux probe. The sample was secured in a cradle and mounted on an adjustable loading cell. For the scope of this research two heights were used, 70mm and 35mm. The intention was to compare the difference in various physical aspects of intumescence as the heat flux was increased. The uniform heat flux at a separation of 70 mm was maintained at 50 kW/m^2 and at 35 mm; it was measured to be 65 kW/m^2. The temperature of the test panel was measured using a thermocouple attached to a data logger. Once the shutter was disengaged, the data logger recorded the temperature of the substrate and the entire experiment was recorded using a thermal imaging camera.

3.3 Impinging flame burner

The burner used in this thesis comprised of a circular fuel nozzle with a diameter of 4.6mm. It was capable of generating flow with Re number ranging from laminar to turbulent regimes. A schematic of the burner is illustrated in the figure 3.3.
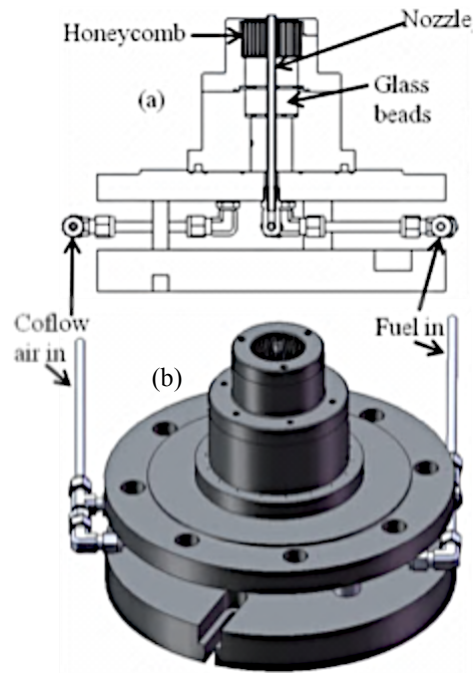
Figure 3.3. (a) Cross-sectional view Impinging flame burner drawing (b) 3-D view with highlighted parts.

A schematic of the burner and the associated plate holding stand is illustrated in figure 3.4. The stand was designed to a maximum achievable plate height of 0.8m. A turning screw system was installed to modulate the height of the plate holding and measured using a scale attached to the vertical side face on the main body of the device.
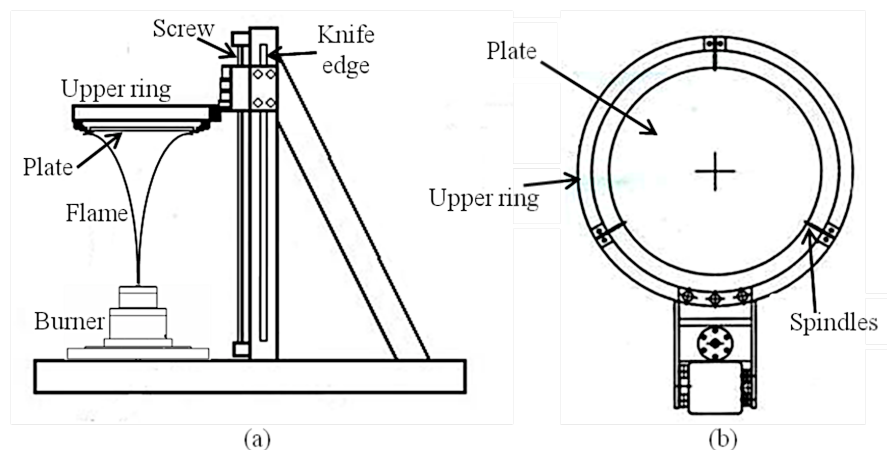
Figure 3.4. (a) Side view- Experimental Rig, Burner and panel assembly (b) Top view of experimental rig-adapted from [94].

Four additional support arms were attached to the circular plate so that a 100mm-square flat or a T-shaped panel can be held horizontally. The length of the arms was such that a cradle of an external length of 120mm could be securely held in position. The schematic of the plate holding device is illustrated in figure 3.5.

42

The cradle was loaded with 100mm square plates, flat or T-shaped, covered in a test coating. 100mm paint coated plates have become a benchmark size for small-scale tests. They gained popularity when they were originally used in cone calorimeter setups. Since then, academia and industry have adopted them. This research used 100mm square plates as well in order to maintain consistency with standard test procedures. The cradle was designed with a depth of 50mm. The cavity behind the test panel was filled with ceramic wool. Therefore, the back surface of the substrate was well insulated from the downstream hot gas exhausts.
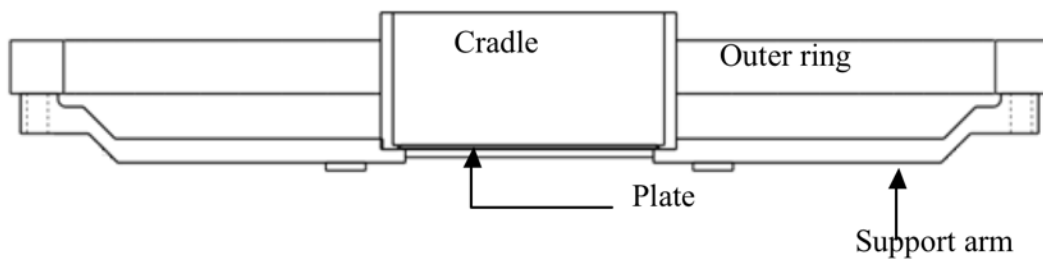
Figure 3.5. Cross-sectional view of the Outer ring, support arms and cradle assembly.

3.4   Paint Preparation

3.4.1 Introduction

A cellulosic fire that is fuelled by cellulose based materials like wood and paper has a stable, low temperature and low turbulent pattern whereas a hydrocarbon fire fuelled by oil, gas etc. has a much higher temperature rise. In ten minutes a cellulosic flame could reach about 650 ^{0}C and hydrocarbon approximately 1000 ^{0}C. Two other major types of fire scenarios are 'jet fires' caused by fuel released through a nozzle and 'rapid rise' fires which occur in confined spaces These fires can achieve temperatures in excess of 1200°C [95].

Four formulations were used in this project designed for either hydrocarbon or cellulosic based fires. The formulation codes used in this research were HPF 1, HPF 2 (Hydrocarbon paint formulation) and CPF 1, CPF 2 (Cellulosic Paint Formulation 1). HPF1 and CPF1 were prepared and applied to test panels at the university. Flat and T-panels coated with HPF2 and CPF2 were supplied prepared.

HPF formulations are designed for hydrocarbon and jet fires. They are currently being used on offshore oilrigs where the risk of a high intensity hydrocarbon fires is very high.

These formulations are designed with focus on mechanical stability over degree of intumescence. HPF1 and HPF2 exhibit similar characteristics. The resulting chars are dense and compact in nature with a low porosity. Hence a typical formulation would intumescence up to a maximum of 40 times its original size.

CPF formulations are designed for cellulosic and rapid rise fires where intensity is relatively low compared to hydrocarbon fires. The risk of such fires is very high in office and public buildings. These formulation produce profuse chars with high porosity and hence a very high degree of intumescence. A higher degree of intumescence is preferred at a compromise to mechanical stability. Hence a typical formulation would intumesce up to a maximum of 100 times its original size. CPF1 and CPF2 exhibit similar characteristics.

3.4.2 Test Panels

Majority of the experiments were performed using 100mm x 100mm flat square steel panels with a thickness of 5mm. A virgin uncoated steel panel was defined as sand blasted and primed steel panel of dimensions 100mm x 100m with a thickness of 5mm. The dimension for the T-panel included a square flange measuring 100x100 mm and a height of 5mm. The web was welded on top of the flange; it was rectangular piece measuring 9x100 mm and a height of 50mm. A cross-sectional image is shown in figure 3.6.
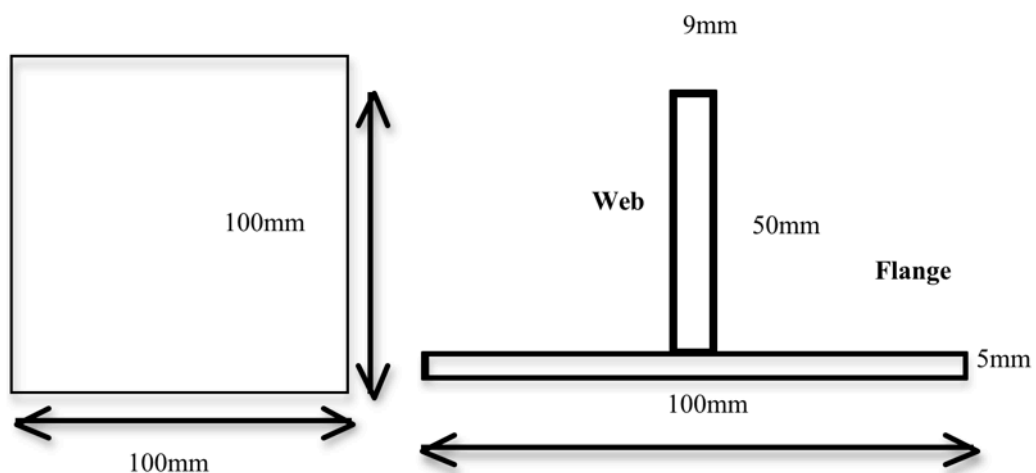
Figure 3.6. Left - flat panel schematic. Right – T-Panel cross-sectional view as used in this research.

The use of flat panels was advantageous due to ease of paint application, relatively simple and symmetrical impinging flow regime resulting in uniform char growth

patterns. Furthermore, the paramount advantage of using 100mm square panels was to record data comparable to other studies which use the same size panels. In T-panel system, movement was two dimensional in nature with a complex interaction mechanism between the two surfaces. Therefore, T-panel system was used to study complex movement pattern and compare char growth mechanisms to simple flat panels systems. The panels were painted with a variety of formulations and tested under various experimental conditions.
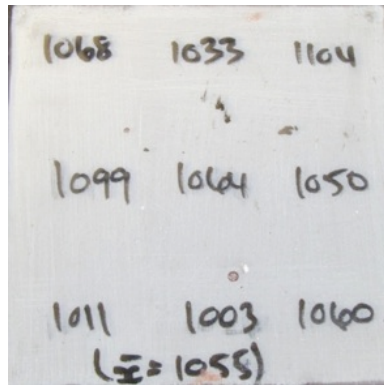
Through the use of flat panels, the research envisaged to study the physical aspects of intumescence in its simplest form. Once, the basic principles had been studied and understood, more complex movement patterns were analysed on complex designs such as the T-panels that reflect the application of intumescent paints on real structures. Both types of panels were studied using a impinging flame and a uniform heating source i-e cone calorimeter as previously discussed in section 2.1.2.1. The results from both heating techniques were compared and are discussed in the next chapter.

3.4.3 Test sample preparation

A generous layer was applied uniformly on each panel using a paint application spatula. It was levelled to a desired thickness using a micrometer adjustable thin film applicator purchased from Sheen instruments. The sample was left to cure for 24hrs under a well ventilated room. Once dry, measurements were taken over 9 equal grid points on the surface of the paint. The mesurements were made using Elcometer© 207 series of Precision Ultrasonic Thickness Gauges. The device was accurate for paint thickness as small as 1mm up to a micron. An avergae thickness value was then obtained from the 9 grid points. A typical prepared paint sample is shown in figure 3.7. All the panels used were subjected to the same method of preparation. After the paint preparation was complete, Type-K thermocouples were then attached to the back surface of the plate. Figure 3.8 and 3.9 show a prepared test panel. Once the sample was cured and the thermocouples attached, it was mounted on the rig using a cradle.

Although, care was taken in each application, sources of error couldn't be eliminated. These included human error during application. The samples were difficult to handle; CPF 1 was very viscous CPF1 and HPF 1 contained solid fibre composites making it harder to obtain a clean draw with the applicator. CPF2 and HPF2, when used were highly viscous that made it considerably hard to achieve a consistent thickness on every

test case. Overall, considering the number of test cases a relative error of ± 5% was recorded, which was within an acceptable range.

Figure 3.7. Generic flat test panel coated with CFP2, measured film thickness coatings and average thickness.
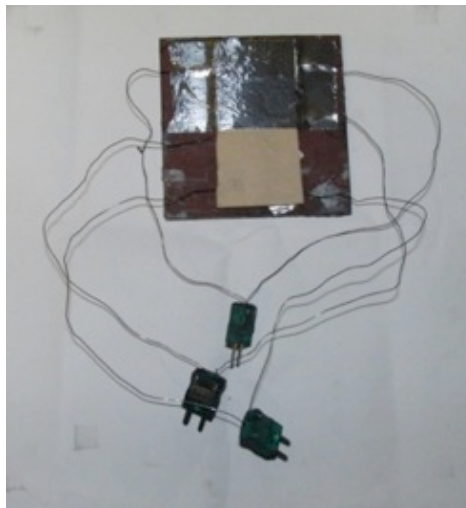
Figure 3.8. Back surface of test panel with attached thermocouple assembly.
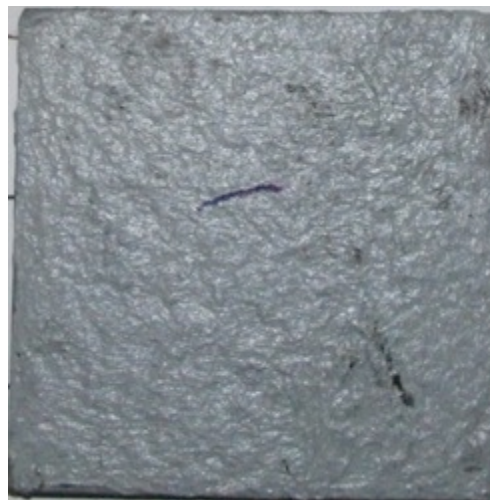
Figure 3.9. Front surface of CPF1 coated on a flat test panel.

3.5 Fuel and Flow Control

The only fuel used in this research was Propane C_3H_8. Propane is readily available, safe to handle and cheap compared to other combustible gases. Furthermore, it is used for the ISO standardised hydrocarbon jet fire and furnace tests.

A pressure regulator mounted gas bottle was maintained at a max pressure of 3.5 bars. The regulator was connected to flow metres using braided stainless steel piping with a diameter of 6mm. The flow rate to the burner was regulated through digital Gas Flow Control (GFC) Aalborg flow controllers. Thin (6mm diameter) polymer plastic piping was used to transport gaseous species to the burner. The output flow rate to the burner was controlled manually in litres/min (l/min) to the nearest 0.1l/min within a range of 0-60 litres.

The diffusion flame and the intumescing paint sample produced soot and copious amounts of spumific gases respectively. Therefore, an extraction system was installed in the laboratory. The extraction was capable of cleaning the air of the entire lab up to 9 times in one hour. The burner was placed directly under the extraction hood to minimise any flow disturbances as a direct result of the draught generated due to extraction system. Furthermore, the extraction was not strong enough to causes any flow variation. The effect on stability of the flame was minimal in all cases when compared to the generic flickering frequency associated with the tip of a flame structure [44]. The lab schematic is shown in the figure 3.10.
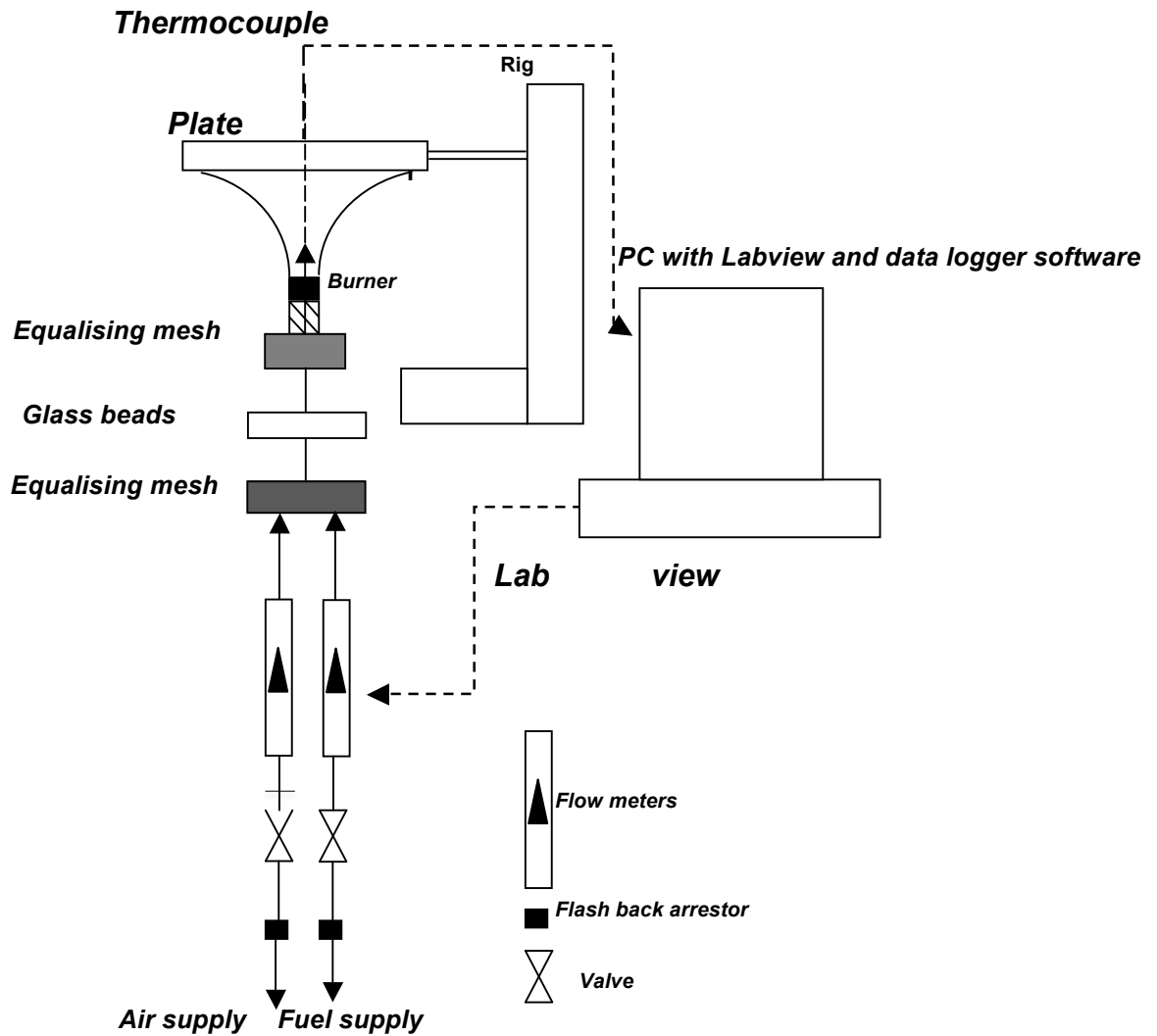
Figure 3.10. Overall experimental setup hardware schematic as used in this research.

3.5.1 Heating rate calibration

The primary objective behind the use of thermocouples was to measure the substrate temperature under various heating rates. Type K thermocouple was used to measure the temperature of the steel plate (substrate).

Due to the different experimental conditions, a method had to be developed to compare the heating rates between the two heating inputs. Thermocouples were attached on the back surface, to measure the rate of change of temperature increase, of blank steel panels. They were heated up to 400 ^{0}C and the Time to failure (TTF) was recorded. This was done at the two heat flux using the CC setup, 65 and 50 kW/m^2, and NTP separations, H/D = 40 to 100 for the impinging flame setup, with and without the shield attached.

TTF were compared assuming it would be approximately the same between the heating inputs, if the heating flux was the same. The NTP separation at which the TTF was approximately the same to the CC was determined. The char samples between these cases were compared. It was envisaged that the results would highlight the impact of a real flame compared to a radiative heat source on the process of intumescence. Further discussion would be presented in the results chapter.

Thermal imaging was the most comprehensively utilised method of studying temperature related intumescent behaviour. Various studies including surface thermal profile, intumescent mechanism, char growth and the effect of various heating patterns were conducted using this technique. Various methodologies are presented in the sections that follow.

3.5.2 Ignition sequence

At the start of an experiment, the diagnostic equipment is set up and kept ready prior to ignition. The fuel input is regulated and ignited manually using a high grade, multi purpose long nose lighter. Once ignited, the thermocouple system was set to record. Thermal imaging system was set to record indefinitely until it is stopped at the end of an experiment. The extra data gather prior to ignition was removed in post processing. The high-speed camera used in Schlieren technique was kept on live recording mode and data was recorded using a manual trigger. The trigger was activated when the desired T_b was achieved. T_b was monitored via thermocouples using the supplied software by Pico technology.

3.5.3 Burnout sequence

Burnout was defined as a small period of time during the experiment when the heating input i-e flame was turned off. The timing of a burnout was maintained at a maximum of 10 seconds. Burnouts were performed in every experiment using the impinging flame setup for two main reasons.

They were required due to a limitation of the Schlieren experimental setup. It was observed that during an experiment, highly localised density variation within the stagnation and wall jet region made it difficult to accurately visualise the char height. During burnout, it was possible to capture an accurate reading of the char height.

Therefore, burnouts were aligned with discrete measurements that were made to track char growth.

There was a limitation in the thermal imaging equipment, which necessitated the use of a burnout sequence. When the flame was present, the thermal camera could not capture the thermal profile of the char. This was because the radiation from the flame would overlap the radiation from the growing char. Thus the camera would only register an inaccurate flame temperature. A burnout was performed periodically in order to capture thermal data for the char surface.

The timing of each burnout was kept the same as the Schlieren char measurement technique. In cases when Schlieren technique was not used, the discrete measurements were still maintained on the same T_b values.

The impact of a burnout on the process of intumescence was also investigated. This was done through analysing whether there was a difference in TTF with and without a burnout. It was observed that burnouts did not impact TTF. The analysis is presented in the next chapter.

3.5.4 Heating techniques

There are three heating techniques that have been compared in this study. First was the non-standard jet fire model where propane based diffusion flame was impinged directly onto a plate that was covered with an intumescent paint. Second, a heat shield was added in front of the test panel. This was done to have a controlled heating input incident on the panel. Finally, a cone calorimeter was used which had a radiation based uniform heating input. Flat plate and T-shaped targets were tested in all three regimes. NTP separation, fuel flow rate and sample thickness were the experimental conditions variations made for techniques 1 and 2 whereas, the heat flux incident on the panel was varied in techniques 3.

The primary objective of the study was to analyse intumescence behaviour under non-homogenous conditions expected in a real fire scenario. This was achieved in technique 1. An uninterrupted jet fire was impinged on a target in an effort to simulate the performance of an intumescent paint sample under non-standardised fire conditions. The flame was in direct contact with the target and completely surrounded the panel and its

support cradle. The term *non-standard* and the need for non-standard testing technique were discussed in chapter 2.

The addition of a heat shield in technique 2 controlled the heat incident on the panel. It focused on conductive and convective modes of heat transfer and eliminated the influence of external heat transfer elements such as radiation that would affect char growth. A reduced heating input was incident on a target sample where the shield ensured the flame was deflected away from the cradle. Such experimental conditions were used in an effort to simulate the performance of a paint sample where the influence of excess external heat was removed. Flow visualisation using Schlieren technique and char growth of HPF2 discussed in Chapter 5 will highlight the motivation behind the addition of the heat shield.

A cone calorimeter used in technique 3 relied solely on uniform radiation as a source of heat input. A uniform heat flux incident on the test panel and the separation between the cone and the test surface were varied. Such experimental conditions were used in an effort to simulate the performance of a paint sample that is heated solely through radiative heat transfer in a fire scenario. Furthermore, the effect of a homogenous heating input on intumescence was compared to a non-homogenous heating input.

Overall, the three heating techniques represented variety of heating conditions in a scenario where fire impinges on a surface protected using a coating of intumescent paint. It was envisaged that through a combination of the three techniques, the performance of protective coatings under a real fire conditions could be better understood.

3.6   Diagnostic Techniques

3.6.1 Schlieren Technique

The primary objective behind the use of Schlieren technique was to visualise the flow as the jet fire impinges on an intumescing paint surface. The investigation was primarily performed on flat plate targets, which upon long exposures to a heat source, resulted in char growth. A z-type Schlieren setup illustrated in figure 3.11 was used.
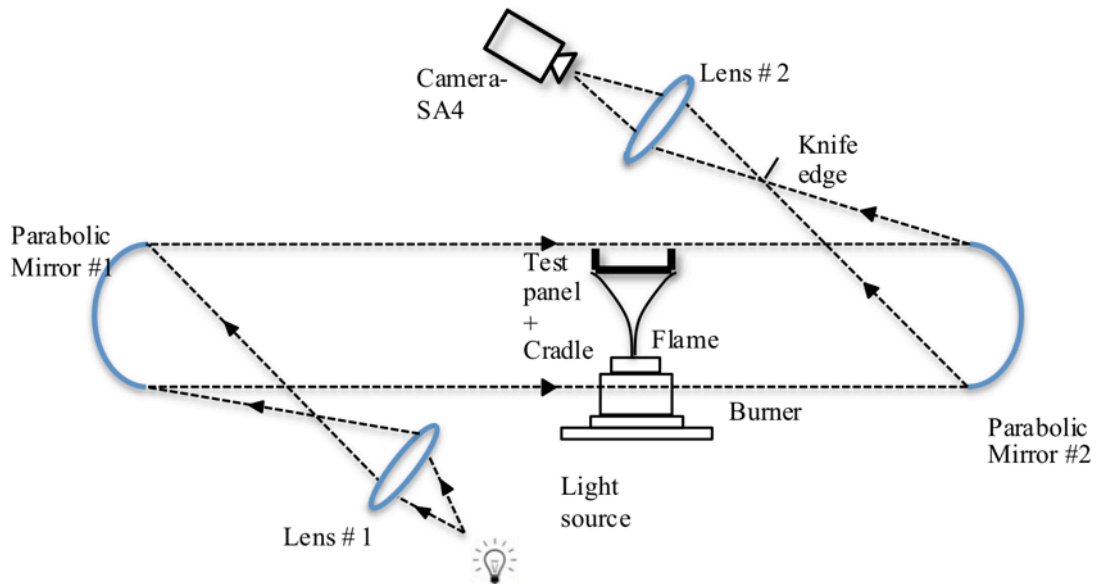
Figure 3.11. Schlieren imaging technique setup schematic as employed in this research.

The technique helped visualise the changes in the flow structure, turbulence and the interaction between the moving flame-char boundary. The technique also enabled the viewer to distinguish various key aspects of an impinging flame jet such as unburnt fuel, flame boundary, convection of the hot gas layer and exhaust gases. An illustration of an intumescing char sample is shown in figure 3.12
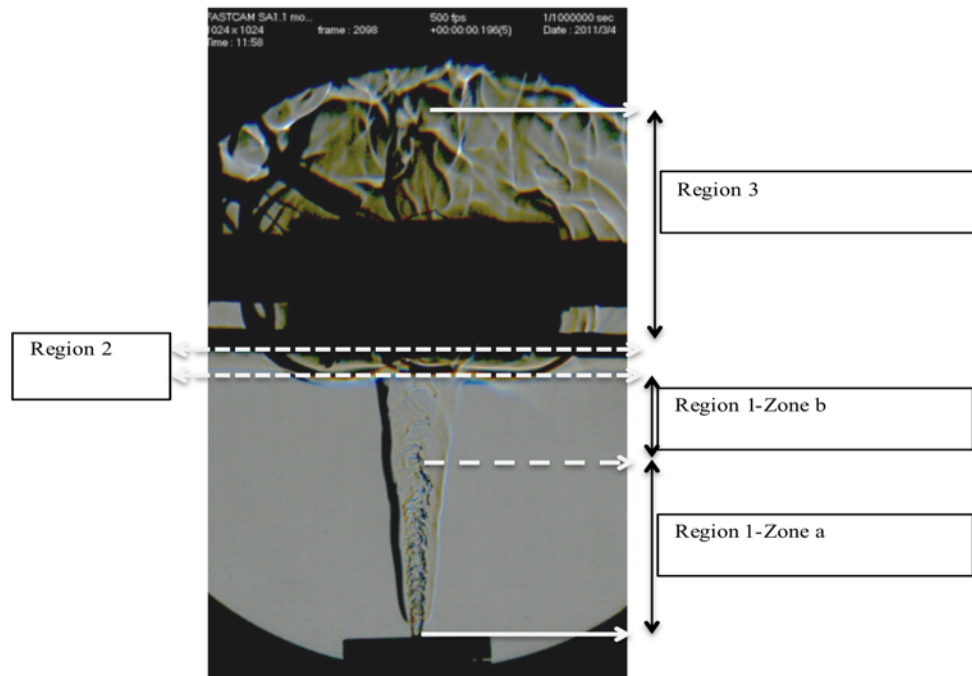
Figure 3.12. Schlieren illustration-Flame impinging on flat target and various regions of flame structure development zones highlighted.

There were three distinct regions that were identified. Region 1 was further split into two parts. These were:

1. Flame fuel/air region between the nozzle and the plate

a. Flame/ reactant rich zone

b. Flame/product rich zone

2. Flame-char boundary near the plate surface

3. Hot gas layer and flame in the exhaust region above the plate

There were various factors that could affect the behaviour of the flow in all these regions such as NTP separation, fuel flow rate, paint thickness and the intumescing char boundary. Schlieren technique helped analyse the behaviour of the flow in all these regions and their effect on the physical aspects of intumescence.

The process of intumescence took a significant amount of time. Therefore, measurements (capture of images) were taken at discrete data points. A typical sample would take between 600 seconds (10 minutes) up to 2400 s (40 minutes) to achieve failure temperature of 400 ^{0}C. The data was captured with respect to substrate temperature T_b because Time To Failure (TTF) was variable and dependent on initial conditions. A maximum of ten readings were taken between Room Temperature (RT) and failure temperature of 400 ^{0}C. It was identified through various pilot tests that the process of intumescence did not start until T_b=125 ^{0}C for most cases and formulations. Hence, ten discrete measurements were made after T_b= 150 ^{0}C was achieved with intervals of 25 ^{0}C up until 375 ^{0}C. At this temperature full intumescence of the char had been achieved and a measurement at 400 ^{0}C was not needed. In some cases, the interval of measurement was varied. These would be identified and discussed later in chapter 4.

3.6.1.1   Accuracy and limitations

The images were captured at a shutter speed of 1 μs that provided adequate background illumination, good temporal resolution and sharp images without blurring even at relatively high flow velocities. The resolution of the camera was high enough to zoom into the images without compromising the quality of the image and analyse the flow behaviour near the char surface.

The cameras operation was limited to storing 5000 frames on a built in flash memory that was later saved to the hard disc of the operating system. The system was limited to make a maximum of 10 discrete measurements per session at a frame rate of 500 Frames Per

Second (fps). This frame rate was fast enough and spread over the complete range of T_b to analyse the behaviour of the flow in the various regions over the complete process of intumescence.

The Schlieren technique is not a 2-D cross section view of a test section. It is a 2-D representation of the complete density variations in a 3-D flow field. Therefore, data in the x-y plane on the front surface will overlap with information over a parallel x-y plane at any distance in the direction of the z-axis. Hence, it was difficult to determine the exact spatial position of char growth and the data could only identify the position of maximum growth.

Furthermore, overlapping was observed between the flame layer near the edges and the middle of the plate. In addition to the overlapping, the flow near the char surface had highly localised density variations. Therefore, it appeared to be thicker in the images obscuring the actual position of the char referred to as an *optical distortion* as shown in figure 3.13 To overcome this problem and measure the char growth the flame had to be turned 'off' and 'on'. This was defined as a *burnout*, which is discussed in section 3.4.3.

When the flame was turned off a dark grey layer, highlighted red in figure 3.14 was observed apart from the black char surface. This was observed to be the release of the spumific gases produced during intumescence, which settled into the multitude of cavities on the uneven char surface. They remained close to the surface of the paint and distorted the position of the char surface.
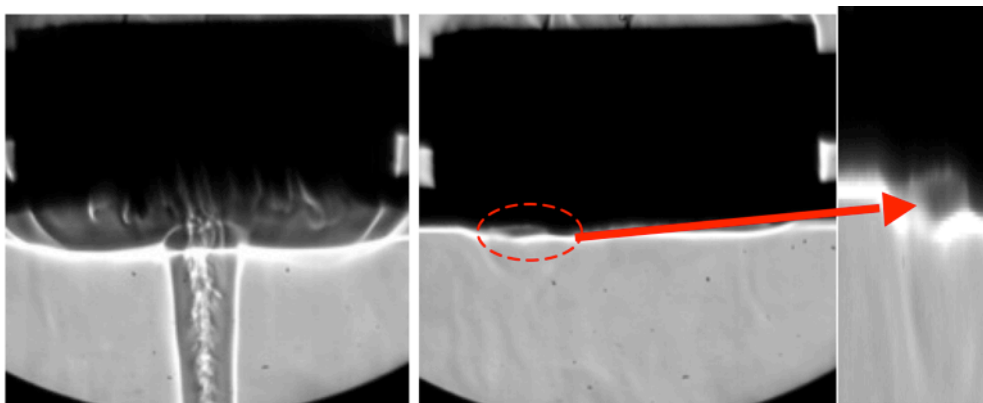
Figure 3.13. A typical Schlieren HPF1 experiment showing two frames 0.12s apart when the flame is on and off. The apparent position of char height relative to real position is highlighted due to dense smoke captured in cavity

All these factors increased the uncertainty involved in analysing the thickness at different timings. Consequently, measurement of char growth for samples such as HPF1, which

did not intumescence greatly, became difficult and relatively less accurate than other samples. It became easier when larger thicknesses were used i-e 2mm and 3mm. The discussion and observations presented in the results section would mainly surround tests with larger thicknesses.
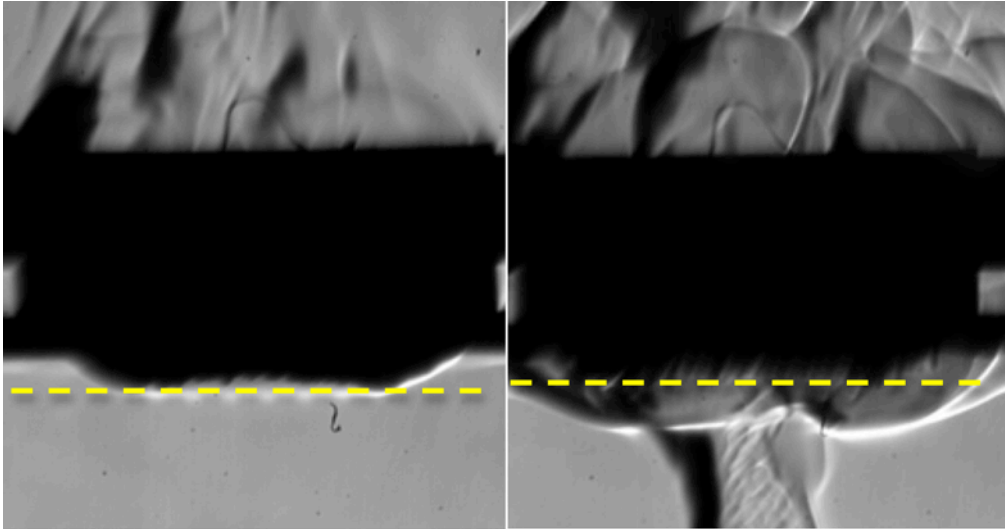
Figure 3.14. A typical Schlieren CPF1 experiment showing two frames 0.12s apart when the flame is off and on. The apparent position of char height relative to real position is highlighted due presence of flame.

Albeit its limitations, the technique provided valuable qualitative and quantitative information particularly when studied in combination with other techniques such as thermal imaging.

3.6.2 Thermal imaging

This study relied mostly on the use of a single thermal imaging camera, ThermaCam SC3000 [87]. ThermaCam SC3000 is a quantum-well infrared photodector based self-cooling system capable of measuring temperatures in the range of -10 ^{0}C up to 2000 ^{0}C. It measured wave length in the spectral range of 8 to 9 μ with an accuracy of ± 1 % for temperatures up to 150 ^{0}C and ± 2% for temperatures over 150 ^{0}C. It operated a nominal framing rate of 50 Hz and up to 250 Hz at a reduced viewing angle with a maximum resolution of 320 x 240 pixels. Although it was capable for field use, the camera was fairly bulky and was mostly used in a laboratory environment.

A second camera was used for the Cone Calorimeter experiments. The FLIR SC640 [96] was a portable hand-held thermal imaging system. It was capable of operating on the same temperature range as the SC3000 at a higher pixel resolution of 640 x 480 pixels

but reduced framing rate of 15 Hz. Both cameras used the same software package namely, ThermCAM [97] Researcher for viewing and post processing data.

Various researches cited suggested that the performance of coatings was related to its ability to withstand the impact of various fire conditions and was measured by the changes in substrate temperature T_b with respect to time. In addition to substrate temperature, this research has aimed to study the thermal characteristics of the paint surface as well.

Although thermal imaging has been utilised in intumescent studies before, it has not been used to study the impact under an impinging flame. Furthermore, there is no evidence that it has been compared with cone heaters- a commonly used equipment to study intumescence. This research has aimed to explore new parameters focusing on thermal characteristics of the char surface as it intumesces. It is envisaged that this data could be combined with T_b studies to gain a novel insight and enhance our understanding of the process. In this section various thermal features, which were studied using thermal imaging, have been discussed.

A relevant limitation that was encountered using the cameras was the systems inability to measure the thermal profile of the char when the flame was on. This was because the radiation form the flame overlapped with that from the char. Therefore, even though the char was visible, its thermal performance could not be measured. Overall, SC3000 was preferred over the SC640 due to its robust nature and reliability.

Experimental setup

Flat Panels

The burner and rig were placed onto a table at a height of 1.25m. The thermal camera was adjusted onto a tripod 0.75m above the ground, angled at 30° from the vertical and focused to capture the entire surface of the plate at all times. The figure 3.15 and 3.16 show an illustration of the lab setup and an image of a flat plate target respectively as seen through the thermal imaging system
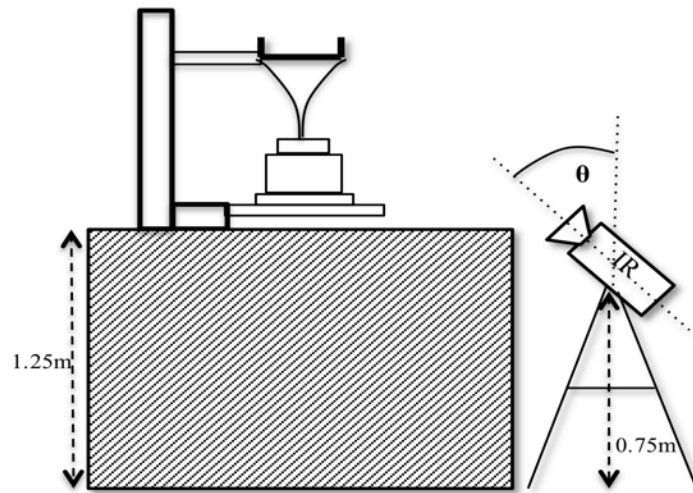
Figure 3.15. Impinging flame and thermal camera lab setup schematic employed as part of this research.
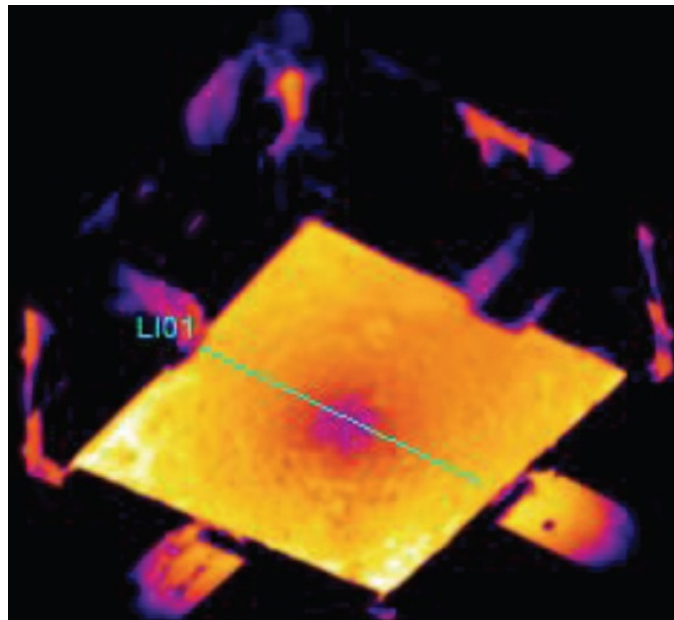
Figure 3.16. Output thermal image at NTP separation of H/D =30.

The image in figure 3.25 shown is for a CPF1 sample at a NTP separation of H/D=30. The lower edge of the plate can be observed as the lowest part of the image. At this point, the camera height was 0.75m above the ground. The tripod height was increased without fluctuating the viewing angle via an extension tube under the camera mount to the maximum separation of H/D = 110. At H/D=20, the angle had to be increased to capture the surface, because the nozzle and the table edges blocked the view of the original setting.

Unlike, the impinging flame setup, the test panel was positioned in an upright orientation and aligned so that the centre of the plate and cone heater were coincident. The thermal camera could only be positioned in front of the cone heater since the setup was

positioned in an enclosed extraction unit. The camera was positioned at a much higher angle compared to the laboratory setup to achieve maximum coverage of the plate.

T-panels

T-Panels exhibited complex two-dimensional movement. Distinctive char growth was observed on the web and flange part respectively. Furthermore, there was combined movement where the two parts were joined together. It was difficult to fully analyse the nature of movement by utilising the same setup as flat panels. Therefore a slight modification was made while using the cone calorimeter setup.

For each experimental condition, two tests using two panels were performed at different orientations. In one orientation, the panel was positioned so the width of the flange faced the thermal imaging system. This was defined as the latitudinal orientation illustrated in figure 3.17. In the second orientation, the panel was positioned so the length of the flange faced the system. This was defined as the longitudinal orientation as illustrated in the figur3 3.18.
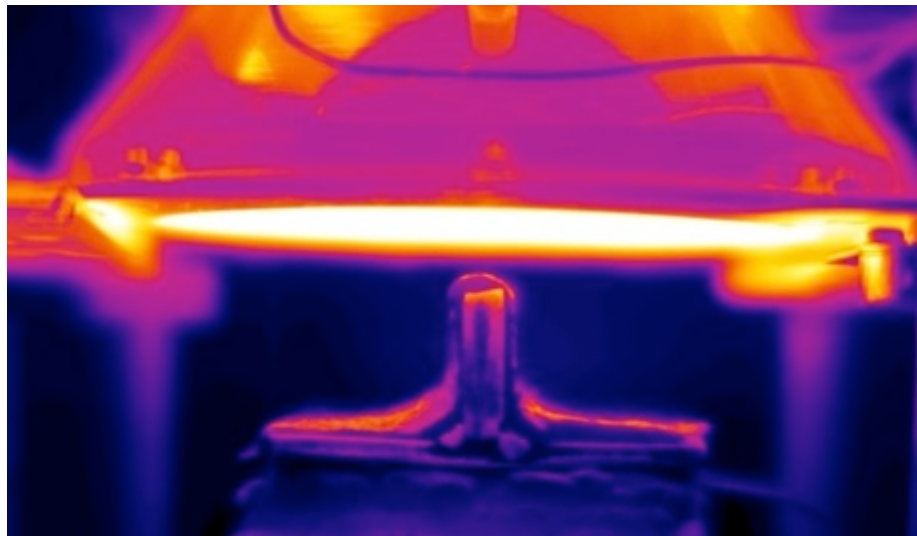
Figure 3.17. Output thermal image from Cone Calorimeter setup illustrating the Latitudinal orientation when testing T-panel systems
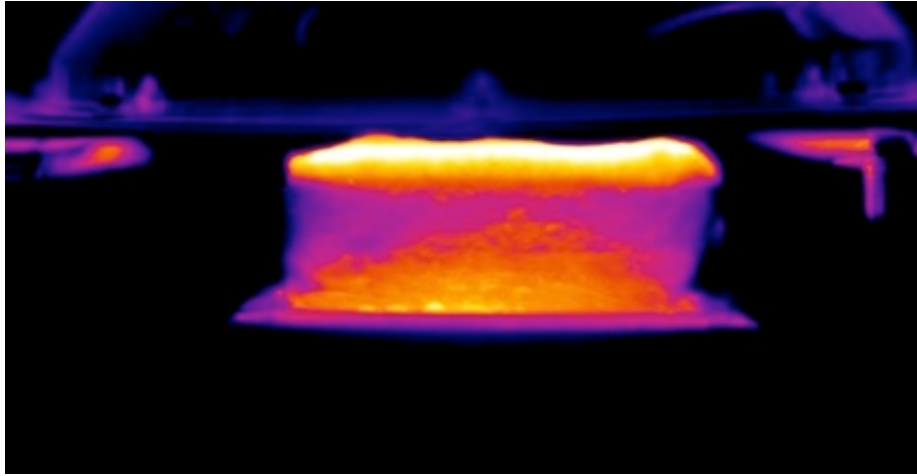
Figure 3.18. Output thermal image from Cone Calorimeter setup illustrating the longitudinal orientation when testing T-panel systems.

Even though, two tests were conducted, it was assumed that the intumescent behaviour would be similar if the conditions were kept the same. Therefore, the results from both tests can be combined to provide a complete analysis.

For the impinging flame setup, only latitudinal cases were studied. The objective was to gather data that could be used in the char tracking technique discussed in section 3.7.7. There were some limitations and challenges during post processing of the results. There discussion would be presented in the next chapter.

3.6.3   Direct imaging

A Casio EX-F1 digital camera was used to capture char samples once a test was completed. The digital images were captured to compare the difference in the physical appearance of the char sample. Casio EX-F1 has a 6 Megapixel resolution capable of manual and autofocus feature and aperture size variation from f = 2.7 – 7.5. It features variable ISO sensitivity from 100 – 1600 based on illumination, 30 to 1200 fps frame rate and shutter speed from 60 to 1/40000 s. The camera was also capable of recording high-speed movies as well [98]. Most images were taken on automatic settings. However, in some cases, exposure times were increased to highlight the black char surface clearly.

3.6.3.1   Accuracy and limitations

The Digital camera used offered a 6MP resolution with an autofocus and auto exposure feature. Thus the images captured offered high spatial resolution that was not

compromised when zoomed up to 20x the original size. Hence, the accuracy of the pixel measurements method was not compromised.

The carbonaceous char presented naturally as black in colour. Also, the soot from the diffusion propane flame settled on the surface of the char as well. This presented as a difficulty when taking digital images. The physical features on the surface of the sample were harder to identify. Long exposure times and an external light source were used to rectify this problem of highlight the features. However, it did affect the presentation and accuracy of the result to some extent.

3.7   Testing conditions

In this section, the variations in experimental conditions are discussed. The discussion focuses on heating rate variations achieved through increasing the Nozzle to Plate (NTP) distance, thermal loading at the nozzle and thickness of coating. This is followed by an overview of ignition and burnout conditions. Finally, changes in heating standards are discussed.

3.7.1 Nozzle to Plate distance

Nozzle to Plate, H, distance is referred to as the separation between the burner nozzle and the surface of the target plate at the start of the experiment. It is normalised as a dimensionless parameter H/D, with reference to the burner diameter, D.

The variation in heating height and the effect it has on the heating profile of a flat surface under an impinging flame was illustrated in figure 2.16. In the review, it was shown that at lower H/D values, the highest temperature was observed away from the centre of the surface with a steep variation in distribution radially along the centre of the plate. Furthermore, it was observed that as the NTP distance was increased the highest temperature shifted to the centre of the plate and the steep distribution radially along the centreline of the plate reduced to a relatively flatter heating profile [65].

The experiment conducted by Hou utilised a premixed methane-air fuel conditions on a water-cooled flat steel plate with H/D values between 2 and 16 [59]. It showed that the value of the measured heat flux reduced with heating height. Studies by Weng that used

flame beds with large diameters that simulated diffusion buoyant fire plumes [49] were also cited as part of the literature in chapter 2.

Intumescence behaviour is highly dependent on temperature. Hence, the effect on intumescence as the NTP separation is varied is of interest. The range of NTP variation in this study was larger than those conducted by other researches. NTP was varied between H/D = 20 up to H/D =110 where nozzle diameter D= 4.6mm. Pilot tests were conducted on samples of CPF1 in order to determine the fuel flow rate conditions that could be explored over a wide variety of separations.

The lower limit of the separation was determined by the degree of intumescence anticipated from the samples which exhibited the highest amount of intumescence. A typical CPF1 specimen intumesced approximately 40 to 50mm. Hence, a minimum separation of H/D 10 was required. For additional safety and ease of instrumentation access H/D 20 was selected to be the minimum value of separation. Table 3.1 summarises the various experimental conditions that were used.

Table 3.1. Nozzle to Plate (NTP) distance variations applied as part of this research

	Flow rate	Flow rate	Paint Thickness	H/D
	Fuel	Fuel		D=4.6mm
	v [l/min]	$x10^{-5}$ [m^3/s]	[mm]	H/D
Nozzle to Plate distance variation	4.00	6.67	1.00	20
	4.00	6.67	1.00	40
	4.00	6.67	1.00	60
	4.00	6.67	1.00	80
	4.00	6.67	1.00	90
	4.00	6.67	1.00	100
	4.00	6.67	1.00	110

A fuel flow rate of 4 litres/minute equivalent to 6.67x10^{-5} m^3/s, converted using D, was used for all separations.. At this flowrate, the flame height was tall enough to interact with the paint sample at the highest separation of H/D=110. This flow rate also offered a nominal heating time for a steel plate tested without any paint. This would be discussed in further detail in section to follow. Finally, time to reach failure temperature of 400 ^{0}C, which is a key performance indicator in this research, was kept comparable

to results found in cone heater tests and good agreement was achieved using 6.67 e-5 m^3/s as the fuel flowrate.

3.7.2 Flowrate

Flowrate is defined as the volumetric flow of fuel that exits the burner nozzle and is completely combusted as a diffusion flame that impinges onto a test target. Parameters such as Reynolds number, thermal loading and fuel exit velocity were directly dependent on Flowrate.

One aspect of the research was focused on variation in fuel flow rate to study the effect of thermal loading and Re number on intumescence. Thermal loading was calculated at the nozzle to simulate various fire loads incident on the paint surface and investigate their impact on intumescence. Re number can have a significant effect on heat flux incident on a flat surface as discussed briefly in figure 2.15. It showed that heat flux incident on a target increased significantly with Re number even though the thermal profile remained consistent. The investigation focused on low separation laminar flow regimes.

Variation in fuel exit velocity combined with flow visualisation would help highlight the impact on various physical aspects of intumescence presented in the results section. Whilst various formulation were tested at H/D=40, the effect on TTF was also investigated. Table 3.2 summarises the various experimental conditions that were used followed by calculated parameters in table 3.3.

Table 3.2 Fuel flow rate variations applied as part of this research.

	Flow rate	Flow rate	Paint Thickness	H/D
	fuel	Fuel		D=4.6mm
	v [l/min]	x10^{-5} [m^3/s]	[mm]	H/D
	2.00	3.33	1.00	40
	3.00	5.00	1.00	40
	4.00	6.67	1.00	40
Flow rate variation	6.00	10.00	1.00	40
	8.00	13.33	1.00	40

3.7.3 Thickness

The primary objective behind this investigation was to explore char growth behaviour as initial thickness was increased. Furnace and jet fire tests have shown that at higher thicknesses, the char can intumescence to such an extent that it cannot support it own weight and breaks off. This can result in exposure of the substrate to direct heating that results in failure. The mechanism of growth that eventually leads to char breakage has not been investigated before and would be studied using Schlieren and thermal imaging techniques.

CPF1 and HPF1 samples were studied in a variety of thicknesses: 1mm, 2mm and 3mm thickness samples, were investigated at a NTP separation H/D =40 and v = 6.67 x 10^{-5} m^3/s.

The paint supplier recommended a minimum sample thickness of 1mm. Pilot tests on CPF 1 sample less than 1mm thick showed that TTF was smaller than expected. It did not intumesce enough to highlight any physical characteristics of interest. Therefore, 1mm was chosen as the smallest thickness for testing.

CPF 2 was very viscous in nature and when 1mm samples were tested, in an inverted orientation under an impinging flame, the char grew and broke off in every test. Therefore, some tests were also conducted on a coating of thickness 0.5mm. At 0.5mm, the char remained intact with the substrate. Using this as a pass criterion, 1mm char samples of CPF1, HPF1and HPF2 were compared to a 0.5 mm char sample of CPF2. 1mm CPF2 samples were solely used to analyse excessive growth that eventually resulted in the breakage and regrowth of the char. Table 3.3 summarises the tests conducted.

Table 3.3.Sample thickness variations applied as part of this research.

	Flow rate	Flow rate	Paint Thickness	H/D
	Fuel	Fuel		D=4.6mm
	v [l/min]	x10^{-5} [m3/s]	[mm]	H/D [formulation]
Thickness variation	4	6.67	1	30 [CPF 1]
	4	6.67	2	30 [CPF 1]
	4	6.67	3	30 [CPF 1]
	4	6.67	0.5	40 [CPF 2]
	4	6.67	1	40 [All except CPF2]
	4	6.67	2	40 [All except CPF2]
	4	6.67	3	40 [All except CPF2]

3.8   Measured properties

3.8.1 Measurement of char growth

The objective behind the measurement of char growth was to analyse rate of reaction of an intumescing paint sample keeping in mind the piecewise mechanism suggested by Vandersall [11] discussed in Section 2.2.1.

The method, used to study flow patterns, offered further benefit by allowing measurement of intumescing char. Selected images of an intumescing char from a CPF1 sample are illustrated in figure 3.19.
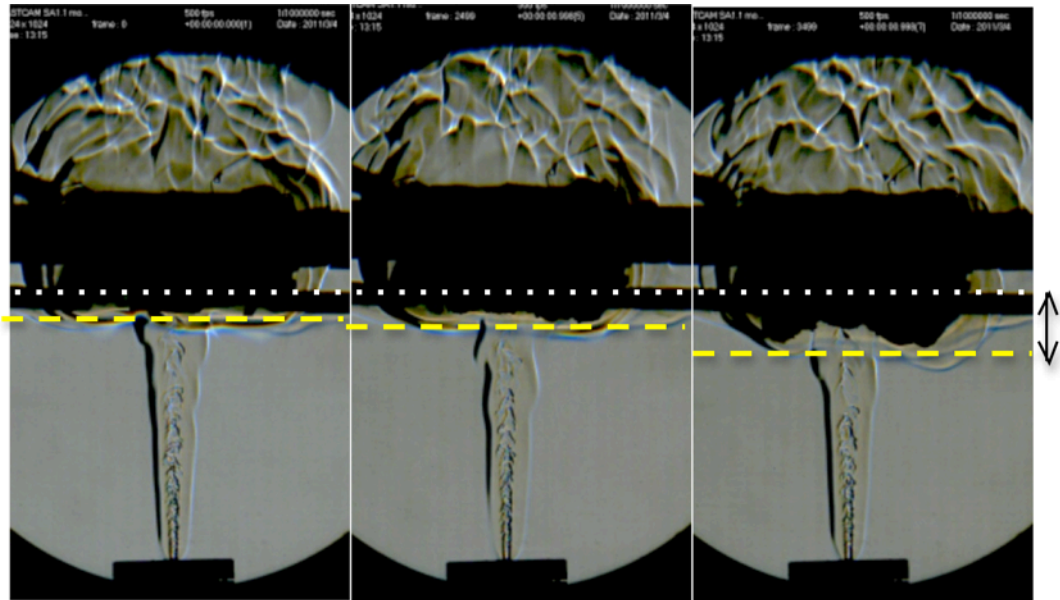
Figure 3.19. Schlieren images for v= 5e-5 m-3-/s at time = [60, 240 and 360] s highlighting char growth and tracking technique.

In the images, the cradle and the support arms can be seen fixed at their position. In addition, the intumescing char layer can be observed. Ten measurements were made for every test case and using a pixel measurement tool, part of the FASTCAM software, the height of the char from the surface of the plate was recorded for various experimental conditions.

It was observed that the thermal degradation processes typically started around $T_b = 200$ ^{0}C in the piecewise mechanism (section 2.2.1) of the intumescence process. Through this method, the substrate temperature at which the process begins and intumescence started was quantifiably identified. This temperature was defined as the Expansion Activation Temperature (EAT): the substrate temperature at which intumescence started. Various samples that are designed for a variety of fire conditions were used in this research. Through this technique, the author intended to identify whether EAT_b can be different based on the composition of the paint sample and heating conditions.

3.8.2   Internal structure and surface texture

Physical features such as surface pustules, degree of intumescence and bubble (internal) size were examined and analysed under varying experimental conditions. Once a test had finished and the char sample was removed from the rig, digital images from various angles were taken. The two main angles were top view and cross-sectional view.

65

Pustules are an inherent surface feature when a paint sample intumesces. They are formed as little gas pockets escape through the char surface in the early stages of intumescence. Experimental conditions and therefore, heating rate had an impact on the size of the pustule.

Larger degrees of intumescence and bubble size have been reported to enhance the thermal resistive properties of coatings. This study verifies that a similar behaviour was observed using an impinging flame setup. It was also observed that degree of intumescence and bubble sizes were larger than those observed using the cone heater heating method for a similar value of heat flux.

Figure 3.20 shows the difference in degree of intumescence between CPF1 samples tested at H/D =30 and H/D = 80. The difference in char shapes is due to the changes in heating rate as the separation was increased. The heating rate was also observed to have a direct impact on other physical aspects such as surface texture and internal structure. Such aspects were studied in greater detail through comparison of digital data.

The majority of the analysis was qualitative in nature. Size measurements were made using a pixel measuring technique in a commercial imaging analysis software. Analysis of the physical features would be presented in the result chapter further on in this thesis.
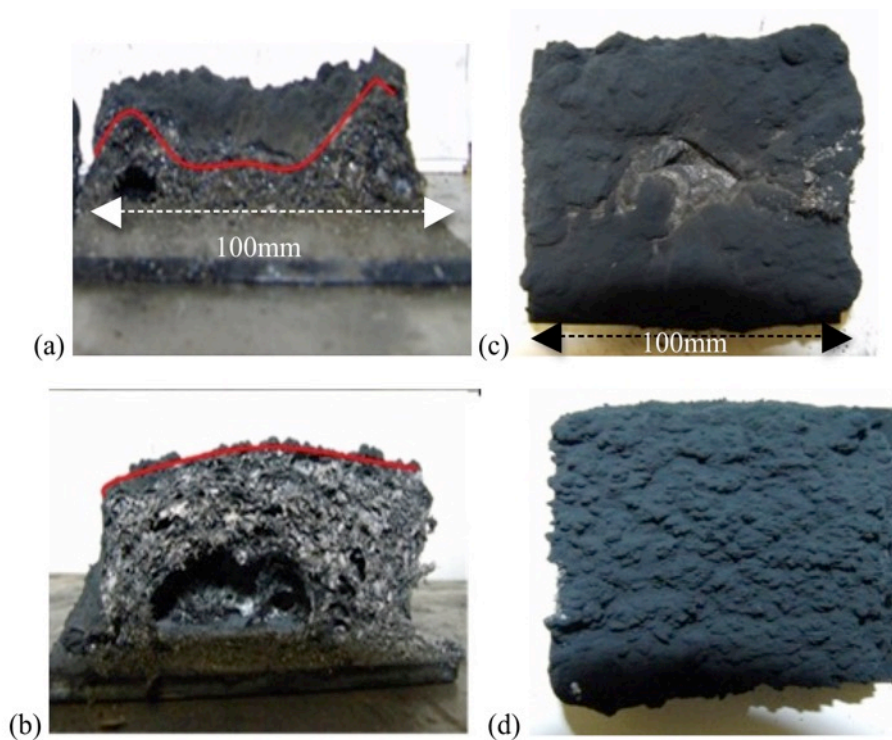
Figure 3.20. (a) & (b) cross sectional view of char structure at H/D=30 and H/D = 80 respectively. (c) & (d) Top view of char surface H/D=30 and H/D = 80 respectively.

3.8.3 Process of intumescence

The advantageous ability to see past a luminous diffusion flame using a thermal imaging system was utilised to study the process of intumescence. The camera system was set to record once the flame was switched on. The spectral range of the camera was set to capture temperatures in the range of 0 ^{0}C to 500 ^{0}C at a framing rate of 50 fps. The process of intumescence and physical aspects unique to individual formulations were identified and analysed through this technique. During intumescence, there were two key stages identified that were consistent in all formulations.

A typical physical feature observed was the appearance of *pustules*. Pustules were defined as bubbles that appeared on the surface of the paint. There appearance was a result of sporadic expulsion of spumific gases near the surface in the initial phase of char formation. Once the appearance of pustules was complete, it was marked by the start of the second stage in which the sample started to intumesce and the char was observed to grow away from the surface of the substrate. Duquesne [8] suggested that during the process of intumescence, the surface of the sample dehydrated and the surface texture was observed to change form a semi-viscous liquid to a solid frozen char. Once frozen, the char was observed to intumesce. Similar behavior was observed amongst the formulations tested in this work. The appearance of pustules overlapped the dehydration phase followed by the growth phase. The figure 3.21 illustrates test case for CPF1 formulations and both key stages have been identified. Pustules were seen as high temperature hotspots relative to a cooler surface.

Appearance of pustules (0-180 s)

67
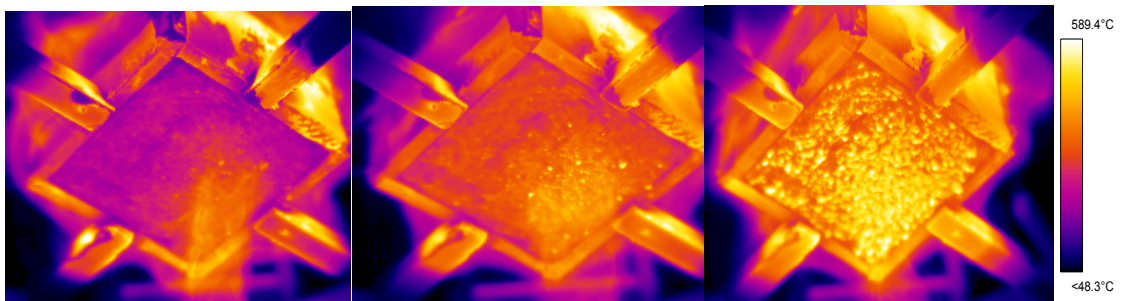
Phase shift- Char starts to intumescence (180-480s)
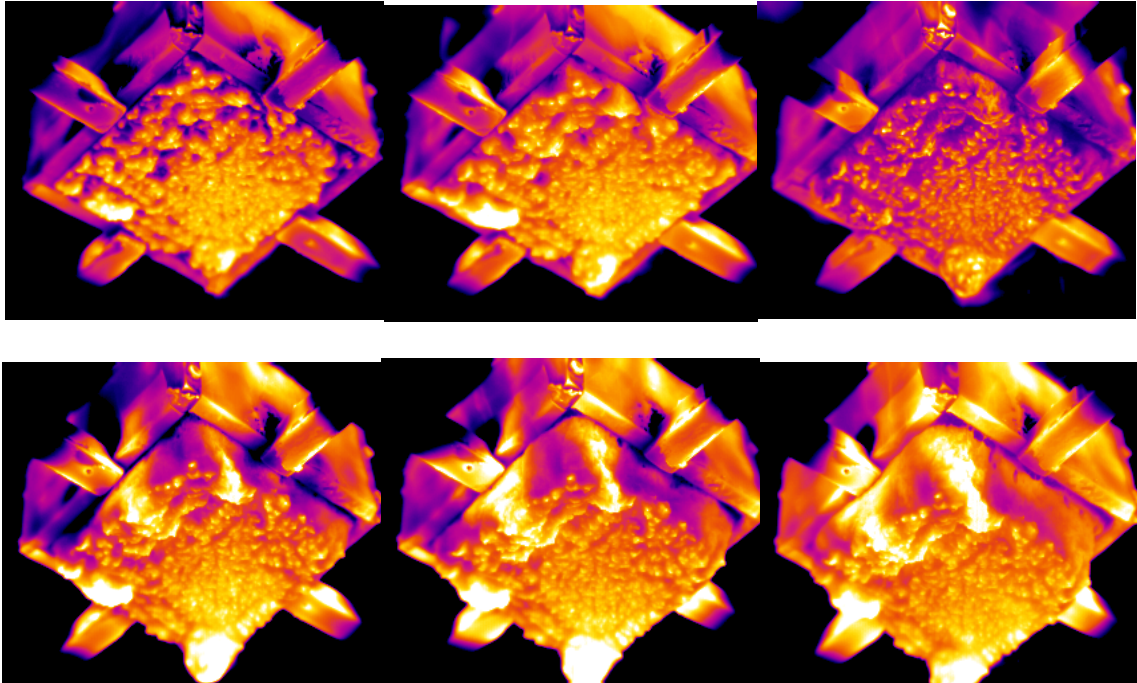
Figure 3.21. *Thermal imaging for H/D=60 t=1mm v = 6.67 m^e/s at 60s intervals 0-480s highlighting key phase shift as it occurred- first half shows development of pustules on surface followed by bulk of char expansion.*

The density, frequency, size of pustules and the second stage of growth varied based on experimental conditions, type of formulations and the heating technique. Furthermore, there were similarities between formulations designed for a specific fire condition as well, which are discussed further and presented in the chapter 4.

3.8.4   Surface Thermal Profile

The temperature variation across the surface i-e *surface thermal profile* of the sample was analysed using the ThermaCam software. The software comprised of a simple GUI (Graphic User Interface) that allowed its user various tools for temperature analysis as shown in figure 3.22.

The resulting output of the GUI comprised of a thermal image with an associated colour coded temperature range as shown in the figure 3.22. Any changes in the viewing area were seen whilst the data was recorded offering the user an instantaneous analysis of the test section. The *spot* and the *line* tool, also illustrated in the figure 3.29, were handy input tools that were used frequently to measure various temperature-based parameters. They are discussed in the light of the parameters measured.
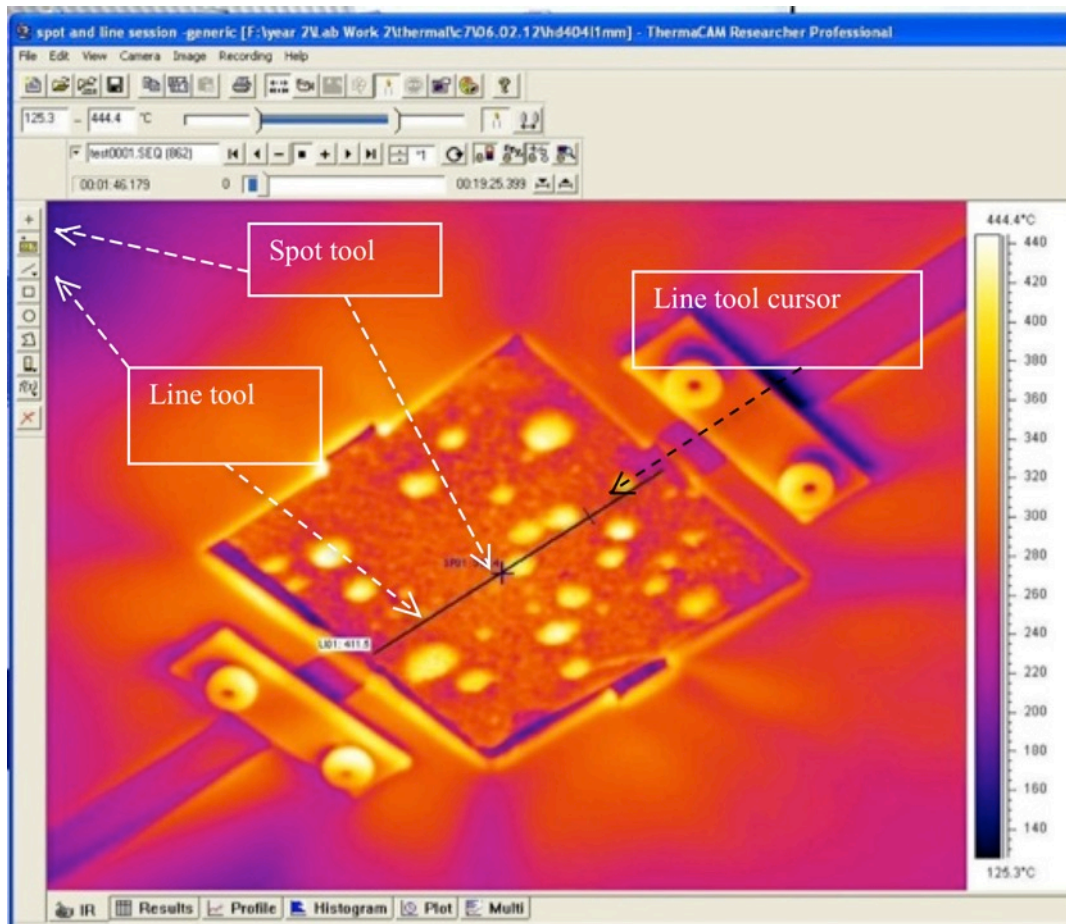
Figure 3.22. ThermaCam software GUI highlighting spot and line tool; HPF1 sample

In most cases, the line was drawn through the centre of the plate. The resulting thermal profile varied from being highly uneven due to appearance of pustules, to a smooth curves based on amount of intumescence. It is proposed this is also because the incident heat flux from the impinging flame setup is non-homogenous in nature. Further parameters such as average, maximum and minimum temperature were useful to analyse the impact of experimental conditions and heating techniques on various formulations. The thermal profiles between the cone setup and impinging flame were compared as well.

3.8.5 Expansion Activation Temperature (EAT)

Expansion Activation Temperature (EAT), EAT_b, was defined as the substrate temperature at which a phase shift occurred during the process of intumescence. The shift occurs from the appearance of pustules stage to growth of char. Similar observation made by Duquesne[8].

EAT was measured using the spot tool function in the ThermaCam software. The spot tool was used to measure temperature at individual points on the surface of the paint. This was not possible if the flame was turned on. Therefore, the temperature at the centre of the panel was measured at discrete substrate temperature T_b during the *burnout* sequence for flame setup. A burnout sequence was not required when measuring under the cone heater setup.

Figure 3.23a illustrates the GUI of the thermal imaging software during measurement of the surface temperature at a typical burnout. Furthermore, a combination of discrete measurements in a single test case is also presented figure 3.23b.
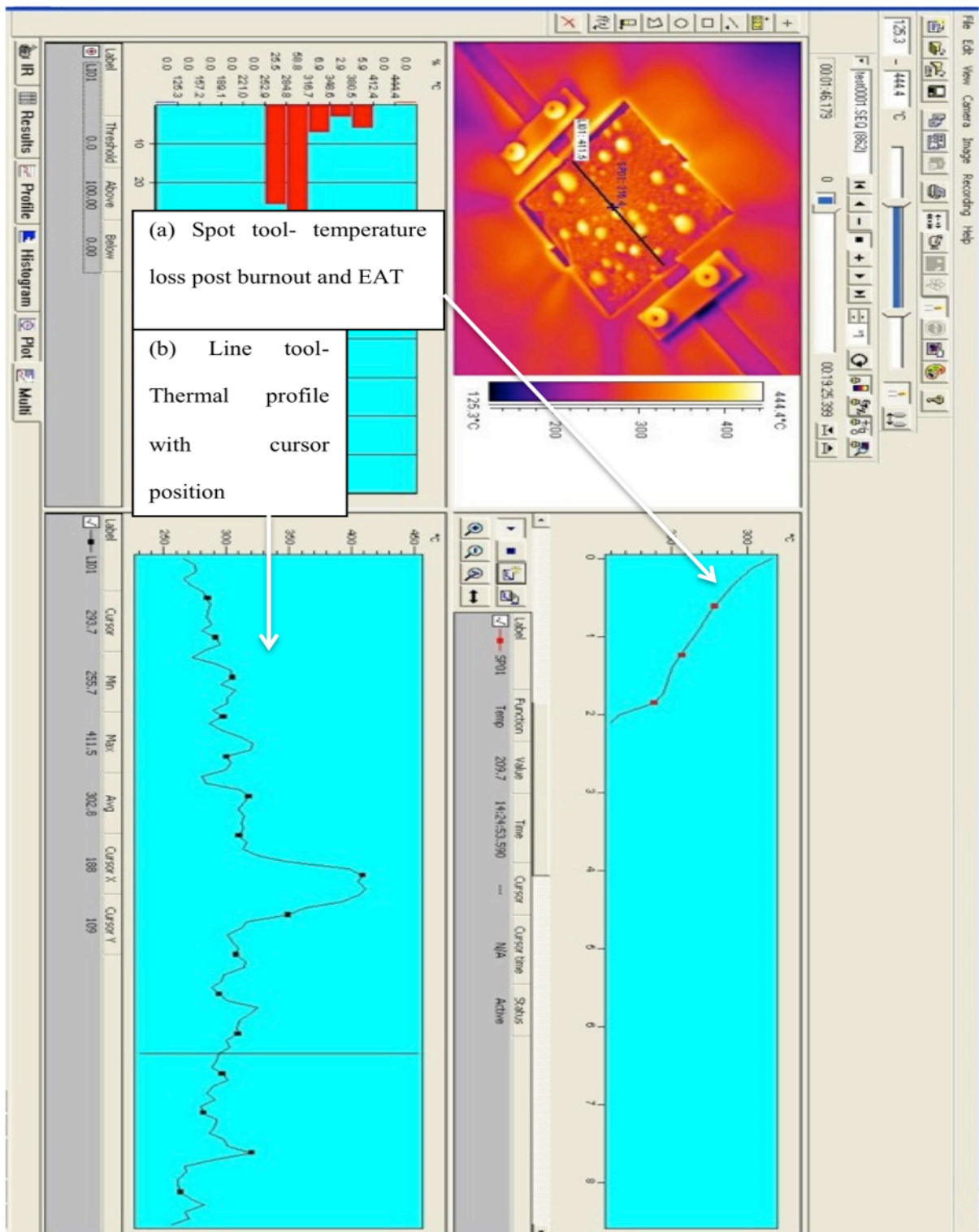
Figure 3.23(a). ThermaCam analysis GUI (a) Spot tool heat loss curve (b) Line tool Thermal Profile
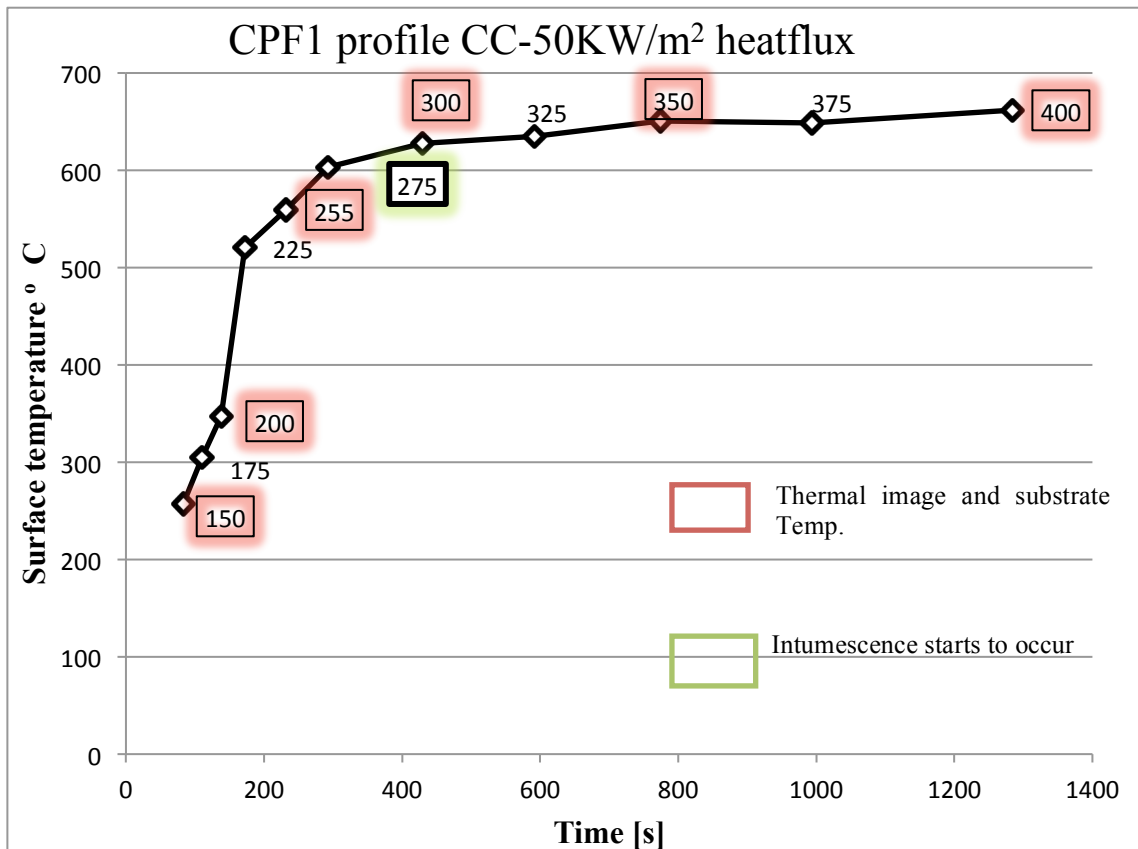
Figure 3.23(b). Surface temperature profile for CPF1 under cone heater- highlighting EAT$_b$.

The results, discussed in the next chapter, highlighted that the value of EAT$_b$, in most cases, was consistent in a formulation irrespective of the heating height. It was also found to be independent of the surface temperature. Different behaviours prior and after the EAT were observed unique to the formulation being tested. The discussion and the effect of experimental conditions will be presented in the next chapter.

3.8.6 Heat Loss Rate

The char produced through intumescence is thin light and crumbly in nature. Therefore, it has a very low thermal inertia that gives it the ability to release heat very quickly. The heat loss rate and rate of change of temperature of a char sample was observed using the spot tool in the ThermaCam software. A cursory investigation revealed that when the flame was extinguished during a burnout sequence, the char sample dissipated heat up to a rate of up to 100 K/sec and achieved steady state within a relatively small timeframe. The nature of the formulation and degree of intumescence that were directly related to the experimental conditions had an impact on the rate of heat loss as well.

3.8.7 Measurement of char growth

The thermal imaging camera was positioned to observe the T-panels as they were heated under the cone heater. The samples were positioned so the cross section of the panel is perpendicular to the viewing plane of the camera (latitudinal view).

The data was captured as a complete recording of the experiment in a movie format. Images were extracted at discrete temperatures points. These temperature points were recorded for the substrate by the thermocouple. The captured data is illustrated in figure 3.24. The maximum temperature that was recorded was 400^0C. Once the substrate reached this temperature, the time to reach this critical temperature was recorded.
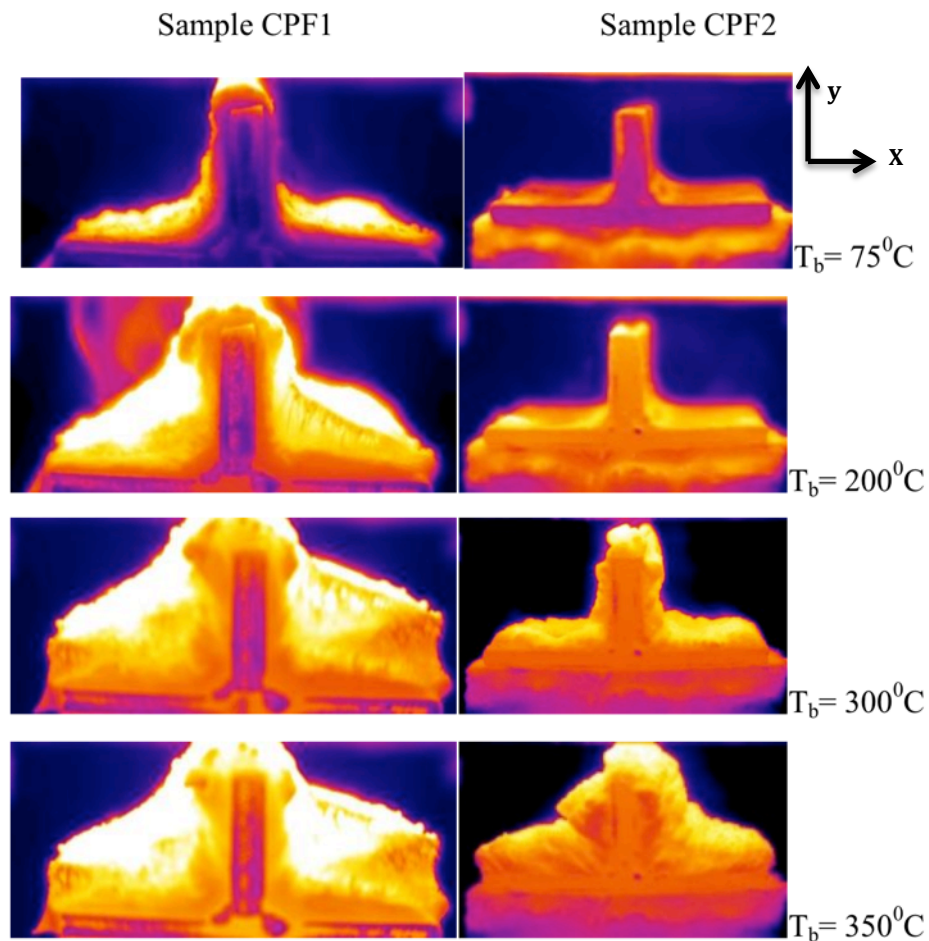
Figure 3.24. Sample CPF1 (left) and CPF2 (left) char growth patterns at various substrate temperatures heating rate measured under a cone heater at 65kW/m2.

The extracted images were imported into MatLab and using a basic image analysis code the boundary of the growing char is tracked with respect to T_b (^0C), temperature of the substrate recorded by the thermocouple, and time (s). The in-house code was designed to first crop all the images with the base of the panel as the reference. The basic RGB (Red

Green Blue) values were enhanced and the best representative of the enhancement was selected. In this case, the blue element of the every pixels individual RGB value was enhanced.

The code was designed to read every pixel as a 3x3 matrix. In the matrix the read pixel becomes the central element, the remaining 8 elements represent the immediate 8 adjacent pixels. This 3x3 filtration matrix allowed the moving boundary to be tracked very accurately. The processed images were then subtracted in a sequential order. The resulting array of values represented the rate of change of pixel i-e the change in the height of the char.

The processed images were converted into black & white to clearly highlight and track the growing char layer. The algorithm tracks every pixel and a white pixel has a value of 1 whereas a black pixel is 0. The pixels were tracked top to bottom (-y axis) for every value left to right (X axis). The converted thermal images from figure 3.31 are illustrated in figure 3.25.

Finally a single row vector was generated in which every value represented the pixel height. The pixel height is the growth of the char from the base of the panel for a specified time or temperature, T_b.
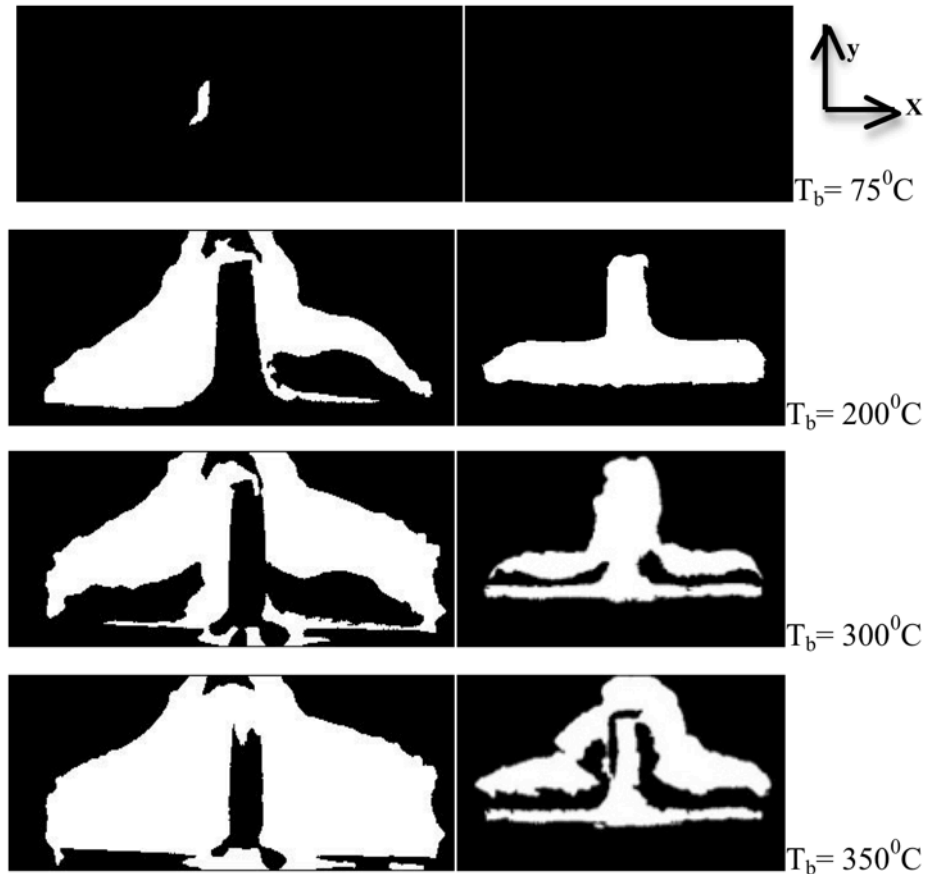
Figure 3.25. CPF1 (left) and C2 (right) char growth patterns converted and tracked using image processing algorithm. The methodology was successfully implemented to track char growth in complex shapes under a uniform radiative heat flux.

After the CC testing, the method was used to track char growth in flat and T-panels under an impinging flamer setup to compare and analyse the char growth patterns. Several difficulties were encountered that presented as inaccuracies. The presence of the flame could not be filtered using the Matlab algorithm and affected the output char growth values. The burnout times was increased to ensure the flame was completely extinguished to improve the accuracy of the results. However, the char cooled down too quickly and the resulting values had an unacceptable level of inaccuracies.

Finally, some pilot tests were conducted using a premixed flame. A premixed flame, as discussed earlier in chapter 2, is not as luminescent as a yellow diffusion flame. Therefore, the tracking method had some clear prospects when used with a premixed flame than a diffusion flame. Further discussion in light of the results would be presented in the next chapter.

3.9   Conclusion

The details of the experimental setup have been discussed in this chapter. This included the specification for the two burners used, experimental rig setup and the plate holding device including the use of the heat shield. A brief overview of paint formulations used, test panel specification, paint application and test panel preparation has been also presented. LabView and its use to control the fuel flow rate, the variation in experimental conditions and the use of a burnout sequence were discussed in light of the objective of this work- investigate the physical aspects of intumescence under an impinging flame setup.

The use of the imaging techniques introduced in Chapter 2 including Schlieren technique Digital and Thermal imaging have been discussed. The use of thermocouple to measure substrate temperature was also presented. The experimental setup of each technique with respect to the heating input, impinging flame and the cone calorimeter, has been given. A variety of methodologies designed to study intumescence using these techniques have been presented. These include flow visualisation focusing on the flame-paint interaction as intumescence occurred followed by a method to measure the rate of char growth. Once a test was complete, digital imaging was used to analyse a variety of physical aspects of intumescence. These included surface and cross sectional texture of the resulting char.

Thermocouples were primarily used to measure substrate temperature with time. The method of studying the time to reach a failure temperature, defined as time to failure (TTF), for a variety of experimental conditions has been presented. Their use was also extended to develop a method that would allow comparison of heating rate between a non-uniform (impinging flame) and uniform (cone meter) heating input. The temperature curves were also used to investigate the effect of a burnout on TTF.

Thermal imaging was used in almost all modes of investigation and proved to be a highly productive diagnostic technique. Formulations were applied to flat and T-panels and studied under impinging and a cone heater setup. A number of methodologies developed have been discussed. These included studying the process of intumescence, thermal profile of the char surface, Expansion Activation Temperature (EAT) and heat loss rate. Finally, an image processing method has been discussed highlighting the use of thermal imaging to track char growth during complex intumescence on T-panels.

Overall, the Schlieren technique, used for the first time in such studies, has helped visualise the flame and paint interaction highlighting the impact on intumescence due to separation between source and target and a variety of other parameters. The combined temperature based information gained from the use of Thermal imaging (surface) and thermocouples (substrate) has added an extra and innovative dimension to the study of intumescence.

The greatest advantage of using these techniques is the ability to study the process of intumescence in its entirety and not just rely on information gained from strategically positioned thermocouples. The use of such diagnostic techniques in the field of fire protection, specifically intumescent paints, is unique and novel in nature. A variety of physical aspects have been studied using these techniques that have not been studied in great detail before. The results and analysis will now be presented in the following chapters.

Chapter4.   Results   and   Analysis: Impinging flame setup

4.1   Introduction

This chapter analyses the results of tests conducted using various heating configurations. The primary technique used was an impinging flame configuration onto a flat square. The results focus on different fundamental properties of intumescent coatings such as the process of intumescence, char structures, expansion time history, char failure and thermal resistivity. The impact on the four formulations designed for cellulosic and hydrocarbon based fires is presented. They are studied using the previously discussed diagnostic techniques. TTF data from the thermocouples is used to analyse the impact of heating rate, thermal loading and film thickness on intumescence. The effect on the physical appearance of the char for different coatings is also discussed focusing on surface topology and internal char structure. The Schlieren technique is used to visualise the variation in flow as the char intumesces.

4.2   Process of intumescence

A summary of the intumescence process was presented in chapter 2. It was described as a series of complex chemical reactions that result in the production of copious amounts of gases within a visco-elastic matrix. The matrix expands as the gases try to escape. Simultaneously, crosslinking reactions cause the matrix to harden. The end product is a swollen carbon rich char comprising of a multi cellular internal structure that acts as a thermal barrier between the heat source and the substrate surface.

These observations were found to be consistent with a CPF 1 sample observed under an impinging flame using a thermal imaging system. In addition to the expansion and visco-elastic behaviour, the appearance of pustules was also observed. Images were taken at an interval of 60s from 0 up to 480s as shown in figure 4.1.

Between 0 - 120s the appearance of small pustules covering the surface were observed. The density and size of the pustule was dependent on the heating conditions.

The pustules started to grow from 180 to 240s. The surface behaved as a semi-solid/liquid visco-elastic mix. Such behaviour is difficult to observe or identify in still frames but it was clearly seen when thermal recordings were reviewed as a video. Pustules were observed to amalgamate with each other and form bigger pustules, which is indicative of first signs of intumescence.

After 240s, a series of exothermic reactions resulted in the formation of gases under the surface of the char. The complete surface of the panel intumesced and the char thickness increased. Char expansion was a direct result of these gases trying to escape from the surface. During this time frame, dehydration occurred as part of the intumescence process and the surface texture changed from a semi-liquid phase to a solid frozen carbon rich char[3].

As the char started to grow it was also observed to shrink from the sides, figure 4.1 (480s frame), and the corners of the substrate were slightly exposed. This shrinking phenomenon was observed in all the experiments conducted and occurred near the corners of the panels. This was due to the mass loss associated as part of the intumescence process[3] that resulted in the contraction (shrinkage) of the initial applied layer of paint and exposeing the edges of the steel plate. . Various TGA experiments performed on a variety of combination of APP/PER/MEL coatings and their derivatives have reported that, due to thermal degradation, gases are formed at the expense of the mass of the original film thickness. The mass loss can vary between 40 to 80 % of the original mass [25, 26, 99-102].

The formulations were tested under similar conditions. Even though the overall process of intumescence remained the same, a few differences were noted. CPF2, a formulation also designed for cellulosic fires, exhibited a delayed start (appearance of pustules) and a significantly more profuse char expansion than any other formulation. It also exhibited a highly viscous char under a heat source that shrank and dried instantly when the heat source was turned off.

In HPF 1, the char structure was predominantly flat apart from the appearance of some large pustules. Their appearance was sporadic in terms of position and depended on application accuracy and heating regimes. They only appeared in the initial stages of intumescence similar to other samples. Their appearance was observed at very early

stages of the test relative to other formulations. HPF 1 did not show any visible characteristics of a visco-elastic mixture in contrast to the other coatings
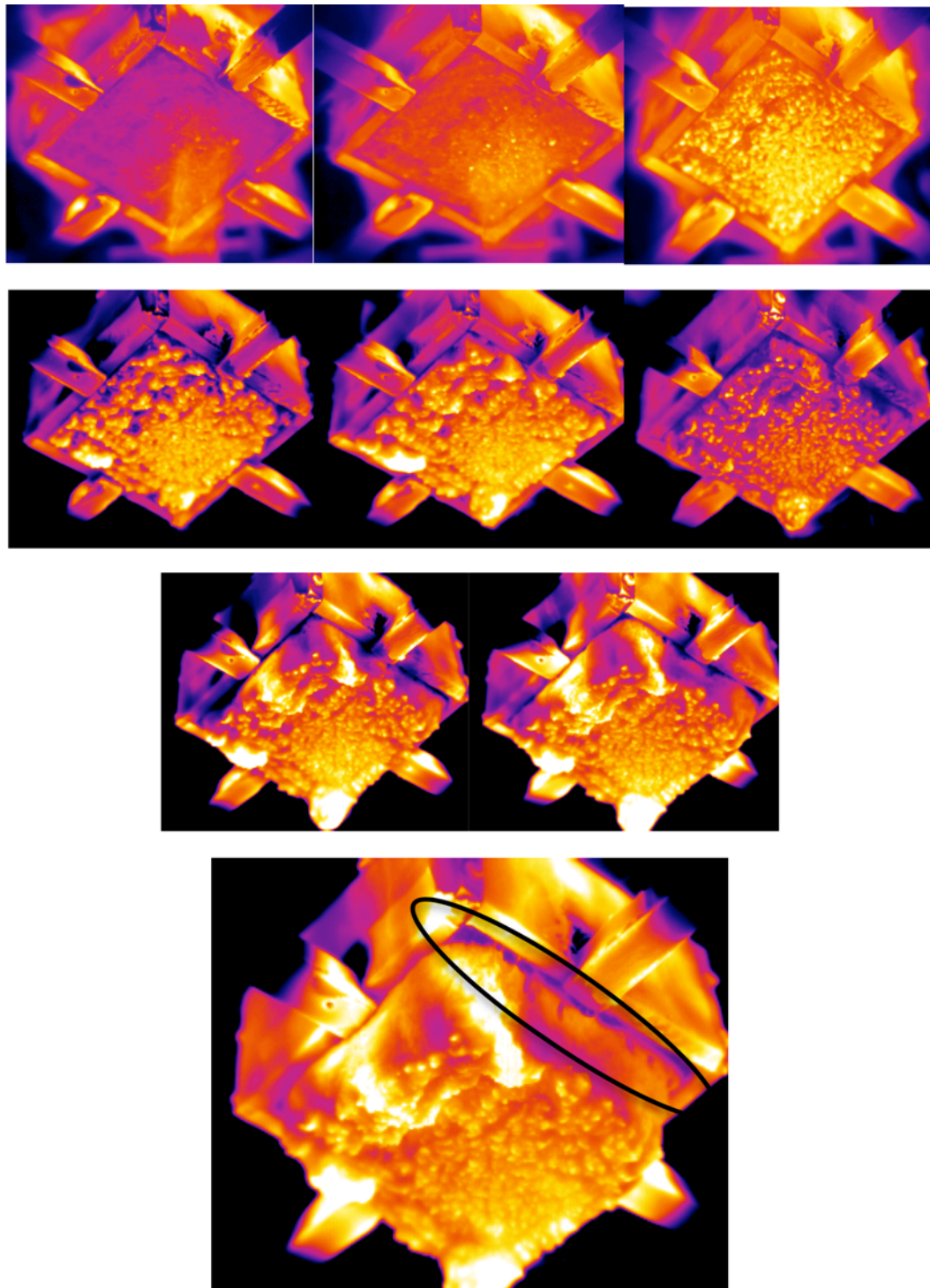
Figure 4.1. Thermal imaging for H/D=60 t=1mm v = 6.67 m^e/s at 60s intervals for 480s for CPF 1 highlighting appearance of pustules on the surface, expansion of char followed by shrinkage at edges.

HPF 1 had a rigid flat expansion. The expanded char replicated the exact shape of the flat panel with sharp edges and features. Due to small expansion ratio, it was extremely difficult to observe when the intumescence had started. Expansion process was slow and

over a long duration of time. The appearance and settling of the pustules at very early stages in the experiment indicated that the process of intumescence started at a lower substrate temperature (confirmed by further analysis).. Finally, when the sample had fully intumesced, a solid char covering the complete panel was observed. There was no shrinkage at the corners of the sample implying a small mass loss. Figure 4.2 illustrates that with increasing thickness of application the size of the pustules became bigger. Furthermore, the brighter yellow colour also suggests that the pustules were at a higher temperature than the rest of the surface.
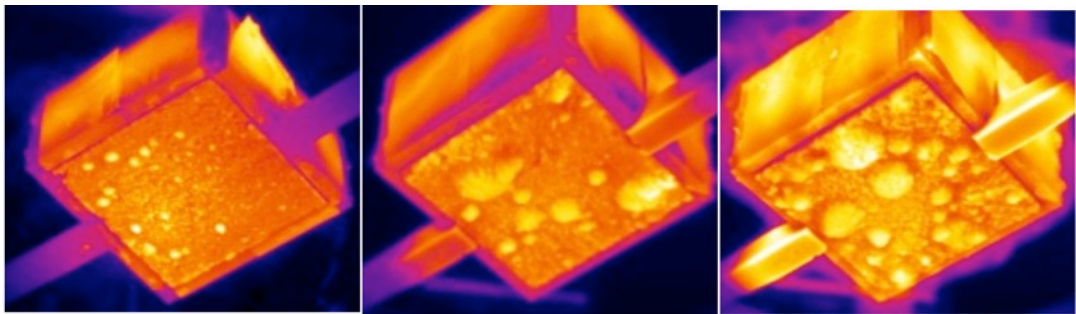
Figure 4.2. Thermal imaging illustrating pustule appearance and size at t=1, 2 and 3 mm respectively -HPF 1.

In HPF 2, the initial stage and appearance of pustules was similar to that of CPF 1. Pustules were distinctive in size and shape and dominate the complete surface of the sample. Unlike HPF 1, the sample was visibly viscous in nature. However, it was less so than the CPF coatings.

The appearance of pustules was observed up until $T_{b,} = 300 \ ^{0}C$, . This was followed by the start of the expansion stage. During the expansion process, the spumific gases were produced under the surface, similar to the other formulations and steady growth of the char was observed. However, around $T_{b,} = 310 \ ^{0}C$, a sudden swelling of the char was observed. The released gases exerted a force on the char. The growth appeared to be swelling-like rather than intumescence. It happened very rapidly over a very small amount of time (10s). The released gases escaped leaving cracks on the surface of the char. This was different to the other coatings.

Shown in Figure 4.3 are schlieren images taken at sequential time interval of 15 seconds between $T_b = 300 – 310^{0}C$ and highlights the sudden expansion seen in HPF 2. The sudden swelling over a period of 30 s can be obsereveed in the last 3 images. The parabolic shape of the intumescing char is very distinctive. Based on the sequence of

images it can be seen that the expansion of char occurs very abruptly, over a small period of time. This behaviour was not observed for any other formulation.
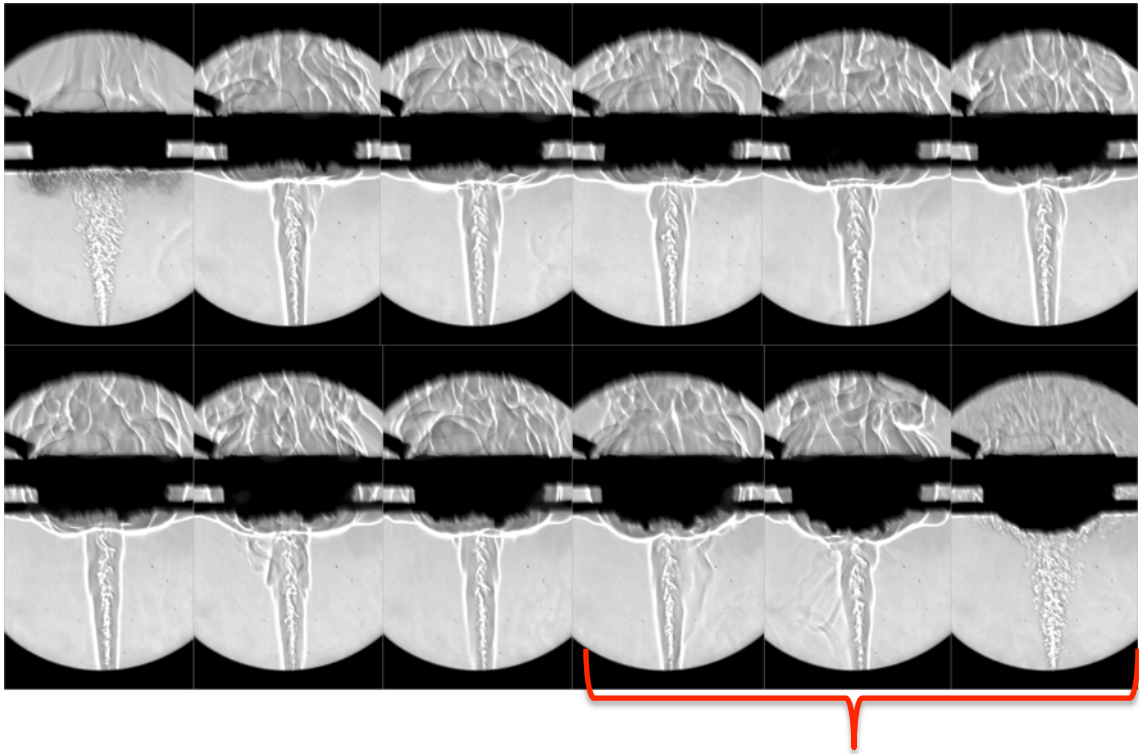
Figure 4.3. Sequential *Schlieren images at 15 s apart for H/D = 40 v= 6.67 m³/s t= 1mm test between Tb = 300 ^{0}C – 310^{0}C – HPF 2*

The performance of coatings under an impinging flame can provide useful information to formulators. It can assist them in choosing a suitable coating for different applications. In this case, HPF 1 can be used in scenarios where high mechanical strength, low expansion ratio and minimum mass loss are important criterion. This is relevant to off shore oilrigs where the risk of high-pressure leaks resulting in jet fires is very likely. Similarly, CPF1 can be a good all round coating in conditions where high expansion ratios and TTF are part of the design requirements.

The other two formulations have profuse char expansions and delayed reaction sequence which could be valuable in scenarios where such a characteristics can be incorporated in a fire fighting strategy.

4.3   Expulsions and Pustules

The appearance of pustules was analysed further using the Schlieren imaging. Tests were conducted under different Schlieren sensitivities, illustrated in figure 4.4, revealed the reason why pustules appeared during the process of intumescence. It was observed

that when the build up of gases under the solid char surface tried to escape, it resulted in the formation of a pustule. These gases would occasionally break the surface resulting in an 'expulsion'.
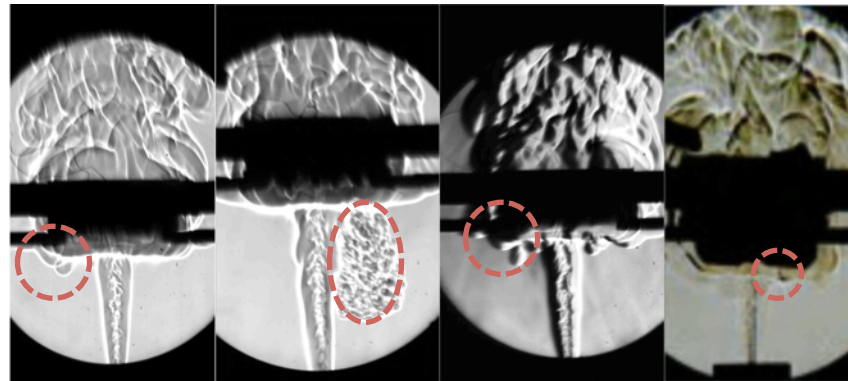
(i) HPF 2   (ii) HPF 1   (iii) CPF 2   (iv) CPF 1

Figure 4.4 Changes in the Schlieren system sensitivities and expulsion shown for each coating.

Expulsions were observed in all the coatings. In HPF 2 during the process of intumescence the surface was very active. Small and frequent expulsions were observed resulting in pustules that were small in size. Successions of images captured at the rate of 50 fps 0.02 s apart are shown in figure 4.5 where the expulsions in HPF 2 are highlighted.
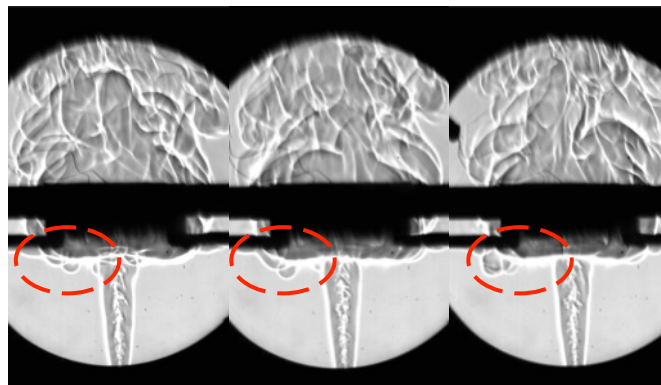
Figure 4.5. Sequential images 0.02s apart for various expulsion strength and patterns in HPF 2

The expulsion pattern of the HPF 1 was very different to HPF 2. In HPF 1 the pustules were sporadic in appearance and frequency. Some pustules would crack resulting in a forceful expulsion of gas through the flame/paint boundary (Fig. 4.4 (ii)) indicating that the gases were trapped under high pressure.

In CPF 2, the highly active surface resulted in a popping sound heard due to expulsions. Schlieren imaging showed that this was because of little bursts of gases through the surface of the flame from the beginning of the test. They stopped once the expansions

started. A sequence of images 0.02s apart is illustrated in figure 4.6 and similar to HPF 2 the little expulsions can be observed near the flame/paint boundary.
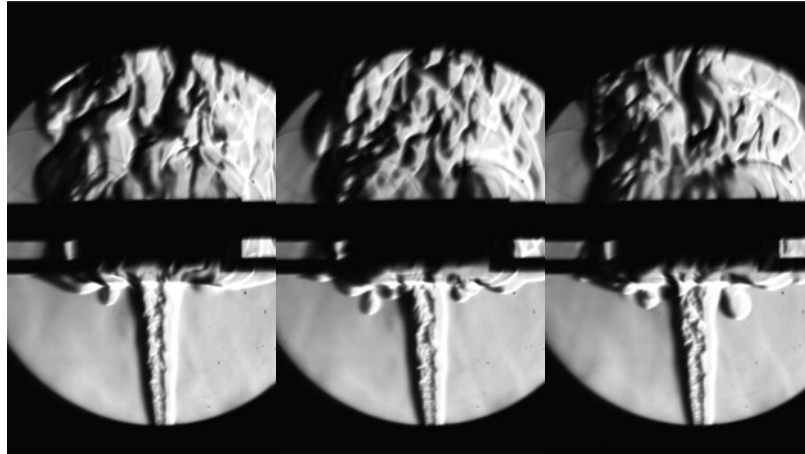
Figure 4.6. Sequential images at 0.02s apart for various expulsion strengths and patterns – CPF 2

The release of gases as pustules form on the surface of the char was uniquely captured through the use of the Schlieren technique and has not been reported previously. It was not possible to determine the spatial positioning of the expulsions using Schlieren imaging. However, thermal imaging revealed that they were dispersed over the surface. This is a good example of how this research unified analysis from two different techniques in order to gain understanding of a previously unreported phenomenon.

Once the expulsions and pustule appearance had stopped, it meant the char surface had fully developed. This was followed by the char expansion stage. This phenomenon was also studied using the Schlieren technique and the Expansion Activation Temperature (EAT) was determined. Furthermore, the technique was used to track char growth and determine rate of char growth which is discussed in the following section.

4.4   Surface texture

The appearance of pustules on the surface of a coating changed its surface texture. These pustules were temperature hotspots. They contribute towards localised uneven heat transfer through the coating. It was also found that their number, size and appearance changed with the Nozzle to Plate (NTP) distance.

The variation in CPF is illustrated in figure 4.7. The appearance of pustules increased with separation. At H/D=20, no pustules were observed. As NTP was increased to H/D=30, the first signs of pustules were observed. At both separations the centre of the panel had a cool core. This meant that the heating rate and therefore, the visco elastic

behaviour were restricted. Expulsion did not break through surface of the char, explaining the lack of intumescence and pustules.

The highest density and size of pustules was observed at H/D=80 where TTF was the smallest. This implied that at approaching this separation the rate of heat transfer, chemical reaction and therefore, thermal efficiency was at its maximum. Hence it can be concluded that heating rate had an impact on the appearance and quality of the pustules.

Figure 4.7. (Top left L-R) surface texture of char highlighting variation in pustule size and density for NTP separations of H/D = 20, 30, 40, 60, 80, 90, 100, 110 - CPF 1

The surface texture at low and high separations for CPF 2 is shown in figure 4.8. In all the tests conducted, the resulting char had a smooth surface with no evidence of pustules. Thermal imaging data revealed that pustules did form during the first stage of intumescence (surface activity). However, the viscosity of the mix was so high that they were not able to hold shape or size.
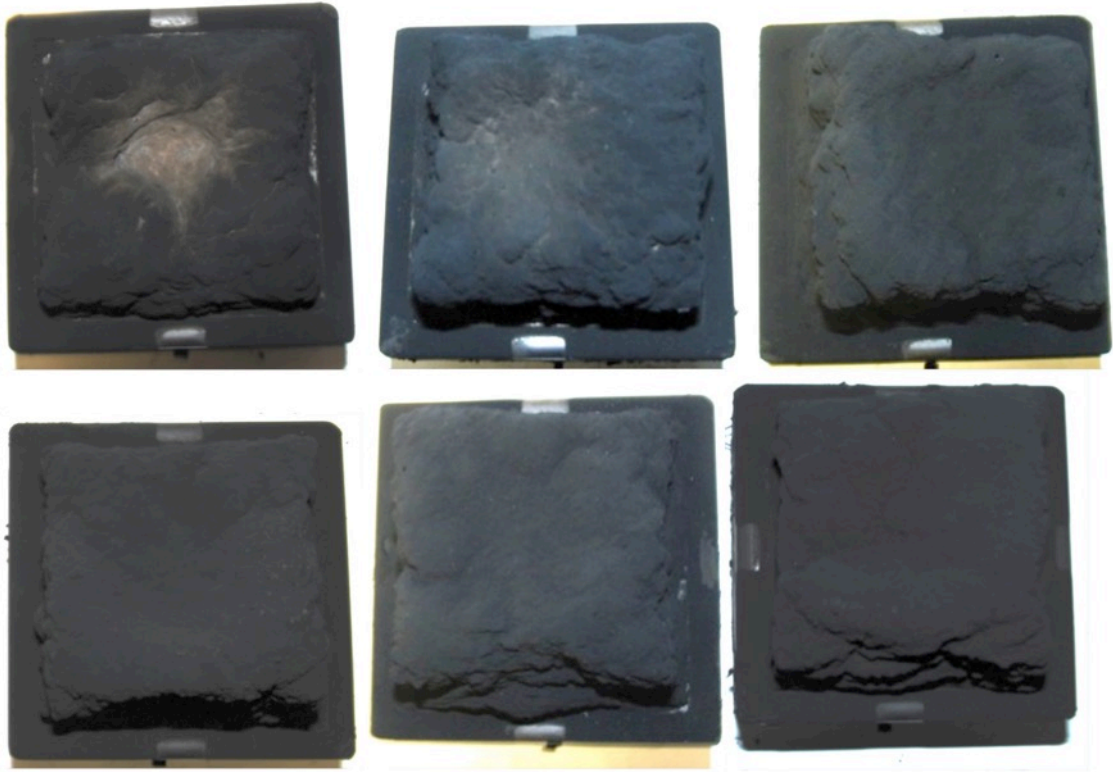
Figure 4.8. (Top left L-R)) Surface texture of char highlighting variation in pustule size and density for NTP separations of H/D = 30, 40, 60, 70, 80, 90 – CPF 2

The combination of small expansion ratio and soot deposits on the surface of a black char made it difficult to observe and analyse the surface of HPF 1. Pustules were observed on the surface during tests. Their appearance was clearly visible to naked eye when coating thickness was increased. Figure 4.2 highlighted that the appearance of pustule was very sporadic. The relative size of the pustule was significantly larger than any other formulation. Cracks or any other significant feature were not observed in this formulation.

The surface of HPF 2 was dominated with pustules that had a very distinctive shape. The size of the pustules was effected by heating rates. At higher separations, a smaller pustule size was observed. There were cracks on the surface and the edges. This was primarily due the spumific gases, which forced their way out of the surface in a sudden burst. This resulted in swelling of the char structure, which consequently lead to the formation of deep cracks in the char. Figure 4.9 compares various char surface structures at a variety of separations. Furthermore, a comparison of the pustule size at H/D = 30 and H/D = 70 is shown in figure 4.10.
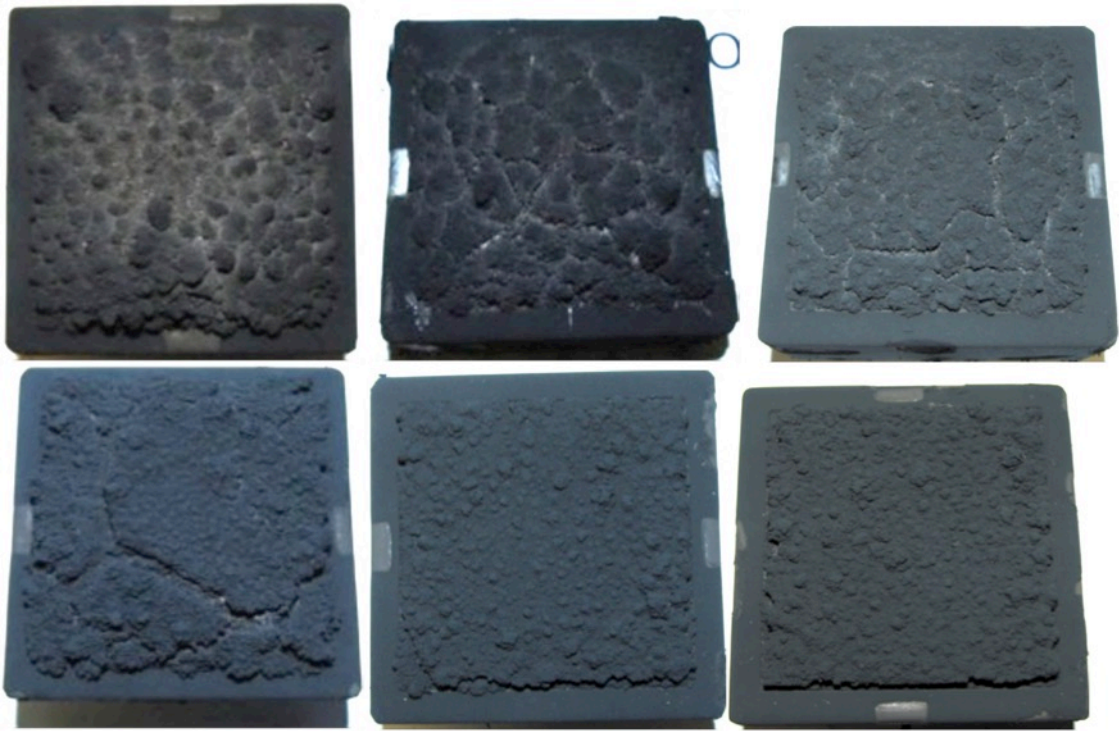
Figure 4.9. (Top left L-R)) surface texture of char highlighting variation in pustule size and density for NTP separations of H/D =30, 40, 60, 70, 90, 100 – HPF 2
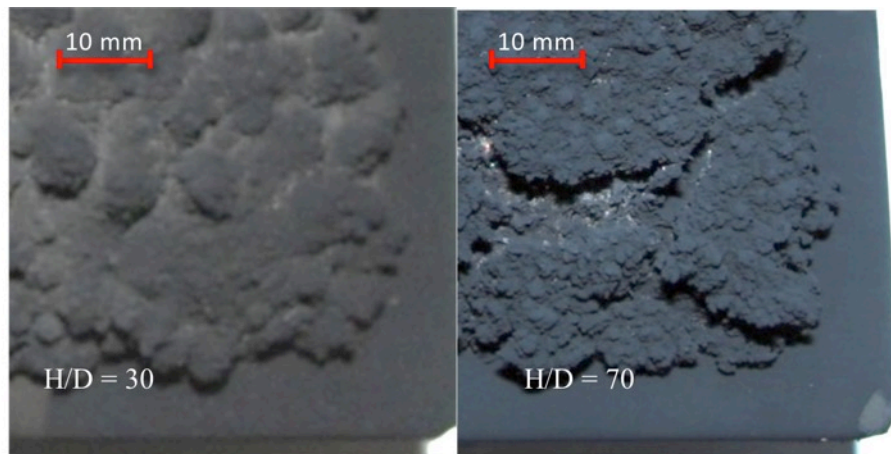
Figure 4.10. Pustule shape and size and appearance of cracks in HPF 2 observed at H/D – 30 and 70.

4.5   Rate of Char growth

Image processing software was utilised to extract char thickness data from the Schlieren images. Data was recorded at 10 different timings during each experiment. The intention was to capture images of the growing char and calculate char thickness with respect to time.

A set of sample images are shown in figure 4.11. The char thickness was observed clearly and easily measured using the pixel measurement technique. Intumescence was

measured using the pixel length between the initial and final level of intumescence. Measurements were calibrated using the height of the cradle as a reference length.
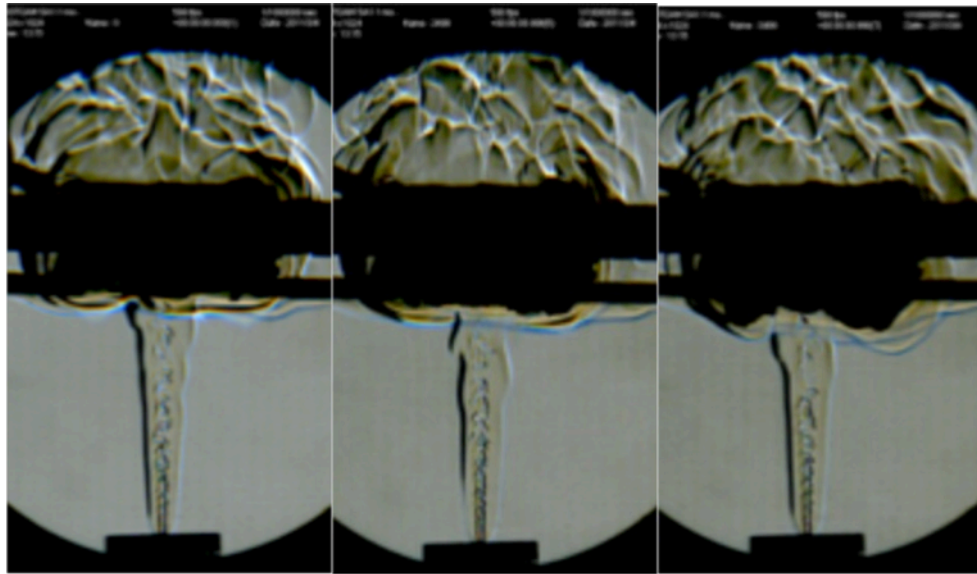
Figure 4.11.Schlieren images for v= 5e-5 m-3-/s at time = [60, 240 and 360] s for CPF 1 highlighting the increased turbulence in flow structure of the flame and hot gas upstream.

The char heights were measured for various flow rate configurations at H/D =40 and film thickness = 1mm. Only the maximum char height was measured irrespective of its position. Char height measurements were made for flowrate values summarised in the table 4.1.

Table 4.1. Experimental conditions for Schlieren measurements

Flow rate	Flow rate	Paint Thickness	H/D
Fuel	Fuel		D=4.6mm
v [l/min]	1e-5 [m3/s]	[mm]	H/D
3.00	5.00	1.00	40
6.00	10.00	1.00	40
8.00	13.33	1.00	40

Char thickness against time plots are shown in figure 4.12. Thermal loading had a significant impact on maximum char growth. A 4th order polynomial provied the visual possible fit. The expansion ratio was recorded to be as high as 44 for a fuel flow rate of 13.3x10^{-5} m^3/s as compared to 25 at 5x10^{-5} m^3/s. The expansion ratio increased proportionally to thermal loading.

The rate of reaction presented a similar trend across different flow variations. It increased significantly at approximately 200 s. It continued to increase until almost

complete intumescence was achieved near the 400s mark. The timing of the increase in rate of reaction coincided with the surface freezing indicating that the process has moved to step IV of the piecewise mechanism presented earlier in section 2.2.1.

(a)

(b)

(c)
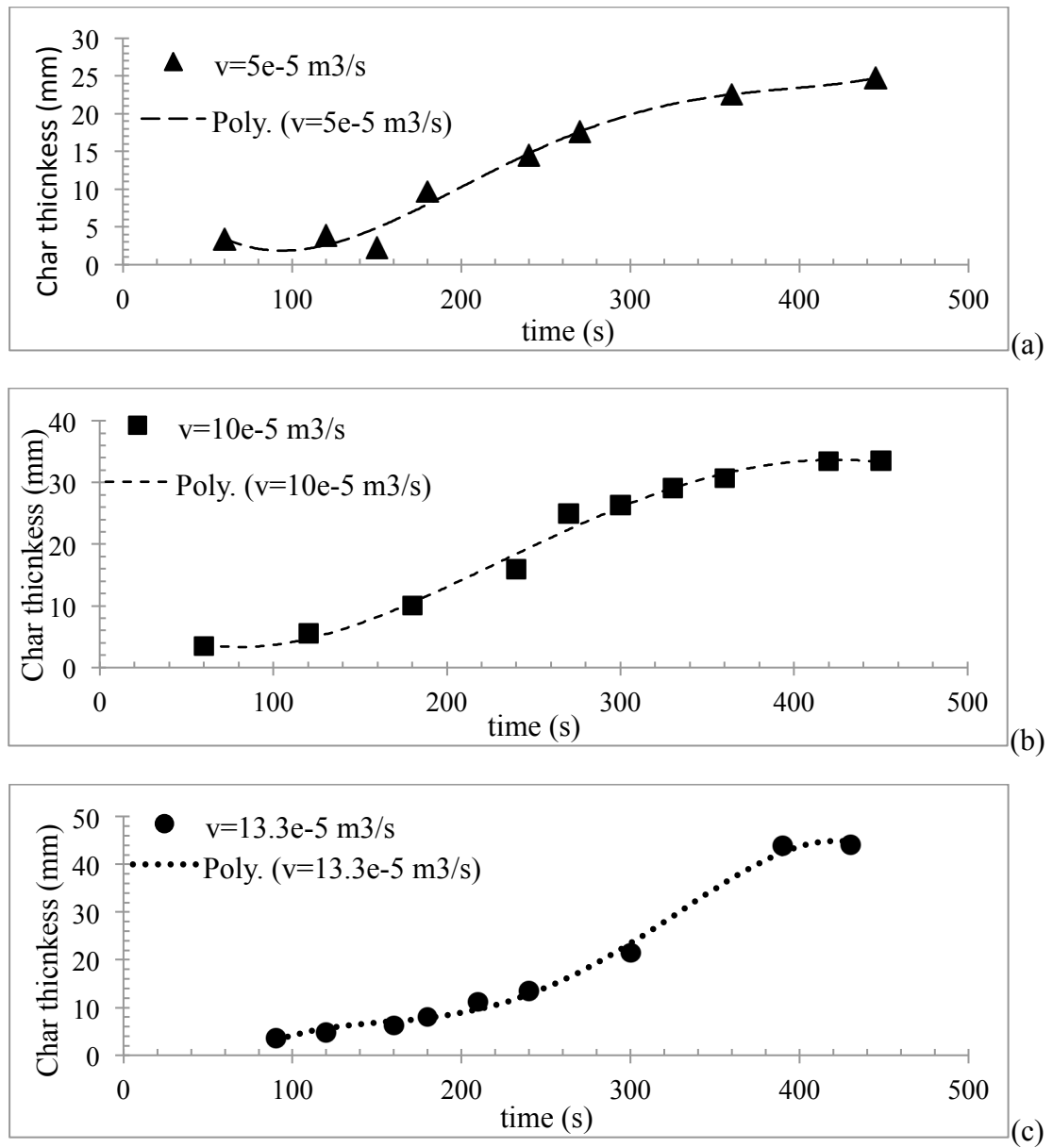
Figure 4.12. Char thickness against time for fuel flow rate of (a) 5e-5 m³/s (b) 10e-5 m³/s (c) 13.3e-5 m³/s – CPF 1

Rate of char growth was analysed with respect to substrate temperature T_b as well and is illustrated in the figure 4.13. Similar trends of growth were observed for the three flow rates. A surge in char growth was observed at approximately $T_b = 275\ ^0C$. This was identified as a potential Expansion Activation Temperature (EAT), EAT_b, for CPF 1. EAT was explored further and the analysis is presented in the next section.
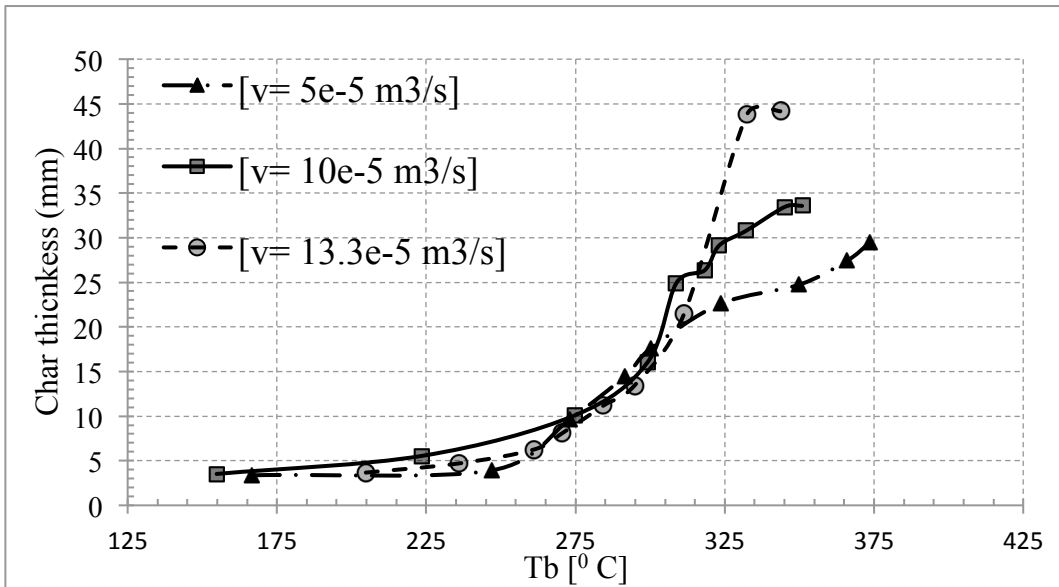
Figure 4.13. Char thickness against Tb for different flow rates using CPF 1

It can be deduced from this data that the thermal loading did not have an impact on the rate of char growth. However, it did have an impact on the maximum char expansion that was higher when the thermal loading at the nozzle was increased. This trend was found to be consistent across all the coating types.

The impact of NTP separation on char growth was also analysed. Figure 4.14 illustrates rate of char growth for a number of NTP separations. The rate of growth varied for different separations. The highest expansion ratio of 33 was recorded. The highest ratio was observed for H/D =60 and the lowest for H/D =30. This is because a higher heating rate was observed at H/D =60 than H/D =30.
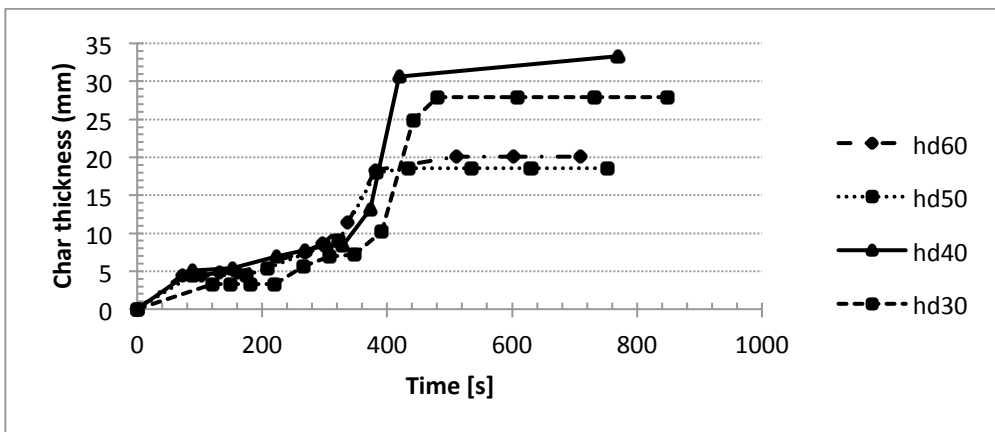
Figure 4.14. Char thickness against time for different NTP separations – HPF 2

Schlieren imaging also provided insight into the diffusion flame structure that was not visible to the naked eye. Figure 4.15 compares the different diffusion flame structures observed using Schlieren technique compared to a digital image. The interaction of the flame with the growing intumescent char can be clearly observed from the Schlieren

images. The amount of fuel impinging onto the surface increased with fuel flow rate. The structure of the flame became broader and the intensity of the flame downstream of the cradle increased. The flame lift off from the burner ring can be observed at v = 10e-5m^3/s.
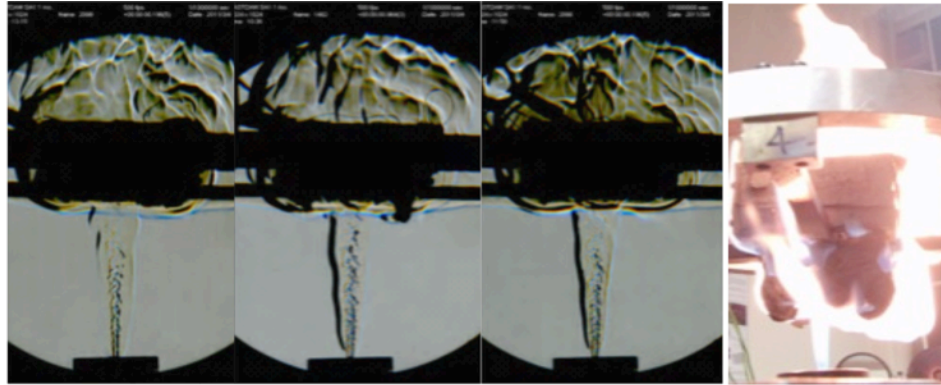
Figure 4.15.Flame structure at different flow rates of v= [5, 10, 13.3 e-5 m3/s] vs. diffusion flame as observed by naked eye

4.6   Expansion Activation Temperature (EAT)

The expansion activation temperature is the substrate temperature at which the rate of char growth increased significantly. This research has indicated that, at this point, all coatings underwent a stage change from surface based activity (expulsion) to profuse char growth (bulk intumescence). The value of EAT was different for each coating due to their unique chemical composition.

CPF 2 exhibited the highest expansion ratio and a distinct change between stages over a small range of substrate temperature. Therefore, its expansion behaviour is presented in order to discuss the phenomenon of EAT. The sample was observed to be very inactive for the first half of the experiment and hardly any expansion was observed. After T_b= 200 ^{o}C, the surface became highly active with numerous tiny expulsions. The main bulk of the intumescence phase was observed within the range of T_b= 320 ^{o}C and 350 ^{o}C. The schematic in figure 4.16, taken at time intervals of 15 seconds between T_b = 310 – 350 ^{0}C, highlights the sudden expansion procedure.
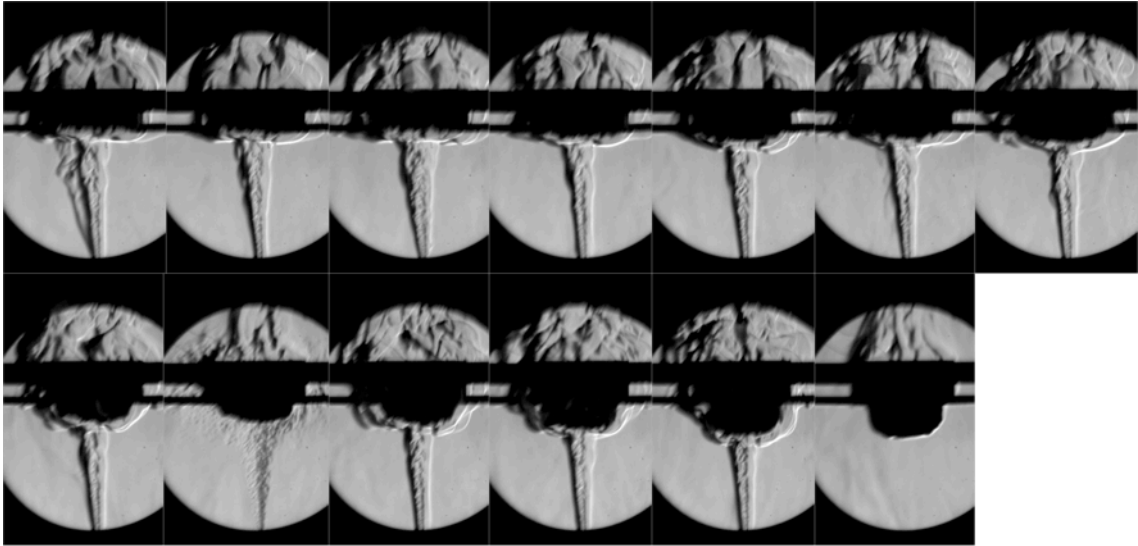
Figure 4.16. Sequential Schlieren images at 15 s apart for H/D = 40 v= 6.67 m3/s and t=1mm test between Tb = 310 ^0C – 350 ^0C – CPF 2

The expansion started at T_b = 320 ^{0}C and was identified as the Expansion Activation Temperature, EAT_b,. Figure 4.17a illustrates the rate of char growth against T_b. The highest rate of growth and expansion ratio were observed for H/D = 60. Char thickness of 45mm were recorded; equivalent of an expansion ratio of 90.
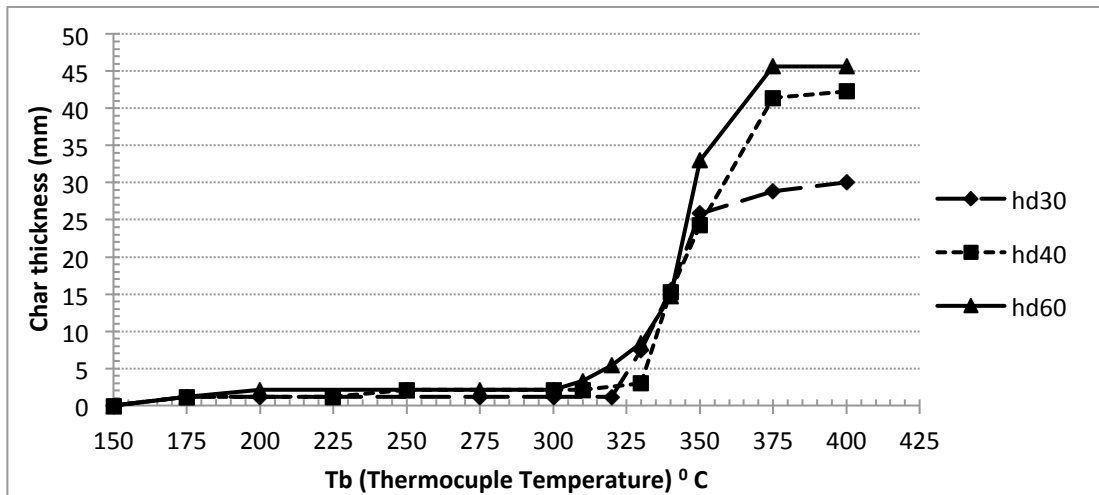
Figure 4.17a. Char thickness against T_b for different NTP separations – CPF 2

Further investigation was performed using the spot measurement tool in thermal imaging analysis. The surface temperature, T_s, was measured at the centre of the panel. Figure 4.17b illustrates the behaviour of T_s and char growth against T_b. T_s, as expected, increased as the sample started to intumesce. Furthermore, the steep change in T_s coincided with the steep change in char height.
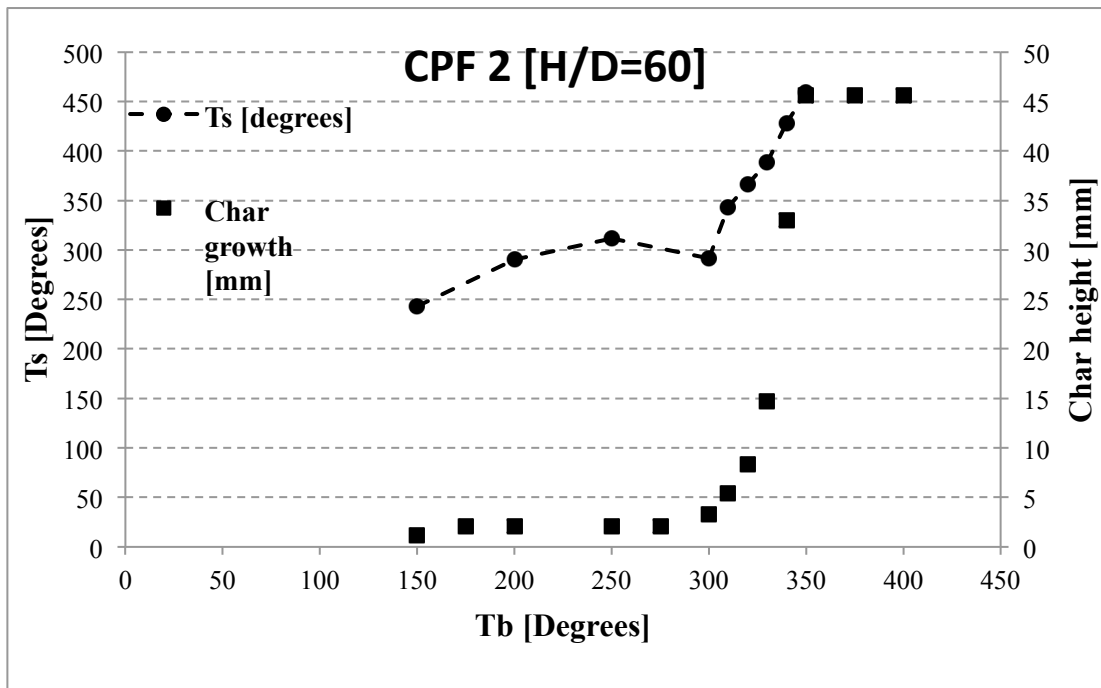
Figure 4.17b. Surface temperature, T_s and Char thickness against T_b – CPF 2

4.7 Expansion-Time History

The objective behind the study was to investigate the effect of heating rates, expansion ratios and thermal loadings by varying NTP separation, film thickness and fuel flow rate respectively on intumescent formulations. The section is divided into subheadings that present the results, observations and analysis based on the experimental conditions. Temperature-time curves, mode shapes and expansion profiles are discussed focusing on observation made in CPF 1. Observations made in other formulations are summarised in adjacent subheading.

4.7.1 Temperature Time curve of the substrate

The observations made during a process of intumescence were presented in section 4.2. The discussion was based on observation made using a thermal imaging system incident at the surface of the coating. It was summarised that, under the impact of an impinging flame, a typical intumescent process:

1. Started with the appearance of pustules on the coating surface.

• This was due to chemical reaction occurring on/near the surface of the coating

Followed by:

2. Expulsion, of varying sizes erupted, from the surface of the coating which caused the appearance and growth of the pustules

3. The complete surface of the panel intumesced and the char thickness increased.

• This was marked by the Expansion Activation Temperature; the temperature at which the pustules had fully matured and the char started to expand away from the substrate

4. Once the expansion stage had completed, the char started to shrink. This was due to the thermal degradation of the coating under a heat source. The substrate temperature increased until the failure temperature of 400 ^{0}C was reached.

Whilst the coating was being observed, a thermocouple was used to capture the temperature profile of the substrate. A typical temperature profile of the substrate as the coating intumesced in shown in figure 4.18. The initially rapid rate of temperature change can be seen to decrease as the coating expanded.
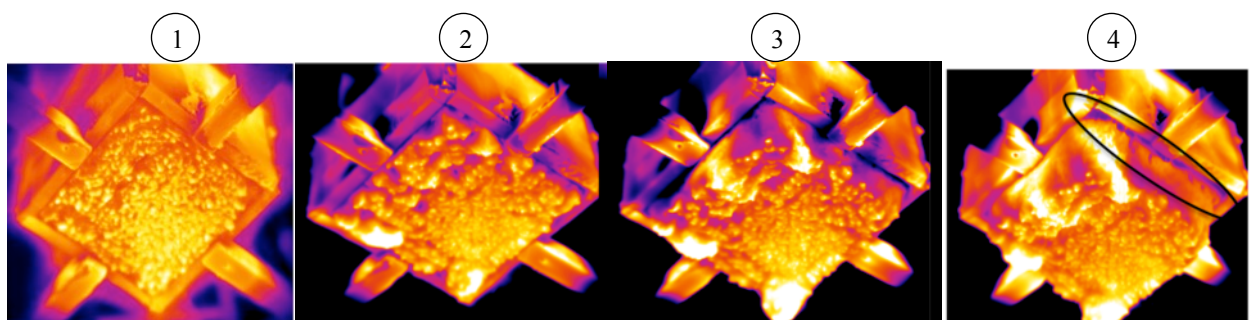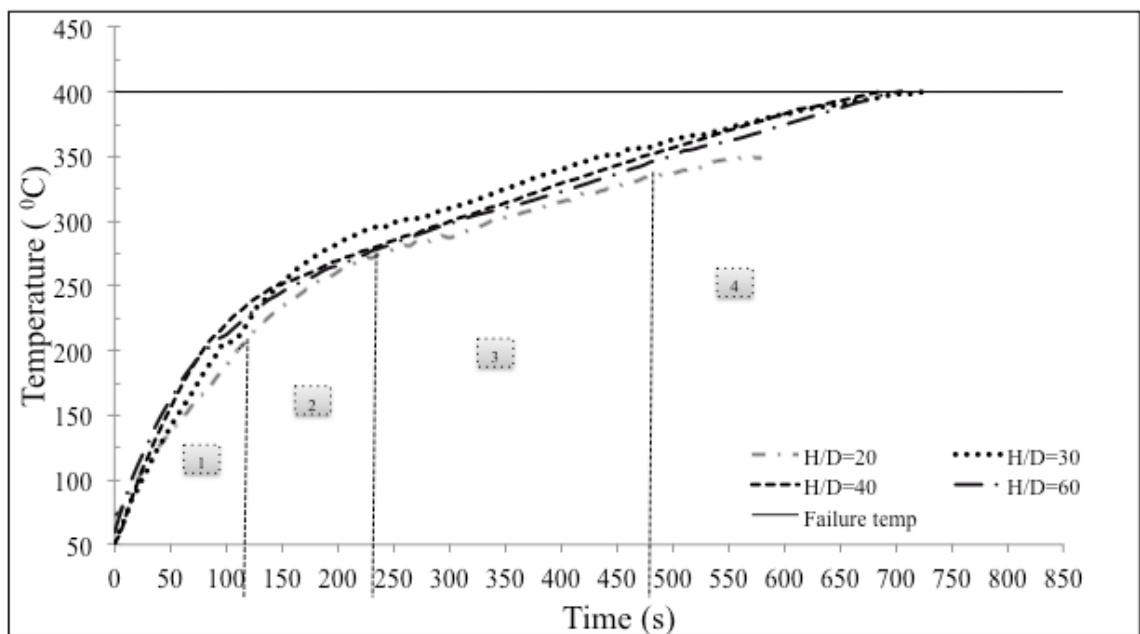
Figure 4.18. Temperature vs. Time curve of H/D= [60] for CPF 1 coupled with thermal imaging of each stage.

The effect of varying the NTP separation on the TTF and expansion patterns was investigated. It was found that the thermal efficiency of the flame changed with

separation and this impacted on the TTF. Other factors that influenced TTF were the char expansion, char shape and internal char structure.
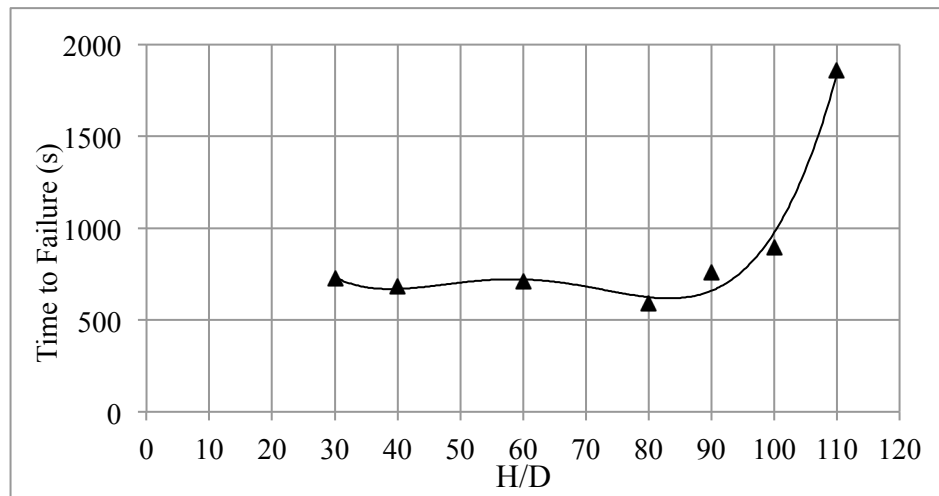
Figure 4.19. TTF against H/D for CPF1 under an impinging flame at v =6.67 m^3/s and t = 1mm.

A TTF trend for CPF 1 is shown in figure 4.19. At low NTP separations, the flame was stable and the heat losses were relatively low. There was still some unreacted fuel that impinged onto the paint surface. This was because air could not entrain to the centre of the flame and support combustion. Hence, TTF was relatively low. At higher separations, the TTF varied significantly and increased with H/D. The flame was unstable with considerable flickering at its tip. The overall heat transfer rate was not constant and loses had a noticeable impact. At H/D=110, the failure criteria was not achieved and the char provided the necessary insulation to protect the substrate.

The trend in figure 4.19 is similar to observation by Hou and Ko [59] on thermal efficiency and flame height. The behaviour they observed suggested that the thermal efficiency of a flame increased before decreasing as the heating height was increased.

The TTF trend at different NTP separations shown in figure 4.19 illustrated that TTF decreased before it increased for 30≤ H/D≤ 110 confirming the hypothesis that there is dependence between TTF and thermal efficiency based on NTP separation.

95
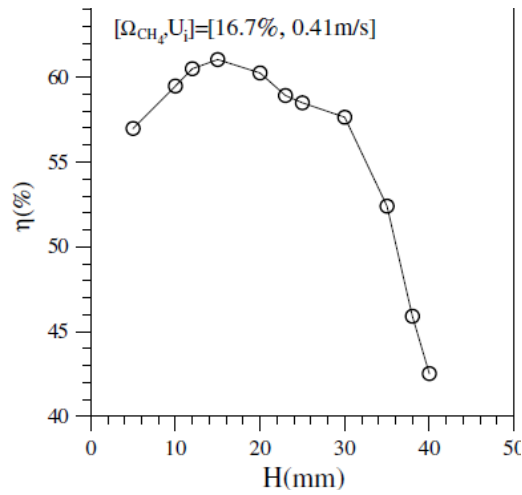
Figure 4.20. The thermal efficiency of a premixed methane flame calculated against heating height. Adapted from [59]

Comparison of the two curves in both figures 4.19 and 4.20 suggests that the thermal efficiency of the flame and thus the TTF is clearly affected by the flame height. Although the flame and fuel were different the combustion efficiency behaviour is related. For a premixed flame, it was reported by Hou [59] and Chander [65] that when the inner premixed zone impinged on the target, highest heat rate transfer values were observed. For diffusion flame, the same could be explained through the air entrainment and species transport phenomena. At very low separations between the nozzle and the target, there was insufficient time for the reactant to completely combust and hence unreacted fuel impinged on the target. Furthermore, there was lack of air entrainment to the centre of the flame. This would result in a flame with a relatively low temperature and a high TTF.

At higher separations between the nozzle and the target, even though the reactants were converted fully into products, excess air entrainment and considerable losses through radiation and convection reduced the peak temperature of the flame that resulted in a high TTF as well. Therefore, it is suggested that somewhere between the two extremes, the conditions resulted in the highest relative thermal efficiency and consequently the lowest value of TTF. From figure 4.19, it can be deduced that would be somewhere close to H/D = 80 as it registered the lowest TTF.

It is relevant to mention that the flow velocity in the present setup was 9 times higher and the fuel used is different than Hou's experiments. Hence, H/D values are considerably higher. However, the relation between the two curves is distinct and it is observed that TTF decreased with increasing thermal efficiency.

4.7.2 Mode Shapes

Figure 4.21 illustrates different intumescence shapes that were observed with changing NTP separations. At lower heights, unreacted fuel impinged on the centre of the plate, which cooled the central region. Therefore, a 'concave' shaped char was observed where the paint on the edges intumesced more than that at the centre of the plate.

As the NTP distance was increased, the amount of unreacted fuel that impinged in the central core region reduced. The char grew evenly on the centre and the edges of the plate. When NTP separation was further increased, a 'convex' shape where the char in the centre intumesced more than that on the edges was observed. At this separation, the highest heat was incident on the centre of the plate and reduced axially along the length of the plate. This behaviour was also discussed in figure 2.16 where the variation in heat flux profile was discussed as H/D was increased.

At H/D=60 the interaction between the flame and sample changed during the test. Initially, no fuel was impinging on the centre of the plate and a convex based intumescence was observed. As the char thickness increased, the amount of fuel impinging on the centre grew proportionally, therefore, the mode of growth switched from convex to concave based and an intermediate mode was observed. Overall, the char product was neither concave nor convex but a combination of both.
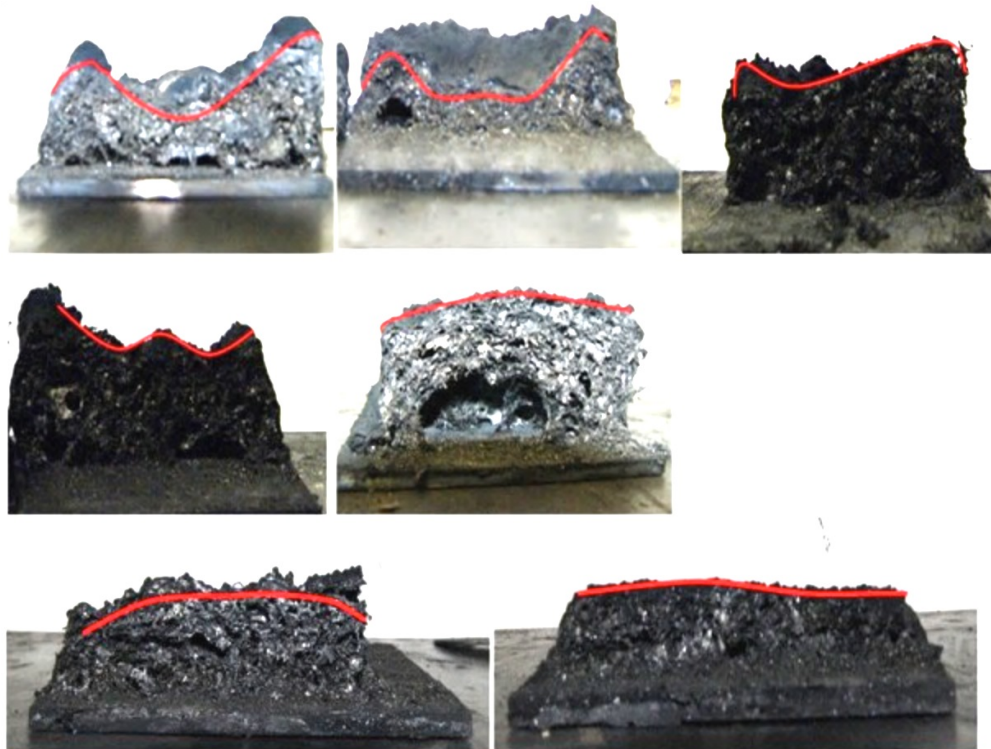
Figure 4.21. Cross-sectional structures and mode shapes of chars observed at various NTP separations (from top left)
H/D=20, 30, 40, 60, 80, 90, 110 - CPF 1

97

The total char thickness for different flow rates at H/D = 40 and t =1mm for CPF 1 is presented in the figure 4.22(a). The surface texture and pustule density was similar for all variations in flow rate. The mode shape is concave because of a cool central core and the char thickness increased with flow rate. These measurements were made once the experiment was completed and the char cooled down. It was observed that the measured char height at this stage was significantly less than measurements made during the experiment. This was the result of char shrinkage as dehydrated char absorbed atmospheric moisture. Char samples left overnight and inspected the following day were full of moisture and the 'crispy' texture, observed at end of flame exposure, became soggy and sponge like.

(i)

(ii)
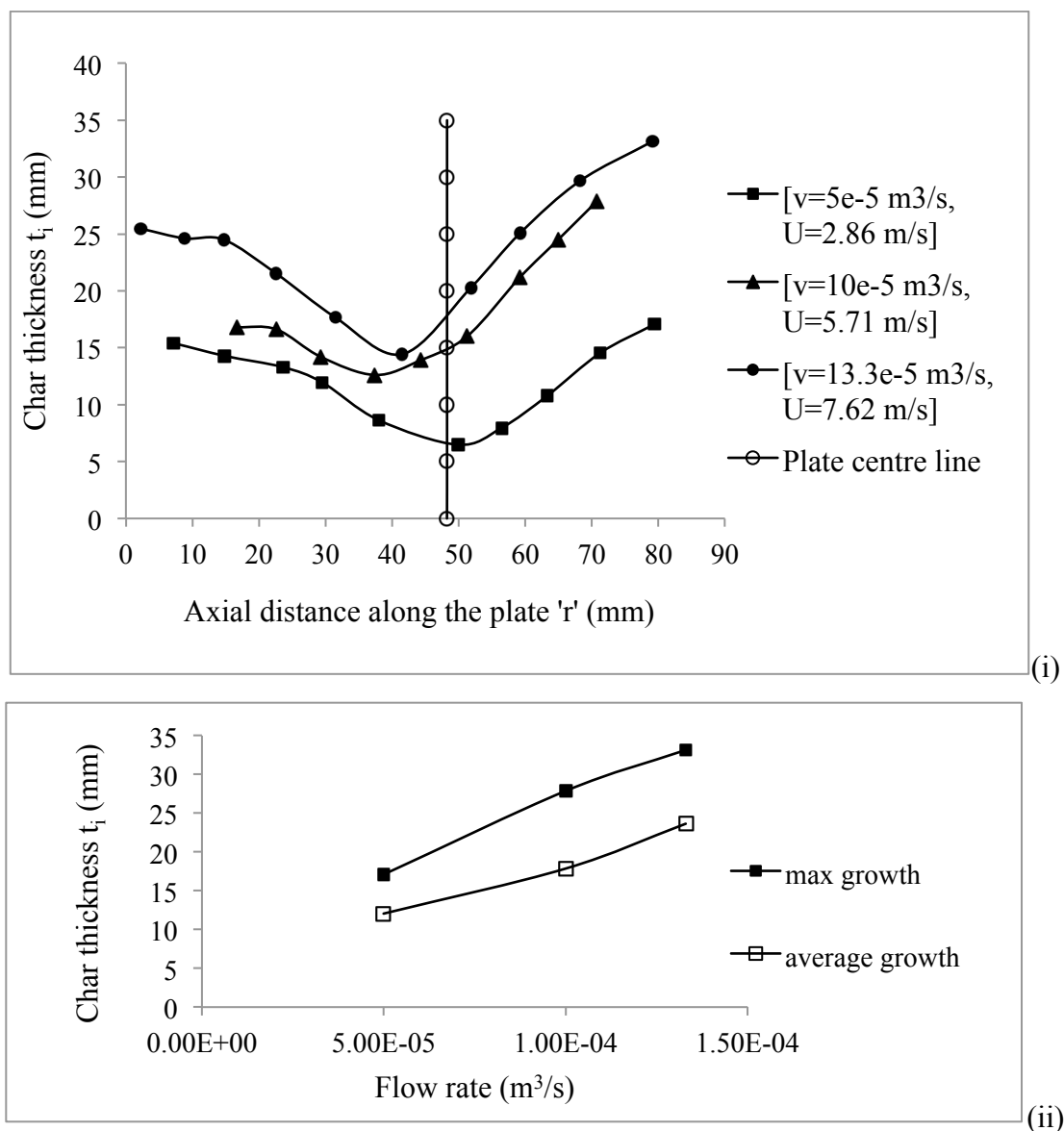
Figure 4.22(a). (i)Char thickness against axial distance 'r' for different flow rates (ii) Maximum and average growth tend for CPF 1

4.7.3 Expansion-Time history

In this section - the char expansion is discussed which is responsible for providing effective protection to the substrate against heat. A high expansion ratio char provides a low thermal conductivity, K [W/m.K] and empty gaseous pockets. Together, these factors allow char coatings to have a relatively lower thermal conductivity and offer greater resistivity to thermal heat transfer to the substrate.

Digital imaging processing software was used to measure the char thickness using the image of a cross sectional cut of the char across z=0, the midline of the flat plate. The variation in char height is shown in figure 4.22(b) below. It is clearly evident that despite having the highest TTF (Fig 4.19), H/D =110 had the lowest char expansion ratio. Whereas, H/D = 60 exhibited the highest TTF and char expansion in the range of 40 < H/D < 90. In this range the impact of heat losses and flame instability were low and thermal efficiency was high. Therefore, the high TTF of H/D=60 is attributed to the high expansion ratio.
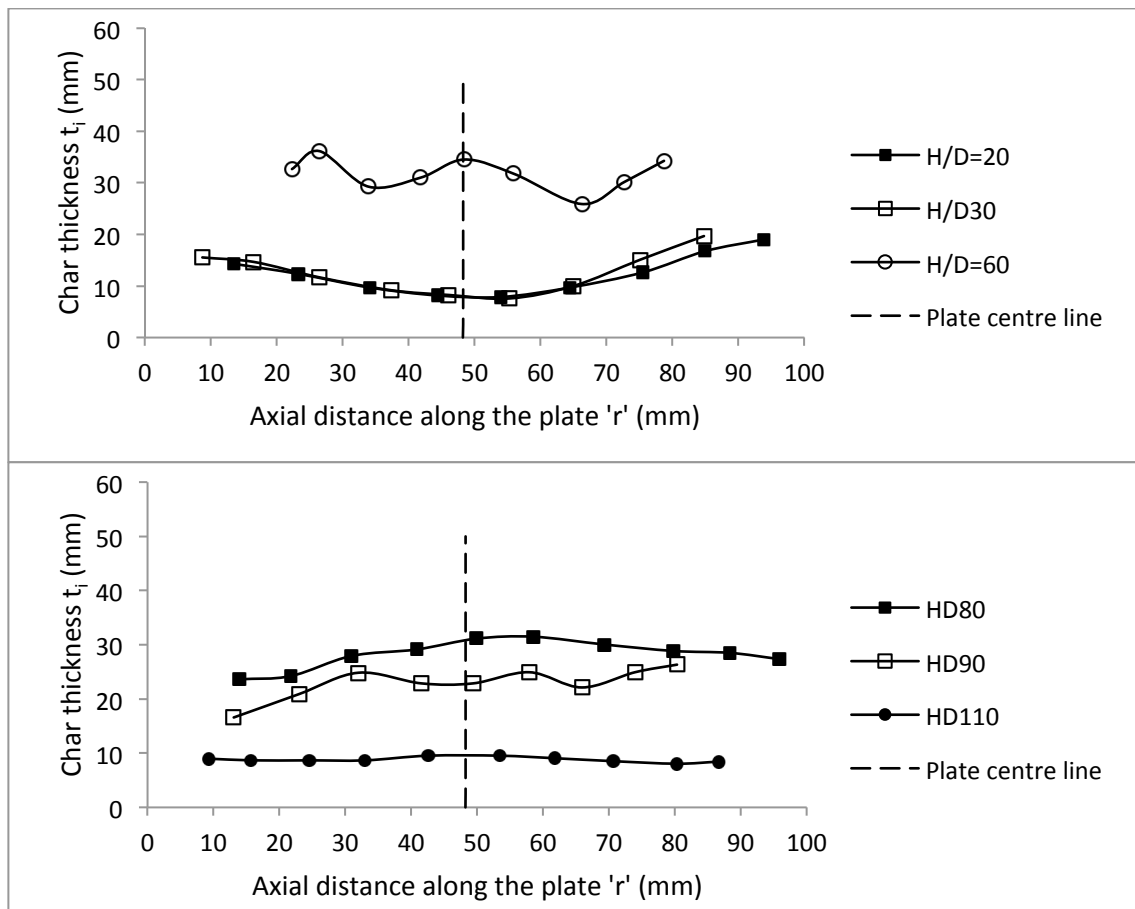
Figure 4.22(b). Intumescence thickness against axial distance along the plate 'r' observed at various NTP separations.

The effect of expansion ratio was further investigated by investigating the impact of film thickness on TTF. Various thicknesses for CPF 1 (figure 4.23) were tested at

H/D = 40 and a fuel flow rate, v= 6.65x10^{-5} m^3/s. A value of H/D= 40 was chosen because it of the high thermal efficiency at this separation combined with the ability to record Schlieren imaging data.
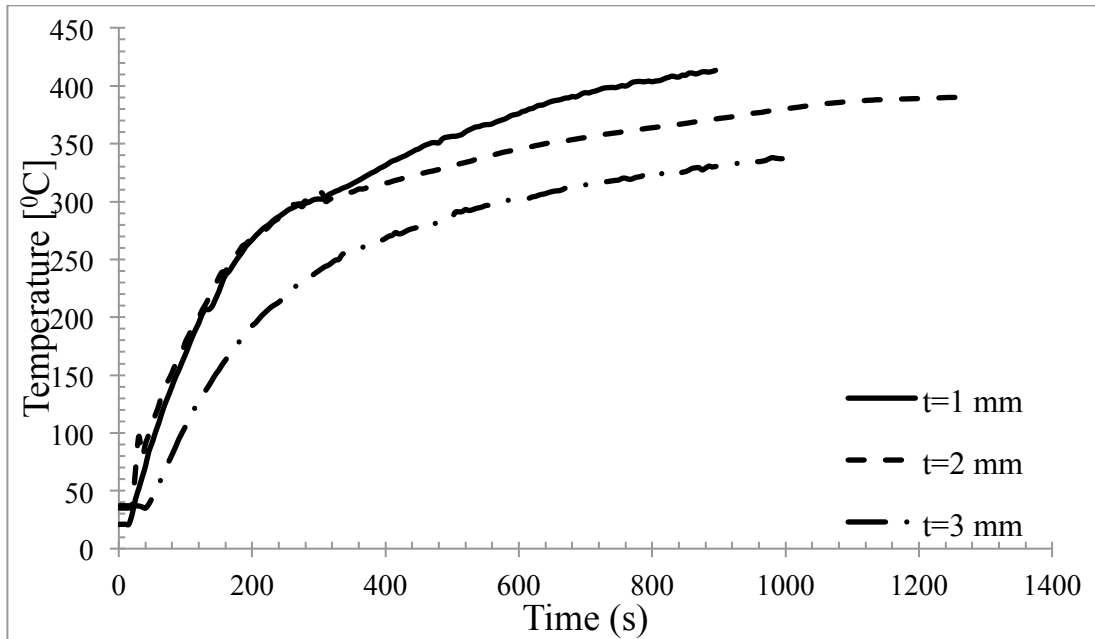
Figure 4.23. Temperature vs. Time coating thickness t= 1, 2 and 3mm CPF 1 H/D 30

The observed result was as expected. The TTF increased with film thickness t. As the char thickness increased it was able to provide better protection to the substrate against the flame. Furthermore, at higher expansion ratios, the porosity increased resulting in a char with a lower thermal conductivity. The target failure temperature of 400 ^{0}C was not achieved for t= 3mm. The result shows that very effective protection can be achieved using larger thickness layers. However, the movement of the intumescing char could become increasingly complex with increasing thickness as shown in figure 4.24.
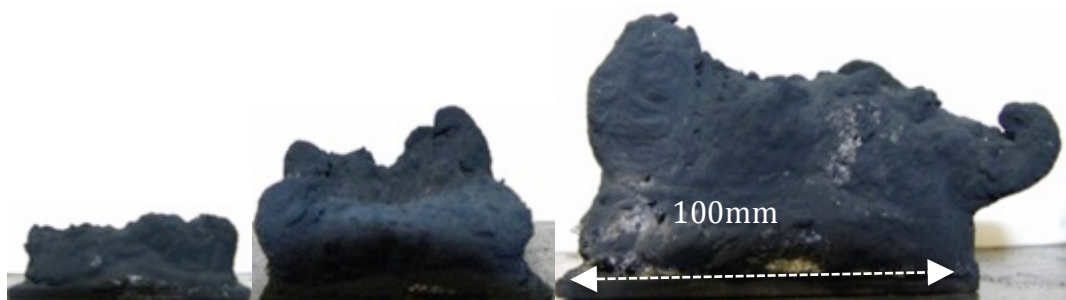
Figure *4.24. Resulting char structures when film thickness of 1,2 and 3mm respectively – CPF 1*

Different thicknesses were observed for constant flow rates of v= 6.67m^3/s at H/D=30 for t= 1mm and 3mm. The overall char still intumesced in a direction perpendicular to the flow of the impinging flame. However, surface irregularities resulted in complex char formation at higher thicknesses. The differences can be observed between figure

4.25 and 4.26 where the behaviour of the flame both upstream and downstream of the intumescent char becomes more distorted with time.

The flow rate didn't have an impact on the rate of growth of the char as mentioned earlier. However, figure 4.27 shows that the char growth increased with film thickness t of the intumescent paint layer. At t=3mm, the heating rate was not high enough to achieve complete degradation of the applied film thickness.
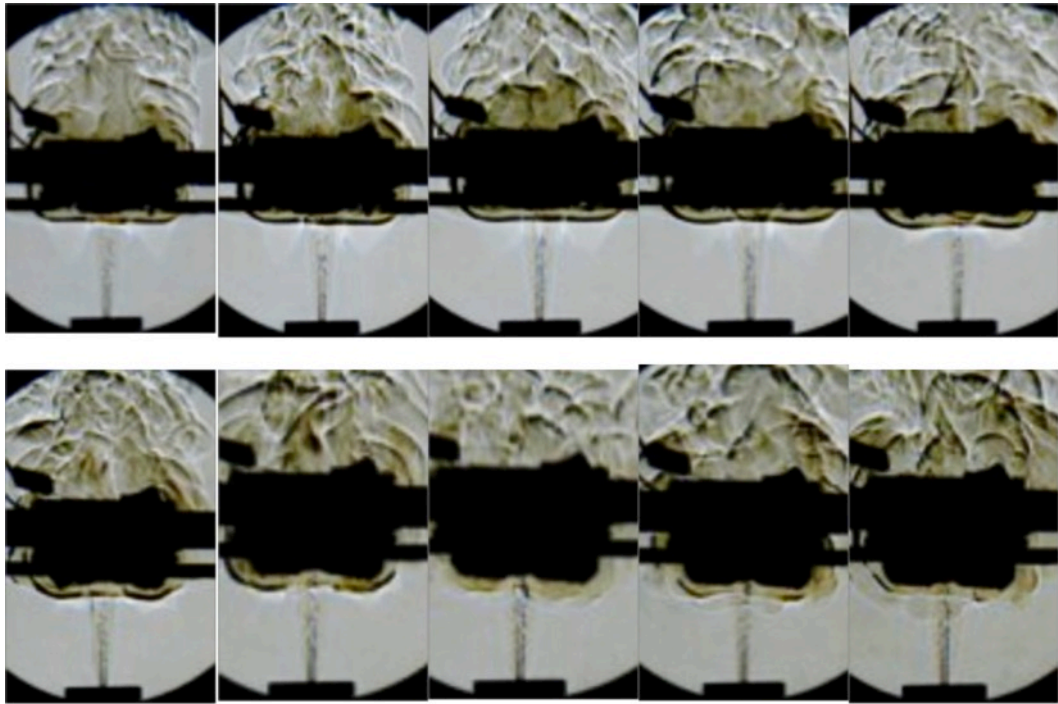
Figure 4.25. Schlieren imaging for t=1mm at different time intervals highlighting char growth, changes in flame and hot gas structure – CPF 1
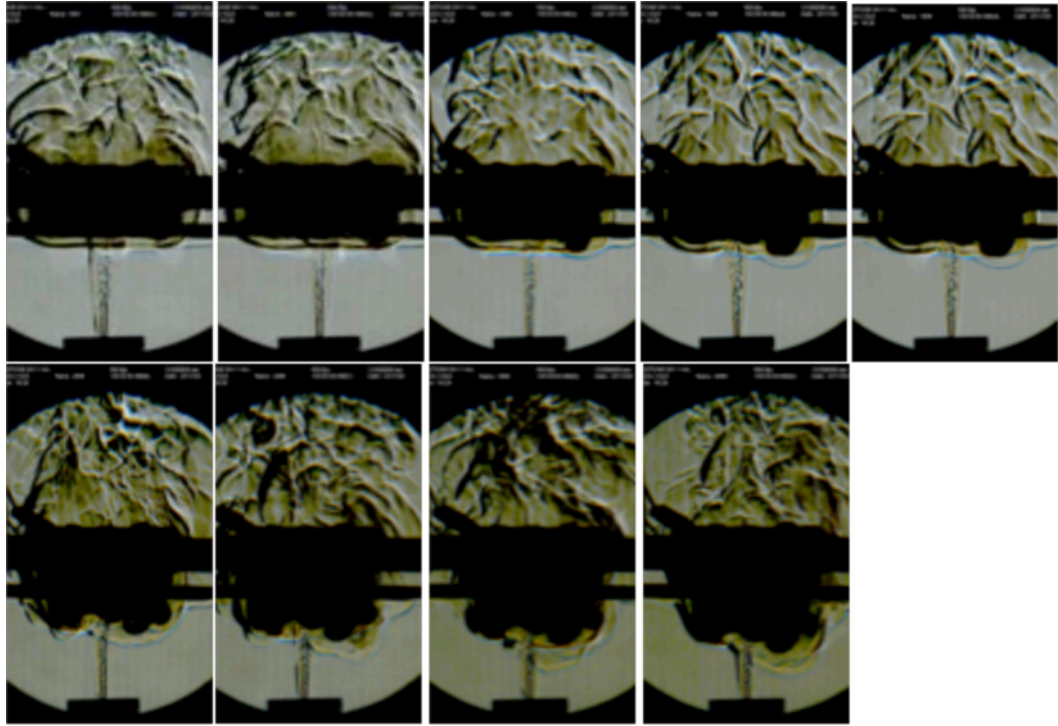
Figure 4.26. Schlieren imaging for t= 3mm at different time intervals highlighting char growth, changes in flame and hot gas structure – CPF 1
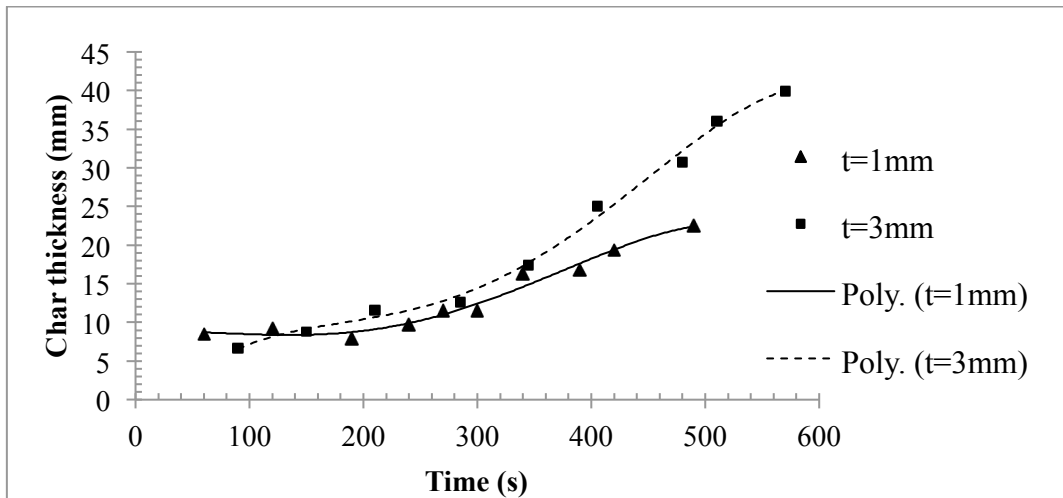
Figure 4.27. Char growth rate with time for t= 1 and 3 mm – CPF 1

HPF 1 was tested in the same was as CPF 1. Unlike CPF 1, the failure temperature was achieved at 3mm thickness of HPF 1, figure 4.28.
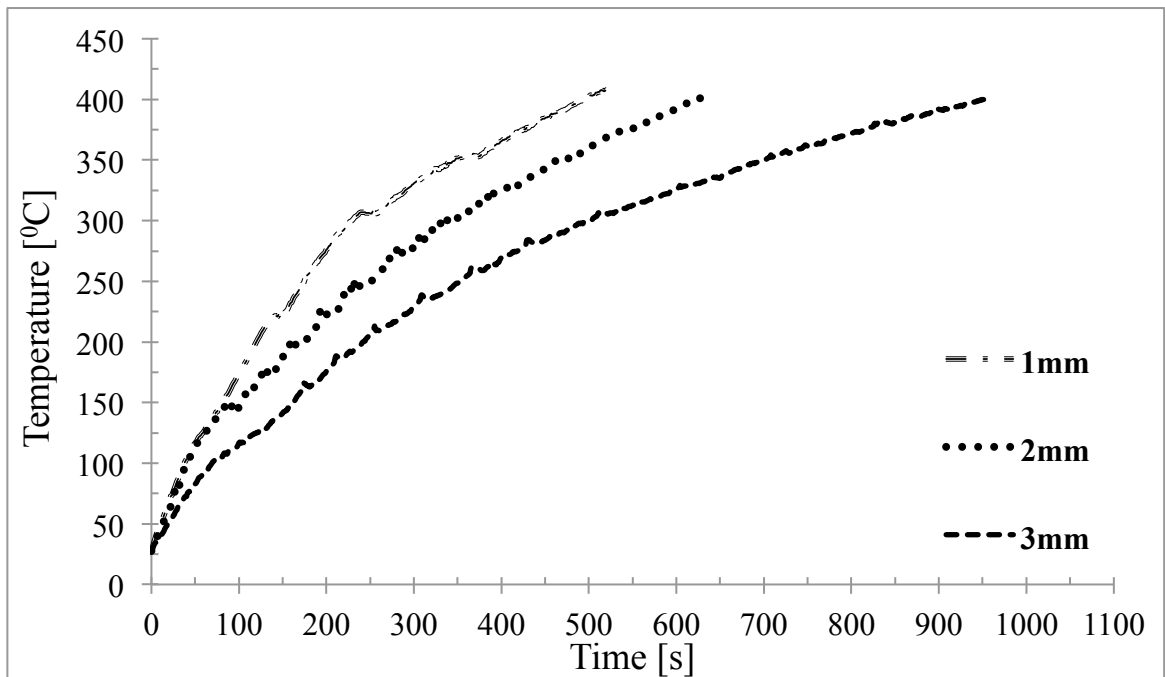
Figure 4.28. Temperature vs. Time coating thickness t= 1, 2 and 3mm HPF 1

Expansion ratio plays an important role in the thermal resistance of the char. CPF 1 provided sufficient thermal protection at 3mm thickness however, the shape and movement of the resulting char was complex in nature. HPF 1 did not present such problems due to its relatively smaller expansion ratio and high mechanical strength. At 3mm, the char structure was flat and uniform similar to the original film. The movement of the intumescing char remained controlled at higher thickness. Small pores appeared in some location as shown in the cross section of the char sample for t=3mm in figure 4.29 and the integrity and char strength was not compromised. The mass loss and shrinkage associated with the sample is relatively small. Hence, the edges of the plate were not exposed. This provides evidence to the strength of the sample and why it is used under extreme conditions in off shore oilrigs platforms.

The information in this work can assist applicators and researchers alike because separation range used in this research is an equivalent of distance between fire source and the coating in real life scenarios. One can determine the TTF, expected expansion ratios and performance of a coating.
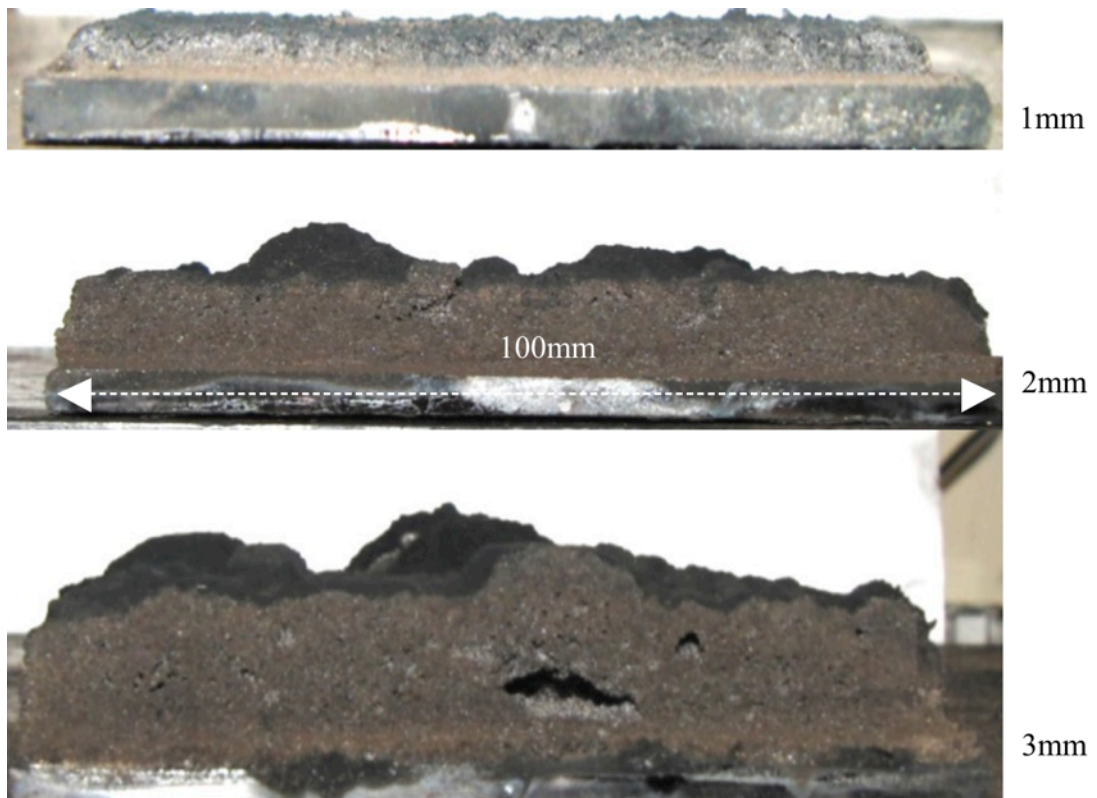
Figure 4.29. Cross section char structures at the end of a test for HPF 1 samples at t= 1, 2 and 3mm.

4.7.4 Mode Shapes other formulations

Figure 4.30 shows the cross sectional char texture at varying separations when an initial film thickness of t=0.5mm was tested of CFP2 was used.
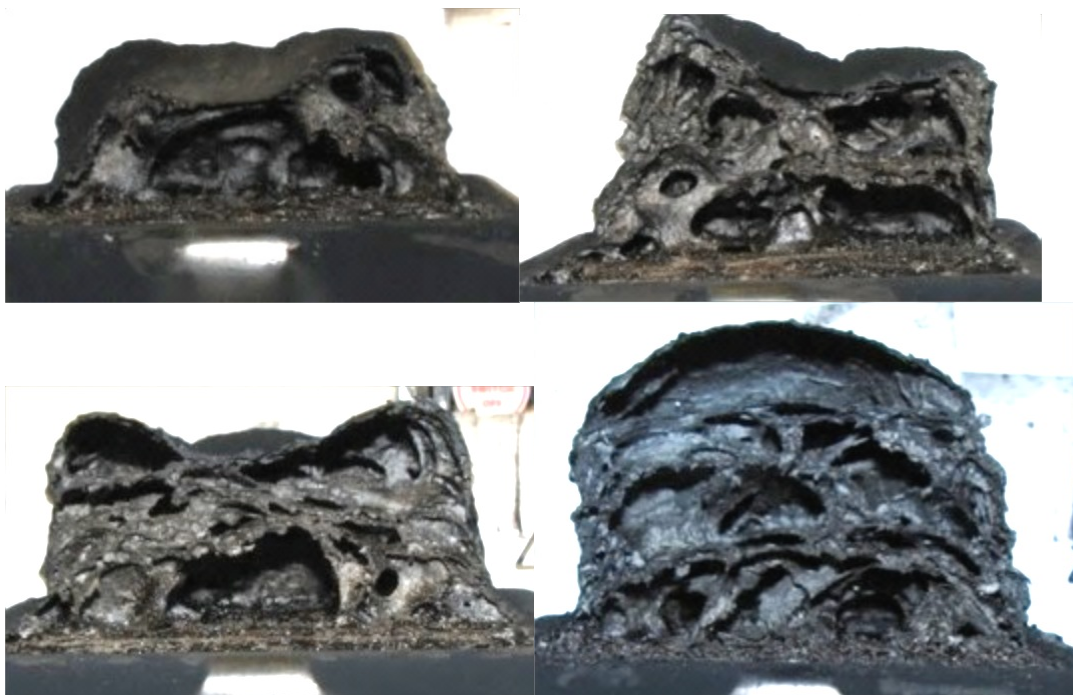
Figure 4.30. Cross sectional view of char samples at the end of an experiment at NTP separation of   H/D [30 60 80 110] - CPF 2

The nature of intumescence was different to CPF 1 and had some unique distinct features. The char structure comprised of thin crispy layers around hollow voids of different sizes that were larger than for other formulations. The growth was influenced by unreacted fuel - exhibiting two distinct mode shapes similar to CPF 1. Furthermore, expansion ratio was not affected by separation. It can be hypothesised that at higher separations, when the resultant thermal flux was lower, it allowed the hollow voids to achieve bigger sizes. Consequently, this resulted in a higher degree of intumescence.

HPF 2 has a distinct intumescence pattern. Figure 4.31 shows the mode shapes and internal structure of a typical test sample. At lower heating heights, the intumescence pattern had a parabolic mode shape. The char separated from the substrate surface and left a hollow void. This might be due to the entrapment of spumific gases under the surface during the intumescence process. It remained attached at the corners. Therefore the char had a very fragile structure. The thickness of the solid char layer was measured to be similar for all separations. The structure of the solid char layer was similar to that observed in HPF 1- denser granular char with low porosity. The size of the hollow void reduced at higher separations resulting in a flatter mode shape of the char. This is shown in Figure 4.31 (a-c).
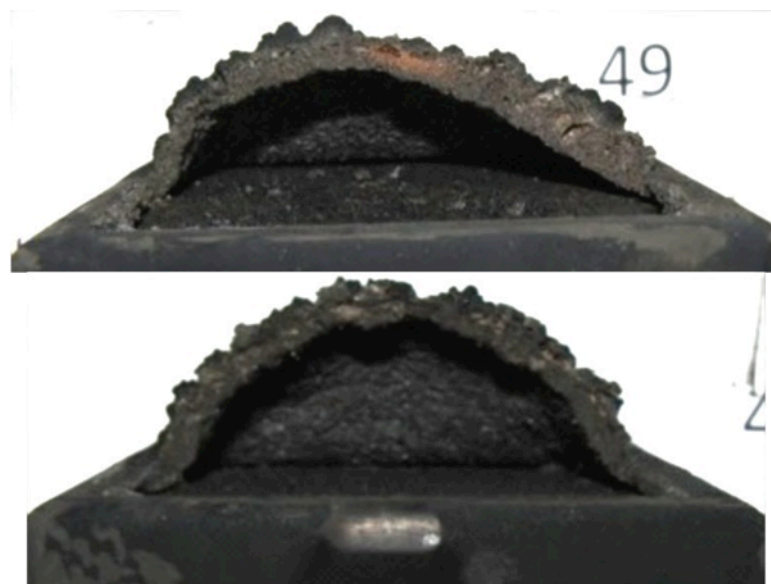
Figure 4.31(a). Cross sectional illustration of the char structure at thee end of an experiment at NTP separation of H/D30 and H/D40 - HPF 2
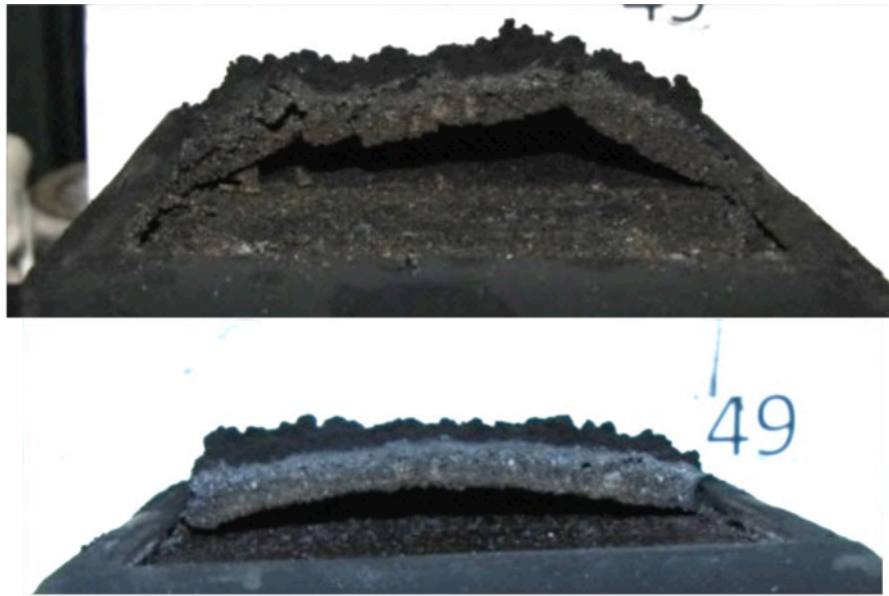
Figure 4.31(b). Cross sectional illustration of the char structure at thee end of an experiment at NTP separation of H/D60 and H/D90 char patterns – HPF 2

Figure 4.31(c). Cross sectional illustration of the char structure at thee end of an experiment at NTP separation of H/D110 char pattern – HPF 2

The nature of char growth may also be influenced by the surface temperature profile. The temperature of the flame decreases axially as 'r' is increased in the wall jet region, illustrated in figures 2.14 to 2.16 (section 2.2.2). Therefore the lowest temperature occurs near the edges of the panel. This phenomenon drives the growth of the char towards the central axis of the plate where temperature is higher. Therefore, the highest expansion is observed in the centre of the panel. Where there was a cool central core, the point of highest expansion was offset from the centre. However shrinkage at the edges was observed in all the test cases with and without a cool central core.

4.7.5 TTF other formulations

The performance of the remaining formulations were investigated using the same experimental conditions as CPF 1. The was one exception for CPF 2 which was tested at t= 0.5mm. This is because at, t=1mm, the char growth was unable to support its own weight and it would collapse. This phenomenon is discussed in section 4.7.6.

The results for TTF are presented (figure 4.32) and discussed as follows.
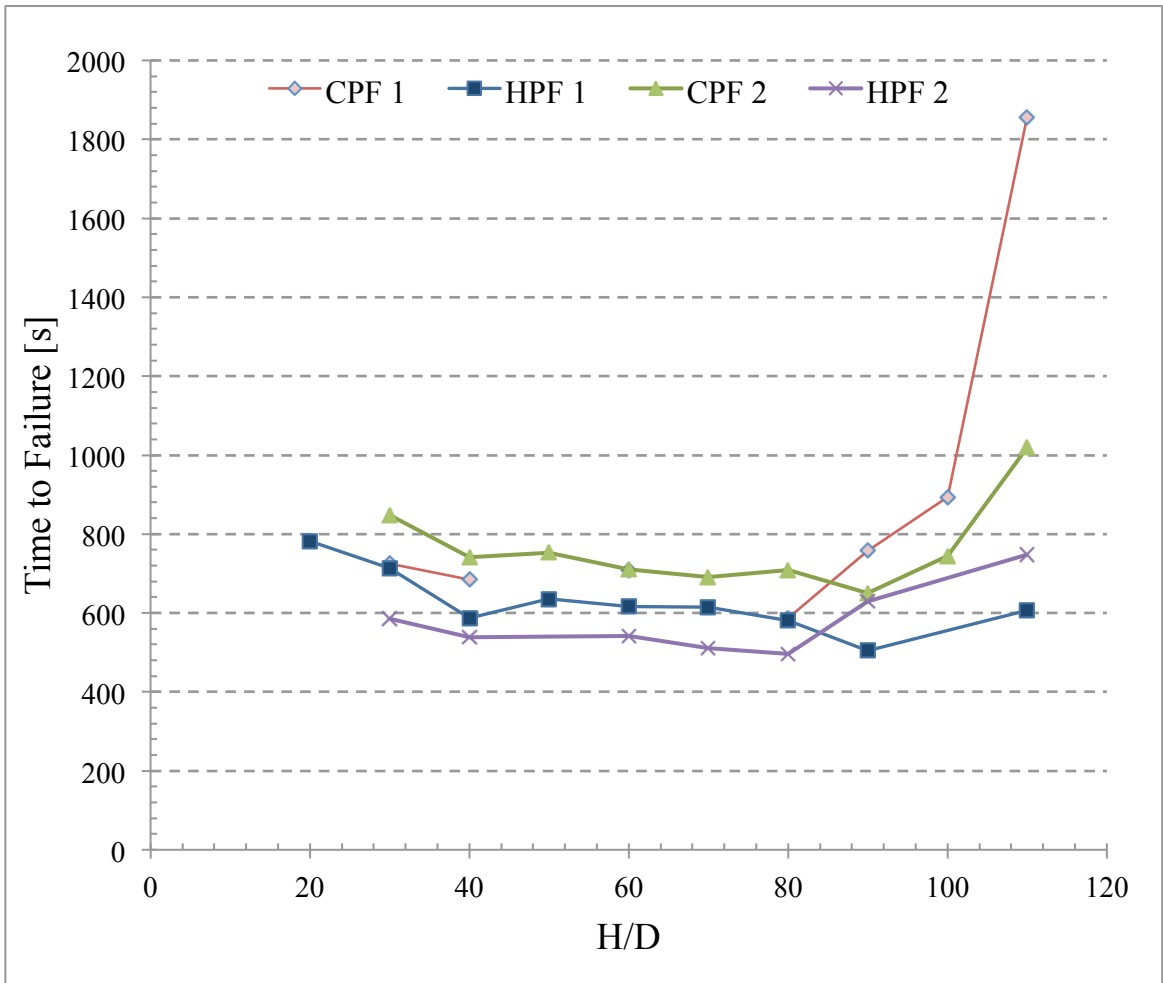
Figure 4.32. Temperature vs. H/D comparison for all formulations.

Table 4.2 TTF comparisons between CPF and HPF formulations- at various NTP separations.

	CPF 1	CPF 2 (t= 0.5mm)	HPF 1	HPF 2
H/D	TTF [s]	TTF [s]	TTF [s]	TTF [s]
0	725	586	714	848
0	685	538	587	742
0	708	542	616	710
0	587	496	581	709
0	758	630	504	650
10	1855	747	607	1019

A comparison between HPF 1 and HPF 2 showed that HPF 2 had higher TTF than HPF 1. This suggests that HPF 2 has a stronger resistance to heat transfer through the

surface thus providing higher resistance times. CPF 2 was only tested at t=0.5mm. Therefore, it was expected CPF 1 would have provide better thermal protection.

Comparison between all formulations demonstrated that all formulations performed in a similar manner. For values of H/D from 40 to 80 all formaulations had a similar failure time. The high thermal efficiency of the flame jet was counter balanced by the effective thermal resistance of the char coating. However, at lower [H/D = 20, 30] and higher [H/D = 90, 100. 110] separations, TTF increased significantly. The variation increased significantly at higher heights; at H/D = 110, CPF 1 took approximately 30 minutes before reaching failure temperature. This behaviour has been discussed earlier in terms of the thermal characteristics of a flame and how it changed with flame height. The thermal efficiency of a flame, rate of change of heat transfer, reduces at both high and low heights.

4.7.6 Char Failure

Initially CPF 2 was tested at film thickness of t=1mm. it was discovered that the char expanded profusely and could not support its own weight. Therefore, it eventually detached from the panel surface. Afterwards, the paint left on the panel resumed intumescing. The 'falling off' of char was considered as a failure scenario and therefore, the testing of CPF 2 was continued using a film thickness of t=0.5mm for all further tests. Thermal and Schlieren images are presented in figure 4.33 and 4.34 that highlight the falling off of the char.
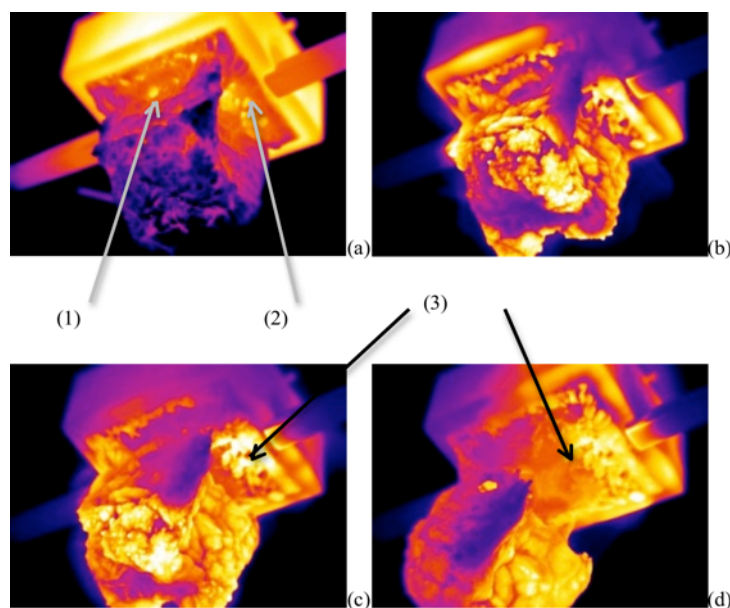
Figure 4.33. (a) Excessive char growth about to crack (b) bottle neck at the base of char (c) first signs of cracking in the right corner of the panel (d) char breaks and falls off. H/D40, v= 6.67 e -5 m³/s, t=1mm.

Figure 4.33 shows a sequence of images, as the char is about to detach from the surface of the panel. In (a), the char was still fully attached to the surface; it had started to stretch away, revealing the edges of the panel. Feature (1) highlights the appearance of holesthat grew bigger as the char intumesced further. Feature (2) shows shrinkage at the base of the char that was moving away from the surface of the panel. This makes the structure weaker. Finally, in (c) and (d) the char peeled and broke away (feature (3) from the right corner and fell off. It left behind paint in some parts and in others substrate surface was exposed.

The Schlieren image in figure 4.34a illustrates the growth of the char sample just before fracture occurs. The calculated growth was approximately 100mm resulting in an Expansion Ratio of 100. At such high expansion ratios, CPF 2 was unable to stay intact to the substrate. Figure 4.34b presents a sequential schematic for test case H/D=60 v= 3.33 m^3/s and t =1mm. The figure illustrates the char breaking apart and falling. The images are taken at an interval of 0.04s.
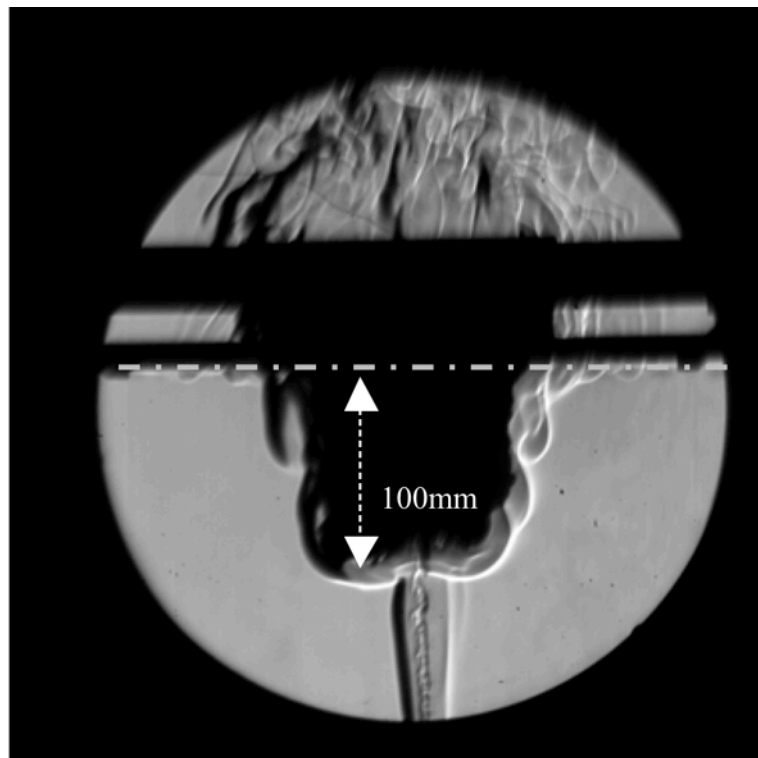
Figure 4.34a. Expansion of t=1mm of CFP 2 coating at H/D40, v= 6.67 e -5 m3/s
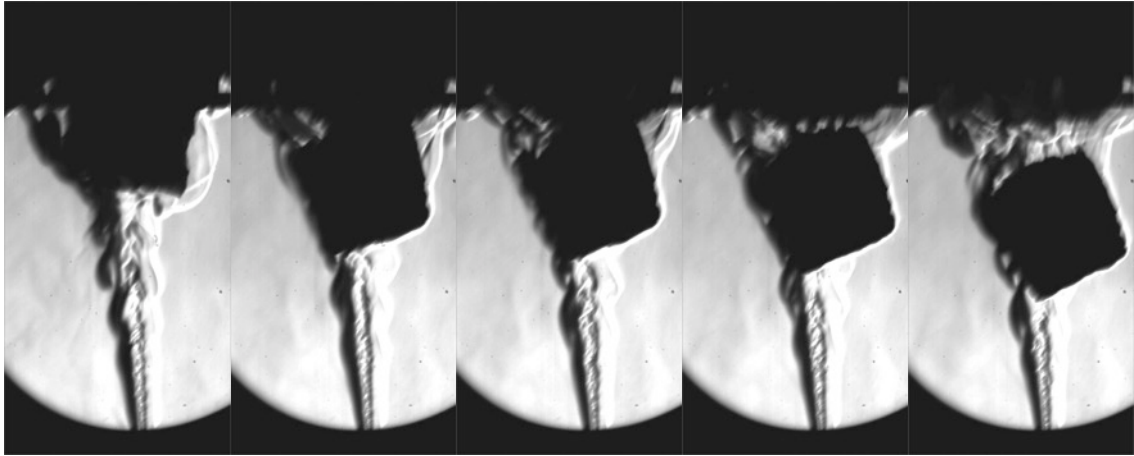
Figure 4.34b. Expansion of t=1mm CFP 2 coating at H/D60, v= 3.33 e -5 m3/s, interval of 0.04s.

An end user/formulator has to consider such behaviour carefully. Coatings with expansion ratios in excess of 100, such as CPF2, can be hazardous. This is true if they are used on ceiling where they will be unable to support their own weight and can peel off posing a significant risk. However, their extreme reactiveness and profuse expansion can be an asset in small enclosures to reduce oxygen and choke the fire.

4.8 Thermal performance of coatings

It is useful to understand the thermal properties of an intumescent coating in order to optimise its application as a fire protective material. However, this task can be very difficult as properties change during the expansion process; are difficult to calculate without expensive large-scale experimentation or change dramatically due to small variatons in the formulation matrix.

The surface temperature of a coating is a desirable to know in order to characterise the thermal performance of a coating. Combined with the substrate temperature and coating thickness, a relatively simple heat transfer model can help estimate the thermal conductivity during the expansion process. The knowledge of the thermal conductivity can be useful to applicators in order to determine required thickness coatings for various applications.

Studies in the past have used expensive large-scale setups to determine the thermal performance of coatings in commonly found application e-g full-scale support columns and beams [103, 104]. To curtail the cost and time involved in such testing methods, researchers have developed various heat transfer models in order to characterise the thermal performance of coatings [71, 105-108]. Data has been collected using cone

calorimeters [109] where a uniform heat flux is used. A good correlation was found between experimental results and theoretical models.

Some studies have used a uniform heating source in the form of a cone heater and a point source thermocouple reading in order to determine an overall heat transfer model of a coating. Unlike these studies, this research has used an impinging flame, which offers a non-uniform heat flux. It is done so in an attempt to characterise the non-linear nature of the surface temperature.

The following sections present the non-uniform nature of the surface temperature observed during the various stages of intumescence. It also analyses the high rate of heat loss through the char surface when the heat source was turned off. Although, the scope of work has been kept purely experimental, it is expected that the results can be used towards heat transfer modelling.

4.8.1 Surface temperature variation during the expansion process

The surface temperature variation was analysed at 1) prior to pustule appearance, 2) after their appearance and 3) during intumesce (char expansion). The observation and analysis with respect to various formulations is presented. The line and spot tool (Section 3.7.4) were used in post processing of the thermal imaging system data. Variation in the surface thermal profile along the centre of the square panel and heat loss through the surface were both analysed. Combined they provided an understanding of the thermal behaviour on the surface of the char during the process of intumescence. The recorded temperature was compared for the different formulations for a variety of experimental conditions. A generic measuring GUI was used (figure 3.23a). The measurements conditions for each stage are summarised in table 4.3 below. Tests were conducted at H/D = 40, t=1mm at a fuel flow rate of 6.67×10^{-5} m^3/s.

Table 4.3. Measurement conditions for surface temperature profile

Sample Type	T_b = Substrate Temperature [^{0}C]		
	Stage 1	Stage 2	Stage 3
CPF 1	215.0	250.0	310.0
CPF 2	250.0	310.0	330.0
HPF 1	125.0	200.0	270.0
		300.0	

4.8.1.1 Thermal Profile

The results are discussed and presented below. T_s measurements were taken across the length of the panel. The position of measurement was kept at the centre of the panel axially along the length of the plate. Figure 4.35 illustrates the measurement positions for the line (Ll01) at $T_b = 215\ ^0C$ (stage 1), 250 ^0C (stage 2) and 310 ^0C (stage 3).
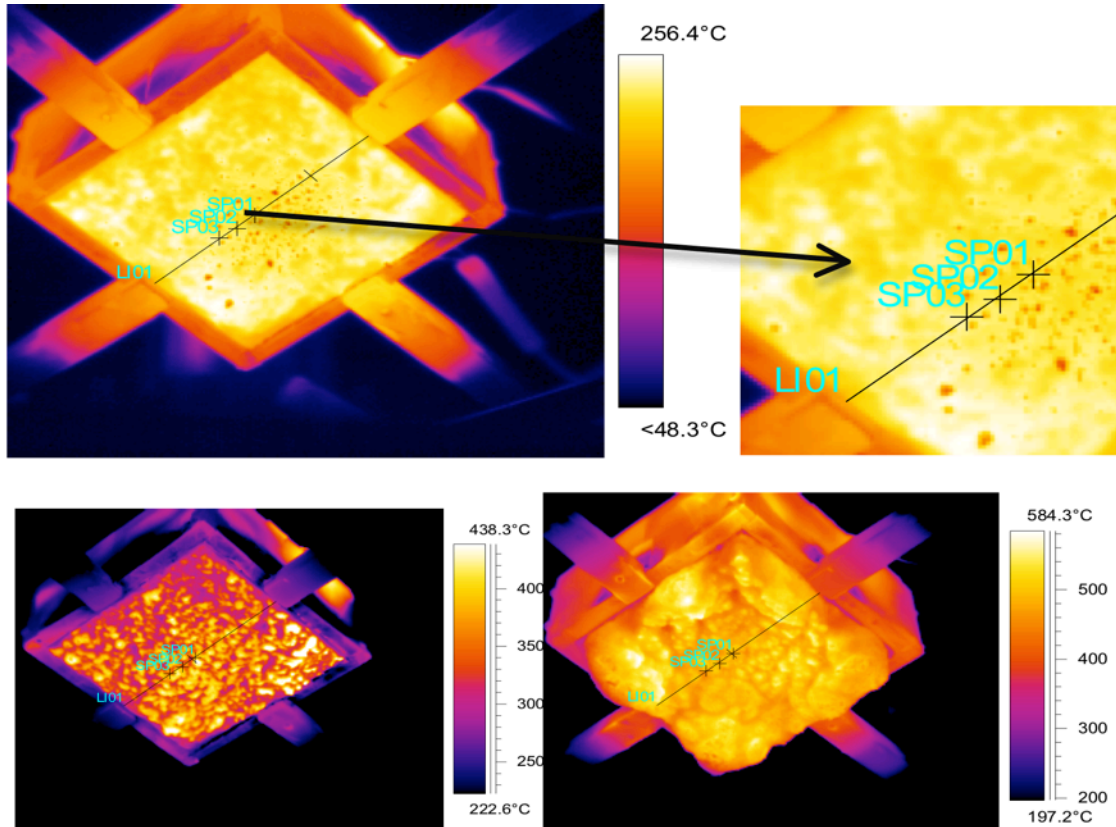
Figure 4.35. Measurement positions for the line (Ll01) and spots (Sp01, SP02 and SP03) at Tb = 215 ^0C (stage 1-top left), 250 ^0C (stage 2-bottom left) and 310 ^0C (stage 3-bottom right) – CPF 1.

The temperature variation along Ll01 is illustrated in the figure 4.36 for all three stages. It can be observed that the surface temperature at the time of the burnout had a very uneven thermal profile.

At $T_b = 215\ ^0C$, there was little or no evidence of the pustules. Therefore, the uneven thermal profile was attributed to the impact of the highly uneven and localised heat flux generated from the impinging diffusion flame. After burnout, the surface cooled to have a smooth profile with a relatively stable temperature of $T_s = 250\ ^0C$.

At $T_b = 250\ ^0C$, pustules had appeared on the surface of the char. T_s was highly uneven. The uneven nature increased due to the pustules, as they were relatively hotter than the surface of the char. A relatively smooth profile was observed 0.75 seconds after the

burnout. The average temperature of the surface changed from approx. $T_s = 375\ ^0C$ to $275\ ^0C$. The average surface temperature was also higher than that at $T_b = 215\ ^0C$.

The profile in figure 4.3(b) comprised of various peaks and dips. The peaks corresponded to the position of the pustule on the surface and the dips, the surface itself. The density of pustules in CPF 1 was high and therefore, a large number of peaks were observed. It can be seen that 0.75 s after burnout the peaks had turned into dips and vice versa. Once the surface had started to cool down, heat was dissipated through the pustules at a higher rate than the surface itself. Furthermore, instead of equilibrium and an even temperature distribution, the peaks changed into dips (highest temperature to lowest). It is hypothesized that this was because the space between the two pustules (surface) became a cavity that acted as a heat sink and did not dissipate the heat as rapidly as the pustules. The highly complex heat transfer mechanisms that act in porous char based systems can help highlight such behaviour and they are still a subject of ambiguity and further research.

(a)

(b)
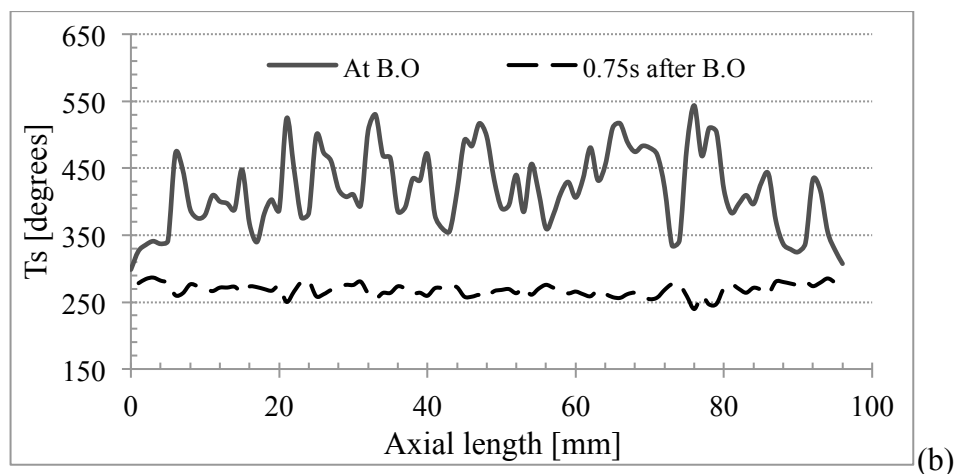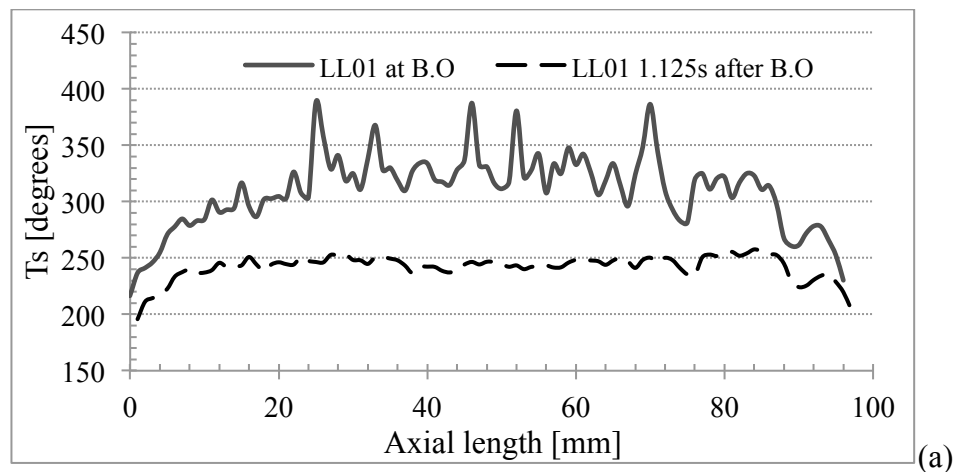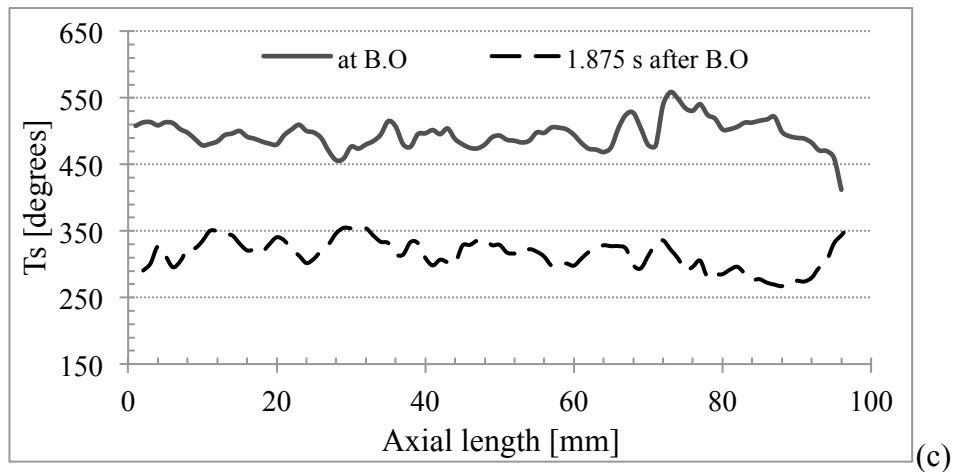
Figure 4.36. Surface thermal profiles at T_b = 215 ^0C (stage 1), 250 ^0C (stage 2) and 310 ^0C (stage 3) – CPF 1

Figure 4.37 shows thermal images for stage 3, T_b = 310 ^{0}C taken at burnout, 1s and 1.5 s later. The pustules had intumesced and transformed into an expanding char structure. The profile is smoother at burnout, the peaks represents positions that exhibit maximum expansion. Once cooled, the inverse relation between the two curves is clearly evident. The peaks temperatures changed to points of lowest temperature after 1.875 s. It also shows how the hotspots (yellow in colour) change from top of the char to the cavity in the middle.
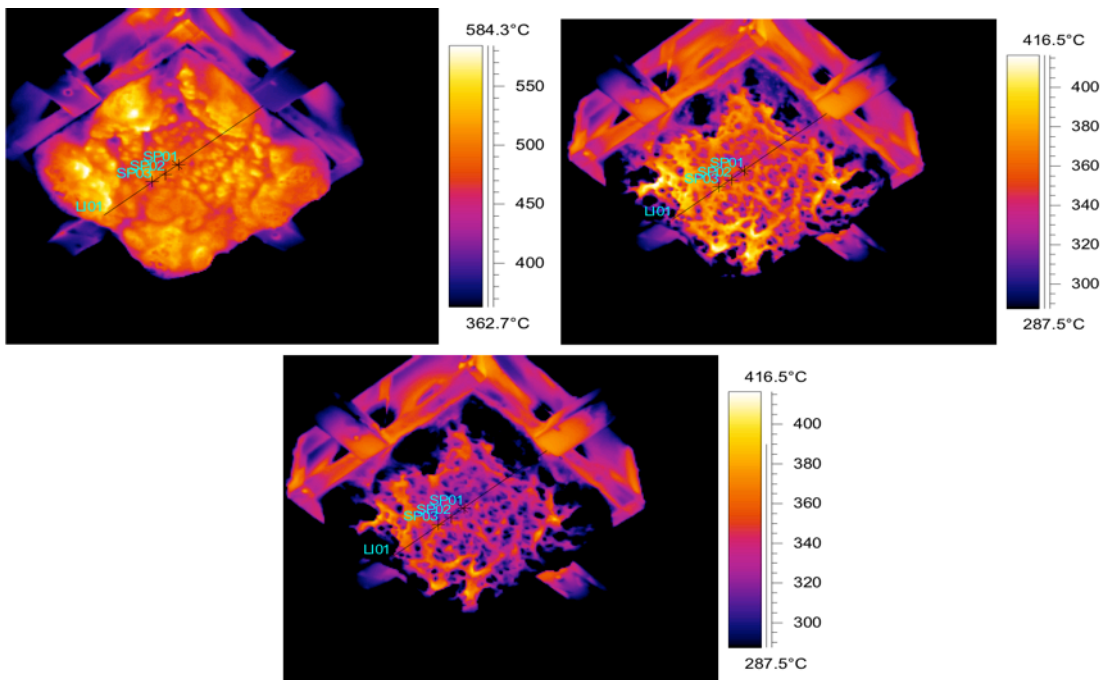
Figure 4.37. Hotspot variations during cool down after burnout in stage 3, sequential images 0.5 s after burnout – CPF 1

Thermal data for CPF 2 was investigated using the same method and under the same experimental conditions. The difference was the film thickness, t=0.5mm for CPF 2. The results are presented and discussed in this section. Figure 4.38 illustrates the thermal profiles at the three aforementioned stages.
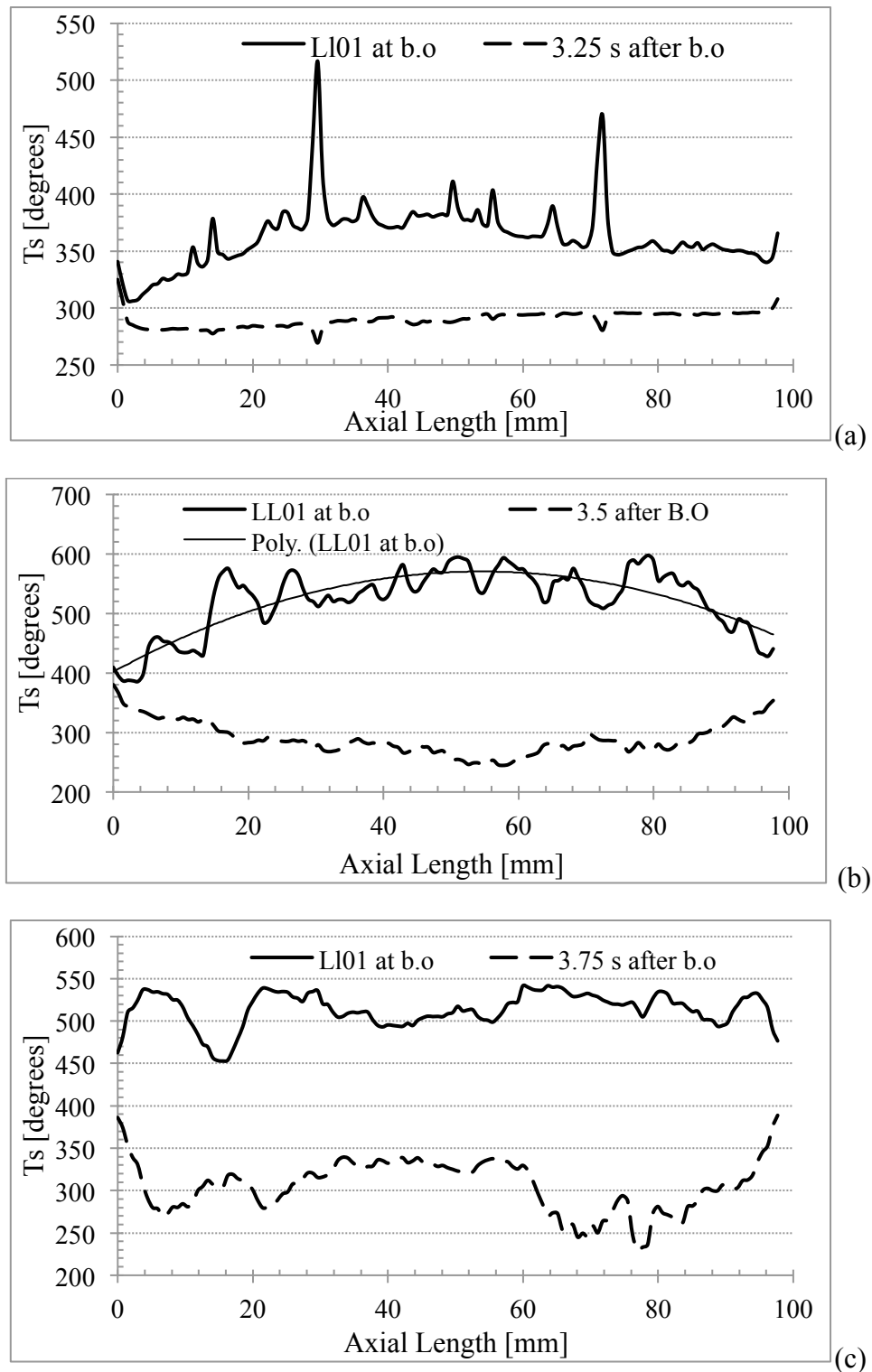
Figure 4.38. Surface thermal profiles at $T_b = 250\,{}^0C$ (stage 1), $310\,{}^0C$ (stage 2) and $330\,{}^0C$ (stage 3) – CPF 2

The appearance of sporadic and infrequent pustules resulted a few large peaks in an otherwise, smooth surface profile in stage 1. Once cooled, the temperature distribution was small resulting in a smooth and constant thermal profile.

Once pustules developed in stage 2, the number of peaks increased, see figure 4.38(b). The shape of the peaks was not as sharp and defined when compared to CPF 1. Each high temperature occurrence was distributed over a relatively larger area of the plate.

115

This means the shape and size of the pustule was smooth and large, unlike CPF 1. Images shown in figure 4.8 revealed that the char surface was fairly smooth and pustules did not appear in any distinct shape or size. The highly viscous nature of the formulation prevented the sustainable development of pustules on the surface. It can also be seen in figure 4.38(b), that the curve showing T_s distribution at burnout has an approximate parabolic shape with a maximum temperature in the middle of the panel. This is indicative of a thermal profile that has a maximum heat flux in the stagnation region of the flame which would eventually result in a distinctive char mode shape.

Once the char started to intumesce, a uniform thermal profile was observed. The inverse relation between peaks and dips over the course of a burnout was consistent in both CPF formulations.

It is already established that HPF 1 did not intumesce a lot. The size and shape of the pustules were small and their occurrence was infrequent compared to CPF coatings. Hence, smooth T_s profiles were observed post burnout. Distinctive peaks in all three stages were positions of pustules on the surface. Over the three stages, T_s profile at burnout was relatively smoother when compared to CPF formulation trends. The curves are illustrated in figure 4.39.

116
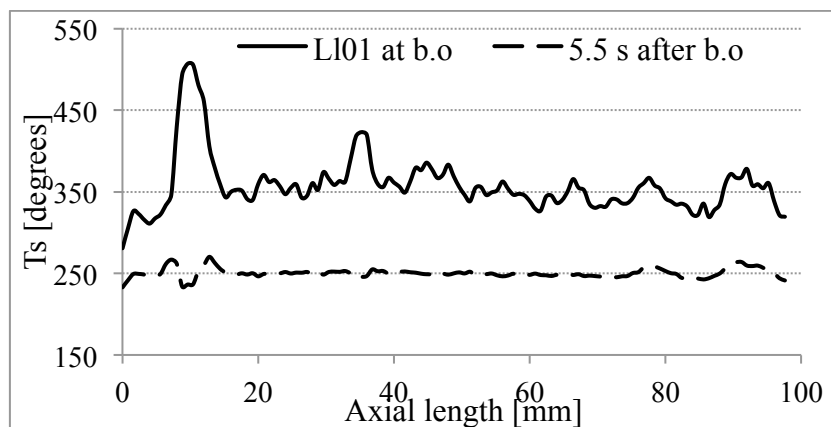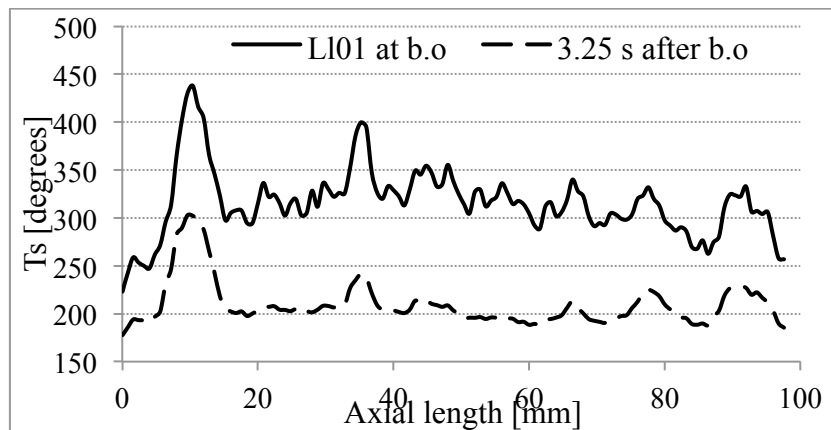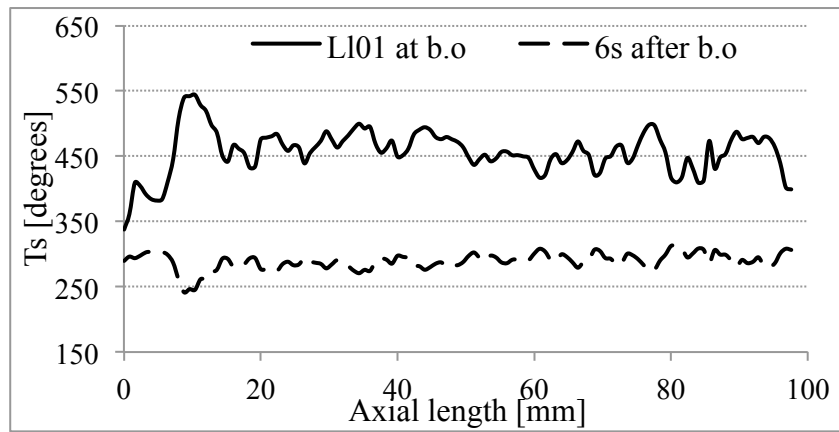
Figure 4.39. Surface thermal profiles at T_b = 125 ^0C (stage 1), 200 ^0C (stage 2) and 270 ^0C (stage 3) – HPF 1.

HPF 2 was different to HPF 1 in stage 2 and stage 3, as shown in figure 4.40. Pustules were a dominant surface feature and therefore, the T_s profile was erratic with a multitude of peaks across the length of the plate. However, the peaks were not as sharp and defined as in HPF 1 (figure 4.39). This was due to the frequency of their appearance rather than size or shape. Digital images, presented in fig 4.7-4.10, of the final char product revealed that the size and shape of the pustules was very distinct in nature.

(a)
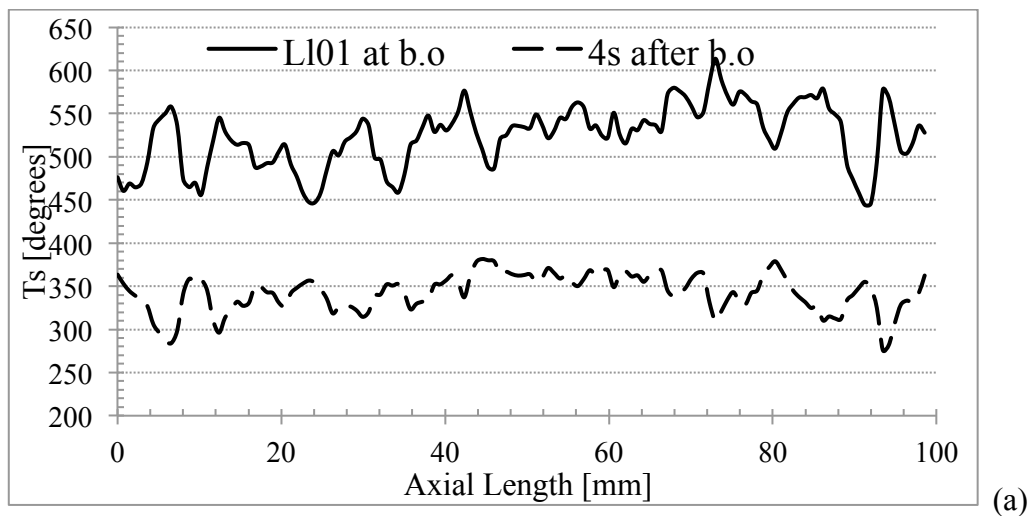
Figure 4.40. Surface thermal profiles at Tb = 300 ^0C (stage 2)

4.8.1.2 Heat Loss through the surface

The spot tool was used to track the change in temperature at the centre of the panel and two adjacent positions along the centreline of the panel, Sp01, SP02 and SP03 as shown in figure 4.35. The change in temperature was recorded on the ThermaCam software and copied out directly. These were compared with the maximum temperature along the line Ll01. The results are illustrated in the figure 4.41. The graphs were exported

117

directly from the thermal software. The vertical axis shows T_s against time on the horizontal axis. A legend is presented highlighting various measurement positions. The sudden dip or spike at the end of each curve indicates the burnout was complete and fuel or flame started impinging on the surface.

It was observed that the rate of temperature change was different for all three stages. The highest rate of change was observed in stage 2, pustule development stage. The starting temperature of the three spot measurement positions had significant variation in stage 1 and stage 2. Whereas, in stage 3 once the char had formed and started to intumesce, the temperature at all three positions was similar.

Mcdaid [89] investigated the thermal inertia of a 10 mm thick steel plate and observed that at steady state conditions, the steel plate maintained its temperature. When the heat source was removed, the temperature changed by $1\,^0C$ in approximately 20 seconds due to its high thermal inertia. Intumescent systems have an extremely small thermal inertia. Spot temperature measurements highlighted that char was capable of losing heat rapidly. This is attributed to the carbon-based char composition, coupled with thin, porus and light layered based composition. In stage 2, Ll01 max temperature changed from approximately 550 ^0C to 300 ^0C in approximately 1 second.
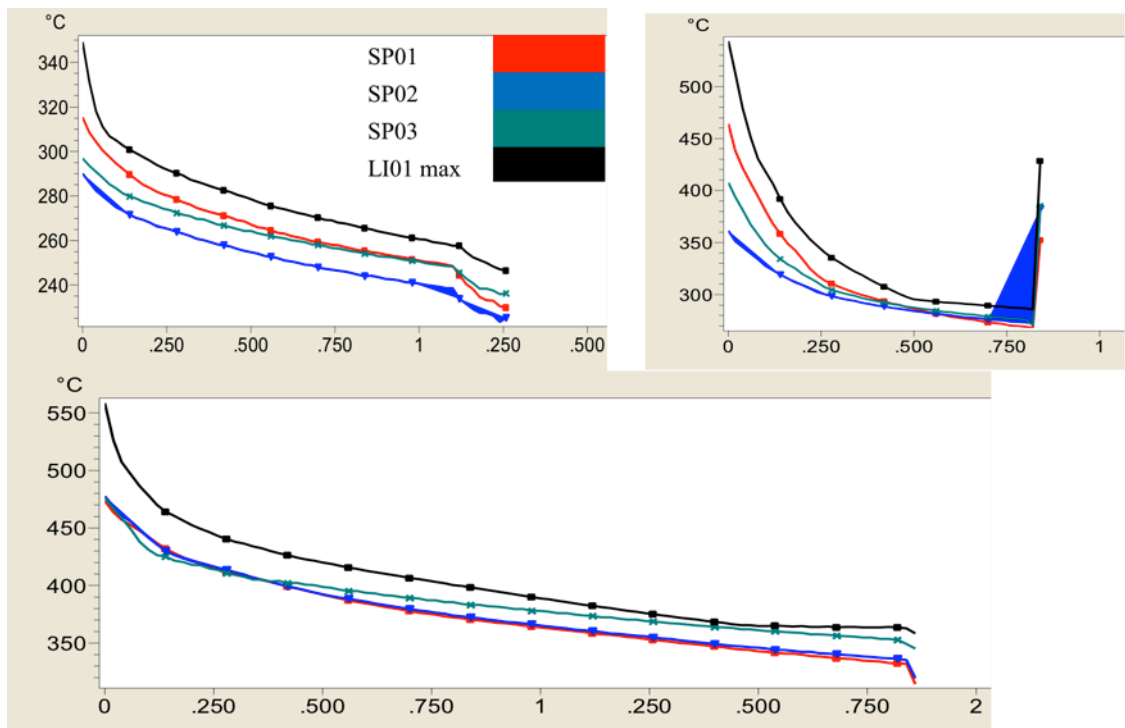
Figure 4.41. Rate of temperature change at Tb = 215 ^0C (stage 1), 250 ^0C (stage 2) and 310 ^0C (stage 3) – CPF 1

Similar analysis was conducted for larger NTP separations. At higher NTP separation the starting temperature for Sp01, Sp02 and Sp03 was higher. Similar trends were observed with respect to the change in temperature with time.

In CPF 2, the spot temperature measurements revealed a similar heat loss trend with one key difference. The heat loss rate was faster than CPF 1. Therefore, a steady state temperature was achieved quickly in stage 1 and stage 2. For stage 3, steady state conditions were not achieved even after 4 s (twice the time compared to CPF 1) as shown in figure 4.42 below. It is hypothesised that, when the evidence for the char structure, process of growth and thermal profiles is combined, CPF 2 had better thermal protection properties than CPF 1.
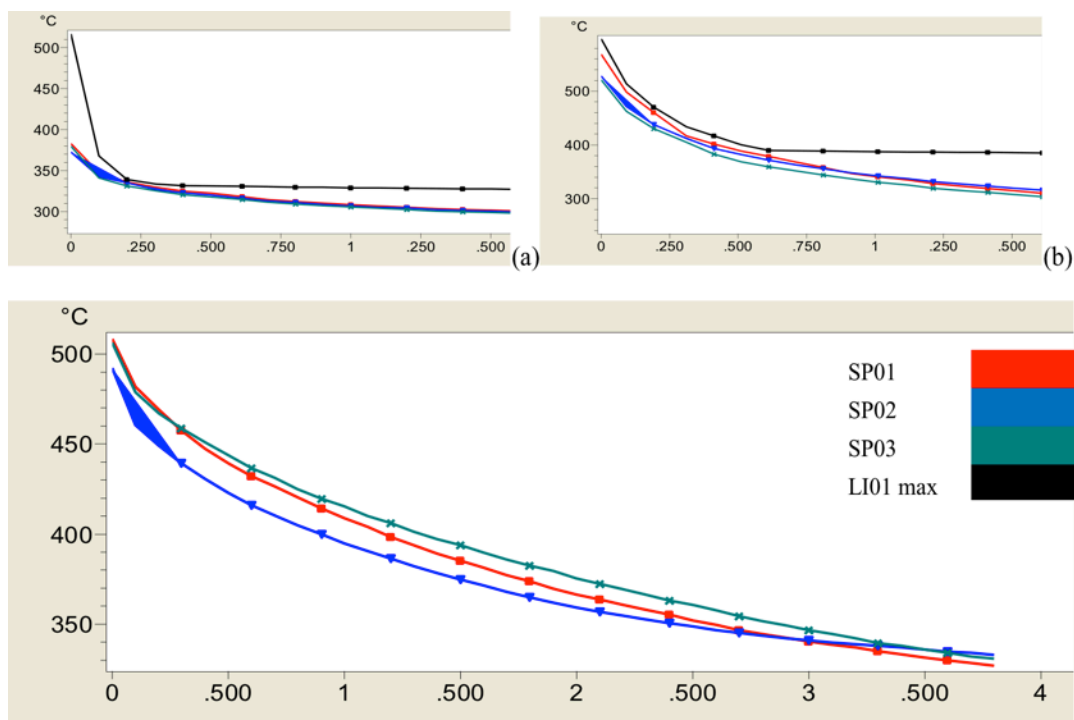
Figure 4.42. Rate of temperature change at Tb = 250 ^{0}C (stage 1), 310 ^{0}C (stage 2) and 330 ^{0}C (stage 3) – CPF 2

4.9 Repeatability of results

Reparability and reproduction of results is a very important aspect of any scientific work. Therefore, it was important that evidence should be recorded and presented which highlights the repeatability for the work conducted as part of this research. Therefore tests were conducted using CPF 1 and HPF 1 with a heat shield in position and HPF 2 without a heat shield. The experimental conditions used were H/D= 40, fuel flow rate of v= 6.67m^3/s and film thickness t =1mm. the standard deviation of the thickness was within 5% of the target thickens. The TTF curves for up to 4 tests

conducted using the same conditions are illustrated in figure 4.43. The TTF values achieved were within 1% of each other. Therefore, the experimental setup and methodology were accurate to a satisfactory standard.

(a)

(b)
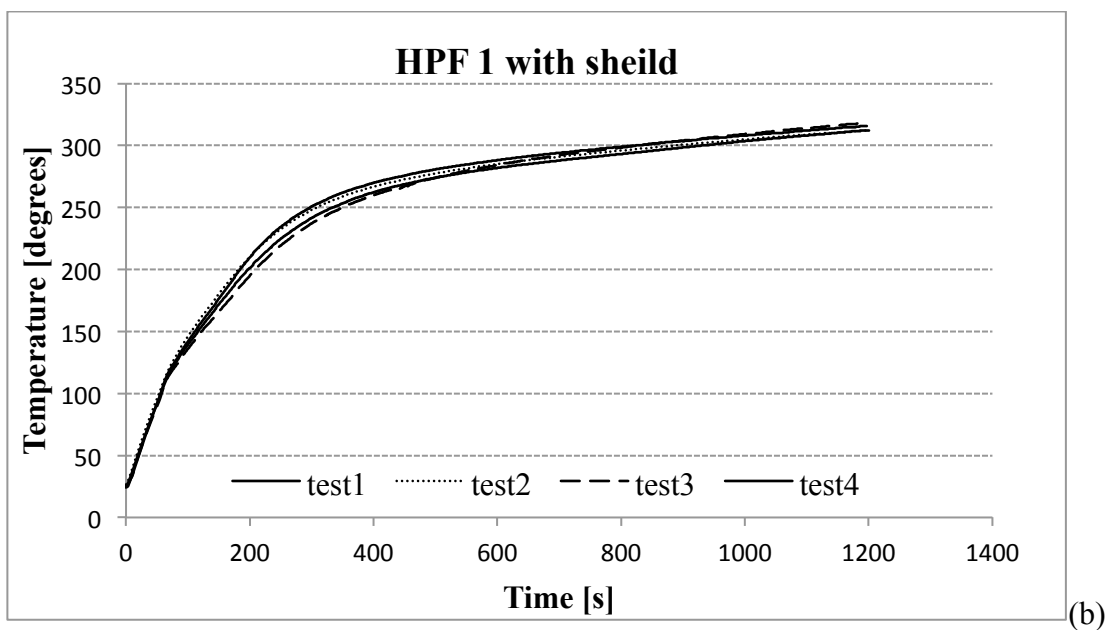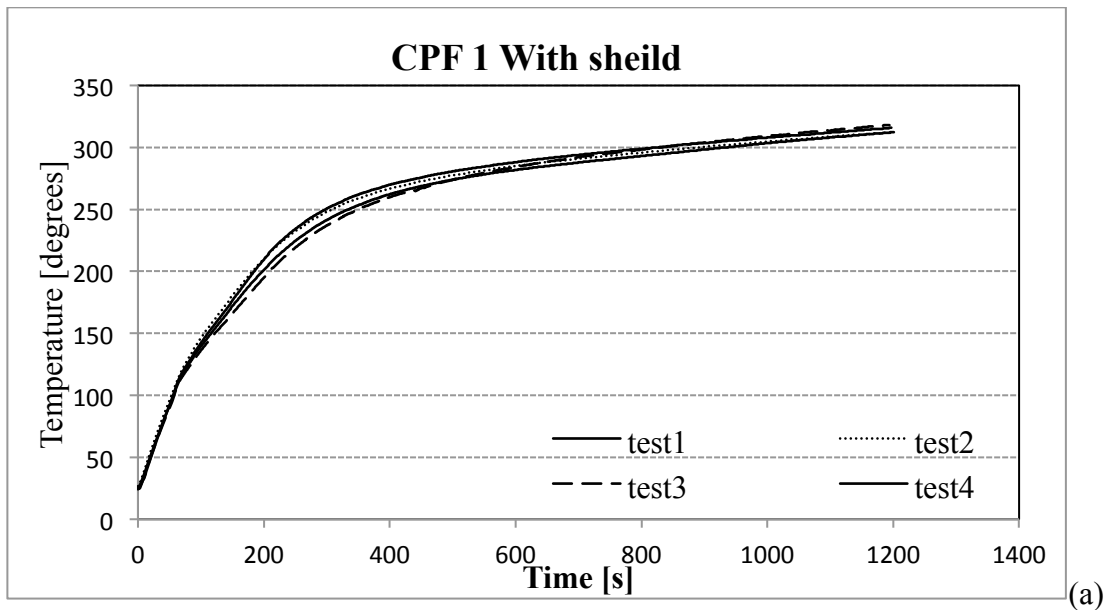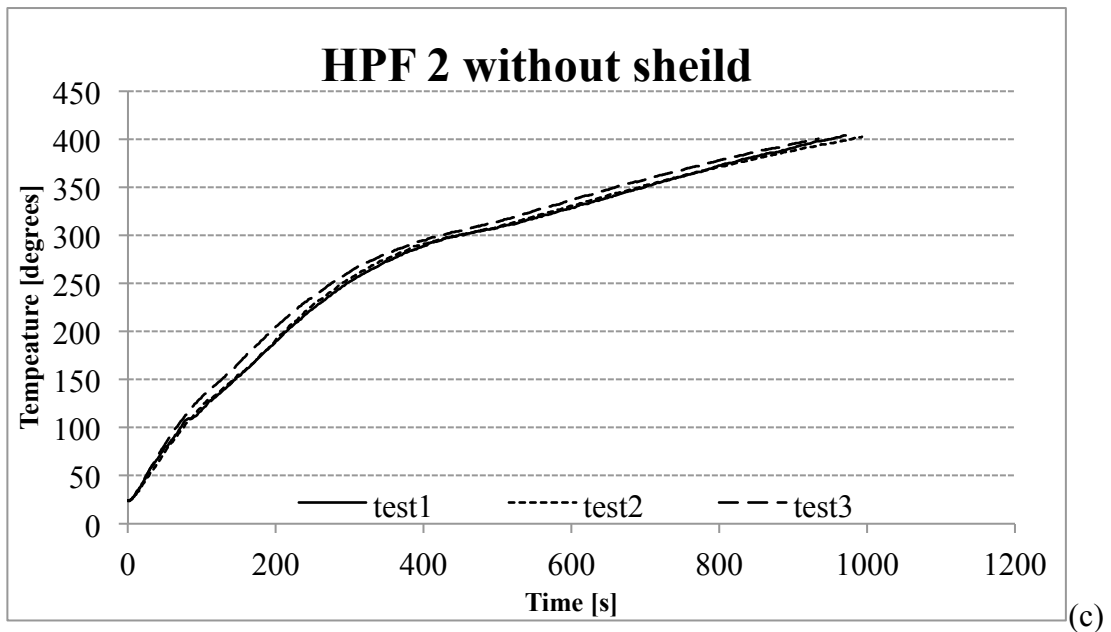
Figure 4.43. TTF repeatability conducting experiment at same experimental conditions for (a) CPF 1 (b) HPF 1 (c) HPF 2.

4.10 Conclusion

In this chapter, the effect of various experimental conditions was discussed for a variety of intumescent paint formulations. The formulations were studied using a variety of diagnostic methods under an impinging flame heating input. A variety of physical aspects have been observed, investigated, analysed and discussed in this chapter. Evidence and results have been presented to test the initial hypothesis that the use of advance imaging based diagnostic techniques will allow us to gain new insight into the process of intumesces. Furthermore, efforts are made towards identifying whether these techniques could be used to study fire protective coatings at lab scale and use the information to predict their performance in real fire scenarios.

The variation in experimental condition included NTP separation (heating rate), fuel flow rate (thermal loading at nozzle exit) and paint film thickness. It was observed that

- The process of intumescence has been studied for the different formulations under a thermal imaging system. It was concluded that:
    - During the expansion process, the surface of the coating developed pustules. These pustules were a result of pockets of gases that escaped through the surface. Once the pustules had fully developed, the coating started to intumescence.
    - During intumescence, mass loss and the exposure of plate edges were observed.

- o Although the underlying mechanism remained the same, the chemical compositions of each coating can be altered. In doing so, formulators can influence the intumescence process. Coatings varied between small rigid expansions with high mechanical stability to profuse chars with significantly delayed reaction sequences. Hence, a wide variety of fire scenarios can be potentially covered.

- The occurrence of expulsions was a unique phenomenon discovered through the Schlieren technique. It was the first time such evidence was collected showing spumific gases, trapped under the surface, released as bursts of different intensities. These bursts resulted in the appearance of pustules or bubbles on the surface of the intumescent coatings.

- Surface textures were dependant on the nature of the expulsion. The intensity of expulsions and consequently the bubble size varied due to the formulation type and heating conditions. Coating designed for turbulent flames exhibited large pustules and infrequent powerful bursts. Whereas, coatings designed for cellulosic fired exhibited smaller pustules. The size of the pustules became smaller as the incident heat flux was decreased.

- The unique application of the Schlieren flow visualisation technique was used to conduct accurate tracking of the rate of char growth and identify the Expansion Activation Temperature, EAT_b. Char growth rate was observed to be unaffected by the fuel flow rate. However, higher thermal loading, NTP separation and coating thickness increased the degree of expansion. It is recommended that fire engineers should consider NTP separation and expansion ratios, as key indicators during the application of coatings in various fire scenarios to achieve desired TTF ratings. EAT_b indicated that majority of the expansion occurred once substrate temperature were in the range of 300 ^{0}C.

- NTP separation was a key factor. It was observed that there was a strong dependency between TTF and NTP separation. This was driven by thermal efficiency. Thermal efficiency reduced significantly with NTP separation, which in turn resulted in extremely high Time to Failure (TTF). Therefore, formulators and applicators should consider thicker coatings close to ignition source.

- Characteristics such as mode shapes, internal char structure and surface texture were also investigated.

- o CPFs exhibited large expansion ratio and consequently higher time to reach failure temperatures.

- o Mode shapes varied between convex and concave due to the impingement of unreacted fuel impinging on the plate resulting in a cool central core. Char structures had high visible porosity and a soft fragile texture.

- o CPF1 surface was densely populated with pustules that changed with heating height. Whereas, CPF 2 had a smooth surface. HPF based coatings had thin densely packed chars designed for strength in extreme conditions. However, it was observed in HPF 2 that the char presented with a swelling once it had intumesced. This resulted in a huge void under the layer of the char that reduced its structural integrity completely.

- • TTF increased significantly when film thickness or NTP separation were increased. However, the char structures became increasingly complex in shape and size.

In this chapter the majority of the analysis conducted over the course of this research has been presented. The following chapters would only focus on results that were found to be different due to the changes in the heating technique.

Chapter5.   Results   and   Analysis: Cone calorimeter setup

5.1   Introduction

Cone heaters have gained popularity for testing lab based fire protective coatings systems. They are simple and robust in construction and allow researchers to measure various important parameters during the degradation process of an organic coating [36]. Wang [6, 110] and Staggs[109] have compared furnace testing with cone heater testing in an effort to increase awareness about small scale lab tests to study fire protective coating. In this work, the observations, results and analysis from cone heater based testing is compared against impinging flame systems. First, some of the key differences between the heating techniques are highlighted.

Direct Flame Impingement

- **Pros**

    – Heat transferred primarily through forced convection, among other mechanisms

    – Covers almost every aspect of thermal fluid phenomena

    – Ease of instrumentation access

    – Uneven heat flux generated similar to real fire conditions

    – Contact based heating method

- **Cons**

    – Element of secondary heating through exhaust gases

    – Diffusion flame setup; Burn outs required

Cone heater

- **Pros**

    – Uniform heating through radiation

    – Negligible secondary heating-rising hot gases extracted

- Ideal to identify basic characteristics and draw comparison

- No burn outs required

- **Cons**

    - Limited variations in testing procedures

    - No impingement of the heat source

5.2 Calibration with impinging flame

In order to compare the results between the two heating techniques, a calibration study was conducted. NTP separation and thermal loading variation using an impinging flame were compared with cone heater heat-flux measurements for blank steel panels. The TTFs are illustrated in figure 5.1.
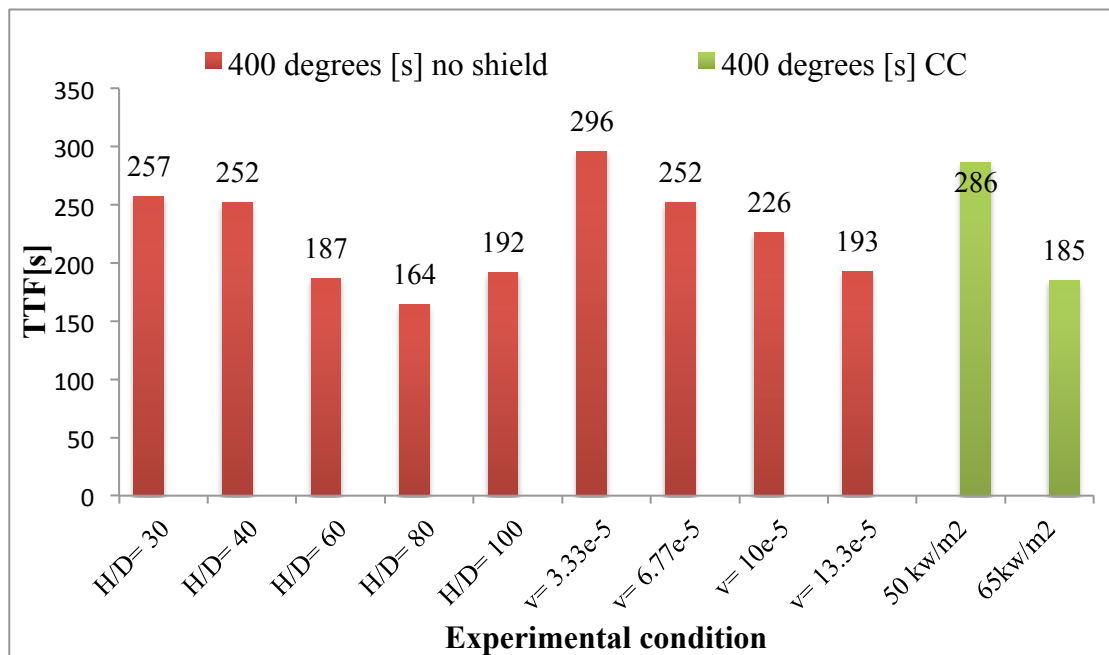
Figure 5.1. Comparison of TTF against various experimental conditions.

It was assumed that the heat rate between the two techniques was equivalent if it took the same amount of time to reach 400 ^{0}C. For a heat flux of 50 kW/m^2, the time was 286 s. It can be seen that NTP separation of H/D = 30 and 40 are within a 10% margin. Table 5.1 summarises, comparable test cases to the two heat flux values used in cone heater. These test cases were used to compare resultant char structures.

Table 5.1. Comparison matrix of experimental conditions between cone and impinging flame heating techniques.

	Impinging flame conditions
50 kW/m^2	H/D = 30
	H/D = 40
	v= 3.33e-5 m^3/s
	v= 6.77e-5 m^3/s
65 kW/m^2	H/D = 80
	H/D = 100
	v= 13.3e-5 m^3/s

5.3 Flat Panel Tests

5.3.1 Process of intumescence

A combination of digital and thermal imaging was used to record and analyse the process of intumescence. Unlike the impinging flame setup, digital images provided clear evidence of when expansion took place during the test. Consistency was observed between the heating techniques with respect to the process of intumescence, surface texture and EAT_b. The key difference was observed in the degree of intumescence and internal structure which were different for each technique. This is attributed to the incident heat flux and the heating rate experienced by the coating.

Figure 5.2 shows the digital data collected for CPF 2 under a cone heater. Inactive surface activity at beginning of heat exposure, the expansion process and post intumescence shrinkage can be observed. The surface temperature is also shown. The surface was inactive until $T_b = 260^0C$ was achieved. This was similar to observation under a diffusion flame. Intumescence was recorded between $T_b = 300^0C$ and $T_b = 350^0C$. Char shrinkage was observed between $T_b = 350^0C$ and $T_b = 400^0C$. The appearance of pustules on CPF 2 can be seen, this was not the case for the flame based heating techniques.
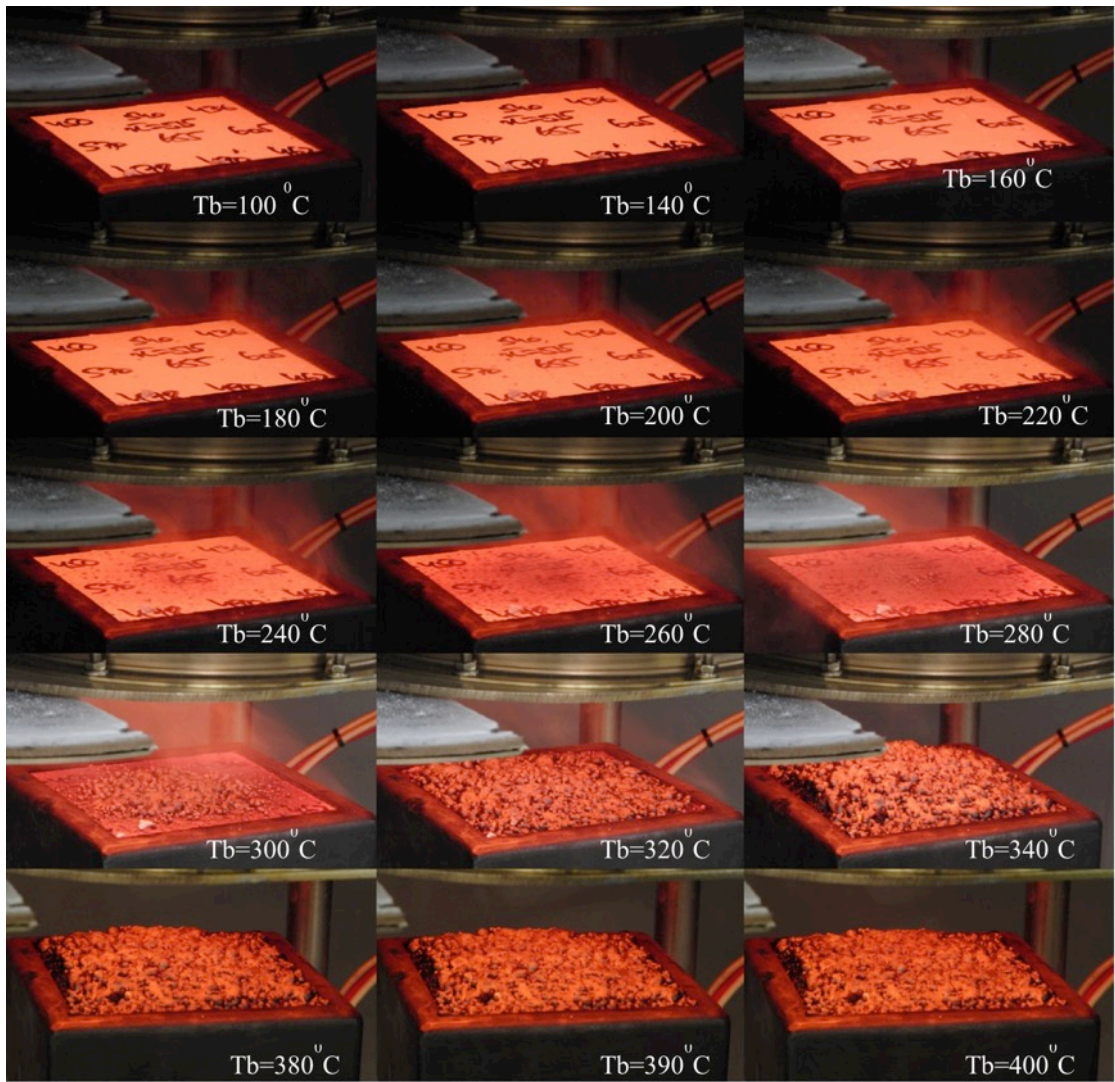
Figure 5.2. Series of digital images illustrating char growth - CPF 2 at 50kW/m2

Images at $T_b = 380^0C$ and $T_b = 400^0C$ have been enhanced and shown in figure 5.3 to highlight the shrinkage of the char.
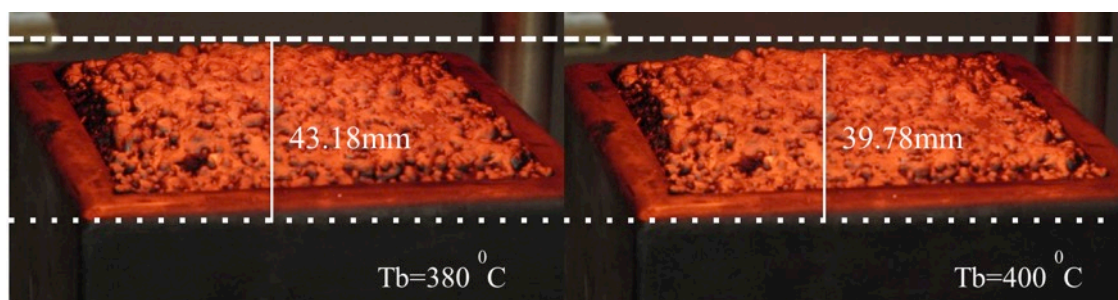
Figure 5.3. Char shrinkage between Tb = 380 and 400 ^0C - CPF 2 at 50kW/m2

5.3.2 Time to Failure and char structure comparison

Time to failure

Time to reach temperature of 300 ^{0}C, was compared for the different formulations. The data is presented in figure 5.4. The difference in the results shows that the change in heating technique had a significant impact on thermal performance of a coating. Cone heaters exhibited higher TTF compared to flame setup. This was because the forced convective heat transfer component found in impinging flame setups resulted in higher heat fluxes at the substrate surface.

TTF [300 DEGREES]

	CPF1	CPF2	HPF1	HPF2
■ 50KW	429	233	450	454
■ 65KW	467	115	320	368
■ H/D 40	305	211	246	329
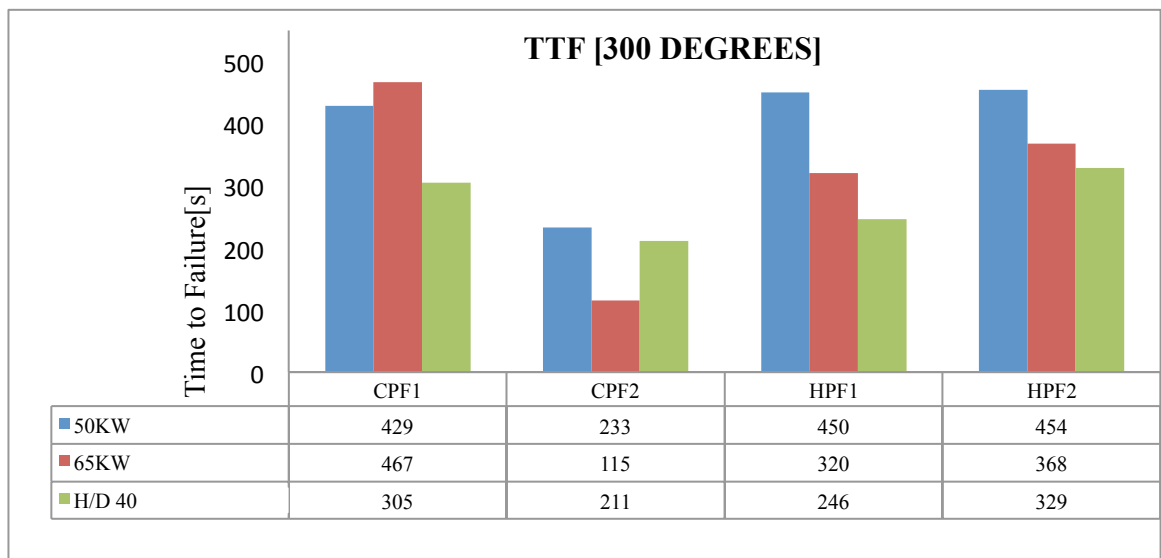
Figure 5.4. Comparison of TTFm for various formulations for cone heater settings against chosen conditions with and w/o heat shield.

Degree of intumescence

The degree of intumescence was significantly reduced under a cone heater. This may be because of the loading cell in a cone heater had the panel facing upwards compared to the inverted orientation in the flame setup. Therefore, the effect of gravity and direction of growth could have large impact on intumescence. The greatest difference was observed in the expansion of CPF 2. In an inverted orientation, with the help of the gravitational pull and its highly viscous nature, CPF 2 expansion ratio was the highest. However, when tested facing up, its expansion ratio reduced significantly.

<u>*Mode shapes*</u>

Using the cone heater, char samples did not exhibit any variation in mode shapes. The char intumesced uniformly with maximum expansion observed in the middle of the panel as a result of the uniform heat flux. The two heat flux measurements were made at 70mm and 35mm respectively. Therefore, it was expected that at 35mm, where a greater heat flux was incident on the test panel, expansion ratio would be higher than that at 70mm separation.

It was observed that the char intumesced to a maximum expansion and started to shrink during a test. This was observed for all tested formulations.[1]Shrinking was observed during flame-based tests as well. The reason for such behaviour is not yet fully understood and is a subject of further investigation.

5.3.3 Surface Temperature Profiles

The surface temperature profiles between the heating techniques were compared. T_s profile for various formulations at H/D = 80, shown in the figure 5.5, were compared with heat flux of 65 KW/m^2 in figure 5.6. At the start of each test T_s increased linearly with time. It decreased slightly as the char started to intumesce. The trend was consistent for all NTP conditions.
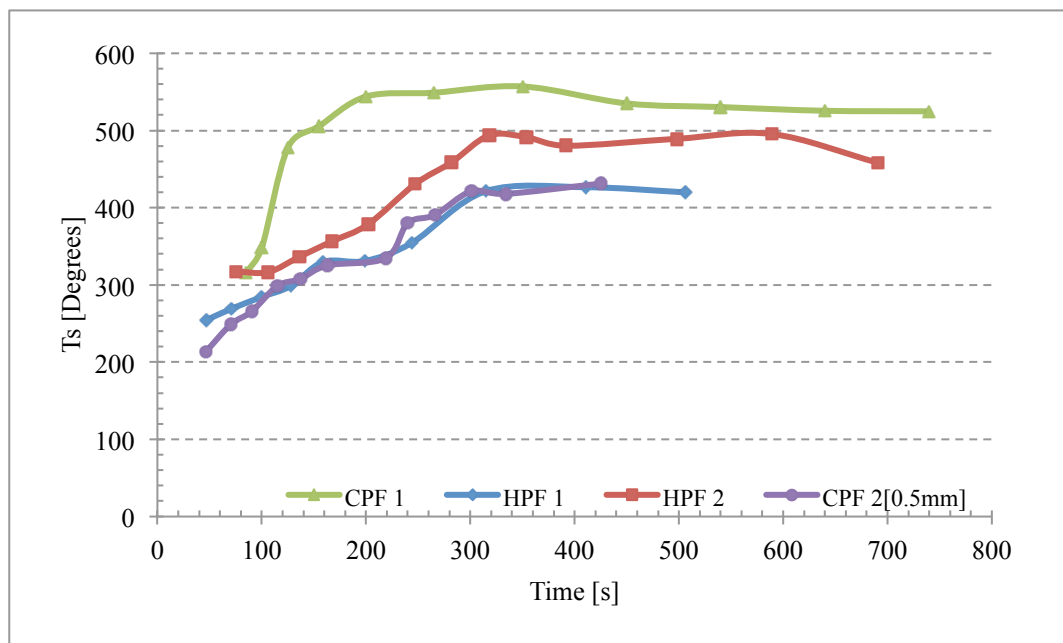
Figure 5.5. Ts profile for various formulations at H/D = 80

The curve illustrated in figure 5.6 is for a cone heater test at a heat flux of 65kW/m^2. The curves exhibits a smooth profile compared to values recorded in the flame based techniques. This was due to the uniform heating offered by a cone heater. The value of T_s was higher than the flame based setup. The values for the different coatings are much closer when compared to the flame based setup highlighting the contrast between uniform and non-uniform heating methods.
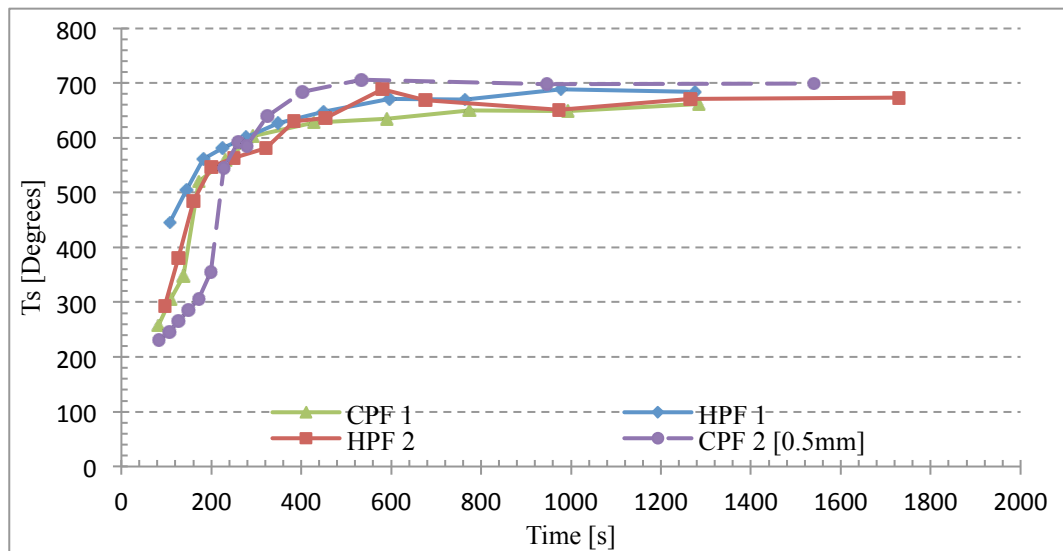
Figure 5.6. Ts profile for various formulations at heat flux of 65kW/m2

Sources of Error

Unlike flame-based setups, there was no need to conduct burnouts in the cone heater and readings through the thermal imager could be taken instantly. This significantly reduced the uncertainty in the measured values. In the flame-based setups, when the flame was turned off the char would cool down rapidly. Therefore, the value of the surface temperature had to be taken instantly. When the value was taken, the influence of the hot gas layer after a burnout could never be completely discounted. This was one of the primary reasons for fluctuation in the recorded values. There was also evidence obtained from the Schlieren technique that a combination of dense smoke and spumific gases settled in the cavities between pustules which could add further uncertainty to the recorded values.

5.4 T-panels: Techniques to study complex char movement

T-panels are representatives of many designs commonly found in steel structures [111]. They include a combination of flat surfaces in various angles and orientations including flanges, webs, curved joints and large fixings such as nuts and bolts. This results in a variety of complex interaction where char growth can be complex in nature. Thus, they are being used increasingly to study more complex intumescent behaviour. The culmination of this work has focused on the movement of char on T-panels under cone heaters using novel diagnostic techniques. A schematic of the T-panel used as part of this work is shown in figure 5.7.
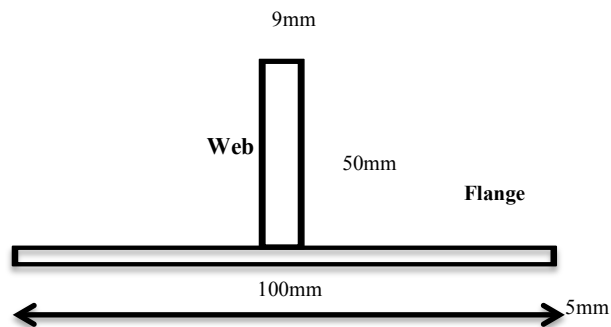
Figure 5.7. Cross-sectional schematic of a T-panel

In this section, the results are presented for tests conducted on samples under the cone heater under heat flux of 50 kW/m^2 and 65 kW/m^2. The thickness of coatings HPF 1, HPF 2 and CPF 1 coatings was 1mm whereas thickness of 0.5 mm was applied for CPF 2. This was to keep consistency in tests with flat panels. Imaging methods can only capture 2-D images at any specific time. Therefore, each sample was tested in lateral and longitudinal direction.

To further enhance our understanding of the char movement, a char growth tracking technique was developed. Thermal images measured at discrete substrate temperatures were post processed using Matlab and the results show that the char growth was successfully tracked using this method.

5.4.1 Process of intumescence

Char growth images, in latitudinal orientation, for a typical test using CPF 1 under a heat flux of 50 kW/m^2 is shown in figure 5.8. The images were taken over a period of time with respect to the substrate temperature. The thermocouple attached to the sample measured the substrate temperature with respect to time.
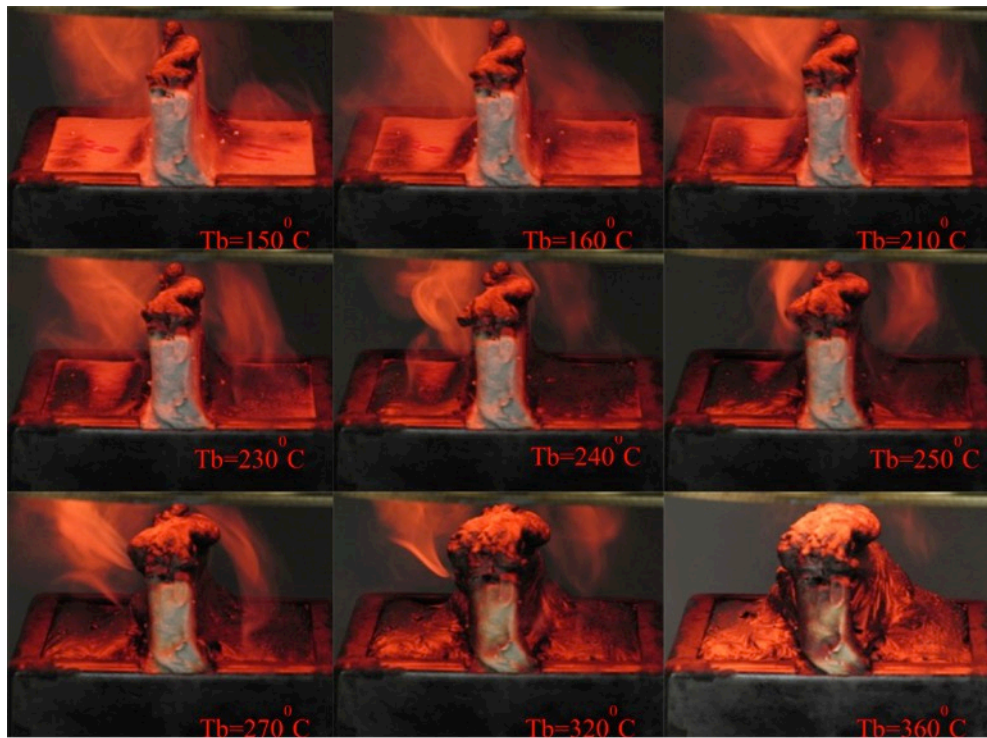
Figure 5.8. Growth sequence of a CPF1 T-panel sample - Latitudinal view

The first evidence of intumescence appears on the top face of the web due to its close proximity to the heater. The flange also shows early signs of intumescence, as the heat flux is directly incident on its surface. Unlike the flange the vertical face of web receives the least heat showing late signs of intumescence. As the reaction sequence progressed, it was observed, when $T_b = 240\ ^0C$, that the char on the top of the flange had fully intumesced and almost all the initially applied film thickness of CPF 1 had reacted.

The second part of the test was to change the direction of the sample to a longitudinal view. A new panel with the same film thickness was used and the char growth is shown in figure 5.9(a). The heating pattern of the flange and the web were similar for the longitudinal view. However, there was an additional observation, on the vertical face of the web, as different parts of the panel started to intumesce, stretch marks

appeared on the surface. As the char under the surface began to intumesce, the marks began to disappear. They did not influence the growth pattern significantly with the exception of the edges of the flange. Upon full growth, the char started to shrink which led to the appearance of cracks on the surface.
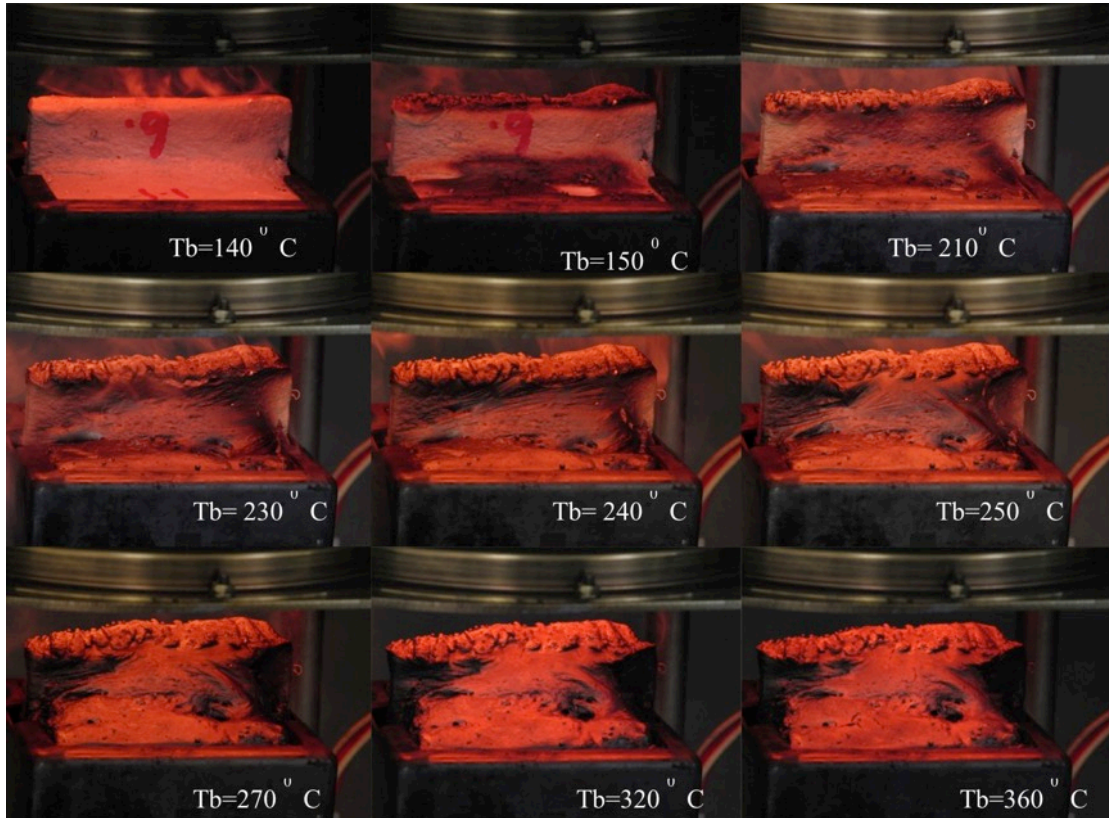
Figure 5.9(a). Growth sequence of a CPF1 T-panel sample - Longitudinal view.

The thermal temperature analysis shows why the stretch marks appeared. Figure 5.9(b), illustrates the thermal footprint at $T_b = 150\ ^0C$ and $T_b = 250^0C$.
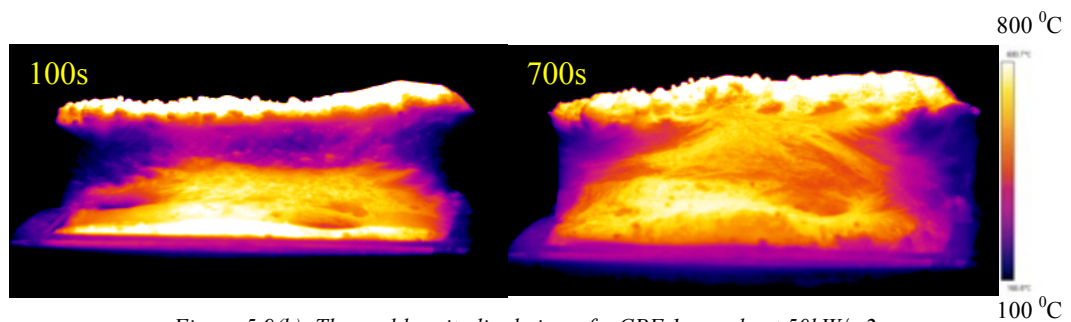
Figure 5.9(b). Thermal longitudinal view of a CPF 1 sample at 50kW/m2.

At the beginning of the test, the vertical face was a low temperature region. This is shown in the image on the left in figure 5.9. Its central part had a higher localised temperature, compared to its edges. Hence, intumescence started in the higher temperature region first. This resulted in uneven expansion patterns that were primarily responsible for the appearance of the stretch marks on the surface. At later

133

stages during the test, image on right in figure 5.9, the complete coating on the face started to intumesce. The low temperature region observed at $T_b = 150 \, ^0C$ disappeared and the stretch marks reduced in size.

The edges of the face were still relatively cooler than the rest of the face. Therefore, as the degree of intumescence increased, the stretch marks near the edges of the panel became more defined in size and shape. The trend can be extrapolated and it can be assumed that at higher thicknesses the uneven exposure could also result in cracks that can expose the substrate.

The process discussed was found to be consistent in all formulations tested but the surface textures and internal structures were unique to each formulation. These have already been discussed in light of the flat panel tests.

5.4.2 Movement of Char

It was observed, that the char intumesced perpendicularly to the surface it formed on - the growth on one surface interacted with and influenced growth on another. This was a general trend observed in the growth patterns in all the samples. It was observed that, the char on the top horizontal surface of the web was supported by the char growth on the vertical faces of the web. The movement of the char on the vertical faces of the web was influenced by the growth on the base of the panel. The base of the panel had the greatest surface area. Therefore, the majority of intumescence would occur over the base assuming all parts of the panel had uniform film thickness.

The combination of char movement on the base and the flange resulted in a diagonal movement pattern (figure 5.10). Such movement was mostly observed near the intersection between the base and the web. Char growth near the edges of the panel was relatively uninfluenced.
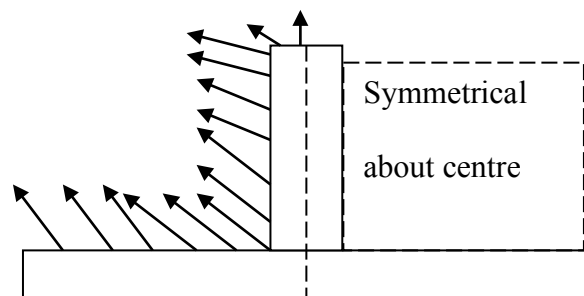
Figure 5.10. Hypothesised char movement schematic for a typical sample

The evidence of diagonal movement was clear, in both digital and thermal images. The appearance of distinctive fault lines at the junction between the web and flange were observed. Figure 5.11, illustrates the appearance of the fault lines as observed in the latitudinal view, for all formulations.

Thermal images for CPFs in the figure 5.11 showed clear evidence of char movement in a diagonal direction. The most distinctive patterns were observed in CPF 2 formulation based char sample. For the HPFs, the evidence was very subtle. This was associated with its rigid texture and relatively low degree of intumescence.
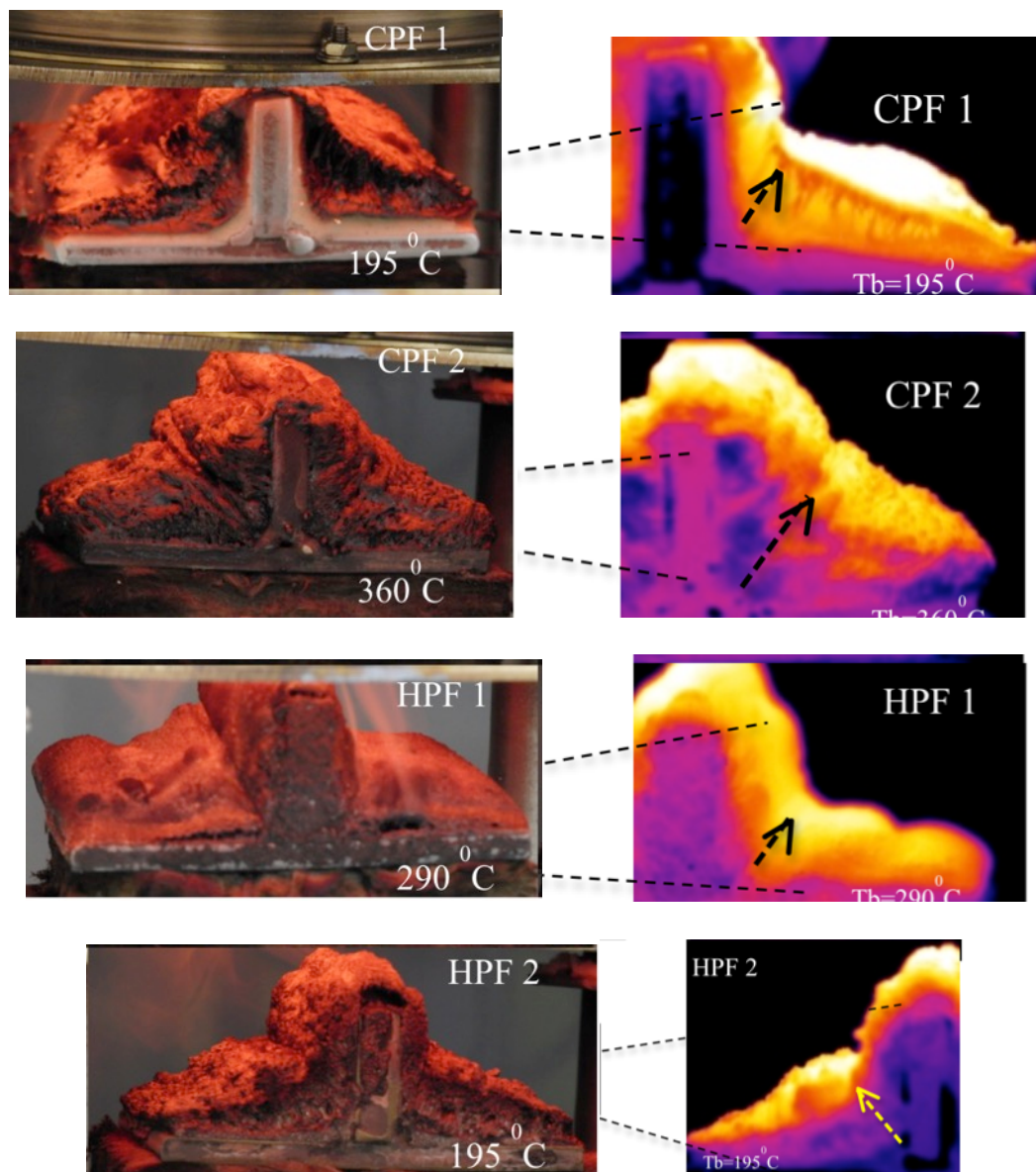
Figure 5.11. Fault lines observed using thermal imaging during growth of char under a cone heater.

The thermal imaging system was also used to analyse the surface temperature profile when the panel was exposed to the cone heater. Values for T_s were measured at the centre of the three visible faces in that orientation. The measurement locations are

illustrated in figure 5.12. Measurements were made on the horizontal face of the web (Sp01), vertical face of the web (Sp02) and the horizontal face of base (Sp03). For the purpose of a basic understanding of the temperature profile, measurements were made at the centre of each face. Figure 5.13 illustrates the changes in T_s against time for a CPF 1 panel, tested at a heat flux of 50 kW/m^2 in a longitudinal orientation.
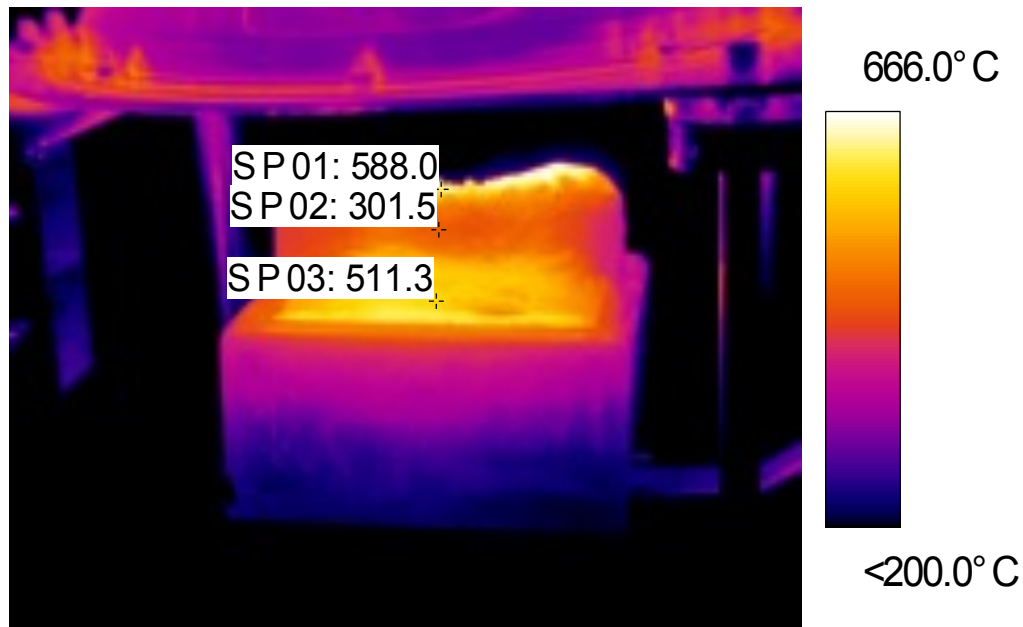
Figure 5.12. Location of spots for surface temperature measurements – CPF 1.
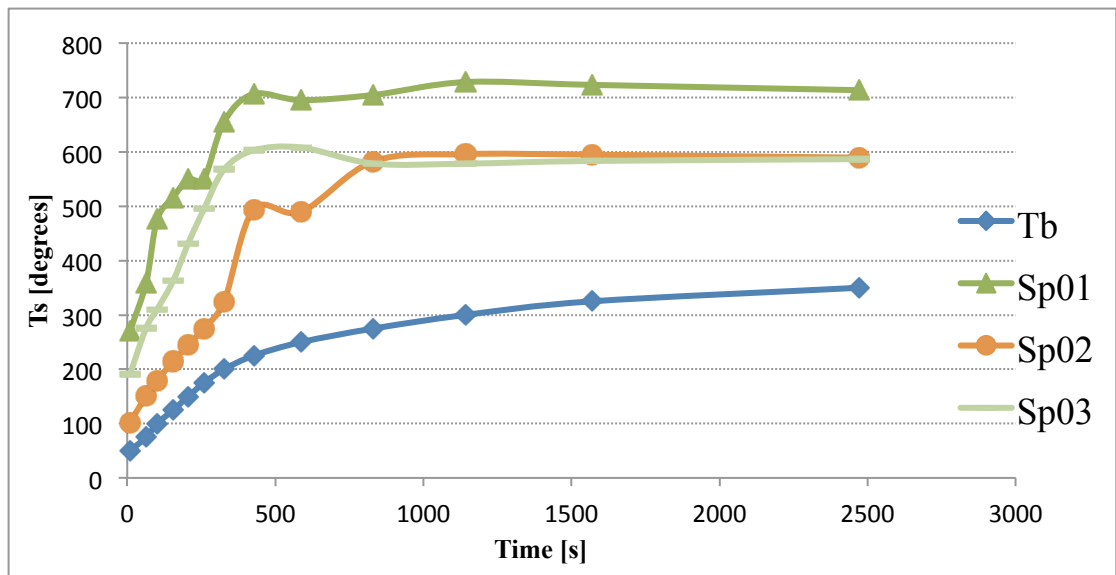
Figure 5.13. Surface temperatures against time CPF 1 panel, tested at a heat flux of 50 kW/m2 in a longitudinal orientation.

The highest surface temperature was achieved at the top of the web. The temperature at the base was higher than that at the vertical face of the web. However, once intumescence increased, the temperature in both parts of the panel became almost the same.

5.4.3 Failure mode

The HPF 2 sample exhibited failure when tested using the cone heater. It was observed that the growth at the base of the plate exceeded that on the web causing an excessive force on the horizontal face of the web pushing the char away from its surface. This led to separation of the char from the surface. The sequential images at T_b= 230 ^{0}C, 240 ^{0}C and 250 ^{0}C, revealed the growth pattern leading to the failure. The first signs were observed at T_b = 240^{0}C, highlighted in figure 5.14. Eventually, the entire char cracked which led to exposure of the substrate. The cracking started at the tip of the web, which was the weakest point of the char.
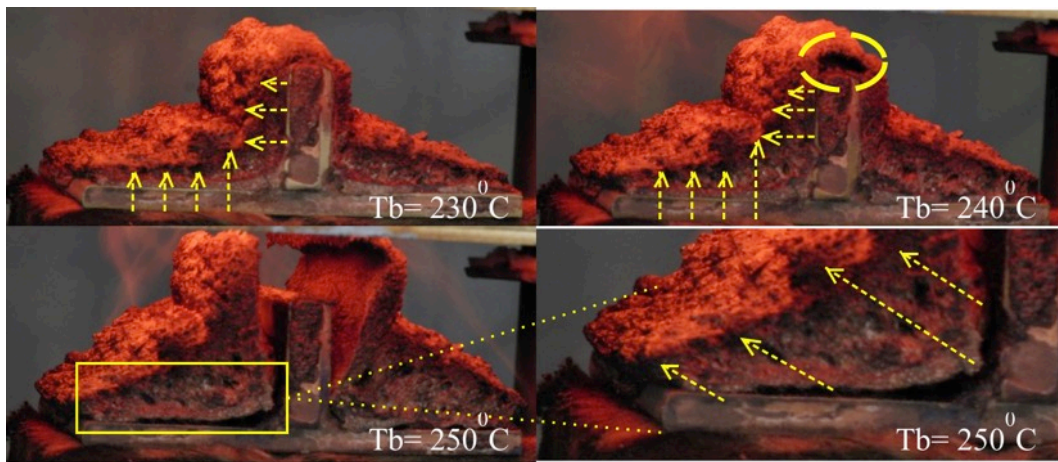
Figure 5.14. Failure in a typical HPF 2 sample

The char on the base and horizontal face of the web started to intumesce earlier than the vertical face because it received the least amount of heat,. This resulted in a distinctive wedge like shape of the char. Figure 5.15 shows a distinctive fault line across the surface of the char. This line represents the position of the original film coating prior to heat exposure, at the junction between the flange (horizontal) and the web (vertical) surfaces.
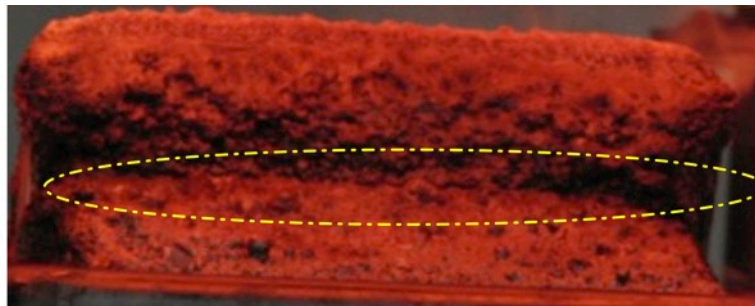
Figure 5.15. Fault line across the surface of an HPF 2 sample-longitudinal orientation.

5.4.4 Comparison between HPF – 2 and CPF - 2

The mechanism of growth of the char was compared for HPF 2 and CPF 2, to highlight the differences in the growth mechanisms. Unlike the HPF 2 sample, CPF 2 was less rigid, i.e. highly viscous during intumescence, allowing it to adapt to the panel shape. During the intumescence process, distinctive fault lines moving diagonally away from the surface were observed, but the char did not crack like the HPF 2 samples. Sequences of growth images are shown in figure 5.16.
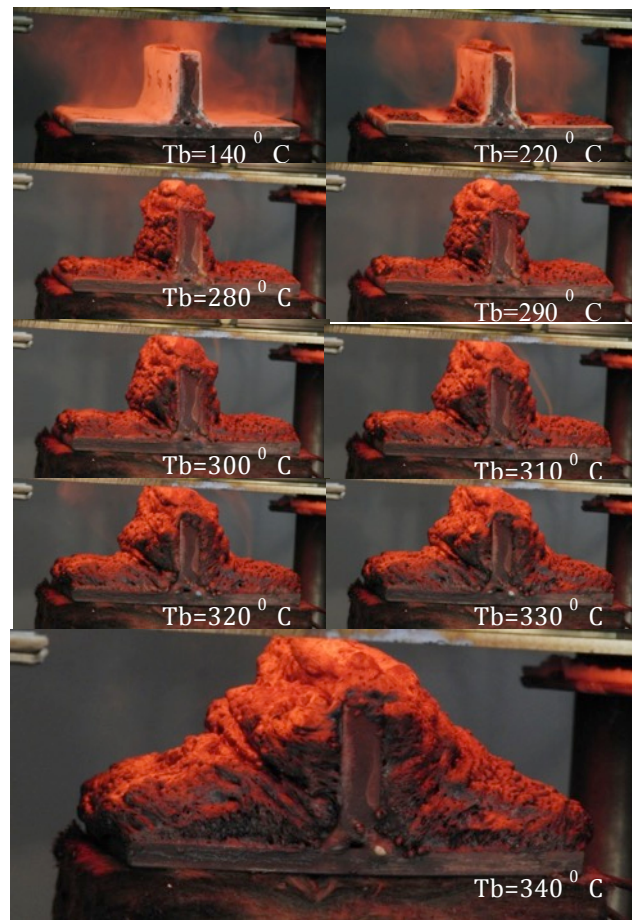
Figure 5.16. CPF 2- Latitudinal view growth sequence

The sample also shrank considerably after the test and there was evidence of hollow voids under the char surface. Furthermore, it was observed in the longitudinal view that the growth of the sample was layer based. This suggests that the growth was not continuous and occurred in phases over a period of time. The three layers of phased-growth are highlighted in figure 5.17.

$Tb=310\ ^{0}C$
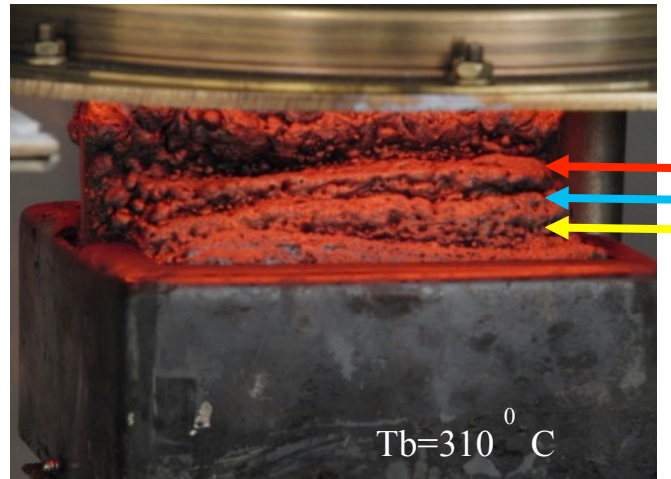
Figure 5.17. CPF 2, longitudinal view, development of a layer based growth highlighted

5.4.5 Char movement analysis - Further Study

Further studies were conducted to examine the initial hypothesis that movement of the char on T-panels was diagonal in nature. To further investigate this hypothesis, only the web part of the T-panel was painted with CPF 2. No paint was applied on the base of the panel. The intention was to observe the movement of char solely on the web without any influence of the char from the base of the panel.

For CPF 2, figure 5.18 illustrates the movement as T_b increased. It is identified at this point that the absence of protection on the flange led to an extremely high rate of change of substrate temperature compared to earlier cases.
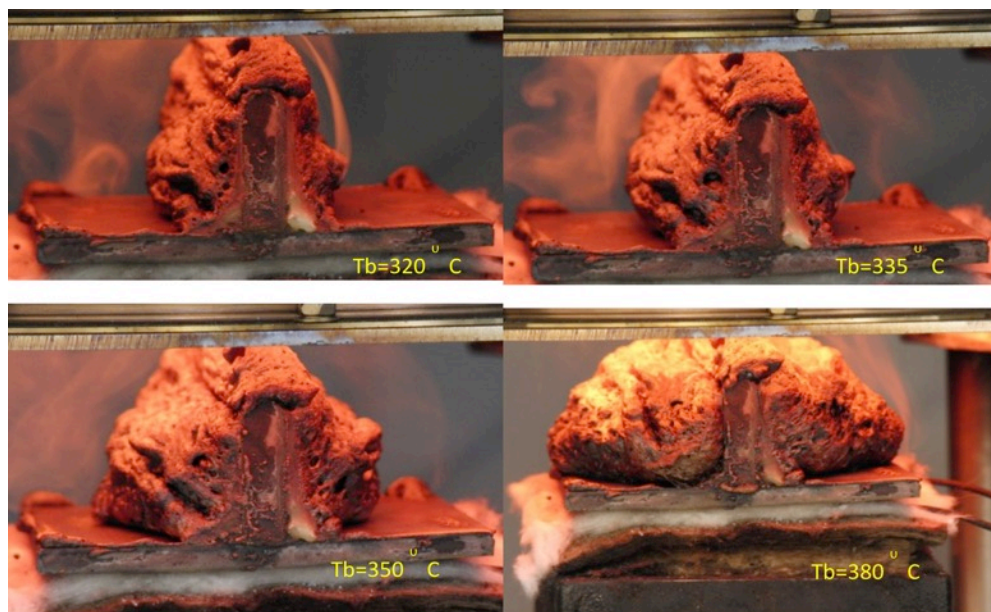
Figure 5.18. Char movement for CPF 2 coated the only on the flange.

The independent movement of the char on the web was in a perpendicular direction away from the flat surface. The paint on the intersection between the flange and base showed the distinctive fault lines that were observed in the earlier cases. However, without any char movement on the base of the panel, the char on the flange continued to intumesce unrestricted and covered the full base before it reached complete intumescence. The fault lines also disappeared. The unique shape of the char that was observed at T_b = 380 ^{0}C was attributed to the highly viscous nature and structural instability of CPF 2, due to which the char continued to grow away from the vertical face of the web

A similar test was conducted using HPF 2 samples and movement in a perpendicular direction was observed until the char cracked. However, the cause of the failure was not the same as earlier cases. In this case, the failure was caused by, char movement in opposite directions on both parts of the flange. Whereas, earlier it was observed that the influence of the growth on the base caused the char to crack near the tip of the web. The images in the figure 5.19 highlight the different failure mode. The first signs of cracking were observed at approximately T_b= 290 ^{0}C near the tip of the web for the test case illustrated in figure 5.19.
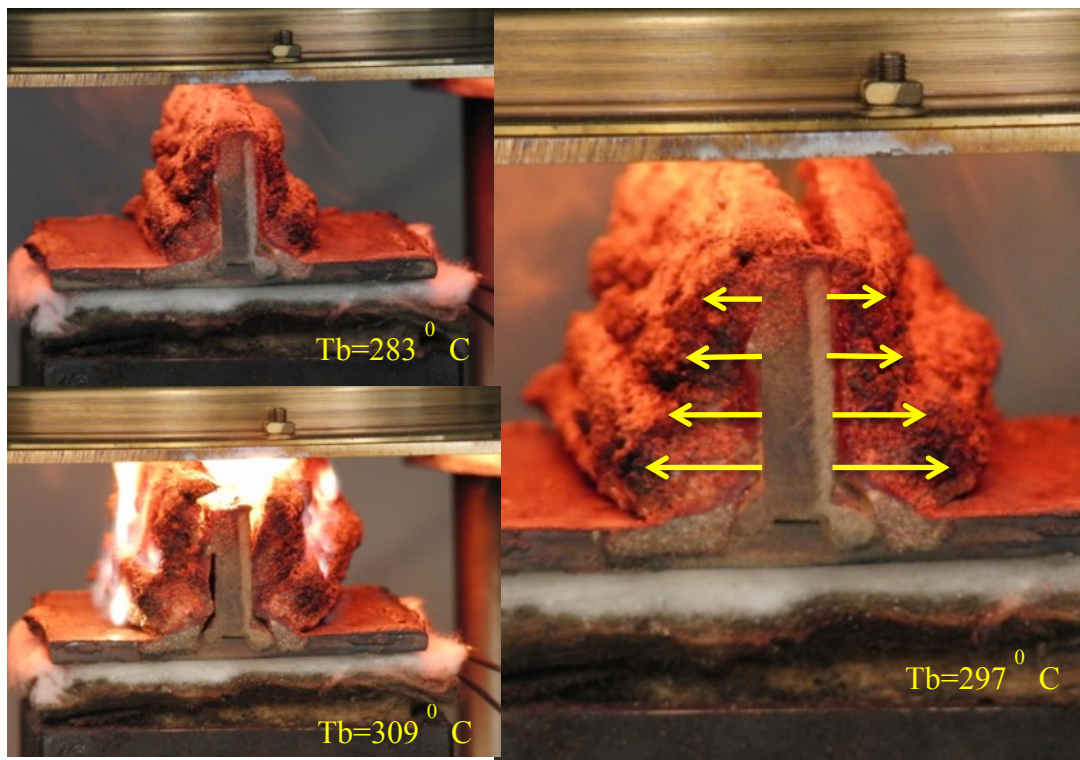
Figure 5.19. Char movement for HPF 2 coated the only on the flange.

5.4.6 Char tracking technique

5.4.6.1   Cone heater

The method to track char growth using thermal imaging system was discussed in section 3.7.7. Thermal imaging data has already helped us gain new insight into the process of intumescence. It has been established that there were clear differences in the char growth pattern based on the nature of the coating and its application conditions. The image processing data can help track the growing char layer and understand it in greater detail. In this section, the char tracking technique has been utilised on experiments conducted under the cone heater. Tests conducted on CPF 1 and CPF 2 along with, the cracking of HPF 2 is presented.

The analysis focused on the direction of movement of char in T-panels as compared to flat panels. Thermal imaging helped reveal the development of hot spots as the sample was exposed under the cone heater. The process of intumescence started at hot spots and had significant impact on the overall movement of the char.

The results from this technique allowed analysis from another perspective about the process of intumescence. One key aspect observed was the phase shift; this was when majority of the intumescence would take place. The variation of this phase among different samples, including cracking in HPF 2, is highlighted using the tracking technique. Furthermore, the substrate temperature beyond which the phase shift occurred was identified, EAT_b.

It was observed in CPF 1 that the process started, approximately when $T_b = 150\ ^0C$ and the majority of intumescence was achieved before the substrate temperature of $T_b = 250\ ^0C$. Therefore the critical phase shift in CPF 1 occurred, approximately at a substrate temperature of 150^oC. This is illustrated in figure 5.20 when CPF 1 was exposed to a heat flux of 50 kW/m^2. Each contour in the figure represents the char height at a specific substrate temperature. Focusing on the left hand region of the panel, identified as x-location 0-60mm, the maximum gap between the contours is observed between $T_b = 125\ ^oC$ and $T_b = 150\ ^oC$.

In region of x-location 60-120mm, there was a big jump in char growth between the contours at $T_b = 125\ ^oC$ and $T_b = 150\ ^oC$. This was an anomaly in the tracking aspect of

the data. It was attributed to the uneven intensity in the original thermal image, which had an effect on the outcome of the processed image. Further evidence was seen in figure 5.21 when the CPF 1 was exposed to a heat flux of 65 kW/m^2. The majority of intumescence was observed after T$_b$=150°C. Similar observations were made for CPF 2 and HPF 1. CPF 2 had a much delayed reaction sequence, the phase shift was observed to occur at T$_b$= 300°C, illustrated in figure 5.22. HPF 2, the phase shift was observed at T$_b$=200°C, figure 5.23.
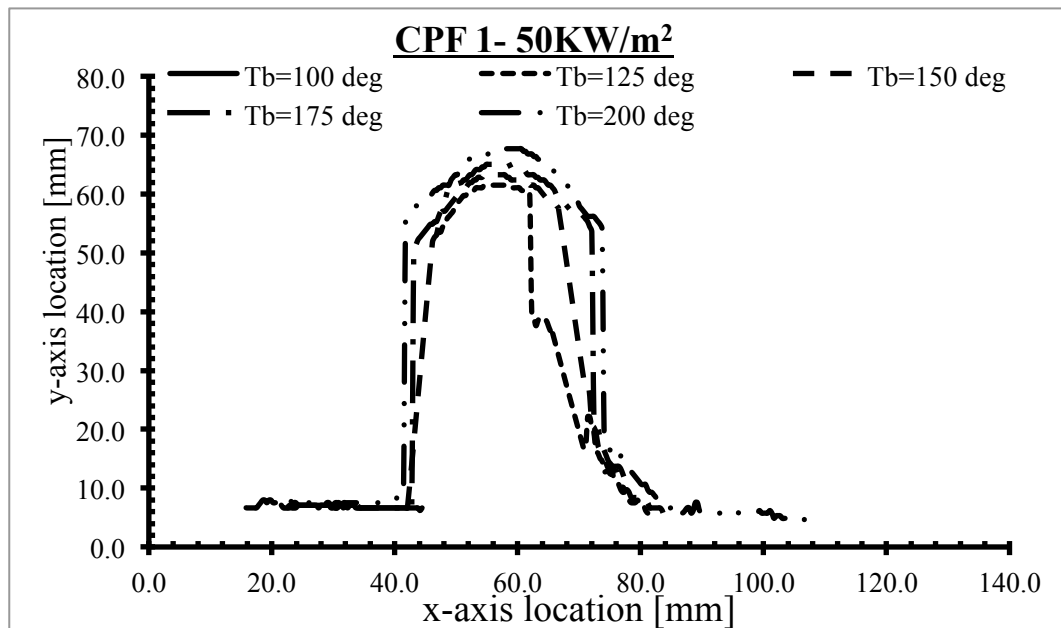
Figure 5.20. Char growth with respect to Tb for CPF 1[100-200 oC] at 50 kW/m2
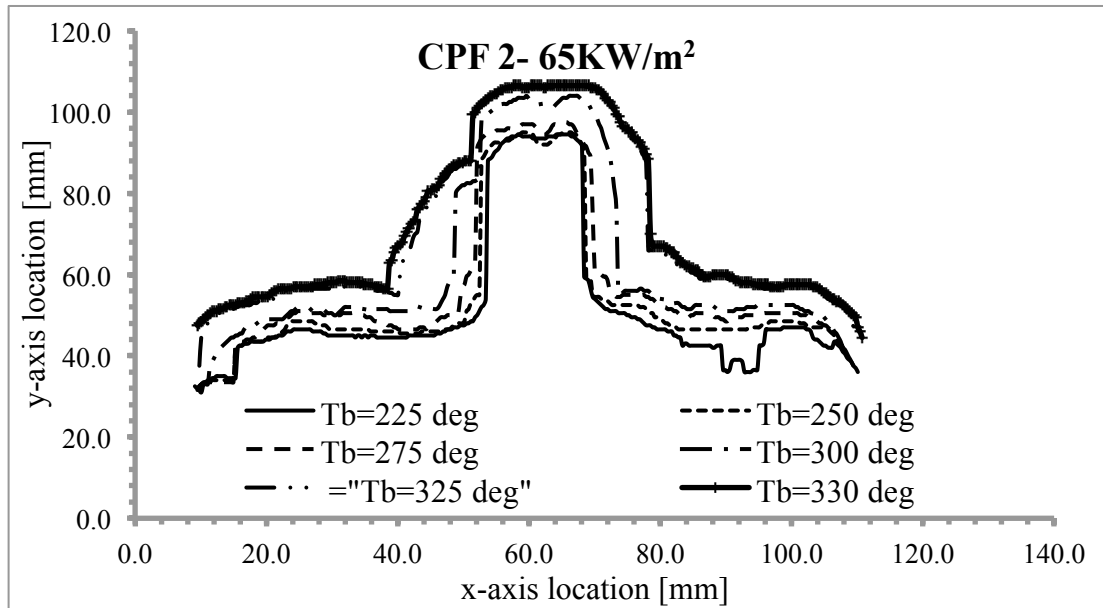
Figure 5.22. Char growth with respect to Tb- CPF 2[225-330 oC] at 65 kW/m2

The char tracking technique can also be used to collect and analyse evidence about when char structures can crack and fail. The instance presented for the HPF 2 showed that char growth could eventually lead to cracking which is considered a failure scenario.
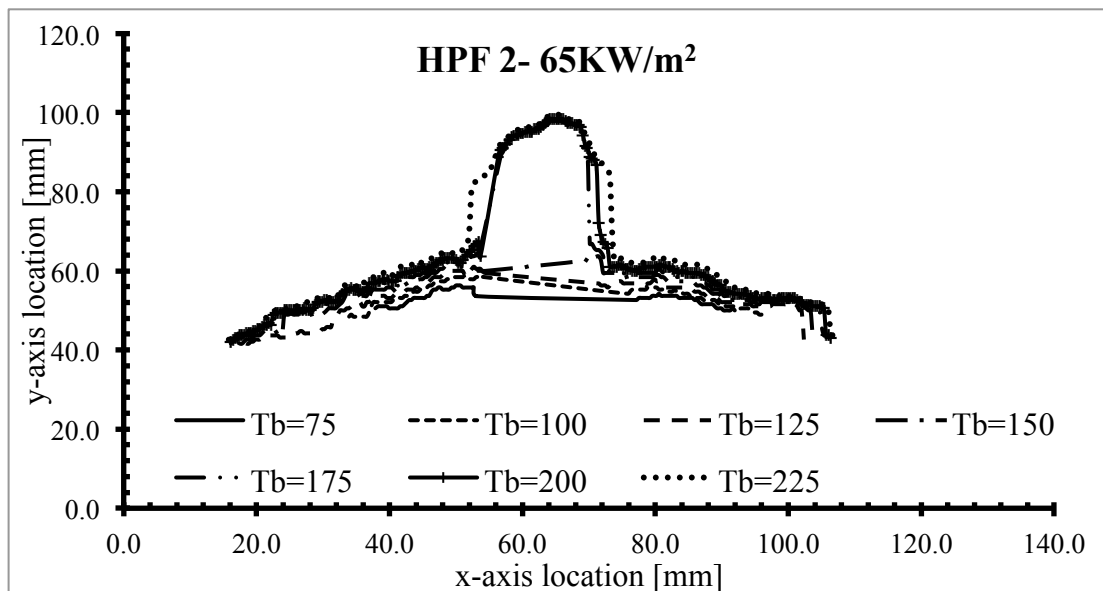
Figure 5.23. Char growth with respect to Tb- HPF 2[75-225 oC] at 65 kW/m2
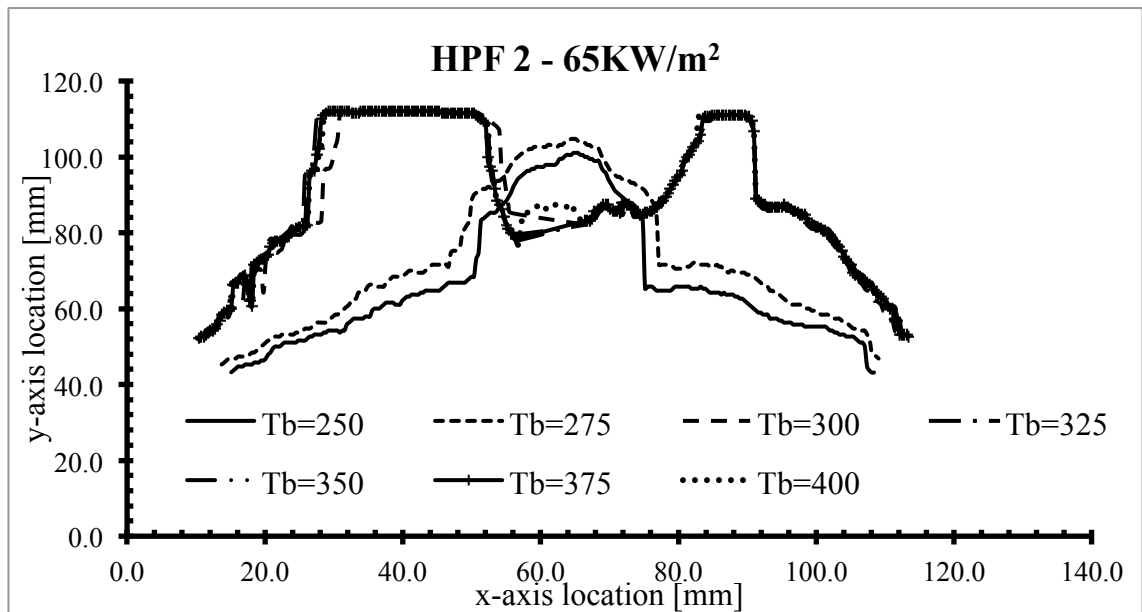
Figure 5.24. Char growth with respect to Tb- HPF 2 [250-400 oC] at 65 kW/m2

Figure 5.23 and 5.24 illustrate the char growth boundary tracked including when it cracked. At $T_b=300^0C$, the change in growth pattern showed a dip in the middle of the panel, providing evidence that the first signs of failure occurred at the flange.

The main advantage of using this method of thermal imaging with addition of image processing allows us to gather qualitative and quantitative data that has not been available before. Given the material properties of the char, it is hypothesized that char growth data can be used to determine the mechanical strength of the chars using this method. The algorithm used improved in accuracy when the char layer growth increased. It was very difficult to track at initial stages of when expansion was relatively small in magnitude. Therefore, it cannot be applied to chars that had small degree of intumescence. However, even small changes, once a considerable expansion had occurred, were easily tracked.

5.5　Conclusion

The initial objective of the thesis, which was to investigate physical aspects of intumescent under a variety of heating techniques using novel diagnostic equipment, has been successfully achieved. Tests have mostly been done on flat panel system that offers an effective method to study the process of intumescence in its simplest form. Internal char structures, surface textures, time to failure, surface temperature profiles and process of intumescence have been discussed using novel diagnostic techniques.

A variety of insightful observation have been made which give credibility to enhance research focus on lab scale based testing using not only cone heaters but flame-based setups as they offer non-uniform heat flux that is closer to what is expected in real fire condition.

The results of coatings tested under a cone heater showed that not all test cases were comparable. Different heating rates between the heating techniques had to analysed to find comparable test cases. Using the heating rate and time to reach failure temperature, certain NTP separations and thermal loading cases were compared.

- TTF_m for cone heaters was very different despite comparable heating rates. The formulations that provided the highest thermal protection based on TTF_m measurements, differed for each heating technique.

- Char structures were found to be very different in the case of the cone heater based heating. The primary difference was the degree of intumescence that was found to be smaller for all formulations. During tests, considerable shrinkage was observed in the char structure. This behaviour was not evident during flame-based tests in any coating or test condition. Shrinkage, specific to CPF 2, only occurred during a burnout. In tests conducted using a cone heater, despite the constant heat source char samples shrank post intumescence.

- The surface temperature profiles were different based on the heating technique used. The highest T_s values were recorded during cone heater tests and the profiles were smooth in nature as well. Reasonable fluctuation was observed in flame-based setups due to the uncertainty introduced by the presence of the hot gas layer when a burnout was conducted.

Once the testing with flat panels was completed, the next step was to study T-panel systems. They are more representative of the complexity encountered in industrial application than the flat panels. Thermal and digital imaging systems were used to collect information and the observations made are summarised below:

- The char movement patterns were more complex than those during tests with flat panels. Intumescence was first observed on the surface of the T-panel that was perpendicular to the incident heat flux, while char growth on the vertical (parallel) faces was delayed as they received less heat.

145

- Panels were tested in two orientations to gain a comprehensive understanding of the char growth behaviour. The general trend, revealed through thermal and digital imaging, of diagonal growth of char was due to the influences of growth from the based to the web of the panel, which also resulted in the formation of fault lines.

- A cursory analysis of the surface temperature revealed that the tip of the web received the greatest amount of heat due to its close proximity to the cone heater, maintaining the highest surface temperature. The flange, base and the vertical face of the web had different temperatures at the start of the tests. However, as the char growth continued both surfaces achieved a similar temperature.

- The HPF 2 sample applied to a T-panel tended to fail due to cracking of the char, which exposed the underlying substrate. This failure was provoked by forces exerted by the char on the base onto the char on the flange, causing the char to crack and break away from the surface of the panel.

- In comparison, CPF 2 samples did not crack owing to the highly viscous nature of the coating.

- In further tests, only the web of the panel was coated, using CPF 2 or HPF 2. In these tests no fault lines were observed, providing further evidence for the proposed cause of the existence of such fault lines in the previous tests.

- A novel method to track char growth has also been presented enabling accurate tracking of char growth with respect to T_b. The phase shifts with respect to T_b were identified for most samples accurately. The T_b values and the nature of the phase shift were found to be different compared to flat panel results. The char tracking method presented can be developed further and used to track live char growth using thermal imaging allowing the formulator to investigate char growth in greater detail.

- The char tracking technique could not be extended and used in diffusion flame setups, due to the presence of the flame in the images. This made the process of boundary tracking very inaccurate and difficult.

- Some pilot tests were conducted using premixed flames, which suggests that there maybe potential for utilising such a setup for char tracking in premixed flame systems.

Chapter6.   Conclusions

This chapter presents the general conclusions regarding the use of diagnostic techniques to investigate physical aspects of intumescence. In this work, impinging flames were successfully implemented as a new lab scale technique to understand intumescence in real fire conditions.

Advanced techniques such as Schlieren and thermal imaging were used in an exploratory role to study new, and previously known, physical aspects of intumescence. These techniques were combined with digital imaging and thermocouple data. Various methodologies were utilised and further developed for these diagnostic techniques.

Intumescent paint formulations are gaining immense popularity as the modern solution for passive fire protection. Their chemical composition has been consistently developing for more than 70 years . However, their performance in real time fire conditions is a relatively new field of study. Large-scale certification tests are very expensive. During these tests, formulators also struggle to observe intumescence as it occurs. In this work we have successfully tested an impinging flame lab scale setup. This setup offers heterogeneous heat flux typical of real fires. The lab scale setup allowed instrumentation access. Hence, multiple diagnostic techniques were used to study the process of intumescence. It is also an inexpensive and small scale representative of large commercial tests. This allows formulators to develop vast permutations of coatings and test their performance cost effectively.

In this work, four coatings were studied in detail. These coatings were designed for hydrocarbon and cellulosic-based fires. The aim of the study was to investigate the impact of non-homogenous fire (impinging flame) conditions on the process of intumescence and the physical attributes of the char. Experimental conditions such as NTP separation, thermal loading and film thickness were. Impinging flame is a contact based heating system. Hence, the flame was in contact with the surface of the paint at all times. This resulted in a very unique thermal profile that changed with the experimental conditions, allowing the author to investigate a range of fire-based conditions.

The four formulations were first applied to flat panels. The results from the heating method (impinging flame) were compared to a non-contact based standard testing

equipment, cone calorimeter. The comparison of the results showed that there was significant difference in performance between contact based and non-contact based heating method, both of which are present in a real fire. Once the tests were completed on flat panel systems, further tests were conducted using T-panel system that exhibited multi dimensional complex char movement and growth behaviour.

Thermal imaging systems ability to see at a target past a diffusion flame, which is not possible with the naked eye. It allowed the author to view past the luminous flame and collect data on the process of intumescence as it occurred. Even though, the target could be seen, it was not possible to take measurements due to the spectral emissivity of the flame. Methodologies have been developed to counter this limitation and the technique was used to study the process of intumescence, thermal variation of the char during the process of intumescence and a novel technique to track char growth using image processing techniques. Furthermore, it was used to suggest and study the critical phase shift phenomenon, the point at which the char started to intumesce. The growth sequence, phase shift and EAT_b were observed to be unique to each formulation. Physical features such as pustules were also observed to be different in size and structure for each formulation. Thermal profiles on the surface were examined at three stages of intumescence. At the start of intumescence, pustule appearance was the dominant feature, which resulted in an erratic thermal profile. Once the char had intumesced, the thermal profile had a smoother trend.

The Schlieren technique combined with the thermal imaging technique has allowed greater insight into the flame paint interactions during the process of intumescence. Certain features observed using thermal imaging were explained using the Schlieren technique such as the appearance of cool central core and the turbulent structure in the flame-paint boundary region, which contributed towards the non-homogenous nature of the incident heat flux. The evidence of reverse heat flow into the back of the cradle, which was responsible for excessive heat transfer to the substrate, was also observed. This was counteracted through the addition of the heat shield to the system. One of the key methodologies developed, in flat panel testing was the char tracking technique. The char height was tracked with respect to the substrate temperature. This allowed the identification of the EAT_b.

The two imaging techniques were combined with data from thermocouples to gain a comprehensive understanding of the performance of various formulations. The

performance of each formulation was observed with respect to its time to reach the failure temperature and various physical features such as mode shapes, surface and internal textures. The flat panel tests also offered a variety of insights that were not specific to the formulations being studied. The majority of the analysis presented in this work can be extended to other coatings, provided the formulation matrix is based on the components or their derivatives that are widely in use and discussed in this work.

The use of these techniques was extended to study complex movement on T-panel system. Primarily relying on thermal and digital imaging, the movement pattern was found to be diagonal in nature. The reason behind such movement was determined as the influence of growth from the flange (base) of the panel on the web. It also led to failure of the HPF 2 coating. Similar to the char tracking methodology using the Schlieren technique, a method was developed using thermal imaging to track char growth in T-panels. The method was limited to cone heaters and has not been extended to flame-based setups.

This thesis has presented numerous interesting results on the physical aspects of intumescence in flat and T-panels. Various formulations were studied using a variety of diagnostic techniques under different heating methods and combining various visualisation and diagnostic techniques. However, improvements can still be made on the accuracy of these techniques, more extensive experimentation could be performed and additional parameters could be studied.

6.1 Scope for future work

6.1.1 Accuracy

The study of the process of intumescence has been presented using the thermal imaging system. It was studied successfully and various new features and characteristics were highlighted and discussed in both qualitative and quantitative aspects. The thermal imaging camera values were influenced by the presence of a hot gas layer and the associated uncertainty could not be removed. This presented as a constraint to study the heat transfer characteristics of the system. Furthermore, the impact of radiation and its dependence on an irregular moving char surface could not be ignored as well. It is suggested that if the system could be calibrated and the temperature readings form the thermal system could be verified. It would be a huge step towards linking the surface and the substrate temperature together and understanding the heat transfer characteristics thought the surface of the paint. Such work could bridge a connection between modelling and simulation and experimental results.

The impact of diffusion flame could not be ignored. Cone heaters and premixed flame heating system should be explored to understand the temperature dependence of intumescence in greater detail. Such efforts can help provide greater insight into the behaviour of char growth in real fire conditions.

Schlieren technique has presented a great potential to study intumescence. The interaction between the paint and flame was a very important aspect which was not studied in great detail due to timing and equipment constraints. Furthermore, the system could not be utilised once the shield was introduced. The reflection form the flame generated unfavourable density gradients. It is recommended for future work that a system with a smaller field of view focused on flame wall boundary should be designed for detailed analysis capable of image processing capabilities. The rig should be modified so the shield and paint surface are tangential and a smooth flame boundary is maintained. The studies should also be conducted on smaller samples using smaller flames. This might help remove the undesirable density gradients.

6.1.2 Further Research

Larger samples could be used to investigate thermal profile in grater detail. The flame escaped around the edges and heated the back of the panel. Testing with bigger samples might compensate for that problem and provide greater detail of temperature distribution along the surface in an axial direction. Furthermore, a larger range of plate height and thickness can be investigated. The losses due to radiation and convection can be calculated to identify the incident heat flux on the surface of the paint sample rather than the thermal loading at the nozzle.

The heat flux incident on the surface increases as the char height grows. The thermal conductivity, as suggested by literature, increases as the temperature increases as well. Furthermore, the porus nature and irregular growth structures add to an increasing complex heat transfer scenario. Information from thermal imaging and thermocouples for the surface and substrate temperature respectively can be combined with thermal conductivity and heat flux variation, as the char intumesces, can form the basis of an experimental based study into the complex nature of heat transfer mechanisms in the char. Digital imaging, image processing and advance microscopic techniques such as Scanning Electron microscopy (SEM) can also add further insight.

T-panels should be studied under an impinging diffusion and premixed flame setup. This was not achieved in this study due to various constraints that include equipment needs, budget limitations, flexible experimental rig and stronger extraction systems among many. A synchronised system using two thermal cameras on a single test case would allow the study of the process and movement of the char in greater detail. Furthermore, similar to flat panel system, the complex heat transfer mechanism is the most important and logical step for future work in this direction.

6.1.3 Summary

The scope for future work discussed in this chapter could not be attempted due to various limitation and constraints. These include time, experimental, budget, stakeholder interests, restrictions again publications and safety concerns. However, there is a huge potential of growth and additional interesting opportunities for further research if these restraints were to be minimised.

Nevertheless, many interesting results have been presented in this thesis over a wide range of experimental conditions using advanced optical diagnostic. The techniques that have been developed will be useful for future research to study the physical aspects of intumescence using impinging flame setups.

Chapter7.   References

[1]   D. R. W. a. V. Thewes. (2004, 10/2004) Foam Protects. [Company publication]. 5.

[2]   G. Camino, L. Costa, and G. Martinasso, "Intumescent fire-retardant systems," *Polymer Degradation and Stability,* vol. 23, pp. 359-376, 1989.

[3]   M. Jimenez, S. Duquesne, and S. Bourbigot, "Characterization of the performance of an intumescent fire protective coating," *Surface and Coatings Technology,* vol. 201, pp. 979-987, 2006.

[4]   ISO22899-1:2007(E), "Determination of the resistance to jet fires of passive fire protection materials-Part 1," 2007.

[5]   M. Jimenez, S. Duquesne, and S. Bourbigot, "Multiscale Experimental Approach for Developing High-Performance Intumescent Coatings," *Industrial & Engineering Chemistry Research,* vol. 45, pp. 4500-4508, 2006/06/01 2006.

[6]   Y. Zhang, Y. C. Wang, C. G. Bailey, and A. P. Taylor, "Global modelling of fire protection performance of intumescent coating under different cone calorimeter heating conditions," *Fire Safety Journal,* vol. 50, pp. 51-62, 5// 2012.

[7]   A. Omrane, Y. C. Wang, U. Göransson, G. Holmstedt, and M. Aldén, "Intumescent coating surface temperature measurement in a cone calorimeter using laser-induced phosphorescence," *Fire Safety Journal,* vol. 42, pp. 68-74, 2007.

[8]   S. Duquesne, S. Magnet, C. Jama, and R. Delobel, "Intumescent paints: Fire protective coatings for metallic substrates," *Surface and Coatings Technology,* vol. 180-181, pp. 302- 307, 2004.

[9]   S. Chander and A. Ray, "An experimental and numerical study of stagnation point heat transfer for methane/air laminar flame impinging on a flat surface," *International Journal of Heat and Mass Transfer,* vol. 51, pp. 3595-3607, 2008.

[10]   J. E. J. Staggs, "Thermal conductivity estimates of intumescent chars by direct numerical simulation," *Fire Safety Journal,* vol. 45, pp. 228-237, 6// 2010.

[11]   H. L. Vandersall, "Intumescent coating systems, their development and chemistry," *J of Fire & Flammability,* vol. 1, pp. 97-140, 1970.

[12]   S. V. Levchik and E. D. Weil, "Thermal decomposition, combustion and fire-retardancy of polyurethanes - A review of the recent literature," *Polymer International,* vol. 53, pp. 1585-1610, 2004.

[13]   S. Bourbigot, M. Le Bras, R. Delobel, P. Bréant, and J. m. Trémillon, "Carbonization mechanisms resulting from intumescence-part II. Association with an ethylene terpolymer and the ammonium polyphosphate-pentaerythritol fire retardant system," *Carbon,* vol. 33, pp. 283-294, 1995.

[14]   M. Jimenez, S. Duquesne, and S. Bourbigot, "Intumescent fire protective coating: Toward a better understanding of their mechanism of action," *Thermochimica Acta,* vol. 449, pp. 16-26, // 2006.

[15]   S. Bourbigot, M. Le Bras, R. Delobel, and J. M. Trémillon, "Synergistic effect of zeolite in an intumescence process: Study of the interactions between the polymer and the additives," *Journal of the Chemical Society - Faraday Transactions,* vol. 92, pp. 3435-3444, 1996.

[16]   S. Bourbigot, M. Le Bras, S. Duquesne, and M. Rochery, "Recent advances for intumescent polymers," *Macromolecular Materials and Engineering,* vol. 289, pp. 499-511, 2004.

[17]   S. V. Levchik, A. I. Balabanovich, G. F. Levchik, and L. Costa, "Effect of melamine and its salts on combustion and thermal decomposition of polyamide 6," *Fire and Materials,* vol. 21, pp. 75-83, 1997.

[18]   S. V. Levchik, G. Camino, L. Costa, and G. F. Levchik, "Mechanism of action of phosphorus-based flame retardants in nylon 6. I. Ammonium polyphosphate," *Fire and Materials,* vol. 19, pp. 1-10, 1995.

[19]   S. V. Levchik, L. Costa, and G. Camino, "Effect of the fire-retardant, ammonium polyphosphate, on the thermal decomposition of aliphatic polyamides. I. Polyamides 11 and 12," *Polymer Degradation and Stability,* vol. 36, pp. 31-41, 1992.

[20]   S. V. Levchik, G. F. Levchik, A. I. Balabanovich, G. Camino, and L. Costa, "Mechanistic study of combustion performance and thermal decomposition behaviour of nylon 6 with added halogen-free fire retardants," *Polymer Degradation and Stability,* vol. 54, pp. 217-222, 1996.

[21]   S. Duquesne, R. Delobel, M. Le Bras, and G. Camino, "A comparative study of the mechanism of action of ammonium polyphosphate and expandable graphite in polyurethane," *Polymer Degradation and Stability,* vol. 77, pp. 333-344, 2002.

[22]   S. Jahromi, W. Gabriëlse, and A. Braam, "Effect of melamine polyphosphate on thermal degradation of polyamides: A combined X-ray diffraction and solid-state NMR study," *Polymer,* vol. 44, pp. 25-37, 2003.

[23]   S. V. Levchik, L. Costa, and G. Camino, "Effect of the fire-retardant ammonium polyphosphate on the thermal decomposition of aliphatic polyamides. Part III-Polyamides 6.6 and 6.10," *Polymer Degradation and Stability,* vol. 43, pp. 43-54, 1994.

[24]   S. V. Levchik, L. Costa, and G. Camino, "Effect of the fire-retardant, ammonium polyphosphate, on the thermal decomposition of aliphatic polyamides: Part II-polyamide 6," *Polymer Degradation and Stability,* vol. 36, pp. 229-237, 1992.

[25]   S. Zhou, L. Song, Z. Wang, Y. Hu, and W. Xing, "Flame retardation and char formation mechanism of intumescent flame retarded polypropylene composites containing melamine phosphate and pentaerythritol phosphate," *Polymer Degradation and Stability,* vol. 93, pp. 1799- 1806, 2008.

[26]   P. Lv, Z. Wang, K. Hu, and W. Fan, "Flammability and thermal degradation of flame retarded polypropylene composites containing melamine phosphate and pentaerythritol derivatives," *Polymer Degradation and Stability,* vol. 90, pp. 523-534, 2005.

[27]   S. V. Levchik, G. F. Levchik, G. Camino, L. Costa, and A. I. Lesnikovich, "Mechanism of action of phosphorus-based flame retardants in nylon 6. III. Ammonium polyphosphate/manganese dioxide," *Fire and Materials,* vol. 20, pp. 183-190, 1996.

[28]   M. Bugajny, M. Le Bras, and S. Bourbigot, "Thermoplastic polyurethanes as carbonization agents in intumescent blends. Part 2: Thermal behavior of polypropylene/thermoplastic polyurethane/ammonium polyphosphate blends," *Journal of Fire Sciences,* vol. 18, pp. 7-27, 2000.

[29]   J. Lindholm, A. Brink, and M. Hupa, "Cone Calorimeter – A tool for measuring heat releasr rate," Finnish Flame Research Committee-IFRF2009.

[30]   K. Carpenter and M. Janssens, "Using Heat Release Rate to Assess Combustibility of Building Products in the Cone Calorimeter," *Fire Technology,* vol. 41, pp. 79-92, 2005/04/01 2005.

[31]   M. Modesti, A. Lorenzetti, F. Simioni, and G. Camino, "Expandable graphite as an intumescent flame retardant in polyisocyanurate-polyurethane foams," *Polymer Degradation and Stability,* vol. 77, pp. 195-202, 2002.

[32]   Z. Wu, W. Shu, and Y. Hu, "Synergist flame retarding effect of ultrafine zinc borate on LDPE/IFR system," *Journal of Applied Polymer Science,* vol. 103, pp. 3667-3674, 2007.

[33]   S. Nie, Y. Hu, L. Song, Q. He, D. Yang, and H. Chen, "Synergistic effect between a char forming agent (CFA) and microencapsulated ammonium polyphosphate on the thermal and flame retardant properties of polypropylene," *Polymers for Advanced Technologies,* vol. 19, pp. 1077-1083, 2008.

[34]   B. Li, H. Jia, L. Guan, B. Bing, and J. Dai, "A novel intumescent flame-retardant system for flame-retarded LLDPE/EVA composites," *Journal of Applied Polymer Science,* vol. 114, pp. 3626-3635, 2009.

[35]   Y. Li, B. Li, J. Dai, H. Jia, and S. Gao, "Synergistic effects of lanthanum oxide on a novel intumescent flame retardant polypropylene system," *Polymer Degradation and Stability,* vol. 93, pp. 9-16, 2008.

[36]   B. Schartel and T. R. Hull, "Development of fire-retarded materials - Interpretation of cone calorimeter data," *Fire and Materials,* vol. 31, pp. 327-354, 2007.

[37]   C. Maluk, L. Bisby, G. Terrasi, M. Krajcovic, and J. Torero, "Novel Fire Testing Methodology: Why, how and what now?," *Proceedings of the Mini Symposium on Performance-based Fire Safety Engineering of Structures as part of the 1st International Conference on Performace Based land Life Cycle Structural Engineering,* pp. pp 448-458, 5-7 December, 2012 2012.

[38]   X. Almeras, M. Le Bras, P. Hornsby, S. Bourbigot, G. Marosi, S. Keszei*, et al.*, "Effect of fillers on the fire retardancy of intumescent polypropylene compounds," *Polymer Degradation and Stability,* vol. 82, pp. 325-331, // 2003.

[39]   Underwrtiers-Labratories, "UL-1709 Rapid Rise Fire Tests of Protection Materials for Structural Steel," Underwrtiers Labratories1994.

[40]   CEN-EN13381-8, "Test methods for determining the contribution to the fire resistance of structural members. Part 8.," BSI, London2010 2010.

[41]   S. Bourbigot, M. Le Bras, R. Delobel, R. Decressain, and J. P. Amoureux, "Synergistic effect of zeolite in an intumescence process: Study of the carbonaceous structures using solid-state NMR," *Journal of the Chemical Society - Faraday Transactions,* vol. 92, pp. 149-158, 1996.

[42]   G. Camino, A. Maffezzoli, M. Braglia, M. De Lazzaro, and M. Zammarano, "Effect of hydroxides and hydroxycarbonate structure on fire retardant effectiveness and mechanical properties in ethylene-vinyl acetate copolymer," *Polymer Degradation and Stability,* vol. 74, pp. 457-464, 2001.

[43]   M. A. Delichatsios, "Air entrainment into buoyant jet flames and pool fires," *Combustion and Flame,* vol. 70, pp. 33-46, 10// 1987.

[44]   D. Drysdale, *An Introduction to Fire Dynamics*: Wiley, 2011.

[45]   D. P. Mishra, *Fundamentals of Combustion*: PHI Learning, 2007.

[46]   G. Cox, *Combustion Fundamentals of Fire*: Academic Press, 1995.

[47]   G. Heskestad, "Virtual origins of fire plumes," *Fire Safety Journal,* vol. 5, pp. 109-114, // 1983.

[48]   B. J. McCaffrey and C. f. F. Research, *Purely Buoyant Diffusion Flames: Some Experimental Results*, 1979.

[49]   W. G. Weng and Y. Hasemi, "Heat transfer to an unconfined ceiling from an impinging buoyant diffusion flame," *Heat and Mass Transfer/Waerme- und Stoffuebertragung,* vol. 42, pp. 652-659, 2006.

[50]   L. Y. Cooper and D. W. Stroup, "THERMAL RESPONSE OF UNCONFINED CEILINGS ABOVE GROWING FIRES AND THE IMPORTANCE OF CONVECTIVE HEAT TRANSFER," *Journal of Heat Transfer,* vol. 109, pp. 172-178, 1987.

[51]   P. L. Hinkley, H. G. H. Wraight, and C. R. Theobald, "The contribution of flames under ceilings to fire spread in compartments," *Fire Safety Journal,* vol. 7, pp. 227-242, // 1984.

[52]   D. Gross, "Measurement of flame lengths under ceilings," *Fire Safety Journal,* vol. 15, pp. 31-44, // 1989.

[53]   G. Heskestad, "Luminous heights of turbulent diffusion flames," *Fire Safety Journal,* vol. 5, pp. 103-108, // 1983.

[54]   T. G. Ma and J. G. Quintiere, "Numerical simulation of axi-symmetric fire plumes: Accuracy and limitations," *Fire Safety Journal,* vol. 38, pp. 467-492, 2003.

[55]   C. Challener, "Fighting fires with greener coating techonologies," *JCT CoatingsTech,* vol. 10, pp. 38-44, 2013.

[56]   M. Jimenez, S. Duquesne, and S. Bourbigot, "Kinetic analysis of the thermal degradation of an epoxy-based intumescent coating," *Polymer Degradation and Stability,* vol. 94, pp. 404-409, 3// 2009.

[57]   R. Viskanta, "Heat transfer to impinging isothermal gas and flame jets," *Experimental Thermal and Fluid Science,* vol. 6, pp. 111-134, 1993.

[58]   S. Chander and A. Ray, "Experimental and numerical study on the occurrence of off-stagnation peak in heat flux for laminar methane/air flame impinging on a flat surface," *International Journal of Heat and Mass Transfer,* vol. 54, pp. 1179-1186, 2011.

[59]   S. S. Hou and Y. C. Ko, "Effects of heating height on flame appearance, temperature field and efficiency of an impinging laminar jet flame used in domestic gas stoves," *Energy Conversion and Management,* vol. 45, pp. 1583-1595, 2004.

[60]   C. E. Baukal and B. Gebhart, "A review of flame impingment heat transfer studies Part 1: Experimental conditions," *Combustion Sceince and Technology,* vol. 104, p. 19, 1995.

[61]   C. E. Baukal and B. Gebhart, "A review of flame impingement heat transfer studies part 2: Measurements," *Combustion Sceince and Technology,* vol. 104, p. 27, 1995.

[62]   C. E. Baukal and B. Gebhart, "Surface Condition Effects on Flame Impingement Heat Transfer," *Experimental Thermal and Fluid Science,* vol. 15, pp. 323-335, 1997.

[63]   C. E. Baukal and B. Gebhart, "A review of semi-analytical solutions for flame impingement heat transfer," *International Journal of Heat and Mass Transfer,* vol. 39, pp. 2989-3002, 1996.

[64]   C. E. Baukal and B. Gebhart, "A review of empirical flame impingement heat transfer correlations," *International Journal of Heat and Fluid Flow,* vol. 17, pp. 386-396, 1996.

[65]   S. Chander and A. Ray, "Flame impingement heat transfer: A review," *Energy Conversion and Management,* vol. 46, pp. 2803-2837, 2005.

[66]   T. H. van der Meer, "Stagnation point heat transfer from turbulent low reynolds number jets and flame jets," *Experimental Thermal and Fluid Science,* vol. 4, pp. 115-126, 1991.

[67]   M. Fairweather, J. K. Kilham, and S. Nawaz, "Stagnation point heat transfer from laminar, high temperature methane flames," *International Journal of Heat and Fluid Flow,* vol. 5, pp. 21-27, 1984.

[68]   L. L. Dong, C. S. Cheung, and C. W. Leung, "Heat transfer characteristics of an impinging inverse diffusion flame jet. Part II: Impinging flame structure and impingement heat transfer," *International Journal of Heat and Mass Transfer,* vol. 50, pp. 5124-5138, 12// 2007.

[69]   I. I. Kantorovich and E. Bar-Ziv, "Heat transfer within highly porous chars: a review," *Fuel,* vol. 78, pp. 279-299, 2// 1999.

[70]   C. E. Anderson Jr, J. J. M. Dziuk, J. Buckmaster, and W. A. Mallow, "Intumescent reaction mechanisms.," *Journal of Fire Sciences,* vol. 3, pp. 161-194, 1985.

[71]   C. E. Anderson Jr and D. K. Wauters, "A thermodynamic heat transfer model for intumescent systems," *International Journal of Engineering Science,* vol. 22, pp. 881-889, 1984.

[72]   J. Buckmaster, C. Anderson, and A. Nachman, "A model for intumescent paints," *International Journal of Engineering Science,* vol. 24, pp. 263-276, 1986.

[73]   ASTM-Committee:E-20, "Manual on the use of Thermocouples in Temperature Measurement," ASTM Committee E-20, Philidelphia1981.

[74]   F. J. White, "Accuracy of thermocouples in radiant-heat testing," *Experimental Mechanics,* vol. 2, pp. 204-210, 1962/07/01 1962.

[75]   M. Salem, S. Staude, U. Bergmann, and B. Atakan, "Heat flux measurements in stagnation point methane/air flames with thermographic phosphors," *Experiments in Fluids,* vol. 49, pp. 797-807, 2010.

[76]   J. A. Qi, C. W. Leung, W. O. Wong, and S. D. Probert, "Temperature-field measurements of a premixed butane/air circular impinging-flame using reference-beam interferometry," *Applied Energy,* vol. 83, pp. 1307-1316, 2006.

[77]   B. W. Albers and A. K. Agrawal, "Schlieren analysis of an oscillating gas-jet diffusion flame," *Combustion and Flame,* vol. 119, pp. 84-94, 1999.

[78]   Y. S. Ko and S. H. Chung, "Propagation of unsteady tribrachial flames in laminar non-premixed jets," *Combustion and Flame,* vol. 118, pp. 151-163, 1999.

[79]   T. Takagi, H. D. Shin, and A. Ishio, "Local laminarization in turbulent diffusion flames," *Combustion and Flame,* vol. 37, pp. 163-170, 1980.

[80]   N. T. Clemens and M. G. Mungal, "A planar Mie scattering technique for visualizing supersonic mixing flows," *Experiments in Fluids,* vol. 11, pp. 175-185, 1991.

[81]   W. H. Wentz Jr and D. L. Kohlman, "Vortex breakdown on slender sharp- edge wings," *Journal of Aircraft,* vol. 8, pp. 156-161, 1971.

[82]   G. S. Settles, *Schlieren and Shadowgraph techniques*. Germany: Springer-Verlag, 2001.

157

[83]   S. B. Dalziel, G. O. Hughes, and B. R. Sutherland, "Whole-field density measurements by 'synthetic schlieren'," *Experiments in Fluids,* vol. 28, pp. 322-335, 2000.

[84]   J. E. J. Staggs, R. J. Crewe, and R. Butler, "A theoretical and experimental investigation of intumescent behaviour in protective coatings for structural steel," *Chemical Engineering Science,* vol. 71, pp. 239-251, 3/26/ 2012.

[85]   M. Vollmer and K.-P. Möllmann, *Infrared Thermal Imaging: Fundamentals, Research and Applications*: John Wiley & Sons, 2011.

[86]   T. L. Williams, "Thermal Imaging Cameras : charecteristics and performance," ed. Florida: Taylor & Francis Group, 2009.

[87]   FLIR systems. (2001, 12/04/2011). *FLIR Iintroduces Thermacam SC 3000 High Speed Thermal Imaging System* Available: http://www.photonicsonline.com/article.mvc/FLIR-Iintroduces-Thermacam-SC-3000-High-Speed-0001

[88]   FLIR. *SC3000 Information*. Available: http://infrapuna.ee/files/FLIR_sc3000.pdf

[89]   C. McDaid and Y. Zhang, "Wall temperature measurements using a thermal imaging camera with temperature-dependent emissivity corrections," *Measurement Science and Technology,* vol. 22, 2011.

[90]   D. Lytle and B. W. Webb, "Air jet impingement heat transfer at low nozzle-plate spacings," *International Journal of Heat and Mass Transfer,* vol. 37, pp. 1687-1697, 8// 1994.

[91]   V. Katti and S. V. Prabhu, "Experimental study and theoretical analysis of local heat transfer distribution between smooth flat surface and impinging air jet from a circular straight pipe nozzle," *International Journal of Heat and Mass Transfer,* vol. 51, pp. 4480-4495, 2008.

[92]   D. J. Bizzak and M. K. Chyu, "Use of a laser-induced fluorescence thermal imaging system for local jet impingement heat transfer measurement," *International Journal of Heat and Mass Transfer,* vol. 38, pp. 267-274, 1995.

[93]   R. D. Cowan, "Proposed Method of Measuring Thermal Diffusivity at High Temperatures," *Journal of Applied Physics,* vol. 32, pp. 1363-1370, 1961.

[94]   C. McDaid, "Developing and Implementing Advanced Optical Diagnostics for the Investigation of Fuel and Flow Effects on Ignition, Flame Structure and Wall Temperature of Impinging Jet Flames," PhD, Mechanical Engineering, University of Sheffield, Sheffield, 2014.

[95]   P. Mather. (2006, 14/02/2011). *Fire Testing, New Technologies and the Shop-Applied Trend in Product Application* Available: http://www.pcimag.com/Articles/Feature_Article/7adac099bbfad010VgnVCM100000f932a8c0____

[96]   FLIR systems. (2001, 20/05/2013). *FLIR Iintroduces Thermacam SC 640 High Speed Thermal Imaging System*. Available: http://www.flir.com/cs/apac/en/view/?id=41965

[97]   FLIR systems. (2001, 20/11/2010). *ThermaCAM Researcher* Available: http://www.flir.com/cs/emea/en/view/?id=42404

[98]   Casio America Inc. (2014, 01.04.2014). *EX-F1 - High speed camera specification*. Available: http://www.casio.com/products/archive/Digital_Cameras/High-Speed/EX-F1/

[99]   M. C. Yew and N. H. Ramli Sulong, "Fire-resistive performance of intumescent flame-retardant coatings for steel," *Materials & Design,* vol. 34, pp. 719-724, 2// 2012.

[100] Z. Wang, P. Lv, Y. Hu, and K. Hu, "Thermal degradation study of intumescent flame retardants by TG and FTIR: Melamine phosphate and its mixture with pentaerythritol," *Journal of Analytical and Applied Pyrolysis,* vol. 86, pp. 207-214, 9// 2009.

[101] A. I. Balabanovich, "Thermal decomposition study of intumescent additives: Pentaerythritol phosphate and its blend with melamine phosphate," *Thermochimica Acta,* vol. 435, pp. 188-196, 9/15/ 2005.

[102] N. Tian, X. Wen, Z. Jiang, J. Gong, Y. Wang, J. Xue*, et al.*, "Synergistic Effect between a Novel Char Forming Agent and Ammonium Polyphosphate on Flame Retardancy and

Thermal Properties of Polypropylene," *Industrial & Engineering Chemistry Research,* vol. 52, pp. 10905-10915, 2013/08/14 2013.

[103]   W. Klingsch, "Fire resistance of solid steel columns," *Fire Safety Journal,* vol. 4, pp. 237-241, 1981.

[104]   Y. N. Shebeko, I. A. Bolodian, V. N. Filippov, V. Y. Navzenya, A. K. Kostyuhin, P. M. Tokarev*, et al.*, "A study of the behaviour of a protected vessel containing LPG during pool fire engulfment," *Journal of Hazardous Materials,* vol. 77, pp. 43-56, 2000.

[105]   A. Bhargava and G. J. Griffin, "Two dimensional model of heat transfer across a fire retardant epoxy coating subjected to an impinging flame," *Journal of Fire Sciences,* vol. 17, pp. 188-208, 1999.

[106]   S. Bourbigot, S. Duquesne, and J.-M. Leroy, "Modeling of Heat Transfer of a Polypropylene-Based Intumescent System during Combustion," *Journal of Fire Sciences,* vol. 17, pp. 42-56, January 1, 1999 1999.

[107]   G. J. Griffin, "The modeling of heat transfer across intumescent polymer coatings," *Journal of Fire Sciences,* vol. 28, pp. 249-277, 2010.

[108]   Z. H. Wang and K. H. Tan, "Green's function approach for heat conduction: Application to steel members protected by intumescent paint," *Numerical Heat Transfer, Part B: Fundamentals,* vol. 54, pp. 435-453, 2008.

[109]   R. J. Crewe, J. E. J. Staggs, and H. N. Phylaktou, "The temperature-dependent cone calorimeter: An approximate alternative to furnace testing," *Journal of Fire Sciences,* vol. 29, pp. 131-151, 2011.

[110]   Y. Zhang, Y. C. Wang, C. G. Bailey, and A. P. Taylor, "Global modelling of fire protection performance of an intumescent coating under different furnace fire conditions," *Journal of Fire Sciences,* vol. 31, pp. 51-72, 2013.

[111]   A. Lyons, *Materials for Architects & Builders*: Elsevier Ltd., 2008.